UNIVERSITY OF LEICESTER

An Experimental Study of Channel Characterization Based on Measurements of non-perpendicular intersections scenarios at 5.9 GHz for Vehicle-to-Vehicle Communications

Thesis submitted for the degree of

Doctor of Philosophy

at the University of Leicester

by

Saddam K. Alwane

Aerospace and Computational Engineering Group

School of Engineering

University of Leicester, UK

December 2019

Abstract

The IEEE 802.11p, which operates at 5.9 GHz, is a standard used for vehicle communications. This thesis presents new measurements of the propagation channel by using new devices such as LocoMate mini2 to measure network performance, signal strength and Doppler propagation conducted for five different non-perpendicular intersections in Leicester, UK.

The study found that the received power and network performance were lower at intersections with fewer buildings. The high signal strength positively correlated to the presence of buildings via multipath propagation. The signal strength measurements were compared with predictions of the path loss model (virtualsource11p) and an average error was found below 5 dB for measurements in these intersections. The model fits well with most measurements but minor modifications to the model are proposed to increase accuracy.

The relationship between car size and Doppler spread is another observation of this study. It is shown that there is a larger Doppler spread when the size of this car is larger. The placement of the antennas also influences the performance. Measurements were taken with different configurations of the transmitter antenna. Results show that changing the height of the transmitter has a strong effect on the received signal within the LOS region, but little effect at greater distances. The addition of an antenna ground plane has a similar effect to changing the height.

Finally, GEMV2-based simulations were performed to show the effects of vehicle and building numbers on the path loss of the V2V communication channel. The results showed that the density of vehicles causes a decrease in the received power when there are few buildings near the road. On the other hand, in intersections with more buildings, the buildings have more effect on the signal attenuation than the number of vehicles.

Acknowledgements

First and foremost, all praises and thanks are due to Almighty ALLAH, the most Gracious and the most Merciful who has created everything and taught the creation which they knew not and may ALLAH's peace and blessings be upon the Prophet Mohammed.

Then, I am very grateful to my supervisor Dr. David Siddle who was abundantly helpful and offered invaluable assistance, support and guidance. I would also thank Prof. Mike Warrington and Dr. Alan Stocker for their numerous help and support.

I am also thankful to the Iraqi Ministry of Higher Education and Scientific Research (MOHESR) and the University of Technology for funding and supporting my research.

I would also like to thank the Iraqi Cultural Attaché in London, in particular Dr. Nahi Yusuf Al-Rikabi and Mr. Laith Mashkoor for their support in completing my studies.

Also, I thank my colleagues at the University of Leicester, especially Radio Systems Laboratory Research group: Dr. Tarik, Dr. Zaid, Dr. Hasanin, Dr. Mohammed Abdullah, and Ameer for their support and beneficial conversations during my study.

Deepest gratitude is also due to Bilal Haveliwala, Dominic Kent, and Michelle Pryce for their help during the period of my study.

The most important thanks are for my family, especially for My father, My mother, My wife and My children for their support and patience throughout the period of my study.

Table of Contents

List of Figures

List of Tables

List of Abbreviation

3GPP ....3G Partnership Project
5GCAR ....5G Communication Automotive Reseach
5GPPP ....5G Public Private Partnership
Bc ....Coherence Bandwidth
BS ....Base Station
CCH ....Control Channel
CCN ....Content-Centric Networking
CDF ....Cumulative Distribution Function
CDMA ....Code Division Multiple Access
CSV ....Comma-Separated Values
CWS ....Continuous Wave System
DD ....Duration of Disturbance
DSPL ....Dual-Slope Piecewise-Linear
DSRC ....Dedicated Short Range Communication
DW ....Doppler spectrum Bandwidth
EDCA ....Enhanced Distributed Channel Access
EM ....Electromagntic
FCC ....Federal Communication Commission
FCD ....Floating Car Data
FDTD ....Finite-Difference-Time-Domain
Fmax ....Maximum Fading Depth
GBD ....Geometry-Based Deterministic
GBS ....Geometry-Based Stochastic
GEMV2 ....the Geometry-based efficient propagation Model
GPRS ....General Packet Radio Service
GPS ....Global Positioning System
GSM ....Global System for Mobile Communications
GUI ....Graphical User Interface
ICA ....Intersection Collision Avoidance
IoT ....Internet of Things
ITS ....Intelligent Transportation System
IVC ....Inter-Vehicular Communications
KML ....Keyhole Markup Language
LOS ....Line-Of-Sight
LTE ....Long-Term Evolution
M2M ....Machine-to-Machine
MIDR ....Median Inter-decile Range
MIMO ....Multiple-Input Multiple-Output
MIPS ....Microprocessor without Interlocked Pipelined Stage

MPP…… Median Peak Power
NGS ....Non-geometrical Stochastic
NLOS ....Non-Line-of-Sight
NLOSb ....Non-LOS due to buildings/foliage
NLOSv .... Non-LOS due to vehicles
NS ....Network System
OFDM ....Orthogonal Frequency Division Multiplexing
OSM .... OpenStreetMap
PDR .... Packet Delivery Ratio
RF .... Radio Frequency
RMS .... Root Mean Square
RSSI .... Received Signal Strength Indicator
RT ....Ray-Tracing
Rx ....Receiver
SCHs ....Service Channels
SISO .... Single-Input Single-Output
SUMO .... Simulation of Urban Mobility
Tc ....Coherence Time
Tx ....Transmitter
V2I ....Vehicle-to-Infrastructure
V2V ....Vehicle-to-Vehicle
WAVE ………………………………………………………………………………………….Wireless Access Vehicular Environment
VANETs ....Vehicular Ad-hoc Networks
WCDMA ....Wide-band Code Division Multiple Access
WiMAX ……………………………………………………………………WordWide Interoperability for Microwave Access
WHO .... World Health Organization
WSN .... Wireless Sensor Network

Variables & Notations

μ	The Mean
B	Bandwidth
C	Curve Shift
$C_{(SISO)}$	Antenna Capacity
c	Speed of Light =3 $x10^8$ ms^{-1}
d	Tx-Rx Separation Distance
d_b	Breakpoint Distance (≈ 180 m)
d_o	Reference Distance
d_r	Distance from the receiver to the intersection centre
d_t	Distance from the transmitter to the intersection centre
E_{LOS}	Line-Of-Sight Component
E_{TOT}	Total Received E-field
E_L	Loss exponent
Em	Median Error
E_o	Ground Reflected Component
E_S	Street Exponent
E_T	Tx Distance Exponent
f_c	Centre Frequency of the Radio Wave
f_d	Doppler shift
G_{Rx}	Antenna Gain of Rx
G_{Tx}	Antenna Gain of Tx
h_t	Height of Tx
i_s	Sub-urban Loss Factor (0/1 for urban/suburban conditions)
L_{SU}	Sub-urban Loss
M	Number of Receiving Antennas
N	Number of Transmitting Antennas
$P_L(d)$	Pathloss at Distance d
P_{Rx}	Receive Power
P_{Tx}	Transmit Power
S/N	Signal to Noise Ratio
v	Speed of the Mobile
w_r	Width of the Receiver Street
x_t	Distance from the transmitter to the wall
γ	Path loss Exponent
θ	Angle of Arrival
λ	Wavelength
σ	The Standard Deviation

List of Publications

S. K. Alwane, D. R. Siddle and A. J. Stocker “The Effect of the Vehicle Size on the V2V Radio Channel" The Birmingham Antennas & Propagation Conference (APC 2019), Birmingham, United Kingdom, 2019.

C. J. Clayton, A. J. Stocker, **S. K. A. Alwane**, and D. Hassan, “Observations of 5.9 GHz radio propagation and 802.11p network performance at road junctions,” Radio Sci., p. 2018RS006643, 2019.

S. K. Alwane and D. R. Siddle, "An experimental investigation into the impact of vehicular traffic on V2V communication channel," *The Loughborough Antennas & Propagation Conference (LAPC 2018)*, Loughborough, United Kingdom, 2018, pp. 1-5.

Saddam K. Alwane, D. R. Siddle, "An Experimental Investigation into the Impact of Vehicular Traffic on V2V Communication Channel" UK/ URSI Symposium 2019, 10 January 2019, National Physical Laboratory, Teddington, London, United Kingdom

Saddam K. Alwane, D. R. Siddle, "Vehicular Channel Characterization" UK/URSI Festival of Radio Science 2017, 5 December 2017, Faculty of Engineering and Informatics, University of Bradford, United Kingdom

Chapter 1: Introduction

Wireless communication is the most established type of communications. Wireless communication started with the discovery of electromagnetic (EM) waves by Scottish physicist James Clerk Maxwell in 1867 (Longair, 2015), and was exhibited later by Heinrich Hertz in 1885 who produced EM waves in his lab. In 1894, Alexander Stepanovich Popov built a radio receiver, and the wireless telegraph system was invented in 1896 by Guglielmo Marconi (Sengar *et al.* 2014). From that point forward new wireless communication techniques have been developed and adopted by the general population all around the globe. The last three decades have seen a colossal development in the utilization of wireless communications. This development was predominantly related to the cellular communication that began in the 1980s when wireless communication became accessible to the masses. Cellular communication began as analogue systems and developed as 2G (GSM, CDMA), 3G (GPRS, WCDMA), 4G (LTE), 5G (5GCAR, 5GPPP) and beyond with the fundamental objective to build throughput and capacity.

The advancements in digital electronics have made hardware gadgets more efficient with a lower price, accordingly making smart gadgets and wireless sensors an integrated part of our day by day life. Moreover, IEEE standards such as 802.11 and inclusion of modern technologies like machine-to-machine (M2M), wireless sensor networks (WSN), internet-of-things (IoT) together with cloud computing have presented a new paradigm that will empower future heterogeneous communication networks. Today, more wireless communication technologies are being improved that are changing our working propensities and have fundamentally impacted our regular day to day existences. The utilization of these new advances is spreading quickly in different fields of life, for example, social networking communication, health, environmental protection, financial matters, transportation and coordination and disaster administration and prevention.

One of the special concerns here is mobility-related applications where transport systems have become critical components of the modern world. They are gainful as far as fast transportation of merchandise and individuals, but they are connected to an expanding number of road accidents around the world. As indicated by the World Health Organization

(WHO), it is assessed that 1.2 million people die every year on the world's streets and half of those are vulnerable street users, i.e., 23% motorcyclists, 22% people on foot and 5% cyclists (World Health Organization, 2015). In the report, it is expressed that in 1990 road accidents were the ninth most common reason for disability/death around the world, and if no further moves are made to counter this then by 2020, road accidents are predicted to be the third common reason for disability/death around the world.

These days, more computerized systems and technologies are becoming a piece of our vehicles and a vehicle in future will be equipped with a wide range of technologies for navigation, location information, safety and inter-vehicle communication. It is foreseen that these systems and technologies can diminish the rate of accidents and additionally they can make the movement more efficacious.

Intelligent transportation system (ITS), (a system which depends on cooperative communication, specifically, among vehicles) can possibly improve on-street safety, driving comfort and traffic efficiency (ETSI 102 637-1, 2010). Following two fundamental paradigms empower cooperative communications in the associated vehicle area: First, vehicle-to-infrastructure (V2I) communications; and second, vehicle-to-vehicle (V2V) communications. However, the ITS system has various communication technologies and protocols which are considered as the base technologies in this system, such as IEEE 802.11p, WCDMA, LTE, etc. (Uzcategui et al, 2009). Moreover, 5G technologies that will enable cars and vehicles to be connected to the networks and also to be able to talk to each other ensuring ultra-high reliability and very low latency. Enabling such kind of connectivity will leverage disruptive new applications that will allow to improve driving efficiency and boost road safety (Fallgren *et al.*, 2018).

V2V communication is more suitable for safety-related applications. It enables vehicles to communicate directly with minimal latency. The essential target with the message swap is to enhance active on-road safety and situation awareness, e.g. collision avoidance, traffic re-routing, navigation, etc. The reliability of V2V safety applications relies upon the nature of the communication link (IEEE Std. 802.11p, 2010), which depends on the properties of the propagation channel. It is the channel that determines the performance of any communication system.

In this thesis, a measurement channel characterization and simulating of V2V channels are presented with the main goal as an understanding of the channels for optimized V2V system design. The measurement-based analysis is performed in three steps: Firstly, the collection of data with channel measurements. Secondly, channel characterization by analyzing metrics such as RSSI, PDR, Doppler spreads, and coherence time to understand key characteristics of propagation. Finally, simulating the channel such that the certain properties of the channel can be reproduced for system simulation and testing.

1.1. Research Scope and Objectives

The scope of this study is characterizing V2V channel to see the communications between cars within intersections with non-perpendicular angles. An outline of the research objectives is as listed below:

- Improve a dual measurement system, used by Clayton (2016) by using new 802.11p MIMO transceiver (LocoMate mini 2).
- Measure channel characteristics (PDR and power) at four non-perpendicular junctions (Y-junction and roundabouts) in Leicester city centre.
- Compare NLOS measurements to predictions from the model, virtualsource 11p.
- Determine the effect of vehicular traffic on signal strength and Doppler characteristics of the signal.
- Investigate the effect on the signal when a vehicle blocks the LOS.
- Investigate the effect on the signal of various different antenna locations.

1.2. Vehicular Communication Overview

Vehicular communication is the exchange of information between two vehicles (V2V communications) or between a vehicle and a fixed infrastructure (V2I communications).

In the V2V communications, Tx and Rx are moving at high speed and there are other objects that may be fixed such as buildings and traffic signals or moving such as cars, buses, and trucks etc. referred to as scatterers. In the V2I communications, one of the stations is in motion and the second is stationary with a high antenna.

Unlike the traditional system of cellular propagation which is stationary and the base station antenna is installed at a high altitude for long-range communications, both V2V and V2I are in motion and short-range communication with antennas mounted at a low altitude (Rubio, *et al.* 2012). The V2I radio channel can be compared with traditional cellular propagation channels only if the access point is installed at high altitude otherwise it will be similar to the V2V channel with only one station is moving. In addition, the vehicular communication channels are affected by obstruction or shadowing caused by the movement of objects.

In V2V communications, the rapid change in the propagation environment results from the rapid mobility of both the transmitter and the receiver. V2V channel parameters are highly variable in time and frequency. This means that the results of cellular channel research cannot be directly applied to vehicular channels and therefore there is a need to perform vehicular channel measurement campaigns in order to gain a deeper understanding of the characteristics of the vehicular propagation channel. The vehicular communications main concept is for all vehicles to exchange safety messages about vehicles positions and speed between them (V2V) and with road infrastructure (V2I). The messages that can be shared include cross-collision warnings, traffic state warnings, pre-crash sensors, wrong driving warnings, and route-changing aids (Mecklenbraüker *et al.*, 2011). This will allow vehicles to take appropriate measures to avoid collisions. Figure 1.1 illustrates the vehicular communication components (Abbas, 2014).

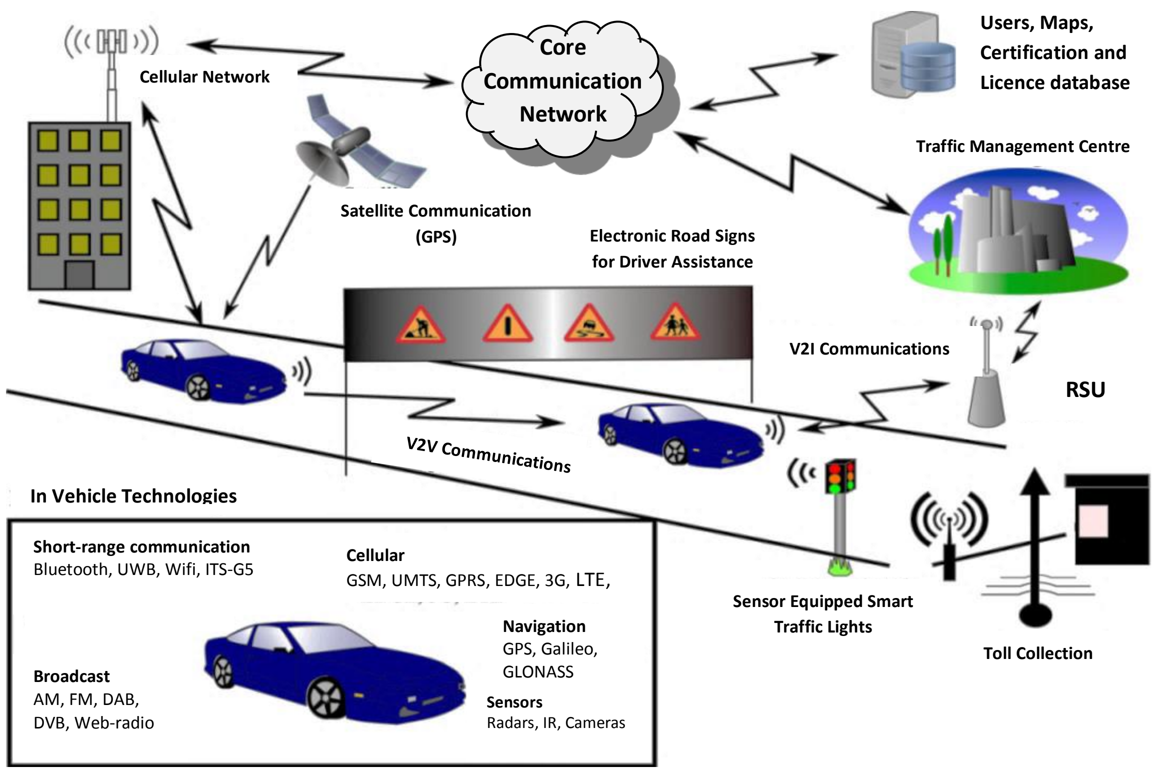

Figure 1.1 Components of vehicular communication (Abbas, 2014)

1.3. Vehicular Communication Characteristics:

There are some characteristics of Vehicular Communication (Vehicular Ad-hoc Networks (VANETs)) which are shared with other ad-hoc networks such as self-organization and decentralization of infrastructure, but it still differs from them due to the changes in the design of the communication system which are impacted by its unique challenges (Elumalai *et al.* 2013).

Some of the unique characteristics of VANET are as follows (Chouha *et al.* 2016).

- A high number of nodes: many vehicles with communication abilities are required to deal with a high number of nodes. In addition, it also deals with a roadside unit which makes VANET to deal with a larger number of nodes.
- The mobility of nodes: a VANET node moves with high mobility. In this case, when vehicles cross each other they have less time duration for an exchange of packets. Furthermore, the movement is limited by the environments and traffic rules.

- Changing of network topology: because of node mobility and random speed of vehicles, the network topology changes frequently.
- Reliable and timely delivery: VANET's application is mainly to avoid accidents and to save lives; it requires a highly realistic and reliable application for data delivery.
- No confidentiality: for safety applications, the main aim of VANET is to avoid accidents; hence there is no confidentiality in the messages.

1.4. Radio Technologies / Standardisation

Currently, IEEE 8021.11p DSRC also known as WAVE is the latest vehicle communication standard designed to make transport safer, more efficient and less harmful to the environment and to provide information and entertainment services (IEEE Std 802.11, 2016). Government radio management organizations have allocated specific bands for the deployment of ITS applications throughout the world. For instance, The Federal Communications Commission (FCC) allowed a 75 MHz band from 5.850-5.925 GHz for DSRC in the USA. Figure 1.2 shows the DSRC channel allocation in the 5.9 GHz band for ITS applications, where channel 178 as the control channel (CCH) which is used for safety communication applications, while other channels (SCHs) are set up for both safety and non-safety applications. Channels 172 and 184 are utilized for safety applications in V2V and V2I respectively (Campuzano *et al.*, 2012).

In recent time, the standardisation associations have designated frequency bands for ITS applications i.e. 5.850-5.925 GHz in North America, 5.875-5.905 GHz in Europe, and 715-725 MHz and 5.770-5.850 GHz in Japan. According to that, most of vehicular channel measurement campaigns managed over the last few years were performed at the 5 GHz frequency band (Paier *et al.* 2010), (Alexander *et al.* 2011). However, other bands can be used for vehicular non-safety ITS applications, such as measurement performed at 2.4 GHz band (Acosta *et al.* 2006) and (Acosta *et al.* 2007), and some measurements with 900 MHz, which is a dedicated band for electronic toll collection systems (Dudley, *et al.* 2007) and (Turkka *et al.* 2008).

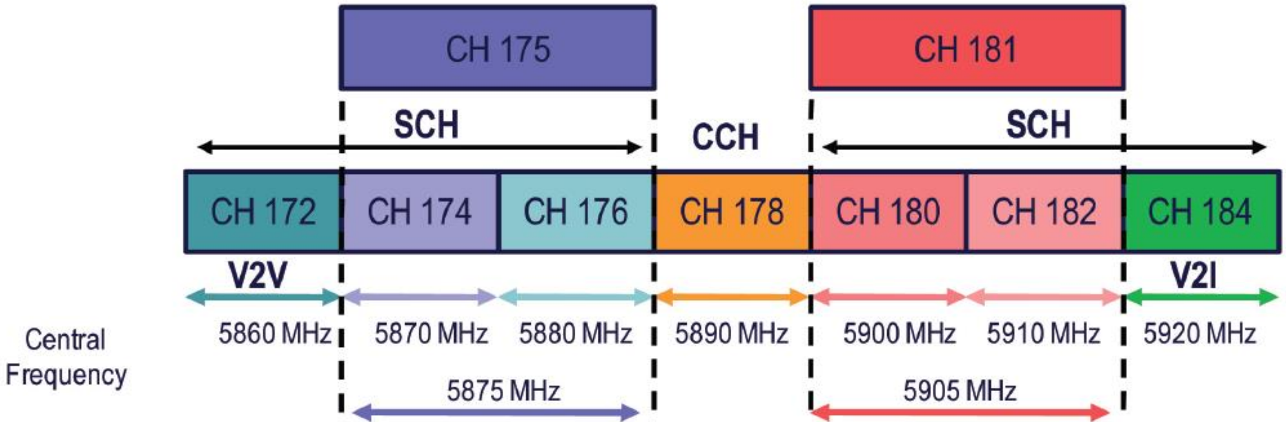

Figure 1.2 DSRC channel allocation in the 5.9 GHz band for ITS applications (Campuzano *et al.* 2012)

The IEEE 802.11p standard is based on orthogonal frequency division multiplexing (OFDM). This scheme transmits data in orthogonal and convergent sub-assemblies and thus can improve spectrum efficiency and deal with harsh channel conditions. Depending on different modulation schemes, it can support data transmission rates ranging from 3 - 27 Mbps (Luan *et al.* 2013). With modifications based on vehicle scenarios, IEEE 802.11p was derived from the famous IEEE 802.11a (WiFi) standard.

1.5. Vehicular Communication Applications

Vehicular communication applications are often categorized classified into three categories traffic safety applications, traffic efficiency applications, and infotainment applications. Figure (1.3) shows vehicular communication applications (Clayton 2016).

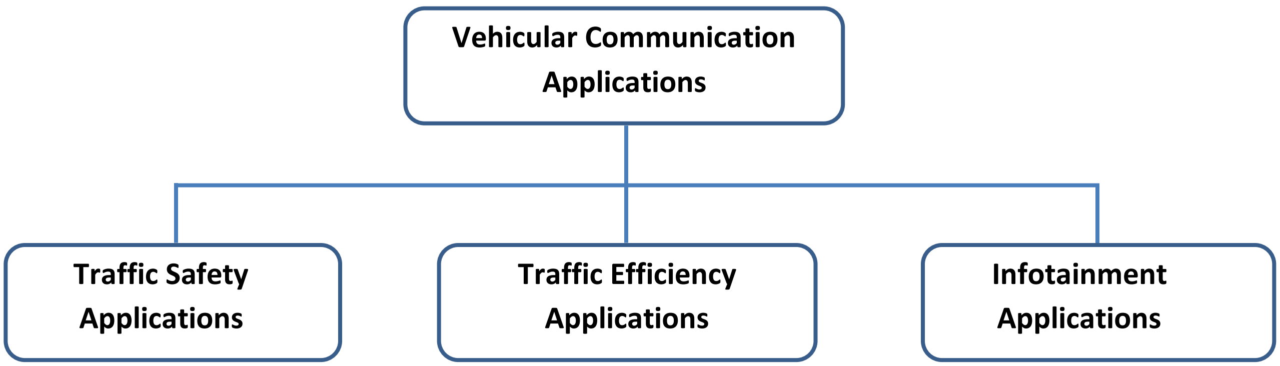

Figure 1.3 Vehicular Communication Applications after (Clayton, 2016)

1.5.1. Traffic Safety Applications

Traffic safety applications aim to further improve the safety of vehicular traffic and reducing the number of accidents and deaths on the roads. During the evolution of vehicles, the goal of reducing accidents on the road was to push aggressively to increase inventions. At present, vehicles are equipped with many systems and techniques that effectively improve traffic safety, such as seatbelts, airbags, and the energy-absorbing construction in the car that reduce the risk of injury when an accident occurs. Some modern cars are equipped with automatic braking systems that enable emergency brakes to reduce the impact of the collision.

Table 1.1 Overview of safety applications

No.	Safety Applications	Describe
1.	**Intersection Collision Avoidance**	1. Traffic Signal Violation Warning 2. Intersection Collision Warning 3. Blind Merge Warning
2.	**Public Safety**	1. Approaching Emergency Vehicle Warning
3.	**Sign Extension**	1. In-Vehicle Signage 2. Wrong-Way Driver Warning 3. Low Bridge Warning 4. Work Zone Warning
4.	**Information from Other Vehicles**	1. Cooperative Collision Warning 2. Vehicle-Based Road Condition Warning 3. Lane Change Warning 4. Blind Spot Warning 5. Highway Merge Assistant 6. Visibility Enhancer 7. Cooperative Adaptive Cruise Control 8. Road Condition Warning 9. V2V Road Feature Notification

Sharing data between vehicles can give additional input to the safety system. For example, sharing car position, speed, acceleration, and other information among all vehicles in the surrounding area leads to cooperative awareness and with conjunction with other available sensor data, serious traffic circumstances can be detected earlier. Another group of applications related to traffic safety is warnings with respect to different types of driving manoeuvres such as turning south/north. In these cases, the driver's warning message is supported in cases where it is not safe to continue manoeuvring. Table 1.1 illiterates an overview of safety application (Olariu 2009).

1.5.2. Traffic Efficiency Applications

The goal of traffic efficiency applications is to increase the efficiency of the traffic system in terms of fuel use, travel times or traffic flow. Existing systems often collect information necessary to increase traffic efficiency through fixed installations such as sensors or cameras. In-car traffic efficiency is supported, for example by navigation systems that offer driving directions to the driver (Olariu, 2009).

The main aim of these applications is to improve the vehicle traffic flow by assisting and coordinating the vehicles. This category can be further divided into two main categories: Speed Management Applications and Co-operative Navigation Applications. Currently, V2V communication systems can provide information covering the entire road network and can inform drivers instantly, individually, and everywhere - because the wireless communication system provides the necessary geographic coverage.

1.5.3. Infotainment Applications

These types of applications cannot be linked to safety applications. It also focuses on a variety of things such as informing passengers of weather, nearest fuel station, restaurants menus and a parking space in a specific car park. Furthermore, it provides to access internet services on the way.

More applications are improved navigation systems, for example, by providing up-to-date maps, traffic information, or GPS correction signals to improve the accuracy of vehicle localization. Another possible application is to improve service maintenance and software updates for the vehicle, either in the garage or even outside.

1.6. Wireless Channel Modelling

Electromagnetic waves propagate through environments where they cross free space or are reflected, scattered, and diffracted by terrain irregularities like walls, buildings, and other objects. As a result of propagation mechanisms, the receiving signal strength can be characterized by almost three independent phenomena of large-scale path loss, large-scale shadowing, and multipath loss. Small-scale fading and multipath propagation can also be described by the physics of these three basic propagation mechanisms (Hie, 2004). These phenomena's are shown in Figure 1.4 (Chisb, *et al.* 2014).

1.6.1. Reflection:

Reflections occur when the dimension of the surface is larger than the wavelength of the incident wave (Azimi, *et al.* 2011). The radio wave can be reflected in any type of obstacles such as mountains, buildings, vehicles. More reflections occur in an urban environment compared to rural areas because the number of reflectors is higher in a dense urban area.

1.6.2. Diffraction:

Diffraction occurs when the radio path between the transmitter and the receiver is obstructed by a surface that has irregularities (Azimi, *et al.* 2011). This leads to curvature of the waves around the obstacle, making it possible to receive the signal even when there is no LOS path between transmitter and receiver.

1.6.3. Scattering:

When the medium through which the wave travels is composed of a large number of objects whose dimensions are small compared to the wavelength, the Scattering occurs (Hie, 2004). Scattered waves are produced by rough surfaces, small objects, or other irregularities in the channel. In practice, foliage, street signs, and lamps lead to scattering in the mobile communications system.

Due to the complexity and time-varying nature of the wireless channel, it becomes hard to obtain an accurate deterministic channel model and researchers resort to statistical channel models, which play a key role in the design of wireless communication system. An understanding of the propagation channel is the key to efficient wireless system design. The purpose of channel modelling is to estimate the first and the higher-order statistical parameters of the fading channel and measure the performance of a transmission system. These parameters include Doppler spread, the time statistics of fading and amplitude probability densities functions.

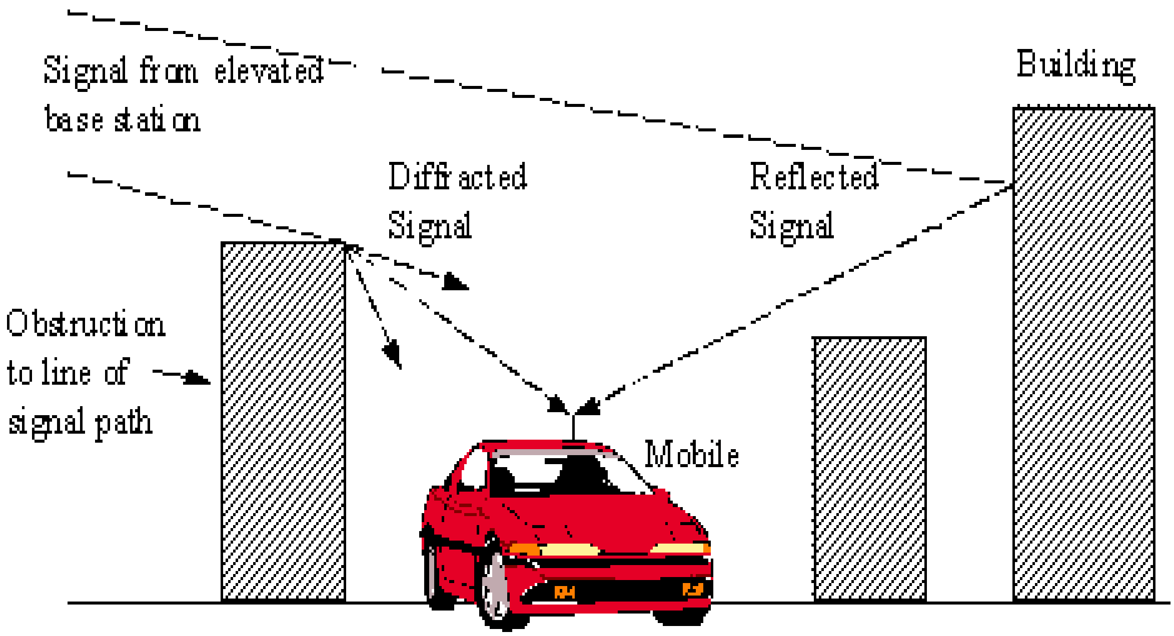

Figure 1.4 Electromagnetic waves propagation (Chisb *et al.* 2014)errfddcc

1.7. Vehicular Channel Modelling

Measurements are being taken to characterize V2V channels along with their modelling. In these models, the transmitter and receiver communicate together without using a base station (BS). The antennas are mounted on the top or inside the vehicles and the speed of vehicles and their directions may be different thereby generating a time-varying channel with the presence of Doppler spread. The obstacles such as buildings and other vehicles around act as scatterers hence generating multipath channel. Depending on obstacles locations the line of sight (LOS) may or may not be present. The transmitter and receiver communicating with each other are normally at the same height but surrounded by a separate set of scatterers. This scenario differs from the base to mobile communication where the BS is usually free of scatterers. Figure 1.5 presents typical V2V communications scenarios (Mecklenbraüker *et al.*, 2011).

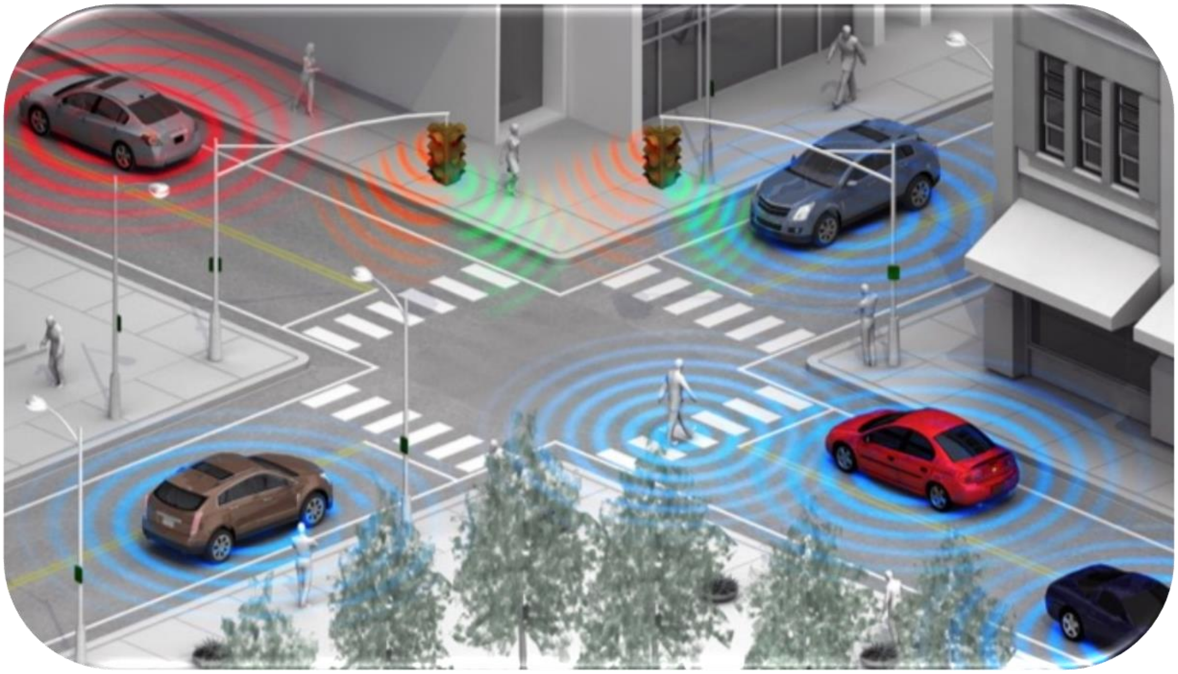

Figure 1.5 V2V communications scenario (Mecklenbraüker *et al.* 2011)

1.8. Channel Modeling Classification

Channel models can be classified according to their most important characteristics into propagation scale, modelling approach, communication type, antenna and environment. Figure 1.6 shows this classification.

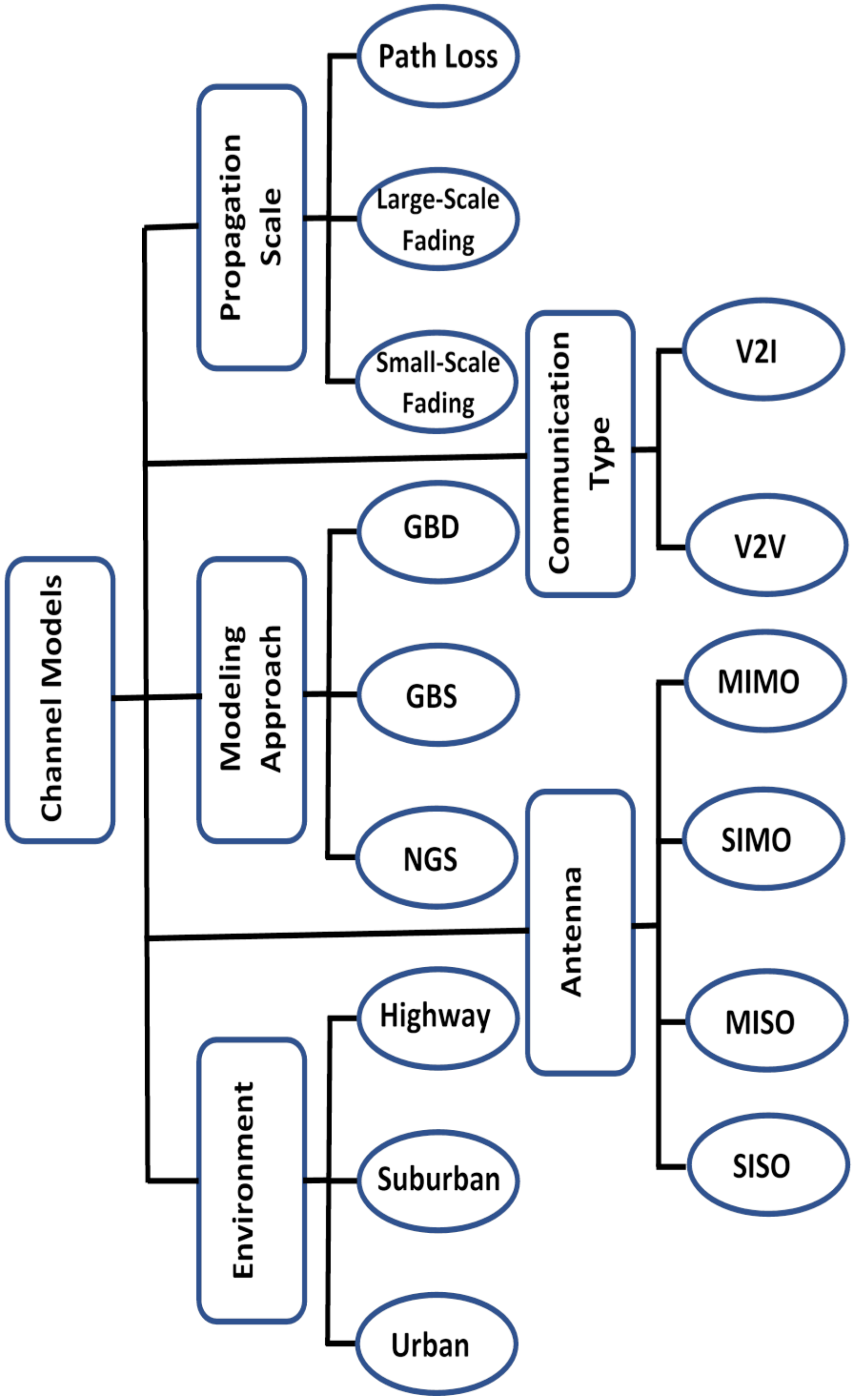

Figure 1.6 Channel model classifications

1.8.1. Path loss, Large-Scale Fading, and Small-Scale Fading

The propagation of electromagnetic waves in complex environments can be understood as an overlap of multipath components (Paier, 2010), where the signal of each path may be reflected or scattered, or diffracted between transmitter and receiver. The most significant parameter characterizing the propagation of the signal is channel loss because it defines the receiving power. In general, the propagation models are typically divided by their scale into:

- Path loss.
- Large-scale fading.
- Small-scale fading.

The path loss is a characterization of the variation of the channel gain over distance. It is a measure of the average RF attenuation signal from the transmitter to the receiver (Paschalidis, *et al.* 2011). One simple model is the free space path loss, also known as Friis' law.

$$\boldsymbol{P_{R_X}\,(d) = P_{T_X} G_{T_X} G_{R_X} \left(\frac{\lambda}{4\pi d}\right)^2} \quad \dots\dots\dots\dots\dots \mathbf{1.1}$$

Where d is the distance between T_x and R_x, λ the wavelength, G_{Tx} and G_{Rx} the antenna gains of the T_x and R_x, and P_{Tx} and P_{Rx} the transmitted power and the received power, respectively. The decreasing of channel gain is defined with increasing distance for the transmitter antenna and receiver antenna in free space, i.e., there are no objects blocking with the wave propagation. Further, more developed, deterministic equations also include propagation mechanisms, reflection, scattering, and diffraction.

The large-scale fading describes the variation of the channel gain over a larger scale, typically a few hundred wavelengths. It is the large difference in the average receiving power by the receiver when measured at different locations despite having the same separation distance (Rowe, *et al.* 2016). The reason this phenomenon is shadowing by large objects such as hills, forests, clumps of buildings, etc., between the transmitter and the receiver.

The small-scale fading describes the channel gain fluctuations on a very short distance, or time comparable with one wavelength. The received signal usually consists of multiple waves which are copies of the same transmitted wave but arrive at the receiver at different times and different amplitudes and phases. These multipath waves create the small-scale fading effects which cause the rapid fluctuation of the received signal over a short period of time or distance (Rowe, *et al.* 2016).

Fading occurs in urban areas because the height of the surrounding structures is much larger the height of the mobile antennas so there may not be a single LOS path to the transmitter. Even when a LOS exists, multipath still occurs due to the reflections from the ground and the surrounding structures. Multiple reflections thus produce many paths between the transmitter and the receiver. Figure 1.7 shows the concept of multipath.

The main feature of multipath propagation is that it allows communication even when the transmitter and the receiver are not in LOS conditions. Multipath propagation of radio waves allows for the effective overcoming of obstacles (e.g. mountains, buildings, tunnels, underground parking, etc.) by circumventing them and helping to ensure almost continuous radio coverage. However, multipath propagation also causes many signal-weakness cases. The three main reasons are the delay in propagation and interference between the paths coming from the transmitter, leading to rapid fluctuations in the signal and the formation of random frequency due to Doppler displacement on different paths (Hie, 2004).

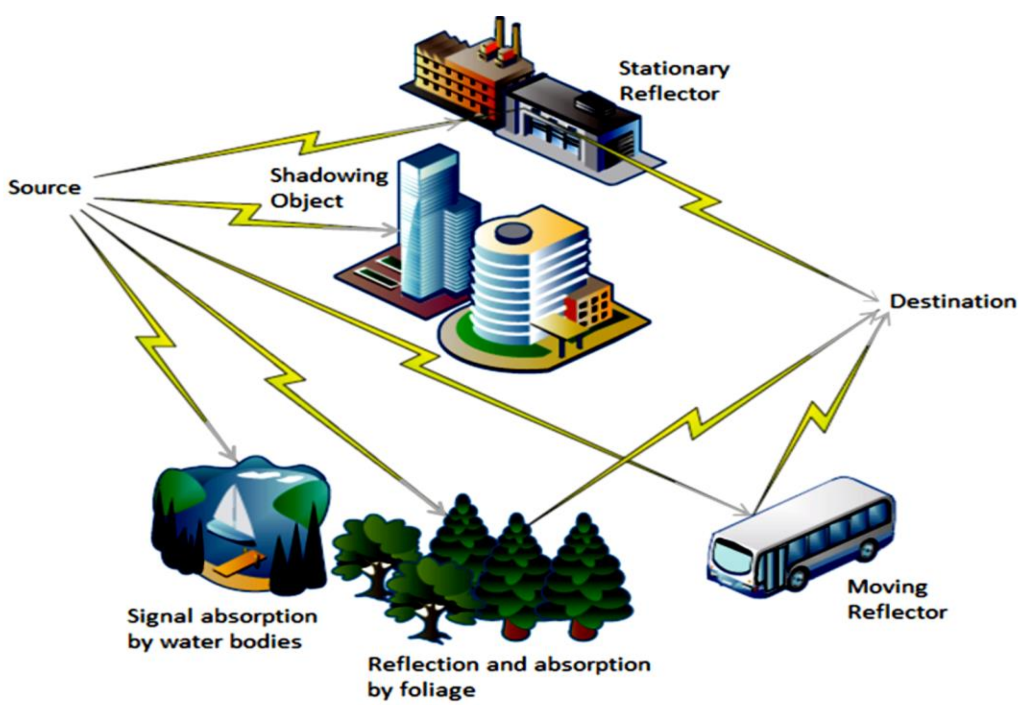

Figure 1.7 The Multipath Concept (Hie, 2004).

1.8.2. Modelling Approach

Channel characterization is used to identify and understand the characteristics of the channel, which is defined when determining the characteristics of the channel in such a way that the channel effects (in a statistical way) of network simulation and system testing can be reprogrammed by channel modelling. There are many ways to model the channel, and the selection depends on the type of channel in question, for example, time-invariant or time-varying, narrowband or wideband, SISO or MIMO, deterministic or stochastic.

Almers, *et al.* (2007) present a generalized classification of channel models based on system assumptions and desired level of complexity. In the following, the modelling approaches are classifying them as deterministic and stochastic approaches.

- **Geometry-based deterministic (GBD) models:** In this approach, the main objective is to reproduce the channel impulse response when the location of the TX and RX with the location, shape, dielectric and conductive properties of all the objects in the surrounding area known (Molisch, 2005). Deterministic models can provide an accurate and effective channel interpretation for a specific location and environment only if a precise description of the environment is available. There are several deterministic modelling methods such as the finite-difference-time-domain method (FDTD) (Schneider, 2017), and so-called ray tracing (RT) (Wiesbeck, et al 2007). The first method is useful when studying near-field problems as they are constrained to structures with limited dimensions. However, the second one, RT is the most widely used deterministic approach, as it gives more appropriate models for far-field propagation environments such as urban areas.
- **Geometry-based stochastic (GBS) models:** In this approach, the statistics of the channel parameters, e.g., received power statistics at a certain delay. Usually, a Cumulative Distribution Function (CDF) of parameters such as path loss, delay and Doppler spread, and fading is used for that purpose. Both location and properties of scatterers are described stochastically according to some probability distributions, and then a simplified ray tracing is performed to model the interaction of propagation waves with the scatterers, which are then combined at the receiver GBS which is also

of main interest in this thesis is capable of describing the time-evolution of the channel by the motion of the TX, RX as well as the scatterers, which makes them useful for non-stationary channels such as vehicular channels (Karedal *et al.* 2009). The simple GBS model used in V2V channel model is the two-ring model (Yuan *et al.* 2015).

- **Non-geometrical stochastic (NGS) models**: generate channel statistics in a completely stochastic fashion, where both the geometrical properties and the channel statistics are generated stochastically. Examples of NGS models used for V2V channel modelling include a tapped-delay-line model.

1.8.3. Antenna

Channel models can be supported by different antennas. There are four types of antennas. Two of these types were used in our developed system. The following is described of these types of antennas:

- **SISO (Single Input Single Output):** in this type of antenna, there is only one transmitting antenna at the transmitter and one receiving antenna at the receiver. It is simplest to implement and easiest to design amongst all the four types of antennas available (Shah, 2017). Figure 1.8 illustrates a block diagram of the SISO system.

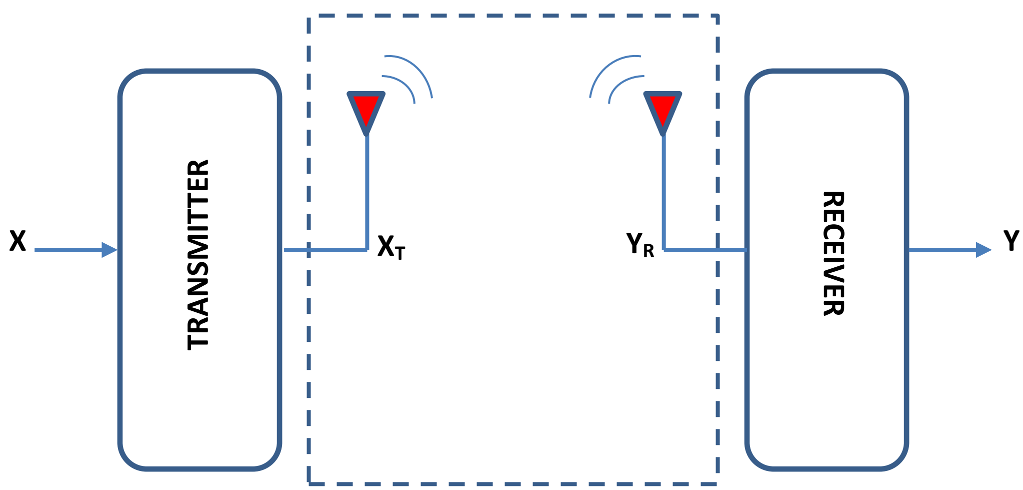

Figure 1.7 Single Input Single Output (SISO) system (Shah, 2017).

In the above diagram, X: input, Y: output, X_T: Transmitting antenna, Y_R: Receiving antenna.

The noise is inserted in the system when the signal is processing from XT to YR. The channel capacity of the SISO system is given as:

$$C_{(SISO)} = B \log_2\left(1 + \frac{S}{N}\right) \ldots\ldots\ldots\ldots\ldots 1.2$$

Where C is the capacity, B is Bandwidth of the signal and S/N is the signal to noise ratio (Nimay *et al.*, 2014).

The advantage of the SISO system is very simple in design and cheap compared with the other types of systems. the applications of this system in Wi-Fi, TV, radio Broadcasting, etc. (Sengar *et al.*, 2014).

This type of antenna is used in the continuous wave part of the system.

- **MIMO (Multiple Input Multiple Output):** MIMO technology has attracted attention in wireless communications. It has obtained the best throughput and efficiency of transmission signals. Because of these properties, MIMO is an important part of modern wireless communication standards as IEEE 802.11n (Wifi), 3GPP, LTE, WiMAX and 5G.

  In MIMO, there are multiple transmitting antennas from which the signal can be transmitted, and also there are multiple receiving antennas which the signal can be received. Figure 1.9 is the block diagram of a MIMO system with N transmitting antennas and M receiving antennas.

  In this type of antenna, multiple channels are available, therefore the MMO channel can be represented as an N × M:

$$\begin{bmatrix} h_{11} & h_{12} \ldots\ldots & h_{1N} \\ h_{21} & h_{22} \ldots\ldots & h_{2N} \\ & & \vdots \\ h_{M1} & h_{M2} \ldots\ldots & h_{MN} \end{bmatrix}$$

  Where h11, h12, etc. are the variables of fading gain between the transmitting and receiving antenna.

The capacity of the MIMO system is given as:

$$C_{(SISO)} = NMB \log_2 \left(1 + \frac{S}{N}\right) \ldots \ldots \ldots \ldots \ldots 1.3$$

Where C is the capacity of the MIMO system, N is the number of transmitting antennas, M is the number of receiving antennas and S/N is the signal to noise ratio (Nimay *et al.*, 2014).

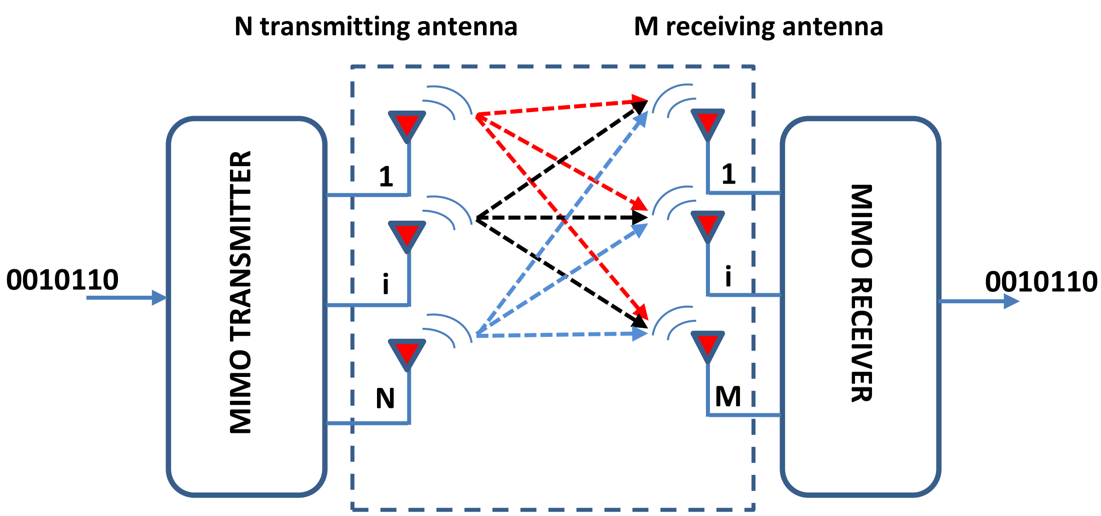

Figure 1.9 Multiple Input Multiple Output (MIMO) system (Shah, 2017)

The advantage of MIMO is that give the best results when compared to the other types because it offers significant increases in data throughput and link range without additional bandwidth or transmits power. It achieves this by higher spectral efficiency (more bits per second per hertz of bandwidth) and link reliability or diversity (reduced fading). Using multiple antennas on both ends of the transmission and receiver.
This type of antenna is used in the network performance part of the system.

1.8.4. Communication Type

Communication links are usually classified into two groups: links between vehicles and links between a vehicle and base station (i.e., infrastructure). Accordingly, communication links can be classified according to three conditions (Abbas *et al.*, 2011):

- The line of sight (LOS) is that the zone is free of obstructions, there is a line of sight between Tx and Rx
- Non-LOS due to static objects (NLOSb) is that the line of sight between Tx and Rx is obstructed by a large object, e.g., a building which completely blocks the LOS.
- Non-LOS due to vehicles (NLOSv) is that the LOS between Tx and Rx is obstructed by another object such as vehicles.

1.8.5. Environment

Vehicular channel models can be classified into the following categories based on roadside environments and traffic characteristics (Molisch *et al.*, 2009). Figure (1.10 shows different V2V Communication Scenarios.

- **Open space and highway environment** are characterized by high-speed motion of vehicles. The roadside environment contains mostly vegetation with a few houses and street signs which are usually located far from the road.
- **The suburban environment** is a mixture of low-rise buildings and open spaces such as park areas and parking lots. These roadside objects are usually set further back from the sidewalk as compared to the urban environment. Low to medium vehicle density and few pedestrians and bicyclists are assumed in this scenario.
- **The urban environment** is a scenario with high traffic densities and a higher density of pedestrians and cyclists. In this environment, objects such as buildings, houses, and street signs are densely scattered along the side of the road and tend to be located very close to the streets.

Motorway vehicular environment.

Suburban vehicular environment.

Urban vehicular environment.

Figure 1.8 V2V Communication Scenarios

1.9. Channel Metrics:

The wireless channel may be varied over different locations and time; several metrics are used to model the behaviour of the channel at a given time and place. In the following important metrics will be mentioned to describe the channel behaviour.

1.9.1. Doppler Spread and Coherence Time

The Doppler spread and coherence time is the parameters that describe the changing nature of the channel over time in a small-scale area. Doppler spread is a measure of the spectral expansion caused by the time rate of change of the mobile channel. It shows how the signal transmitted signal spreads in frequency due to the movement of TX, RX and scatterers (reflectors such as buildings and vehicles). The amount of spectral expansion depends on Doppler frequency shift, which is a function of the relative speed of the mobile and the angle between the direction of mobile traffic and the direction of the scattered waves. The Doppler shift, f_d is the frequency offset experienced by each multipath wave, due to the relative motion between TX and RX. It is directly proportional to the velocity and the direction of motion of the mobile with respect to the direction of arrival of the received multi-path wave. Doppler transformation can be expressed as (Rappaport 2002);

$$f_d = \frac{v\cos(\boldsymbol{\theta})}{\lambda} = \frac{v f_c \cos(\boldsymbol{\theta})}{c} \ldots\ldots\ldots\ldots\ldots 1.4$$

Where v is the speed of the mobile, λ is the wavelength of the radio signal, c is the speed of light 3 x 108 m/s and fc is the carrier frequency of the radio signal θ is the angle of arrival of the signal relative to the velocity vector as illustrated in Figure (1.11).

The coherence time, Tc, of the channel represents a statistical measure of the time period during which the channel impulse response is essentially constant (fixed or highly interconnected) and determines the similarity of the channel response at different times. In other words, the coherence time is the duration over which two received signals have a strong potential for amplitude correlation. If the reciprocal bandwidth of the baseband signal is greater than the coherence time of the channel, then the channel will change during the transmission of the baseband message, thus causing distortion at the receiver.

$$T_C = \frac{1}{f_d} \dots \dots \dots \dots .1.5$$

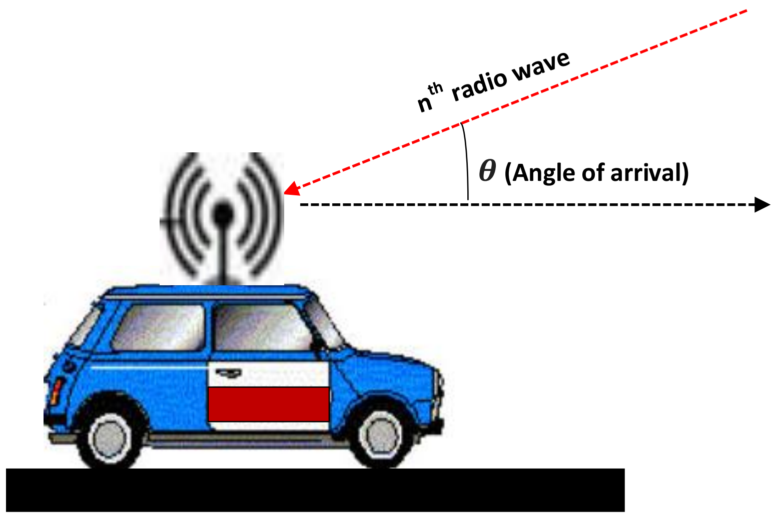

Figure 1.9 Doppler Scenario

1.9.2. Delay Spread and Coherence Bandwidth

Delay Spread and the Coherence Bandwidth are the parameters which describe the frequency selective nature of the wireless channel (multipath delay spread). They provide information about the time-varying nature of the channel due to the multipath environment. However, they do not provide information about the channel's time-variation due to the relative motion between Tx and Rx and the mobile scattering in the channel. Delay spread is a means of measuring the multipath effect of a channel, which is the difference between the time of arrival of the first multipath component and the last multipath component to indicate the destination. Describes how the signal transmitted at the north time is spread by echoes. In V2V communications, the multipath delays vary with time, so the delay spread becomes a random variable. The root means square (RMS) delay spread is the most common characterization of delay spread.

The coherent bandwidth, Bc of the channel is the frequency (or bandwidth) separation in which it is assumed that the channel has the same transfer function (or flat fading channel). The coherence bandwidth of a channel is a statistical measure of the range of frequencies over a channel. It is inversely proportional to the delay spread and significant parameter in the design of many wireless systems. Figure 1.12 illustrates the signals have different delays with different times when they arrive at the receiver.

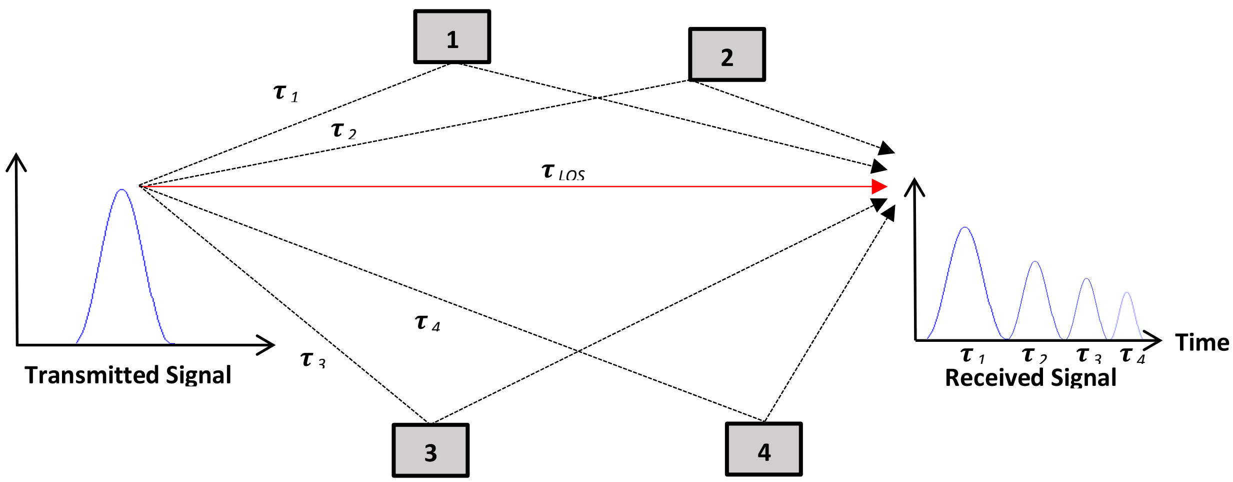

Figure 1.10 Multipath Delay Spread

1.9.3. Received Signal Strength Indicator (RSSI):

In telecommunications, received signal strength indicator (RSSI) is a measurement of the power present in a received radio signal (IEEE Std. 802.11p-2010, 2010). RSSI is usually invisible to a user of a receiving device. However, because signal strength can vary greatly and affect functionality in wireless networking, IEEE 802.11 devices often make the measurement available to users. In an IEEE 802.11 system, RSSI is the relative received signal strength in a wireless environment. RSSI is an indication of the power level being received by the received radio after the antenna and possible cable loss. Therefore, the higher the RSSI number, the stronger the signal. Thus, when an RSSI value is represented in a negative form (e.g. −100), the closer the value is to 0, the stronger the received signal has been.

1.9.4. Packet delivery ratio (PDR):

Packet delivery ratio (PDR) is the ratio of a number of packets received at the destination to the number of packets generated at the source. A network should work to attain high PDR in order to have a better performance. PDR shows the amount of reliability offered by the network (Jain, *et al.* 2014).

$$\boldsymbol{PDR = \frac{Number\ of\ packets\ received\ successfully}{Number\ of\ packets\ sent}} \ldots\ldots\ldots\ldots \mathbf{1.6}$$

1.10. Challenges Faced by Vehicular Communication Networks

The VANET is the largest dedicated wireless network operating in highly dynamic environments that are unforgiving towards radio communication. It is used for critical life-saving purposes, a lot of research and testing is required both, technically and sociologically.

Some of the key technical issues are listed below:

- Packet collisions are more frequent because there is no centralized transmission management system, resulting in low efficiency and network traffic bursts (Hartenstein *et al.* 2010).
- The presence of many reflective objects gives the opportunity to various signals in terms of amplitude and frequency, and the mobility of the environment increases fading. VANETs must be highly robust to deliver low latency communications and deal with the radio fading, Doppler shifts and spreads which will impact upon communications; especially in Non-Line-of-Sight (NLOS) conditions where communication performance drops rapidly (Hartenstein et al. 2010).
- VANET security is of major concern. Trusting information packets requires increased security which reduces the privacy of the sender (Puñal *et al.*, 2012).
- Vehicular communication networks have the ability to provide warnings to drivers in 76% of multiple vehicle accidents but only if vehicle networks are deployed on a wide scale (United States Government Accountability Office, 2013).

- Maintaining a decentralized self-organization network where the nodes are moving at high speeds is difficult. Especially for optimization algorithms aimed at improving channel utilization and communication variability when it comes to re-routing packets (Hartenstein *et al.* 2010).
- Other equipment that shares the DSRC should not reduce the reliability of safety-critical communications (United States Government Accountability Office 2013).

Some of the main socio-economic issues are:

- Cost: The costs of security systems and timelines for development make it difficult to estimate costs (United States Government Accountability Office 2013).
- Drivers will have to respond appropriately in a timely style if vehicular communications are to be efficiently utilized (United States Government Accountability Office 2013).

Chapter 2: Literature Review

This Chapter provides a summary of the state of the art, conducted to evaluate V2V channel characterization and modelling, including analytical as well as measurement-based research on V2V channels. Different propagation environments and their impact on propagation are discussed.

2.1. V2V Channel Measurements

Channel modelling is based on real-world measurements of the channel. The measurements are done to realize the character of the channel, extract model parameters and validate existing channel models. Design and implementation of measurement campaigns should be implemented in a style such that all the major features can be obtained. This assignment is complicated because each measurement is limited by scenarios, measuring tools and measurement conditions (Molisch *et al.*, 2009).

A number of real-life channel measurement campaigns have been carried out for vehicular communication systems, in many different propagation environments and with different measurements setup. The measurement equipment utilized for vehicular channel measurements is substantially comparable to that used for cellular channels. However, V2V measurements are more complex. For example, in vehicle-to-vehicle channels both the transmitter and the receiver are mobile.

In this section, V2V measurement campaigns were classified into three categories (carrier frequency and bandwidth measurement, antenna configuration and scenarios).

2.1.1. Bandwidth Measurement and Carrier Frequency

Several of the V2V channel measurements were implemented at the 900MHz band such as (Davis 1994) and (Turkka 2008). This band is a dedicated band for electronic toll collection systems, targeting an M2M communication system. in 1999, The Federal Communication Commission (FCC) in the United States recognised the importance of dedicated short-range communication (DSRC) in vehicular environments and assigned a 75MHz frequency band at 5.9GHz (Kenney, 2011). For this reason, Alexander *et al.* (2011), Paier *et al.* (2010), Meireles *et al.* (2010), Paschalidis *et al.* (2011), Mangel *et al.* (2011), Sommer *et al.* (2011), Segata *et al.* (2013) and Fernández *et al.* (2013) conducted most of the V2V measurement campaigns in the 5 MHz bandwidth. Cheng *et al.* (2007) used channels sounding equipment at 5.9 GHz while other authors used channel sounder at 5.6GHz which would deliver similar results at 5.9 GHz but some data would be inaccurate such as (Abbas *et al.* 2013) and (Paier *et al.* 2010).

Vega *et al.* (2019) conducted a measurement campaign to obtain empirical information about the spectral characteristics of vehicle-to-vehicle (V2V) and vehicle-to-infrastructure (V2I) multipath radio channels in the 700 MHz band. The collected data were processed to compute the average Doppler shift and the Doppler spread of the measured channels. The obtained results showed that the spectral properties of frequency-dispersive vehicular radio channels can be effectively analysed using narrowband sounding principles.

In addition, some of the researchers such as Acosta *et al.* (2006), Wang *et al.* (2013) made measurements on the V2V measurement campaigns the 2.4 GHz band. They calculated that the 5.9 GHz provide faster data rate at a short distance. While 2.4 GHz offers coverage for farther distance but may perform at slower speeds.

Park *et al.* (2018) presented millimetre wave Doppler measurements for V2I communications. The measurement campaigns were conducted at 28 GHz in a test expressway located parallel to an actual interstate expressway in Korea. Based on the measurement results, it observed high Doppler shifts caused by not only static objects including terrain and structures but also moving other vehicles in an expressway.

Paier *et al.* (2009, 2010), Renaudin *et al.* (2008), and Paschalidis *et al.* (2008) characterized channel conditions using a wideband channel sounder which is often suitable for measuring select channels, such as V2V channels. However, some measurements were performed using narrowband systems such as Cheng *et al.* (2007) and Clayton (2016) where a sine wave generator was used with a spectrum analyser.

2.1.2. Antenna Configuration

Each of the measurement campaigns mentioned in the previous section is different from any other measurement campaign performed even at the same frequency band. The main differences are the types of vehicles used for the TX and the RX, environment and the antenna configuration.

Numerous measurements have been used with the same type of antenna configurations: a roof-mounted SISO antenna configuration such as Vlastaras, *et al.* (2014), Boban *et al.* (2011) and Convoys (2016) or MIMO roof-mounted antenna as in Abbas *et al.* (2015), Onubogu (2016) and Paier *et al.* (2009, 2010). However, there are a few exceptions. Abbas *et al.* (2013) added a number of antennas in a bumper, windscreen, and mirrors of the transmitter and receiver car In addition to the roof-mounted antenna. The results of this added was a good solution for obtaining the best reception in most of the propagation environment, as well as keep line-of-sight between sides and not suffer from shadowing problem. Kaul *et al.* (2007) and Mangel *et al.* (2011) tested five and three different roof positions, respectively.

Kaul *et al.* (2007) and Mecklenbraüker *et al.* (2011) have discovered that the antenna placements are important because it combines with the surface to make a unique radiation pattern for each style of vehicle. The antennas have a significant influence on the channel characterization such as delay spread and the selection of a suitable antenna (e. g., using an array and beam steering) that can reduce the delay spread and found that the packet error rate is quite sensitive to the exact antenna position. Moreover, Park *et al.* (2018) investigated the effect of the antenna positions on a vehicle based on measurements in a typical V2V scenario at 28 GHz. The measurements were conducted at various TX and RX positions, and PL characteristics were analysed. It can be seen that PL varies depending on the distance between TX and RX. Based on the measurement, they investigated path loss characteristics for various transmitter and receiver positions. This work can be useful to answer how to deploy mmWave antennas on a vehicle.

Mecklenbraüker *et al.* (2011) discuss the possibility of enhancing communication using multiple antenna systems for spatial diversity and beam formation. However, improvements in channel estimation by the receiver will also enhance communications along with the development of roadside equipment at the highest possible level. The researchers noted that the immediate environment will affect the radiation pattern, which will significantly affect the performance of the network.

Mao *et al.* (2018) proposed a dual-band full-duplex antenna/array for intelligent transport systems applications. The antenna is highly isolated and designed to operate at different frequency bands simultaneously. Such a property could support the full-duplex operation-mode, which significantly simplifies the complexity of the RF front-end subsystem. The other contribution of this work is that multiple functions such as filtering, duplexing, and radiation are combined into one single device, resulting in a simplified RF frontend. This co-design multifunctional device could also remove the separate filters, duplexers, and interfaces between them, resulting in the reduction of the size, weight, and cost. All the measurements agree well with the simulations, showing two full-duplex channels of 4.58–4.83 GHz and 5.86–6.2 GHz for transmitting and receiving, respectively. The proposed antennas also exhibit excellent performance in terms of channel isolations, frequency selectivity, out-of-band rejections, and gains.

Maier *et al.* (2012) have used multiple system antennas (SIMO) and found that the integration of this type with the system provided a clear improvement of the system due to the additional complexity compared to using a single antenna.

In this thesis, Hyperlink wireless band 4.9-5.9 GHz 6 dBi omnidirectional antenna model HVG-4958-06U is used in the CW part for transmitter and receiver to improve reception and transmission in certain types of terrain as well as have been used (MIMO) patch antennas with low profile, which can be mounted a flat surface, in the network system.

2.1.3. Physical Environment and Scenarios

The characteristics of a V2V channel vary widely in different propagation environments. The propagation environment varies widely from one location to another and from country to country, but in order to characterize V2V channels, a fairly basic generalization of the propagation environments is required. Depending on cellular channels scenarios, V2V channel environments can be classified into urban, suburban, highway and rural scenarios. This scenario classification has been taken in a number of measurements as in Cheng *et al.* (2007), Kaul *et al.* (2007) and Paschalidis *et al.* (2008). Later, it was necessary to find more suitable scenarios for V2V communications. In Paier *et al.* (2009), Sen (2008), Renaudin *et al.* (2008) and Paschalidis *et al.* (2008) the old scenarios were modified by introducing new measurement scenarios to analyze the effects of traffic density and traffic flows.

Currently, the automotive industry with the ETSI ITS standardisation organization in Europe and US-DOT in the USA have identified a core set of ITS applications which has motivated research groups to use more accurate definitions of measurement scenarios related to applications of intelligent transport systems, especially for critical safety scenarios. Paier *et al.* (2010), Meireles *et al.* (2010), Paschalidis *et al.* (2011), Mangel *et al.* (2011), Sommer *et al.* (2011), Segata *et al.* (2013), Abbas *et al.* (2013) and Borhani *et al.* (2013) considered the V2V communication in situations such LOS and NLOS by buildings and other vehicles. They calculated that the radio channel is highly influenced by the rich scattering environments.

Urban environments are characterized by multipath effects and delays associated with a low range due to NLOS conditions. Some authors such as Bai *et al.* (2010), Paier *et al.* (2010), Sepulcre (2012) and Sommer *et al.* (2011) have gathered data in urban and suburban environments.

The intersection is a special case in urban and suburban environments. The propagation conditions in this environment differ from the linear road communication environment and it presents an interesting mixture where NLOS conditions change to LOS conditions increasing the data traffic to vehicle towards the centre of the intersection. At the intersection, buildings will be probably located at the corners where they limit LOS propagation conditions. Buildings act as obstacles to the radio signal, but reception behind these buildings may be possible through reflected and diffracted signal components. However, radio waves lose energy during both diffraction and reflection, and the amount of energy lost depends on the signal frequency and the angle of arrival, as well as the material, structure and shape of the surface (Mangel 2012). Abbas *et al.* (2013), Mangel *et al.* (2011), Schumacher *et al.* (2012), Karedal *et al.* (2010) and Hafner *et al.* (2011) have collected data from urban and suburban intersections areas.

In a highway environment, the expected Doppler spread is large as well as increased coverage in comparison to urban and suburban environments. Kaul *et al.* (2007), Bai *et al.* (2010), Alexander *et al.* (2011), Sepulcre *et al.* (2012) and Paier *et al.* (2010) also gathered the data in highway environments. have experimented a shadowing model in a rural area by gathering data from these environments.

2.2. Vehicular Channel Characterization and Modelling

Numerous researches have been done to characterize and model V2V propagation channels. These channels are highly dynamic and this is one of the main aspects that complicate their characterization and also pose a challenge when it comes to modelling. A number of researches have been published in the past few years in wireless channels in general and in vehicle-to-vehicle channels in particular such as Bernad, (2012) and Bernadó, *et al.* (2013).

A wireless link can be classified into the following three categories:

- Line-of-sight (LOS) is the situation when there is line-of-sight between the TX and the RX. Typically it is free of obstructions.
- Non-LOS_V ($NLOS_V$) is the situation when the LOS between the TX and RX is temporarily obstructed partially by another moving object. Especially blocking by other vehicles.
- Non-LOS_b ($NLOS_b$) is the situation when a larger object, e.g., a building between the TX and RX, completely block the LOS.

In each of these cases, the signal propagation is significantly different from each other as shown in Figure 2.1. The differences are more clearly seen in V2V communications at 5.9 GHz than in cellular frequencies because of important losses when passing through buildings and at diffraction around the edges of buildings.

The use of the channel sounder gives different information about the properties of the channels, such as the power variation, Doppler spread and delay spread. The channel sounder system has a higher resolution and provides a channel snapshot at all times when the receiver is switched on instead of receiving RSSI from the receiver (DSRC) only when the receiver is successful to receive data and decoding of a packet. When the data loss occurs during data collection using transceivers (DSRC), the collected data represents channel characteristics only when the packets are successfully received and deciphered. If the PDR is low, this means that one cannot estimate the channel characteristics for a significant proportion of the time. This limits accurate observations of the debilitating factors of V2X networks when the channel characteristics such as received power, delay spread and Doppler shifts and spreads are disadvantageous and create bias in the data as observed by (Cheng *et al.* 2007).

Yusuf *et al.* (2019) presented measurements of the experimental radio channel sounding campaign performed in an arched road tunnel in Le Havre, France. The co-polar and cross-polar channels measurements were carried out in the closed side lane, while the lane along the centre of the tunnel was open to traffic. They investigated the channel characteristics in terms of path loss, fading distribution, polarization power ratios and delay spread. All these parameters were essential for the deployment of vehicular communication systems inside tunnels. The results indicate that, while the H-polar channel gain attenuates more slowly than the V-polar channel due to the geometry of the tunnel, the mean delay spread of the H-polar channel is larger than that of the V-polar channel. Rashdan *et al.* (2018) presented an extensive wideband measurement campaign for vehicle-to-pedestrian communications. They performed measurements at 5.2 GHz with a bandwidth of 120 MHz. In parallel to the channel sounding measurements, performance measurements were carried out using ITS-G5 system at 5.9 GHz and with a bandwidth of 10 MHz. It has been found that the reflection of the signal by pedestrians causes rapid fluctuations of the path loss around its mean value. In addition, other pedestrians that surround the receiver cause path loss variations and degradation due to shadowing. LOS obstruction by parked vehicles was investigated and the extra path loss which is caused by each individual parked vehicle is distinguished.

Mangel *et al.* (2011b) have used RSSI values when the PDR is greater than 65%. The advantage of using DSRC transceivers is that they can gather the accurate performance of the network. Alexander *et al.* (2011) have used DSRC transceiver which has the advantage of providing Doppler spread but this data was obtained as the part of the channel estimation process and not to measure the channel.

Wang *et al.* (2018) presented a study on Doppler characteristics in vehicular network scenario at 3.5 GHz. the characteristics of small-scale parameters such as the Doppler shift and the coherence time were analysed, respectively. It can be found that most important scatterers are trees and billboards, whereas other cars parked on the roadside do not significantly contribute to the multipath propagation. In summary, the measurements and analysis results in this paper can provide valuable channel information for the future 5G band selection and network planning.

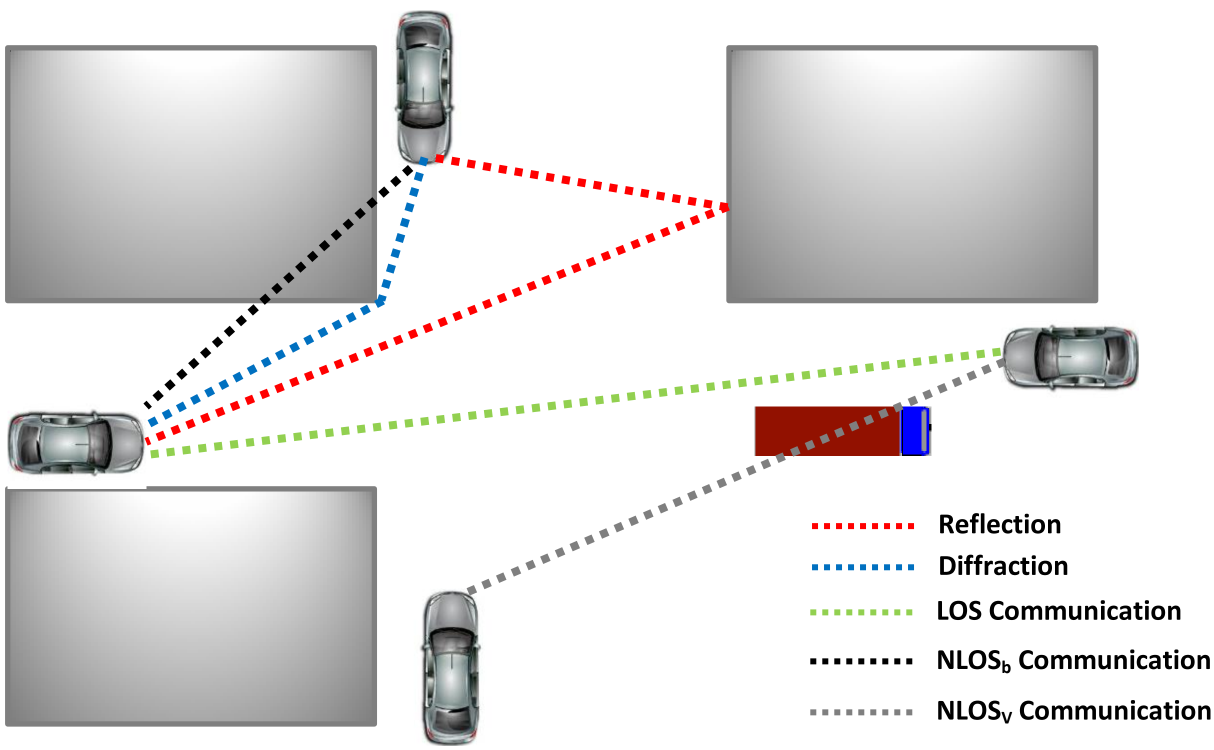

Figure 2.1 Schematic representation of V2V communication links (a) LOS (b) NLOSv (c) NLOSb (Boban *et al.*, 2014) .

Numerous authors have collected data under LOS and NLOS conditions which represent an important factor when it comes to the behaviour and modelling of V2V channels such as Paier *et al.* (2010), Mangel (2011), Somme *et al.* (2011) and Abbas *et al.* (2013). The NLOS conditions can cause considerable changes in channel properties which lead to a significant reduction in PDR at 5.9 GHz. Alexander *et al.* (2011) have gathered data in LOS and NLOS conditions.

Nilsson *et al.* (2018) presented an NLOS path loss model based on analysis from measured V2V communication channels at 5.9 GHz between six vehicles in two urban intersections. They analysed the auto-correlation of the large scale fading process and the influence of the path loss model on this. With these results, the vehicular ad-hoc network (VANET) simulations should be based on the current geometry, i.e., a proper path loss model should be applied depending on whether the V2V communication is blocked or not by other vehicles or buildings.

Some of the authors such as Cheng *et al.* (2007) have used a GPS system that has accuracy 1 m. Abbas *et al.* (2013) used camera video as well as GPS to help them to note the reasons for the change of the channel properties.

Cheng *et al.* (2007) used a 5.9 GHz band, and the radio transmissions between two vehicles driving in a suburban area were measured. A narrow-band signal was generated by a digital signal generator, and a signal analyser was used to identify characteristics of the wireless channel. The study presents the path loss modelling as well as parameters with respect to characterizing small-scale fading. Cai *et al.* (2018) conducted a measurement campaign for vehicle-to-vehicle (V2V) propagation channel characterization. Two vehicles carrying a transmitter and a receiver, respectively, have been driven along an eight-lane road with heavy traffic. The measurement was conducted with 100 MHz signal bandwidth at a carrier frequency of 5.9 GHz. They proposed an approach based on a Hough transform to identify the clusters. Based on the cluster identification results, channel characteristics in composite, intracluster, and time-variant levels are analysed. The parameters investigated include the composite root-mean-square (RMS) delay spreads and power decay versus delay behaviours of clusters and clutter paths, cluster RMS delay spread, cluster RMS Doppler frequency spread, correlations of cluster parameters, and coherence time of parameters of interest. The statistics constitute an empirical stochastic clustered-delay-line channel model focusing on the wideband characteristics observed in the realistic time-variant V2V propagation scenario.

The evaluation of the performance of the VANET is done by measuring PDR under a variety of external conditions mentioned above, for example, the different antenna locations, physical environments, speeds, etc.

Sukuvaara *et al.* (2013) found that IEEE 802.11p is the best protocol for the environment of vehicles compared with the IEEE 802.11g protocol despite the low coefficient of transport. They also designed the WiSafeCar network which is a heterogeneous network combining IEEE 802.11p and 3G mobile services and has been found exploitable synergy between two communication technologies.

Bai *et al.* (2010) have confirmed that the PDR when using 6 Mbps as the data rate is an important measure if not the most important in Inter-Vehicular Communications. Sepulcre *et al.* (2012) and Fernandez *et al.* (2012) used 6 Mbps as the data rate.

Schumacher *et al.* (2012) presented the results of a measurement campaign at urban intersections under NLOS conditions using commercial off-the-shelf wireless interface cards which meet the 802.11p and ITS-G5 specifications using a modified device driver. They evaluated PDR and received power levels under varying conditions with respect to vehicle positioning, intersection geometry and traffic density. They achieved effective reliable communication ranges by calculating the sum of the transmitter and receiver distances to the intersection centre. By knowing the reliable communication range and the speed of the vehicles, the most reliable notification time can be deduced with the assumption of equal distances to the intersection for both vehicles threatened by the collision. Karedal *et al.* (2010) presented the results of an empirical study of V2V wireless propagation channels in street intersections. The results are derived from four different types of urban intersections. They found that the path loss is high when the vehicles are far away from the intersection, with few physical objects actually providing propagation paths. Comparing the results from different intersections in the absence of a line of sight, the coverage is dependent on the availability of significant scatterers such as buildings. Hafner *et al.* (2011) have provided experimental results for a control Intersection Collision Avoidance (ICA) system implemented on modified Lexus IS250 test vehicles at an intersection.

Abbas *et al.* (2015) compared a deterministic channel model for vehicle-to-vehicle (V2V) communication with the measured channel data collected during a V2V channel measurement campaign using a channel sounder. They compared channel metrics, power delay profile, channel gain and delay and Doppler spreads are obtained from both channel sounder measurements and simulation results using a ray-based channel model. They found a high accuracy of the simulation results in the sense that the measured physical phenomena of wave propagation are captured by the ray tracer.

Clayton (2016) presented novel measurements of network performance, signal strength and Doppler spread under NLOS conditions at three T-junctions with different street widths and building layouts. The study found that there was less received power and poorer network performance in intersections with single and dual lanes and fewer buildings on either side of the roads. However, the search did not take into account the effect of traffic on the spread of the signal, nor did it take into account the oblique intersections such as the roundabout intersection Y-junction intersection.

Some researchers took note of the temporary obstacles on the street, such as small and large vehicles (Boban *et al.* 2011, Otto *et al.* 2009 and Takahashi *et al.* 2004). Boban *et al.* (2011) introduced a model that takes into account vehicles as 3D physical obstacles that affect V2V communications. Where they take into account their effect on LOS obstruction, received signal strength, and packet reception rate; the results showed significant blockage of LOS due to vehicles inducing significant attenuation and packet loss. Otto *et al.* (2009) performed V2V experiments in the 2.4 GHz frequency band in an open road environment. The signal reception is significantly worse during a rush hour period in comparison late-night period.

Takahashi *et al.* (2004) reported significantly higher path loss for the crowded scenarios through analysis the signal propagation in “crowded” and “uncrowded” highway scenarios for the 60 GHz frequency band. Rodriguez *et al.* (2016) presented a measurement-based evaluation of large vehicle shadowing at 5.8 GHz in V2X scenarios. The receiver antenna height was fixed to average vehicular height (1.5 m), while the transmitter antennas are located at different heights (1.5, 5, and 7 m) in order to investigate both V2V and V2I scenarios. A truck was used to obstruct the LOS between transmitter and receiver, and a large number of geometrical combinations of the scenario were explored. The statistical analysis of the measurement shows how in the V2V case, the experienced shadow levels are higher than in the V2I scenarios, where the shadow levels depend on the transmitter antenna height. A simple 3D ray-tracing simulation was validated against the measurements, showing a good match with an RMSE of 4.1 dB. Based on both measurements and ray-tracing data, a simple deterministic shadowing model, useful for implementation in system-level simulators, is presented, as the first step towards a more dynamic and scalable shadowing model.

Yang *et al.* (2018) were analysing and modelling of path loss characteristics for vehicle-to-vehicle (V2V) communications with vehicle obstructions. A series of channel measurements were performed at 5.9 GHz in a typical urban scenario for V2V communications. In these measurements, they subdivided into three types of test cases: non-obstruction, small vehicle obstruction, and large-vehicle obstruction. Then the path loss and shadow fading components of the three cases are extracted, compared and analysed. Based on the measurements, we show the influence of different types of vehicle obstruction on path loss and shadow fading characteristics. It is found that small-vehicle obstruction does not significantly affect the mean of path loss, and it leads to additional shadow fading of 3 dB. Large vehicle obstruction brings about 10 dB of additional path loss. Finally, a path loss model is proposed, which includes the influence of vehicle occlusion on path loss and employs the classical long-distance path loss formula. The results in the paper could be used for the performance analysis and system design of V2V communication.

Boban *et al.* (2019) performed V2V channel measurements in four different frequency bands (6.75, 30, 60, and 73 GHz) in urban and highway scenarios. They studied and analysed the impact of the blocker size and position on the received power and fast fading parameters, as well as the frequency dependence of these parameters under blockage. The results showed that there is a strong influence of the size of the blocking vehicle on the blockage loss and the angular/delay spread. The position of the blocker relative to the transmitter and receiver also plays an important role. On the other hand, the frequency dependence is quite limited, with the blockage loss increasing slightly and the number of scattered MPCs reducing slightly as frequency increases. The main conclusion was that V2V communication will be possible in high (millimetre-wave) frequencies, even in the case of blockage by other vehicles.

Acosta, *et al.* (2007) used 5.9 GHz frequency with a bandwidth of 10 MHz to collect data from six different environments classify in form urban, suburban and rural environment situations. The measurements were applied to achieve a small-scale fading model of the according to channels. The results include important characteristics for the six scenarios such as path loss, delay, frequency shift or Doppler analysis. The extracted information is used to be injected into an RF channel emulator. The study shows that the V2V channel clearly is time-selective and frequency-selective.

2.3. Network Simulation and Modelling

Modelling and simulation are cheaper and safer compared to testing new protocols and applications using real-life vehicles. Software modelling decreases the area wanted for a real-life experience comprising a number of vehicles and moving at high speed. It is also more suitable for repeatability and has environment control.

The mobility of the nodes is a key factor of vehicular networks which must be taken into consideration when conducting the simulation to analyze network performance. There are some of the mobility simulators which can be used to simulate traces of a node such as Network Simulator – 2 (NS-2) or QualNet (NS3 Simulation 2019).

The following characterization of some common mobility simulators:

- Simulation of Urban Mobility (SUMO): is a free, open, source road traffic simulation suite designed to handle large road networks. It allows modelling of traffic systems including road vehicles, public transport and pedestrians. It has the capability to produce mobility traces which can be used with other software such as NS-2, QualNet and Matlab. Maps can be manually input or OpenStreetMap can be used if real-world maps are required (*SUMO* 2018).

- Mobility generator for Vehicular networks (MOVE): is based on SUMO. It allows the user to create realistic mobility models to simulate the vehicle network. MOVE provides an interface to automatically generate simulation scripts for ns-2 and QualNet (Karnadi *et al.* 2007).
- VANET Mobility Simulation (VanetMobiSim): can generate movement traces in different formats, supporting different simulation/emulation tools such as NS-2, Glosim and QualNet. It has the ability to simulate road structure and topology as well as traffic signs (Eurecom, 2014).

Jiang *et al.* (2008) simulated a network focused on finding optimal network configurations. 6Mbps were found to provide the highest packet delivery ratio. Mangel *et al.* (2011b) have mentioned a 6Mbps data rate gives a good capacity and signal robustness.

The environment of intersections is a complex environment for wireless communication as well as drivers where conditions NLOS and LOS are mixed. This is the reason why there are many accidents in such areas and this has led to the design of protocols for such environment (Azimi *et al.* 2013). Aygun *et al.* (2016) developed a geometry-based path loss and shadow fading model for V2I links. They modelled the following types of V2I links: line-of-sight, non-line-of-sight due to vehicles, non-line-of-sight due to foliage, and non-line-of-sight due to buildings. They had been verified the proposed model using V2I field measurements. They implemented the model in the GEMV2 simulator, and make the source code publicly available

Yang *et al.* (2019) proposed a cluster-based 3D channel model is used in urban and suburban scenarios for V2V communications and considers the distribution of MPC clusters in both horizontal and vertical domains. This model was based on the measurements conducted at 5.9 GHz in urban and suburban scenarios in Beijing. In the proposed model, all MPC clusters were divided into two categories: global-clusters and scatterer-clusters, and the distribution of the two clusters were characterized by a series of inter- and intra-cluster parameters. It is found that both the azimuth spread and the elevation spread follow the lognormal distribution. In addition, the power of MPCs within a cluster has the truncated-Gaussian distribution, whereas the angle of MPCs within a cluster has the Laplacian distribution. Finally, the accuracy of the model was verified by comparing the measurements and simulations.

Alsuhli *et al.* (2019) proposed a double-head clustering (DHC) algorithm for VANET. This approach is a mobility-based clustering algorithm that exploits the most relevant mobility metrics such as vehicle speed, position, and direction, in addition to other metrics related to the communication link quality such as the link expiration time (LET) and the signal-to-noise ratio (SNR). The proposed algorithm had enhanced performance and stability features, thorough evaluation methodology was followed to validate DHC and compare its performance with another algorithm using different evaluation metrics. These metrics are analysed under various mobility scenarios, vehicle densities, and radio channel models such as log-normal shadowing and two-ray ground loss with and without Nakagami-m fading model. The proposed algorithm DHC had proven its ability to be more stable and efficient under different simulation scenarios.

By using VirtualSource11p in NLOS conditions, Mangel (2011) simulated intersections when the communications channel is contested by many nodes. They found that the network load was highest on the street which did not have the transmitting node. However, the worst-case was still acceptable to receive a safety message on time. In this model, the distance was quantified in a single path-loss equation – shown in Equation 2.1 with a description of the parameters provided in Table 2.1.

$$P_{loss} = 3.75 + 2.94 i_s + \begin{cases} 10\log_{10}\left(\left(\frac{d_t^{0.957}}{(x_t w_r)^{0.81}}\frac{4\pi d_r}{\lambda}\right)^{2.69}\right), & d_r \le d_b \\ 10\log_{10}\left(\left(\frac{d_t^{0.957}}{(x_t w_r)^{0.81}}\frac{4\pi {d_r}^2}{\lambda}\right)^{2.69}\right), & d_r > d_b \end{cases} \quad \ldots\ldots\ldots\ldots 2.1$$

Table 2.1 Parameter descriptions for virtualsource11p

Parameter	Description
$\boldsymbol{d_r}$	Distance from the receiver to the intersection centre
$\mathbf{d_t}$	Distance from the transmitter to the intersection centre
$\boldsymbol{w_r}$	Width of the receiver street
$\boldsymbol{x_t}$	Distance from the transmitter to the wall
$\boldsymbol{i_s}$	Sub-urban loss factor (0/1 for urban/suburban conditions)
$\boldsymbol{\lambda}$	Wavelength (0.0508 m)
$\boldsymbol{d_b}$	Breakpoint distance (≈ 180 m)

As the NLOS path-loss at a certain distance can be calculated by the model, the NLOS received power $P_{RX(d)}$ for a transmitter power $P_{TX(d)}$ can be calculated using the following expression,

$$P_{RX}(d) = P_{TX}(d) - S_{Loss} + G_a - P_L \dots\dots\dots\dots 2.2$$

Where S_{Loss} is the system loss and G_a is the combined TX and RX antenna gain. For comparison, these parameters are assumed to be zero, where the effect of averaged antenna gain and cable losses were removed from the measured channel gain before calculating the receiving power. Figure 2.2 shows the geometry related parameters.

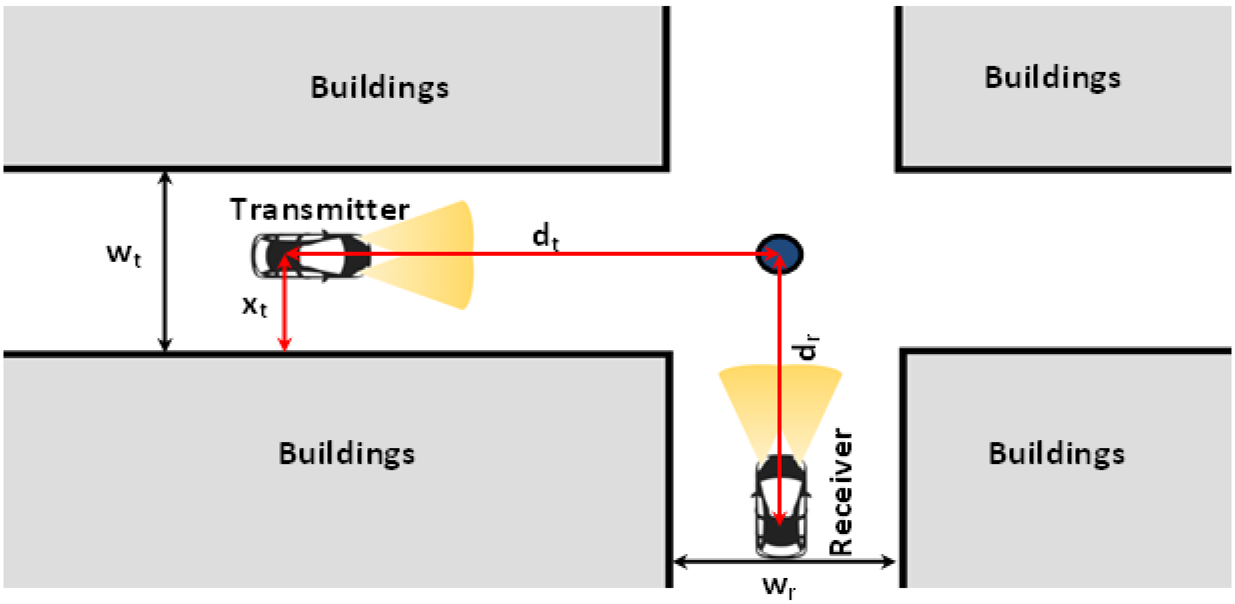

Figure 2.2 Geometric parameters used in the virtualsource11p model

Abbas *et al.* (2013) tested data which were collected in various environments by Virtualsource11p. It was found that the model produces accurate predictions in most locations. One prediction of received power was an underestimate because one of the buildings had large metals sheets in the corner which had assisted the received power levels. It is concluded that, in spite of the accuracy of the model, the intersection gain factor would provide improved forecasts; however, this would require the collection of more data from intersections that could provide variations for propagation.

Karedal *et al.* (2009) designed a V2V channel model based on measurements made in suburban and high-speed environments in the 5.2 GHz band. They analyzed four distinct signal components: LOS, discrete components from vehicles, discrete components from static objects, and diffuse scattering.

Sommer *et al.* (2011) used measurements to calibrate a path loss model that aims to distinguish between LOS and NLOSb conditions. The model calculates the received power based on the length of the transmission across the buildings and the number of walls through which the transmitted beam passes, while the reflected and reflected rays are not calculated.

Boban *et al.* (2017) investigated the evolution of a line of sight (LOS) blockage over both time and space for vehicle-to-vehicle (V2V) channels. Using realistic vehicular mobility and building and foliage locations from maps, they performed LOS blockage analysis to extract LOS probabilities in real cities and on highways for varying vehicular densities. moreover, they modelled the time evolution of LOS blockage for V2V links, they employed a three-state discrete-time Markov chain comprised of the following states: i) LOS; ii) non-LOS due to static objects (e.g., buildings, trees, etc.); and iii) non-LOS due to mobile objects (vehicles). They obtained state transition probabilities based on the evolution of LOS blockage. The results can be used to perform highly efficient and accurate simulations without the need to employ complex geometry-based models for link evolution.

There are some studies that have focused In terms of propagation modelling on a city-wide scale, these reported by Giordano *et al.*, (2010) and Cozzetti *et al.* (2012) where they presented propagation modelling in grid-like urban environments, where the streets are supposed to be straight and intersecting at an angle. While these assumptions remain for some urban areas, in other areas they may not do so.

In addition to improving propagation modelling using site-specific information, Wang *et al.* (2012) have used aerial photography to determine the scatterers density in the simulated area where the level of fading of a particular location on the road is determined by processing the air data to deduce the scattering density.

A number of researches have been carried out in different environments to estimate the channel by conducting measurements and fitting measured data using known models. For example, Paschalidis *et al.* (2011) performed measurements in different environments and fitted the measurements data to the long-distance path loss model.

Abbas *et al.* (2015) designed a stochastic propagation model for highway environments that combines vehicular obstructions and defines the time duration of LOS, NLOSv, and NLOSb states using the measured probability distributions.

There are a number of studies looking at the upper layers of communication to reduce hops such as Amadeo *et al.* (2012), Boban *et al.* (2014). Amadeo *et al*. (2012) utilise Content-Centric Networking (CCN) as instead of the TCP/IP protocol suite. Their simulations demonstrated an increase in network efficiency by reducing the number of hops. Boban *et al.* (2014) presented simulations which used high vehicles as the relaying nodes. they found that the taller vehicles can transmit packets through a wider range after a certain distance, making the packet forwarding process more efficient. in this way, it has been shown that the LOS conditions for most transmissions have been met because of the elevation feature on which the antennas will be placed. This means a higher reception power and fewer hops.

Gong *et al.* (2019) proposed a Geometry Enhanced Winner II V2V channel model (GEWV), which simulates the channel responses among vehicles in arbitrary places with detailed geographical information (e.g., placement of buildings). After exploiting the outlines of vehicles and buildings, the light of sight (LOS)/non-light-of-sight (NLOS) links type are judged. In addition, the multiple-interaction reflections and diffractions are calculated. Then signal variations and multi-links time delays are generated. Therefore, this channel model reflects practical communication conditions more reliable in comparison to some existing LTE V2V channel models. Results validate the importance of the geometry surroundings in comparison with models with simple large-scale and small-scale propagation paths.

Islam *et al.* (2013) utilized the Nakagami model and performed simulations comparing it with the two-ray, free space and the dual-slope piecewise-linear (DSPL) path loss models. They have found that simplistic models such as the free space and DSPL resulted in underrating bit error rates. Schwartz *et al.* (2012) simulated uses 1-hop periodic beacon message issued by each car in a VANET. This has been compared with current delay methods and found to be more effective at controlling the number of vehicles transmitting within each time. Subramanian *et al.* (2012) simulated on top of MAC layer to improve packet reception performance. they have found that the synchronous MAC helped in finding neighbouring nodes as opposed to the asynchronous approach hence increasing safety in DSRC safety applications. Sharafkandi *et al.* (2012) modified the Enhanced Distributed Channel Access (EDCA) mechanism where Packet collisions involving safety-related and high priority packets was reduced.

Boban *et al.* (2014) designed the Geometry-based efficient propagation Model (GEMV2). The main objective of GEMV2 is to model the effective propagation of VANET simulations involving a large number of vehicles in large geographical areas. It utilizes the geographic descriptors to enable location-specific modelling of the V2V channel. GEMV2 uses outlines of vehicles, buildings, and foliage and as well as locations and dimensions of vehicles, which are readily available through geographical databases and mobility traces to recognize three types of links: LOS, NLOSv due to vehicles and NLOSb due to static objects. GEMV2 calculates the large-scale signal variations and small-scale signal variations based on the number and size of surrounding objects. They demonstrated the validity of GEMV2 by intensive measurements in urban, suburban, highways and open environments. The output of this simulation is two groups of files the first group includes Keyhole Markup Language (KML) files to visualize the results. Google Earth or any program that provides support KML format is used. Figure 2.3 shows the Google Earth visualization of the received power calculated by GEMV2. The colours of the lines represent a link between TX-RX pairs shows received power relative to the maximum received power in dBm during the simulations.

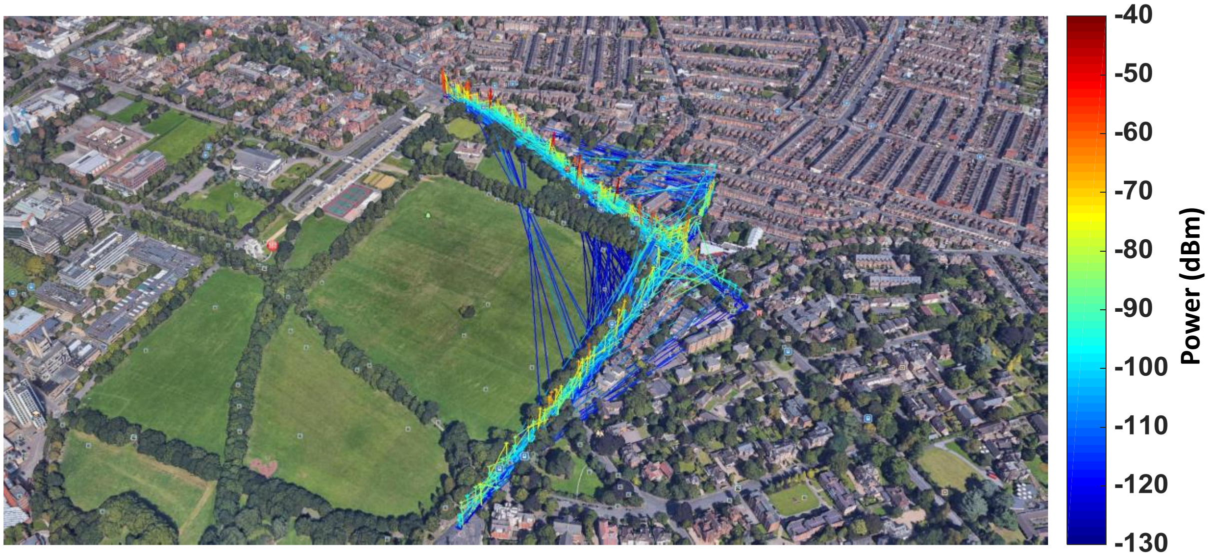

Figure 2.3 The Google Earth Visualisation of a roundabout V2V scenario with a number of transmit-receive pairs in the city of Leicester.

The second type of these files is comma-separated values (CSV) with each variable saved in a different file which suitable for analyzing the results in/outside MATLAB. More details about this model in Chapter 7.

The research contributions found in the scientific literature are summarized in Table 2.2.

Table 2.2 Contributions to vehicular channel characterization and modelling

Author and Year	Contribution
Maurer *et al.* (2002)	Vehicular channel characterization using a narrowband measurement at 5.2 GHz.
Matolak *et al.* (2005)	The V2V channel model was developed at 5 GHz and it was found that RMS delay distribution was provided by lognormal distribution and the greatest value for RMS delay differences was obtained in the urban environment.
Eggers *et al.* (2007)	The antenna placed inside a car leads to higher path loss. this result was found by measurement V2V MIMO channel in rural and highway environment
Tan *et al.*, 2008)	A GPS sounding system was developed to measure V2V and V2I channels at 5.9 GHz. it is found that in time-varying vehicular channels larger packets may face higher error rates.
Kunisch *et al.* (2008)	Path loss characterization for V2V based on wideband channel measurements at 5.9 GHz.
Zaji *et al.* (2008) Pätzold *et al.* (2008)	Statistical SISO and MIMO channel modelling and analysis for mobile-to-mobile (M2M) channels.
Renaudin *et al.* (2009)	Develop statistical channel model for highway environment based on 30x30 MIMO V2V channel measurement at 5.3 GHz.
Karedal *et al.* (2011)	Developed empirical-based path loss models for V2V communication at 5.9 GHz.
Shivaldova *et al.* (2012)	Found that the use of directional RSU antenna instead of omnidirectional RSU antenna increases the coverage range and throughput.
Cheng *et al.* (2013)	Proposed a geometrical channel model for the diffuse component based on scattering objects distributed along the roadside, and use this model to associated predict the Doppler spectrum and angle-of-arrival (AOA) distribution with this component for various V2V scenarios.
Fernandez *et al.* (2014)	Development of path loss model for V2V at 5.9 GHz.
Nilsson *et al.* (2015)	Vehicular channel characterization at 5.9 GHz and found that a large object such as a car will affect the measurement uncertainty, but only to a small degree.
Liu *et al.* (2016)	Tapped-delay line (TDL) channel models applicable to the 5 GHz band were developed. Also, provided measurement and analytical results for V2V propagation path loss and RMS delay spread
Onubogu (2016)	Developed a path loss model for V2V communications based on extensive V2V channel measurements conducted in three different vehicular propagation environments.
Granda *et al.* (2016)	Evaluated some important parameters of a V2I wireless channel link such as Received Power, Power Delay Profile, Delay Spread and Coherence Bandwidth, in an urban scenario using a deterministic simulation model based on an in-house 3D Ray-Launching algorithm.

Avazov *et al.* (2017)	Investigated the statistical characterization of a 3-D propagation model for multiple-input–multiple-output vehicle-to-vehicle (V2V) communications inside a rectangular tunnel under non-isotropic scattering conditions.
Torres *et al.* (2017)	Analysed the applicability of a geometric-based stochastic (GBS) model based on ray-tracing techniques to vehicular-to-vehicular (V2V) intersections
Granda *et al.* (2018)	Presented a deterministic computational tool based on an in-house 3D Ray-Launching algorithm is used to represent and analyse large-scale and small-scale urban radio propagation phenomena, including vehicle movement effects on each of the multipath components.
Rashdan *et al.* (2019)	Developed of a geometry-stochastic channel model (GSCM) for V2P communications. This model presented wideband V2P channel characterization results. Enhanced super-resolution tracking (KEST) algorithm was employed to track multipath components (MPCs) and estimate their parameters based on the measured data
Hofer *et al.* (2019)	Presented a real-time geometry-based channel emulator, which enables the emulation of non-stationary doubly-selective fading channels. This emulator directly uses a propagation path based geometric model that allows for continuously changing path delays and Doppler shifts.

Chapter 3: Research Methodology

There are several measurements mentioned in the literature review in Chapter 2 which can be used as metrics, such as Doppler spread, PDR etc. In this Chapter, the devices used in the construction of the measurement platform will be described.

3.1. Platform Devices

3.1.1. LocoMate mini 2 (Arada Systems)

A multimodal communication device is compliant with the IEEE 802.11p communication standard. The Arada Systems LocoMate mini 2 is a leading developer of technologies for vehicle-based communication network applications, including tools collection, vehicle safety services, and commerce transactions via cars. The Arada Systems LocoMate mini 2 OBU device can provide wireless communication in a vehicular environment while considering different data rates according to the IEEE 802.11p standard. It offers low latency connectivity for both inter-vehicle and vehicle to roadside units. This solution integrates a GPS device for vehicle navigation. It can transmit and receive the packets at 5.7 GHz to 5.925 GHz with 10 MHz and 20 MHz channel bandwidth. In the software it can support for WAVE standard (802.11p/1609.x/SAE J2735), multi-channel synchronization between service users, exclusive packet control, WAVE data and management frame, etc. Figure 3.1 shows the LocoMate mini 2 device (Arada Systems, 2017). It has MIPS processor running at 680 MHz, RAM/Flash- 16MB Flash, 64MB SDRAM (512Mbits). Table 3.1 illustrates more hardware specification of the Loclmate mini 2. Figure 3.2 shows a block diagram of LocoMate mini 2 with Host computer connection (Arada Systems, 2017). It has MIPS processor running at 680 MHz, RAM/Flash- 16MB Flash, 64MB SDRAM (512Mbits). Table 3.1 illustrates more hardware specification of the LoclMate mini 2.

Figure 3.1 LocoMate mini 2 platform

Table 3.1 LocoMate mini 2 specifications

Specific device	Description
Protocol	802.11p
Frequency	5.85-5.95 GHz
Tx	24 dBm
Modulation	OFDM
Rx	-95±2 dBm
Power supply	Compliant to SAE J1113-11, 5 V DC
GPS device	GPS with embedded RF antenna
DSRC message	BSM, SPAT, MAP, TIM
Platform	Linux/Unix compatible/ Windows
Antenna interface	SMA Connector

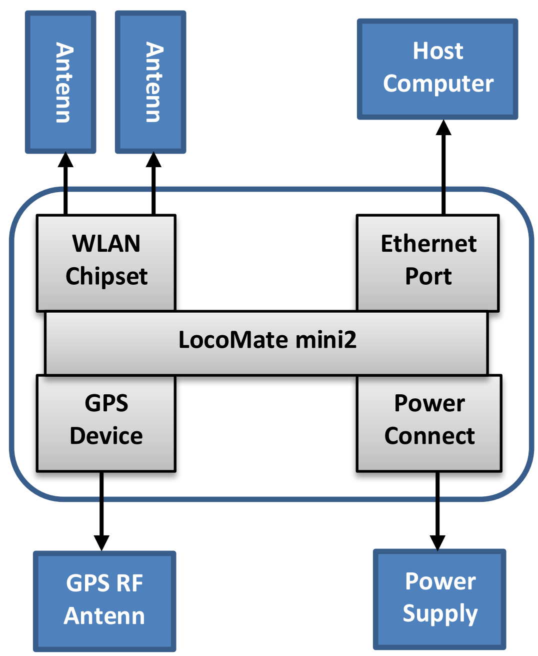

Figure 3.2 Block diagram of LocoMate mini 2

3.1.2. E4440A Spectrum Analyser; 3Hz to 26.5GHz

This measures and monitors complex RF and microwave signals up to 26.5GHz. Phase noise optimization, FFT analysis, a full suite of detector modes (Agilent 2012).

3.1.3. Anritsu MG3692B signal generator

The Anritsu MG3692B is the rf/microwave signal generator covers both RF and microwave frequencies from 0.1 Hz to 70 GHz. it offers the highest output power, unsurpassed frequency coverage, spectral purity, switching speed, modulation performance, size, upgradeability, reliability, and service. Thus the MG3692B is an ideal signal source for RF requirements fully configurable from simple to high-performance applications (Anritsu, 2009).

3.2. Software and Programming Tools:

In this section, the software used to collect and analyse the data are described.

3.2.1. The Network System (NS)

Putty is a free and open-source terminal emulator (SSH.COM 2018). Figure 3.3 shows a snapshot of the Putty utility. It is developed originally for the Windows platform, but it has been ported to various other operating systems such as Unix-like platforms and macOS. It supports several network protocols such as SSH, Telnet. It can also connect to a serial port (Tatham 2017).

3.2.2. The Continuous Wave System (CWS)

The VXI-11 protocol is a communication protocol primarily designed for connecting instruments (such as oscilloscopes, multimeters, spectrum analyzers etc.) to controllers (e.g., PCs) (Electronics ICS, 2019). It has been used to make the necessary connection between the spectrum analyser and the PC, in order to collect the spectra and save them in files that have .log extensions. These saved files were used to analyse the output spectra in further steps.

Instruments may support this protocol directly (e.g., as part of implementing the more recent LXI interface), or maybe connected by way of an adapter (gateway) that attaches to a dedicated bus (such as GPIB) (LocoMate Guide 2013).

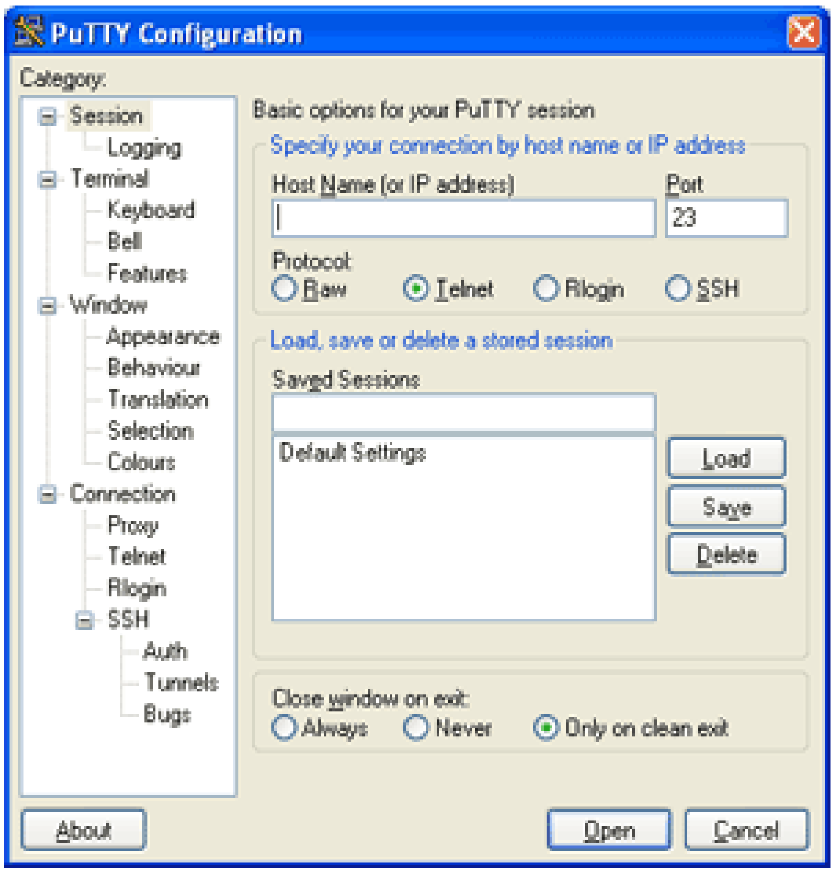

Figure 3.3 Putty snapshot

3.3. The Measurement System

Many measurement campaigns were mentioned in the literature review. Depending on what was mentioned above, the measurement system used similar to that used by Clayton (2016) with some improvements to increase the efficiency of the system. The measurement system is divided into two parts. The first part is a continuous wave system (CWS) to measure channel parameters. The second one is a network system (NS) to measure network performance. Figure 3.4 illustrates the measurement system.

The CWS is been essential in measurement system because the Arada 802.11p transceivers are not capable of channel sounding and RSSI values do not have high accuracy; subsequently utilizing it to model the communications channel may be erroneous.

3.3.1. The Continuous Wave System (CWS)

The continuous wave system (CWS) was utilized to determine the characteristics of the channel at 5.9 GHz including accurate measurements of the path loss and any Doppler effects. The signal generator transmits a continuous wave which is received by the spectrum analyzer.

Hyperlink wireless band 4.9-5.8 GHz 6 dBi omnidirectional antenna model HVG-4958-06U is used in the transmitter and receiver. Figure 3.5 shows the radiation pattern of the continuous wave system antennas.

The antennas are connected with a signal generator and spectrum analyser by coaxial cable, 50-ohm impedance. The parameters in this part are in table 3.2. This part of the system used to analyse the signal characteristics of a continuous wave. During the measurements, each spectrum is stamped according to the laptop's clock.

Table 3.2 The Continuous Wave Characteristics

Signal Generator		Spectrum Analyser			Antenna height
Freq.	Power Level	Centre Freq.	Reference Power	Span	1.5 m
5.9 GHz	+ 18 dBm	5.9 GHz	-30 dBm	500 Hz	

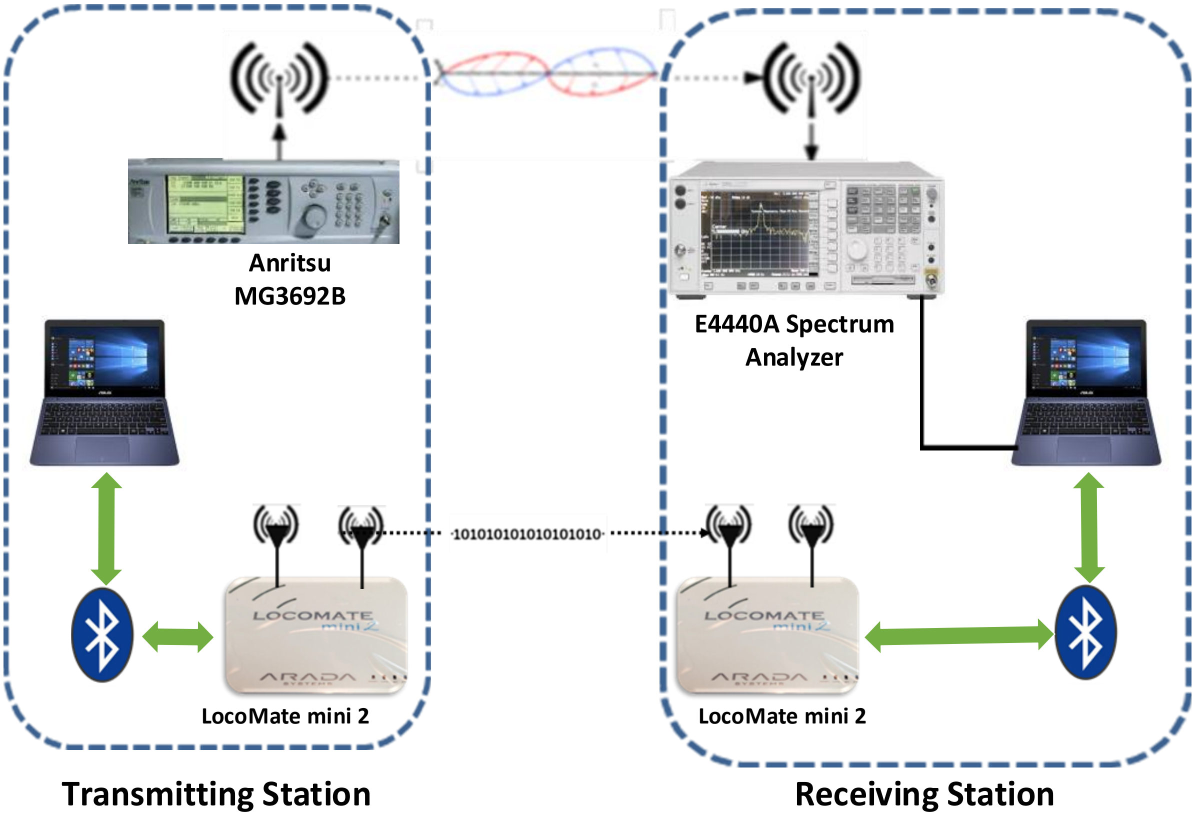

Figure 3.4 The Measurement System

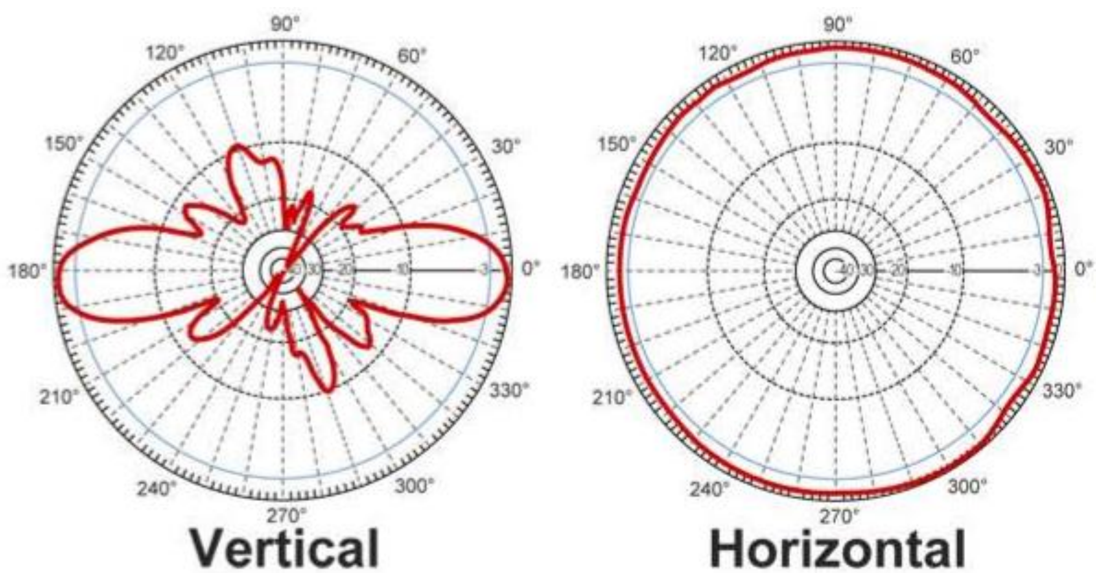

Figure 3.5 Radiation patterns of the Hyperlink 6dBi omnidirectional antenna model HVG-4958-06U (L-COM 2017)

3.3.2. The Network System (NS)

This system is utilized to analyse packet loss in 802.11p network operating at 5.9 GHz which is channel 172 in the FCC channel allocation system. One LocoMate mini 2 transceiver is set up as a transmitter and second as a receiver. Every transceiver is connected to a laptop via Bluetooth to monitor packets sent and received. The antennas used in this part of the system are supplied with the devices. The NS operating parameters are in Table 3.3. The Packet Delivery Ratio (PDR) has been calculated in this part of the system.

The equipment is loaded onto two trolleys. One is the transmitting station and the second is the receiving station. The 802.11p transceivers in both stations are connected with a laptop to monitor the transmitter and receiver packets. The equipment on the trolleys are powered by a deep cycle battery. The data are collected and saved in the receiver part via a laptop which is connected with the spectrum analyser, while the connection with locomate mini 2 device is via Bluetooth.

Table 3.3 802.11p NS Parameters

Parameter	Select Value
Tx power	24 dBm
Packet Size	250 Bytes
Data Rate	6 Mbps
Channel	5.9GHz
Antennas	Patch Antenna
Gain	6dBi
Antenna height	1.25 m

3.4. The Combined System

Figure 3.6 and Figure 3.7 Illustrate the transmitting and receiving trolleys respectively. A laptop has recorded the data from both the 802.11p receiver and the spectrum analyser. To track the positions of the transmitter (TX) and receiver (RX) trollies during the measurements, each 802.11p transceiver measures GPS coordinates with accuracy 1m. These data will be also combined with the measurement data after the measurements have been taken to identify important scatterers. Videos of each measurement were recorded through the webcam set on receiver trolley. GPS coordinates together with video information are used when the analysis of data to know the reasons whenever an unexpected difference between the links is observed because of the variations in a number of pedestrians, traffic density, building and roadside objectives. Figure 3.8 shows a flowchart about how to collect the data from both The Continuous Wave System (CWS) and the Network System (NS) by the 802.11p receiver and the spectrum analyser.

Figure 3.6 Transmitting station trolley

Figure 3.7 Receiving station trolley

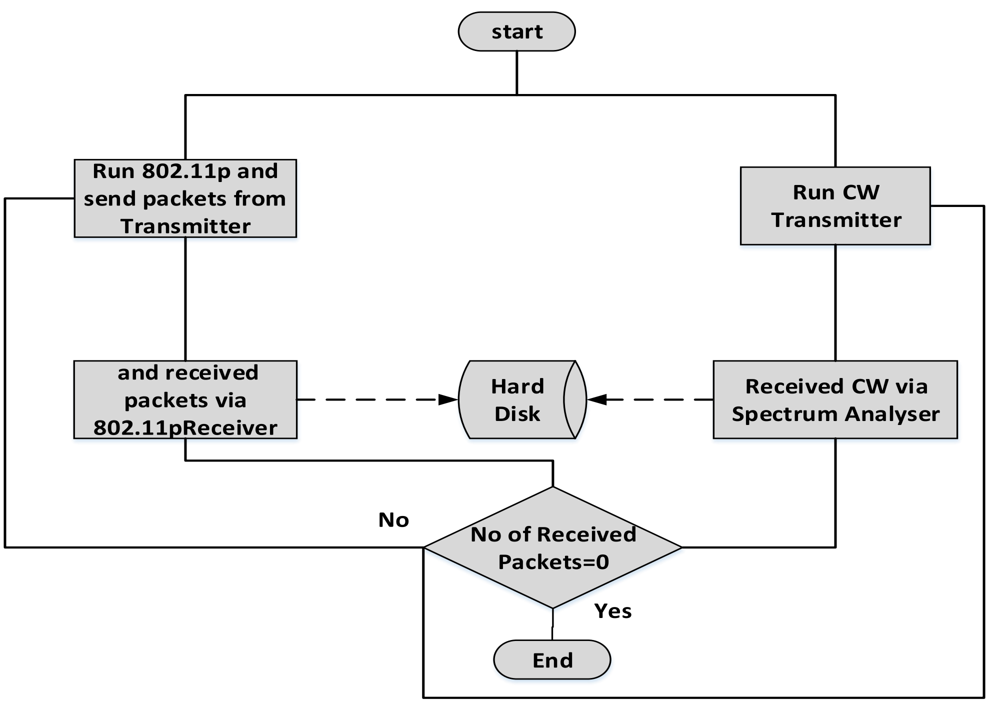

Figure 3.8 Flowchart describing script used to collect 802.11p packets and spectra

3.5. Data Output from the System

3.5.1. Data measured from the CWS

A laptop connected to a spectrum analyzer contains data stored as spectra. 40 spectra are obtained at each location on the data collection path with a bandwidth of 500 Hz. This narrow frequency enables monitoring Doppler spreads resulting from pedestrian and vehicular traffic. A smaller bandwidth is not selected because of each spectrum will take a long time to collect.

A 40 spectra sample is a statistically significant sample that gives a median peak power and provides a good estimate of the change in parameter at each position, all within approximately 50 seconds. The time it takes to move the receiver from one location to another and to prepare to collect data is about 150 seconds, with 50 seconds representing the time of data collection, each position requires about 3.5 minutes. Thus, approximately 50 positions can be covered by 175 minutes, which is an acceptable time to collect data before the batteries die.

Figure 3.9 shows an example of three spectra obtained through an experiment at an intersection. From the spectra collected at each location, the median peak power was obtained which can be used to analyze the path loss versus the distance from the centre of the intersection.The peak power was measured instead of the total power in the spectrum because the peak power is not affected by Doppler spreads as much as the total power in the spectrum and would be more accurate in determining the path loss independent of the physical traffic. In addition to the peak power, the spectra also provide an indication of the size of the Doppler shifts and spreads that occur in the radio channel. These Doppler effects can be compared against the network performance to analyse how the NS could be affected by Doppler shifts or spreads. It was noticed during data collection that Doppler spreads were caused by pedestrians, cyclists and vehicles. Figure 3.10 provides an indication of Doppler spreads and how they differ with the power in them. 40 spectra were collected in one position and combined in a matrix, where rows and columns correspond to frequency and time respectively. This matrix is then printed as an image where the colour of each pixel corresponds to the power.

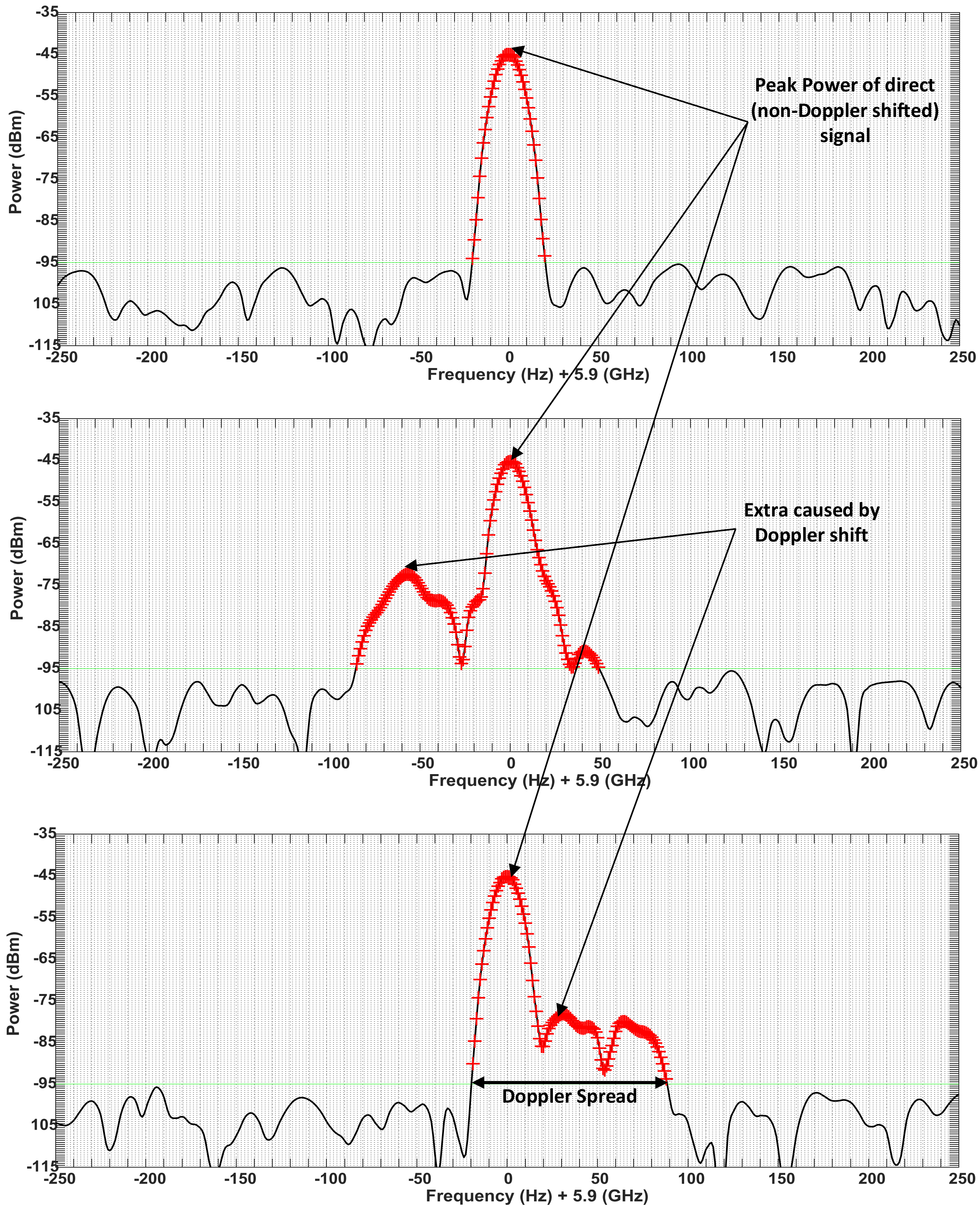

Figure 3.9 Three spectra showing the CW power (red crosses) affected by different sizes of Doppler spreads and power at -95 dBm threshold

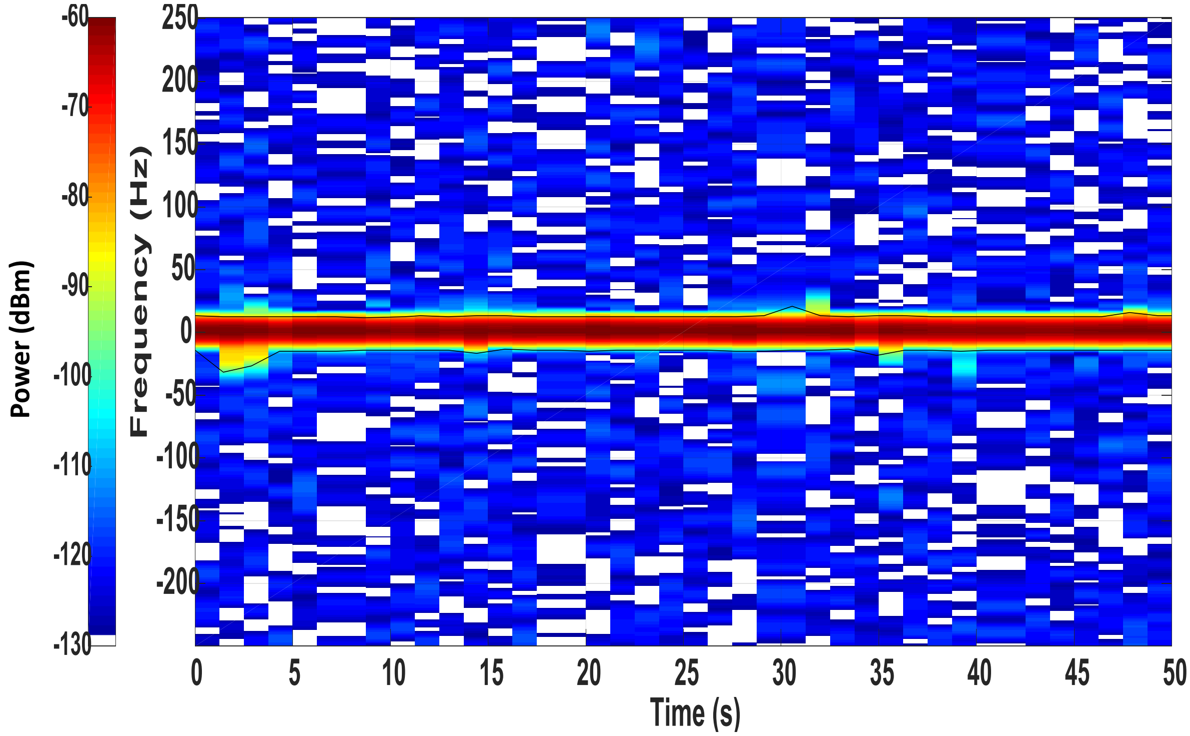

Figure 3.10 Joining all the spectra collected at a certain position

3.5.2. Data measured from the NS

In this part of the system, packets were sent out from one 802.11p transmitter at a rate of 10 packets per second. Figure 3.11 shows a snapshot of network system data.

Each of these packets is stamped with the local time and a unique packet number. In addition, the received packets from the receiving 802.11p transceiver are time-stamped on reception, and the received signal strength indicator (RSSI) is obtained for each packet. These packets are used to determine the packet delivery ratio (PDR).

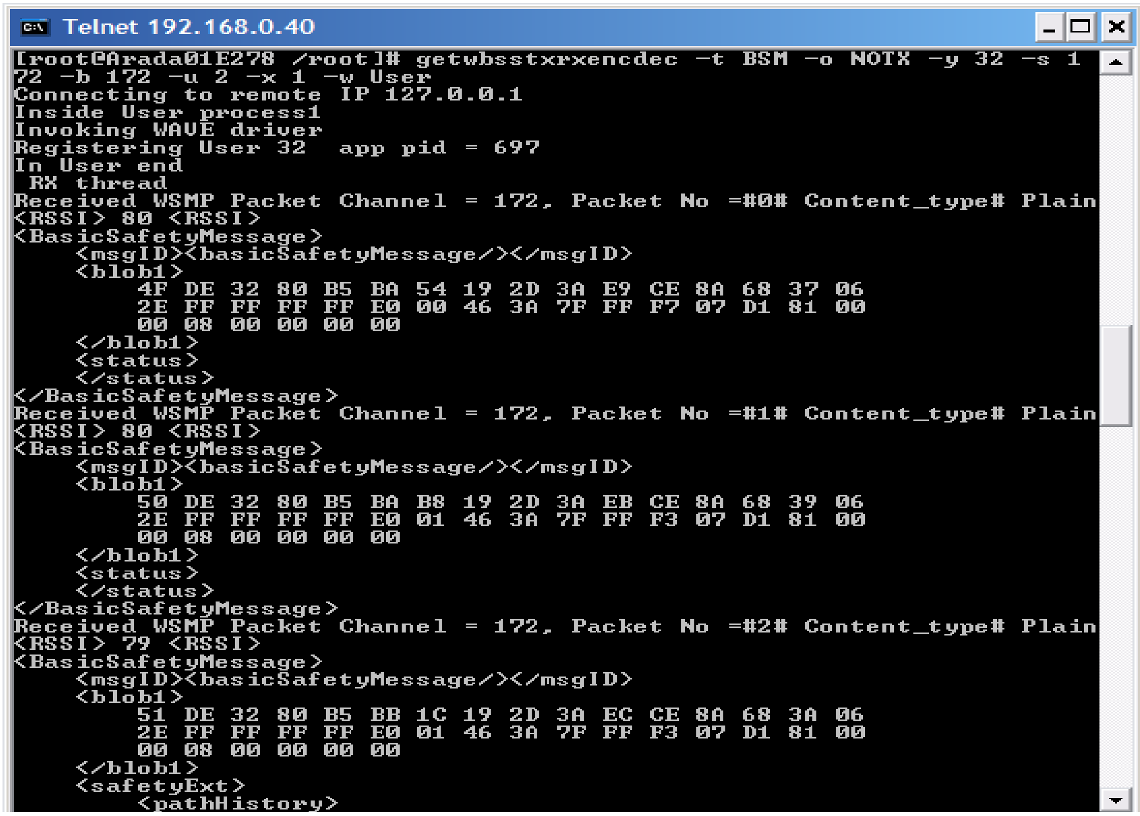

Figure 3.11 Snapshot of network system data

3.6. Power Calibration

The measurement system was tested before the first experiment was done and power calibrations of both parts of the system are performed. In this test, the trolleys were close to each other and the distance between the antennas was 2.5 metres and the spectra and packets were collected while the power level varied from the signal generator from 1 to 18 dBm in steps of 1 dBm. Figure 3.12 shows received power as the transmitted power was increased.

The primary purpose of using the 802.11p transceivers is to exchange messages between each other and is not intended to measure the received signal strength with high accuracy, unlike the spectrum analyser.

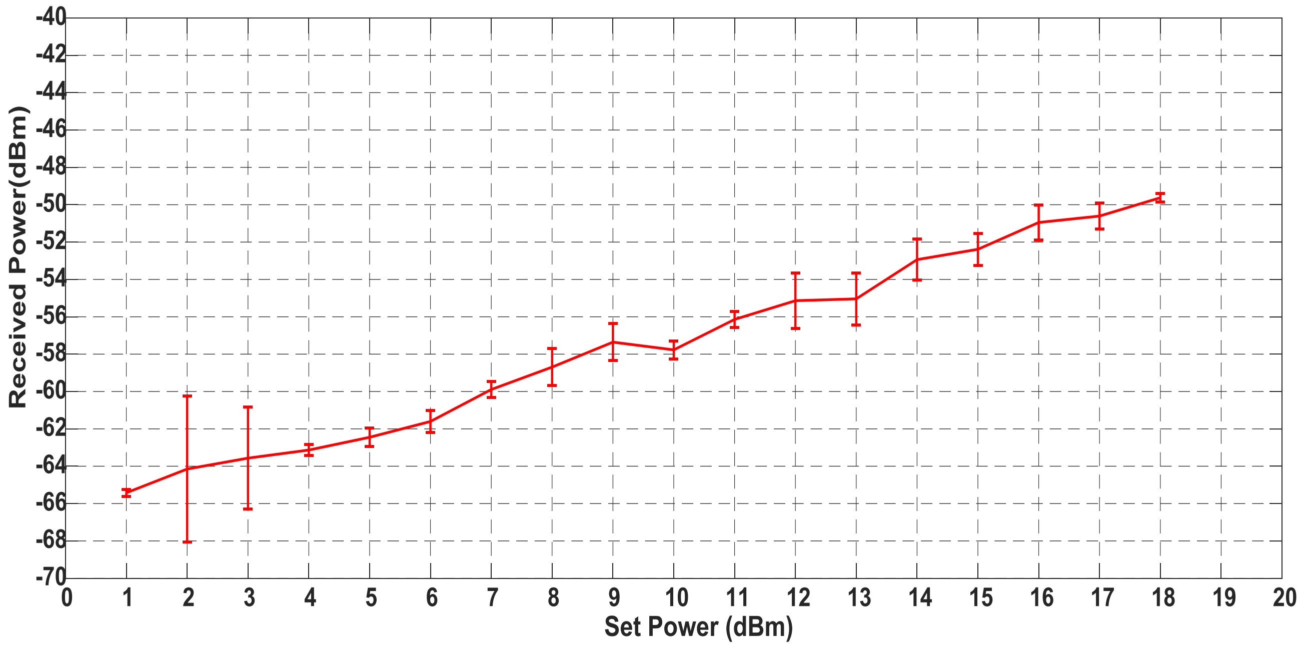

Figure 3.12 Received power vs transmitted power

The data collected provides information about the performance of the 802.11p network. This system has been used in a few studies and in a variety of environments such as straight road and intersections (Cheng *et al.*, 2007, Clayton, 2016). The data collected in this project focuses on the radio wave propagation at non-perpendicular intersections under LOS and NLOS conditions.

3.7. Measurement Scenarios

There is a set of ITS applications defined by the automotive industry together with ETSI ITS standardisation organization in Europe and US-DOT in the USA, respectively, which can reduce the number of road accidents and traffic. Among this special interest are road safety applications and traffic efficiency applications especially at road intersections.

Intersection scenarios are described when more than one road of varying width intersects. In such scenarios, visual contact is often blocked between cars approaching the intersection by buildings of a certain height located at the corner of the intersection. In the

NLOS scenario, the reliability of a V2V link depends on the availability of scattering objects nearby such as buildings, trees, lampposts, street signs and parked vehicles. These objects provide multi-path components which are advantageous for signal reception in the NLOS case.

After safety applications were considered, a number of scenarios were identified, where vehicular channel measurements were made. The measurement locations were carefully selected so that a general conclusion could be drawn about each scenario. All measurement sites are located in Leicester, UK. 2-4 measurements runs were performed in each scenario in order. These measurements may be enough to obtain meaningful statistics because it collected at different times. The scenarios are discussed in detail below.

Chapter 4: Channel Measurements and Analysis

Radio propagation and network performance data were collected in four different intersections with non-perpendicular angles. These intersections were selected based on different ray-path geometries, the density of buildings and sizes. They also provide NLOS propagation conditions of varying degrees.

In each scenario, the transmitter (Tx) was kept in a constant position. Data were collected by moving the receiver (Rx) at regular intervals (each 100 cm) along a specific path. The equipment was always constant during data collection and the distance is a displacement from the centre of the intersection. Traffic was normal during data collection to study its effect on signal propagation in the channel. The distances between one location and another were measured using a laser rangefinder Bosch, (2018) that had an accuracy of 1 mm.

In this Chapter, some important parameters are presented for describing the time-variation of vehicular ad-hoc network communication channels caused by mobile reflectors during the collection of data. These parameters are peak power, PDR, Doppler spread and coherence time which describe the time-varying nature of the channel in a small-scale region.

4.1. Scenario One

Figure 4.1 illustrates the first scenario in which measurements were taken was the roundabout intersection that has been deployed in the four-way intersection with three wider streets and one narrow street. This intersection has two lanes in each driving direction for four-way. This intersection is between London Road and Victoria Park Road. In addition to that, it has a roundabout of radius 15 m. Furthermore; this roundabout has some trees and grass. The intersection was divided into two parts. The first part contains multi-story buildings from one side of the road and the other side contains a green area surrounded by a row of trees. Second part has multi-story buildings situated at each corner of the intersection. The width of the intersection in this scenario is 47 m and the width of the roads was at 30 m at the intersection. These objects (trees and buildings) provide multipath components which are helpful for signal reception in NLOS situation and to block the LOS or act as a scatterer. The transmitter is placed on the narrow street with the receiver moved on both sides of the intersection. The different building geometry on each side of the intersection provided an opportunity to study the effect of buildings on propagation. The open area surrounded by a row of trees offers the opportunity to study its effect on propagation. The data collected from this intersection contained a combination of line-of-sight (LOS) and non-line-of-sight (NLOS) conditions, 30 positions with LOS and 70 with NLOS conditions. Blue circle represent the transmitter location and the yellow circle represent the initial receiver location, respectively. The green arrows in the figure show the path of the receiver. The receiver was on the pavement to avoid any congestion when passing cars during the measurement process. The data were collected in this intersection in two stages. The first stage is as the Rx approaches the Tx. The length of this stage is about 55 m. The second stage was 45 metres long, as the Rx receded from the Tx.

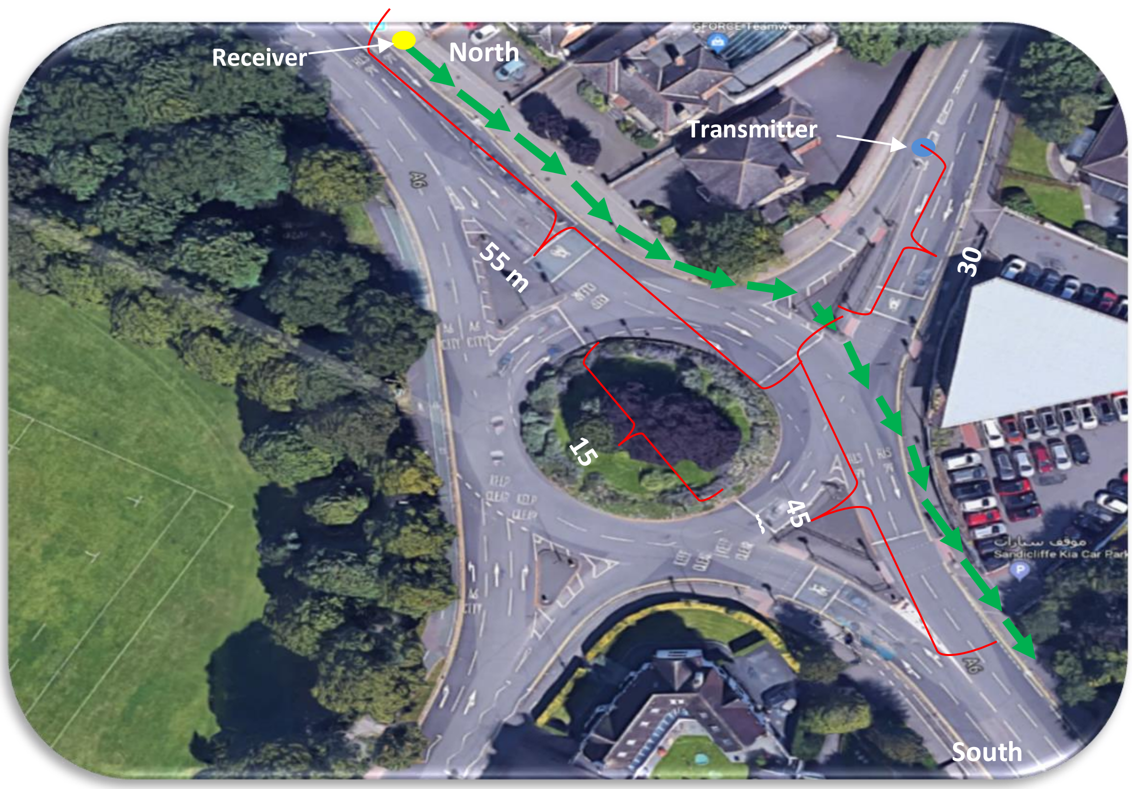

Figure 4. 1 Roundabout intersection scenario (first scenario)

4.1.1. Median Peak Power and Packet Delivery Ratio Analysis

Figure 4.2 and Figure 4.3 show PDR and peak power resulting from the collection of data obtained from six data collection runs on different days in the roundabout intersection. Table 4.1 presented more details about these runs. The average of these data was calculated to produce the graph, which presents the general trend of the PDR and peak power. Individual runs are discussed subsequently. The data were varied as the receiver was moved away from the centre of the intersection in either direction.

Table 4.1 Details of the different measurement runs in the scenario one.

No.	Type of scenario		Distance Range (m)	Distance Resolution (m)	Date	Start time	Vehicles speed (mph)
1	North-side Roundabout intersection	Run1	0 - 55	1	22-10-2017	10:01	30
		Run2				13:05	
		Run3				16:18	
2	South-side Roundabout intersection	Run1	0 - 45	1	23-10-2017	11:00	30
		Run2				14:05	
		Run3				17:01	

In general trend, at the centre of the intersection (LOS region), both the PDR and peak power start high and then decrease as the receiver moves away from the intersection to the NLOS region. The dropping of peak power and PDR is nearer to the centre on the north side where fewer buildings on one side of the road, compared with the south side which has more buildings on either side to reflect the radio waves. That is, when the number of buildings decreases, the received power decreases, resulting in reduced performance. On the north side of the intersection, the PDR is above about 98% up to 15m and drops below 60% within 24 m. On the south side of the intersection, which contains more buildings, the PDR remains at 98% up to 21 m and does not fall below 90% during the first 35 metres.

On the south side, the PDR starts to fluctuate between 0% and 60%. These cases are not suitable for vehicular safety applications. On the other side with the open area, the signal passes through fluctuations after 21 m and start to stabilise at 0% after a distance of 48 m. Therefore, it will not be possible to have vehicular safety applications exceeding about 25 m.

Although there are PDR heights after that distance, the system will not provide reliable connections. There is approximately 10 m extra in the south side of the intersection which is likely to be caused by multipath propagation due to signals reflected by buildings on either side of the road.

In addition to the above, traffic has a strong impact on the success of data transfer. Depending on the state of traffic, moving objects (cars, vans or trucks) that are blocking the LOS between Tx and Rx or as reflectors cause severe performance differences. However, the fluctuations in the signal on the north and south sides of the intersection may be due to the passage of cars of different sizes that acted as reflectors (whose effects will be explained in detail in Chapter 5).

The peak power in these Figures decreases sharply with the entry into the NLOS area but it rises again briefly and can be seen on both sides of the roundabout intersection. The decrease in peak power is not smooth on either side. The fluctuation of peak power in the LOS on both sides is due to uncontrolled traffic flow.

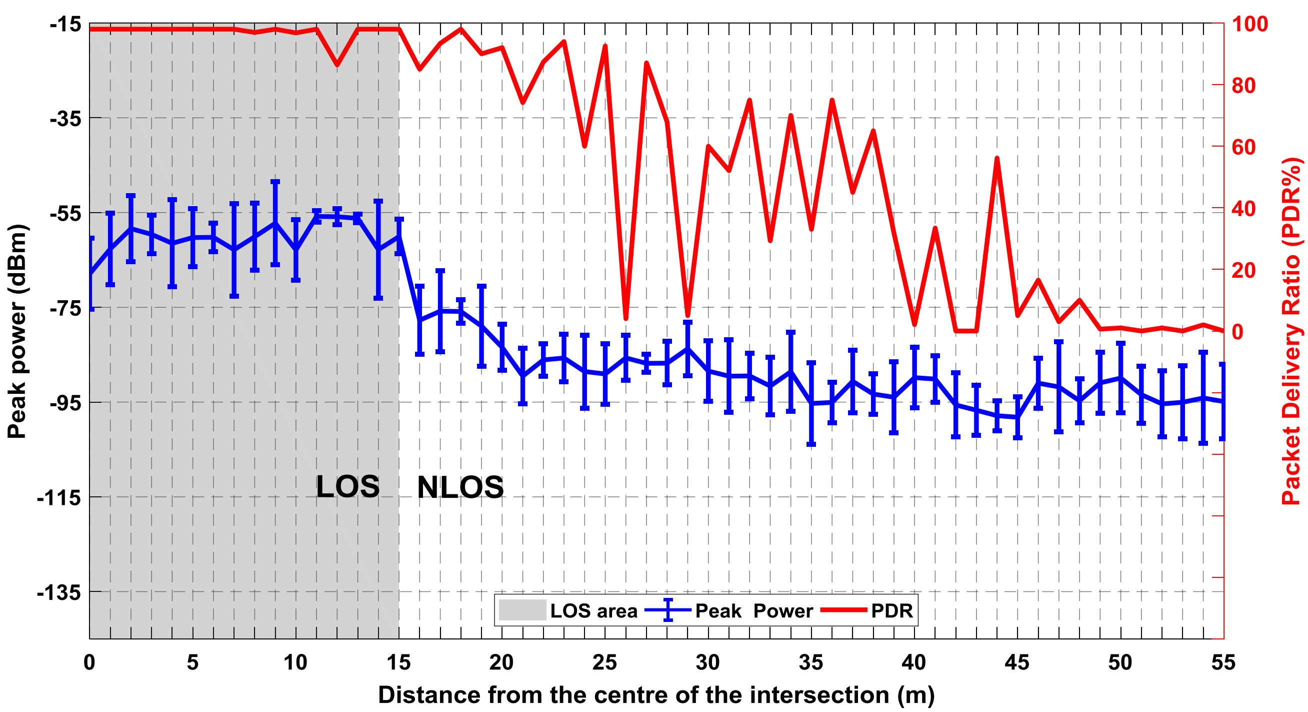

Figure 4.2 Packet delivery ratios and peak power for all the data collected in the North side of roundabout intersection

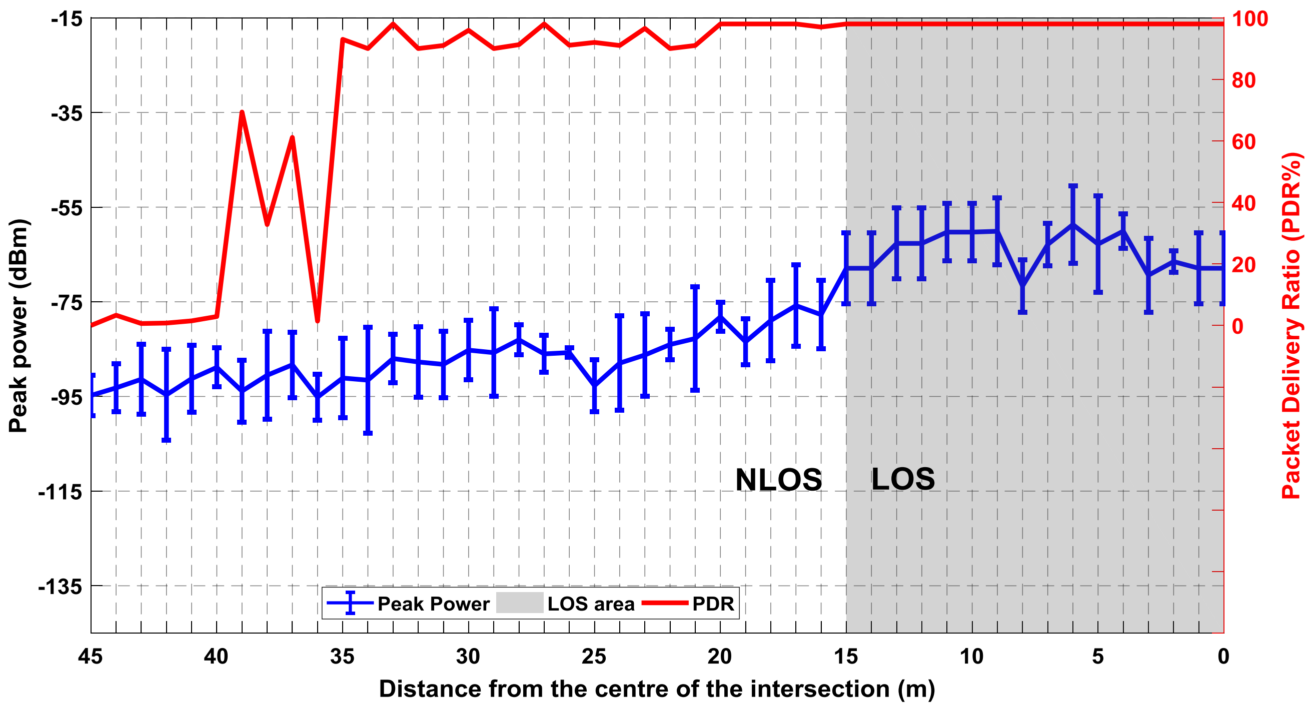

Figure 4.3 Packet delivery ratios and peak power for all the data collected in the South side of roundabout intersection.

Figures 4.4 and 4.5 show graphs of the data collected in the roundabout intersection from the separate runs. On the north side, although there are some similarities in the run between 1, 2 and 3, they have some positions where peak power differs by about 15 dBm.

For example, in run 1, the peak power differs from runs 2 and 3 at 40 m, while the second run differs from the first and third runs by about 7 dBm at position 0 m. The difference in peak power between runs 1, 2 and 3 can be referred to vary in the propagation environment such as parked cars, the size of vehicles and pedestrians which would contribute to the signal fluctuation being higher in certain positions and lower in other positions due to the combination of multipath components at the receiver.

The PDR in run 1 is also approximately 98% throughout with two major dips 2% at distance 26 m and 3% at distance 29 m. This drop may have resulted from a truck passing between the transmitter and the receiver depending on the video recorded at those moments at these distances. After 29 m, PDR suffers from fluctuation of about 75% to 35% to a distance of 40 m then starts to decline until it reaches 0%.

In the run 2 and 3, the PDR declines in the LOS area, but not deeply, up to about 95% and 90% at 8 m and 15 m and 90% at 11 m, in run 1 and 2 respectively. In these runs, the PDR started to fluctuate between about 90% and 45% to 34 m. At 35 m, it is close to 0% then started fluctuation between 0% and 80%. At a distance of 44 m, PDR starts from the drop to reach 0%.

On the south side, data were collected on the same day. Run 2 was the return leg starting from d = 55 m and ending at d = 0 m. Due to the relatively short time between each operation during which the data were collected, it is assumed that the radio channel did not change much, especially in the range of distances (30 – 45 m) between the first and second runs and the range of distance (0 - 15 m) between the second and the third runs. Figure 4.6 shows that the three runs follow a similar pattern of decay when it comes to peak power but there is a significant difference between the data at the range of distances (0 - 3 m), and (13 - 17 m) respectively.

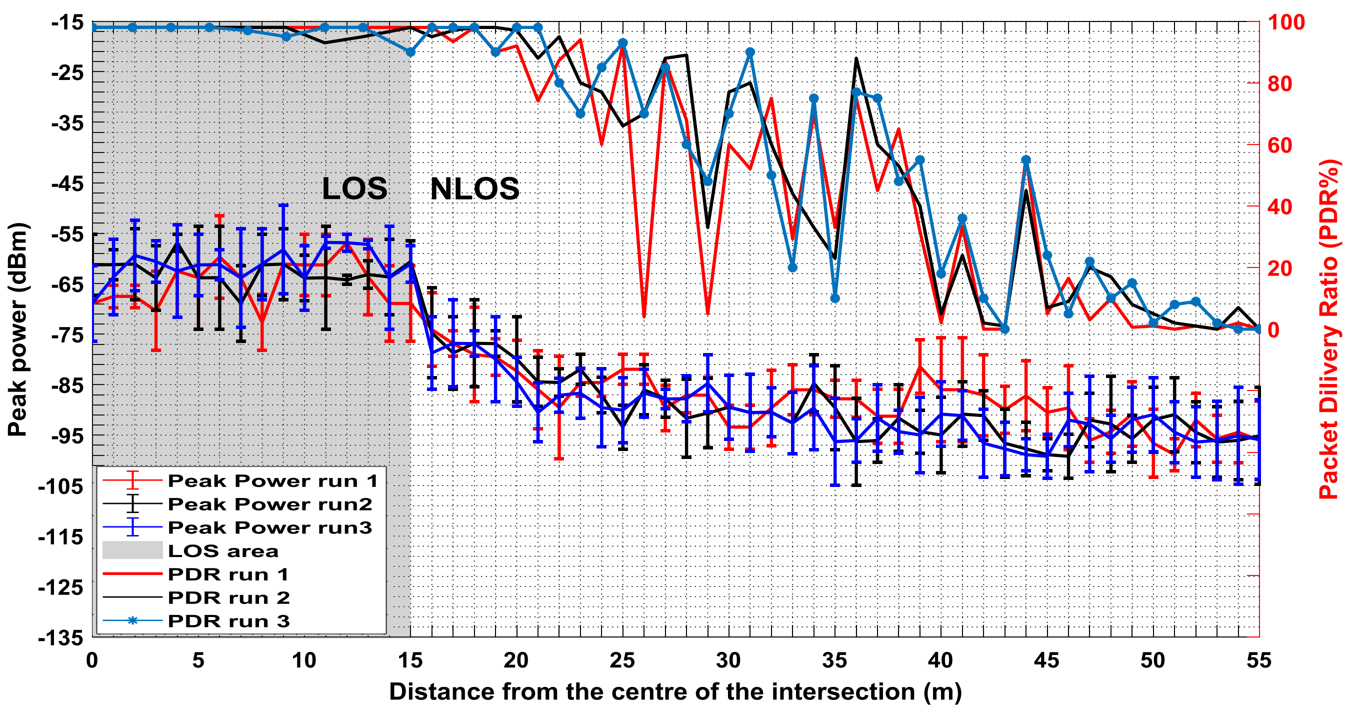

Figure 4.4 Packet delivery ratio and peak power for all the data collected in the north side of the roundabout intersection for each run.

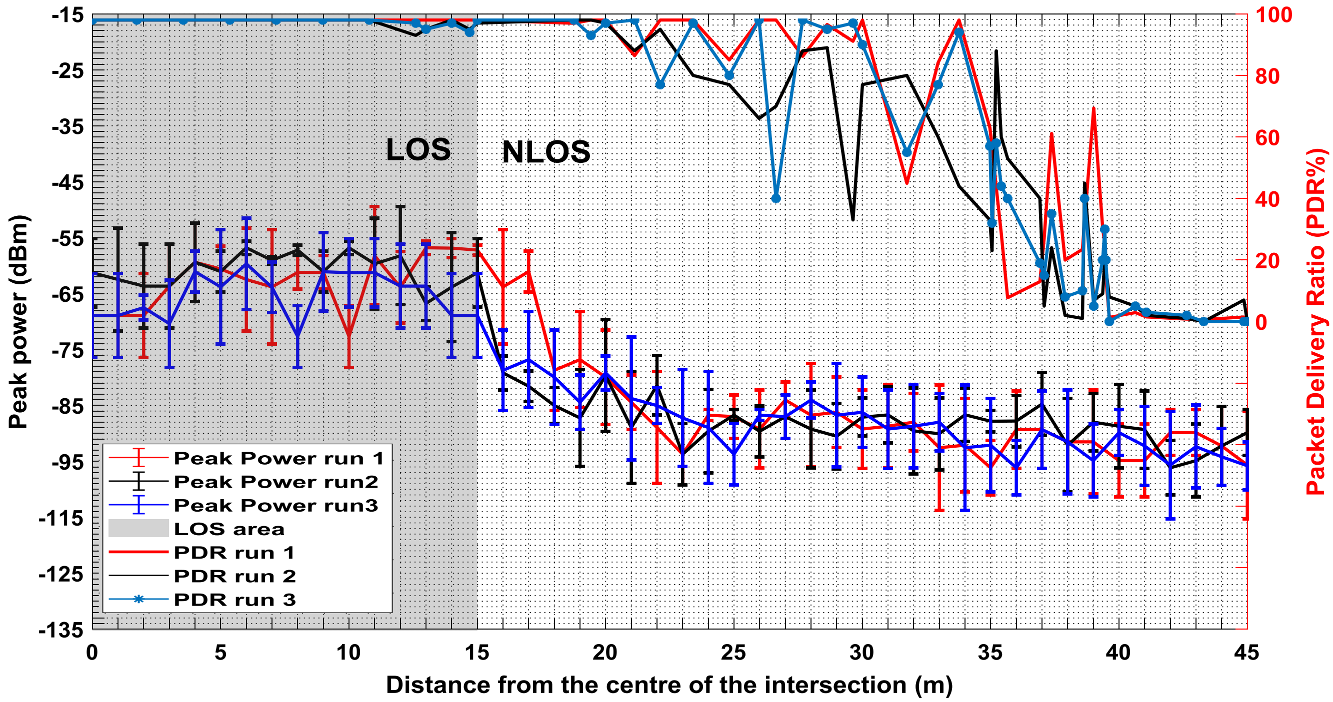

Figure 4.5 Packet delivery ratio and peak power for all the data collected in the south side of the roundabout intersection for each run.

The PDR in the south side seems to be similar up to a distance of 21 m. After this point, a significant difference was observed in the PDR between the three runs, sometimes the difference being approximately 80%, such as at 29 m.

The amplitude difference between runs (denoted by the error bars) in the north side tends to be larger than in the south side runs, where the distances from the intersection centre were similar but different locations (on the other side of the junction). This difference is explained by the few numbers of stationary and moving reflectors in this part of the intersection. As well as the pedestrian traffic, because of which some of the radiation pathways that would have been received would be disrupted, will be reflected elsewhere. The peak power is also varied because, with traffic, ray paths, continue to change, causing a multipath propagation and the receiving waves add constructively / destructively depending on their phase, which depends on the length of the propagation pathway, which depends directly on the mobile reflector.

4.1.2. Comparison of observations of power with the NLOS model

In this Section, the data obtained using the dual-measurement system will be compared against an NLOS path-loss model at 5.9GHz frequency named VirtualSource11p (more details in Section 2.3).

Figures 4.6 and 4.7 illustrate the NLOS peak power of all data collected from scenario one along with the prediction model provided by virtualsource11p (dashed lines) as a function of distance.

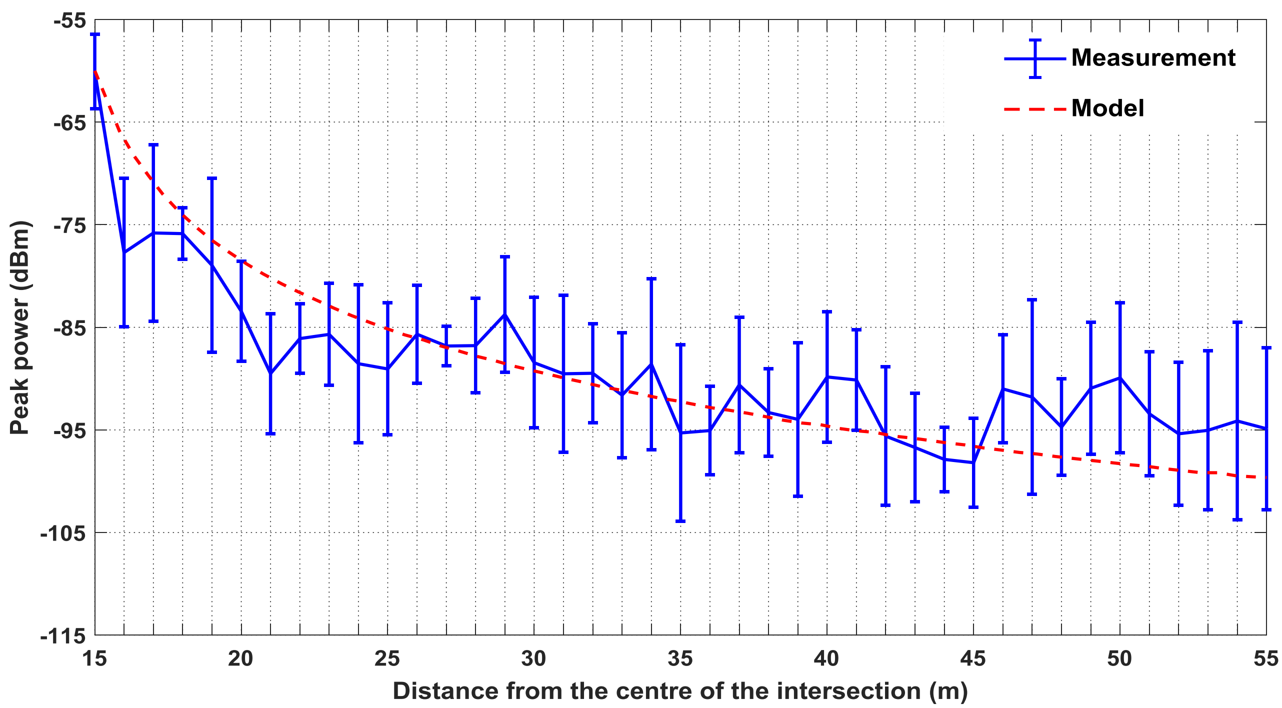

Figure 4.6 Peak power as a function of a distance from the north-side of roundabout intersection: measurement and virtualsource11p model.

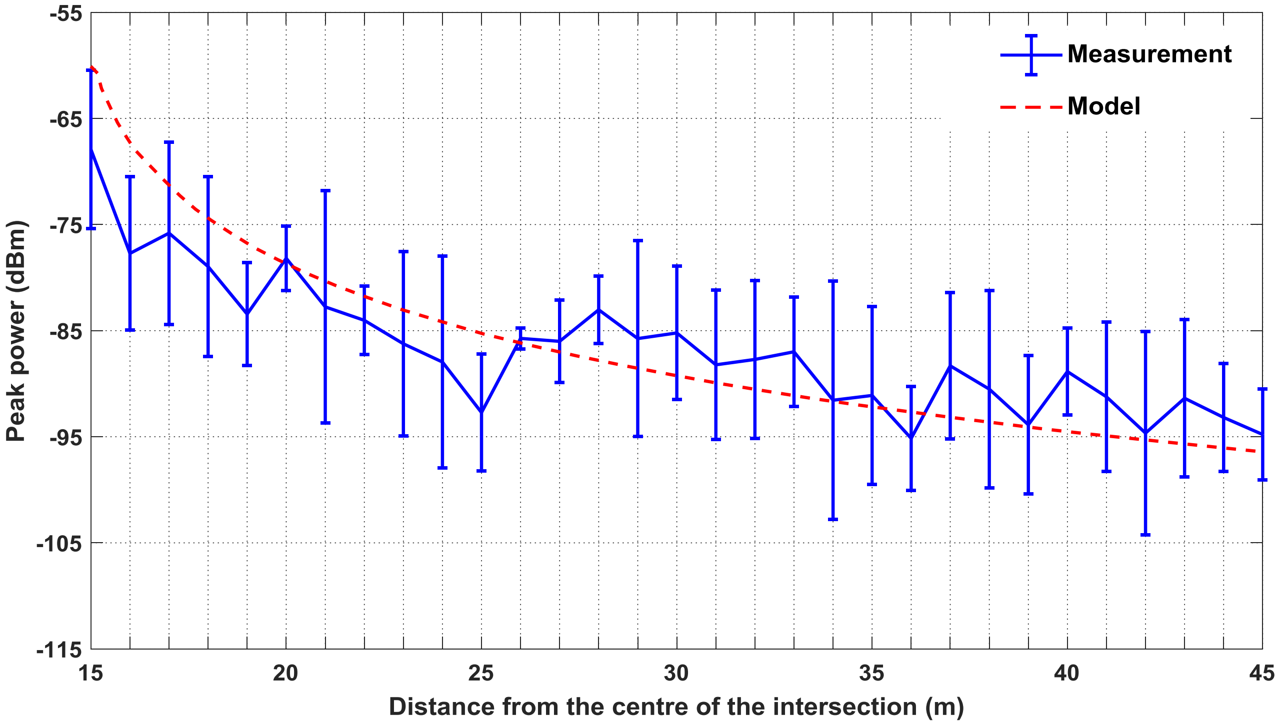

Figure 4.7 Peak power as a function of a distance from the south-side of roundabout intersection: measurement and virtualsource11p model.

It can be seen from this Figure the measurement data contain agree well with the NLOS model although the difference in each position (as shown in the error bars) and the nature of the signal decay change. The difference in the model and measurement starts to grow for distance > 45 m. The reason behind this is the open space on this side of the intersection which has few reflectors. The difference in some of these sites may be due to temporary changes such as the passage of vehicles of different sizes or the nature of the place such as in the sloping streets and differences in the forms and sizes of buildings.

4.1.3. Doppler Spreads Analysis

4.1.3.1. LOS Test

Figures 4.8 and 4.9 show all the spectra collected at LOS conditions on the north side and south the side of roundabout intersection respectively. The spectra which were collected at each position are grouped together and the power in the continuous (CW) wave is shown by the horizontal coloured band which goes through the middle of the chart. The centre frequency is located at 5.9 GHz with an observation span of 500 Hz, and the observed noise level has -95 dBm. It is possible to view all the spectra collected through data collection along with visualizing the Doppler spreads caused by traffic. The chart also offers how the power in the CW changes at each location. An advantage visible in each of the mesh is that the frequency of the CW drifts by a few Hertz. The Doppler spreads are long, these are all caused by traffic. This was noticed on the spectrum analyser screen during data collection. On some distances near the centre of the intersection, it was simply not possible to record accurate information about moving wave reflector numbers.

In Figure 4.8 the data were collected on the north side of the intersection where there are more open spaces than the other side of the intersection. Doppler spreads have a large range and are within 450 Hz of where the peak of the CW. Depending on the wave reflectors, Doppler spreads fluctuated between 50 and 450 Hz. Table 4.2 shows some of the interesting areas where Doppler spreads have occurred.

In the south side of the intersection (Figure 4.9), there are more Doppler spreads in these data sets as there were a lot of moving reflectors (vehicles).

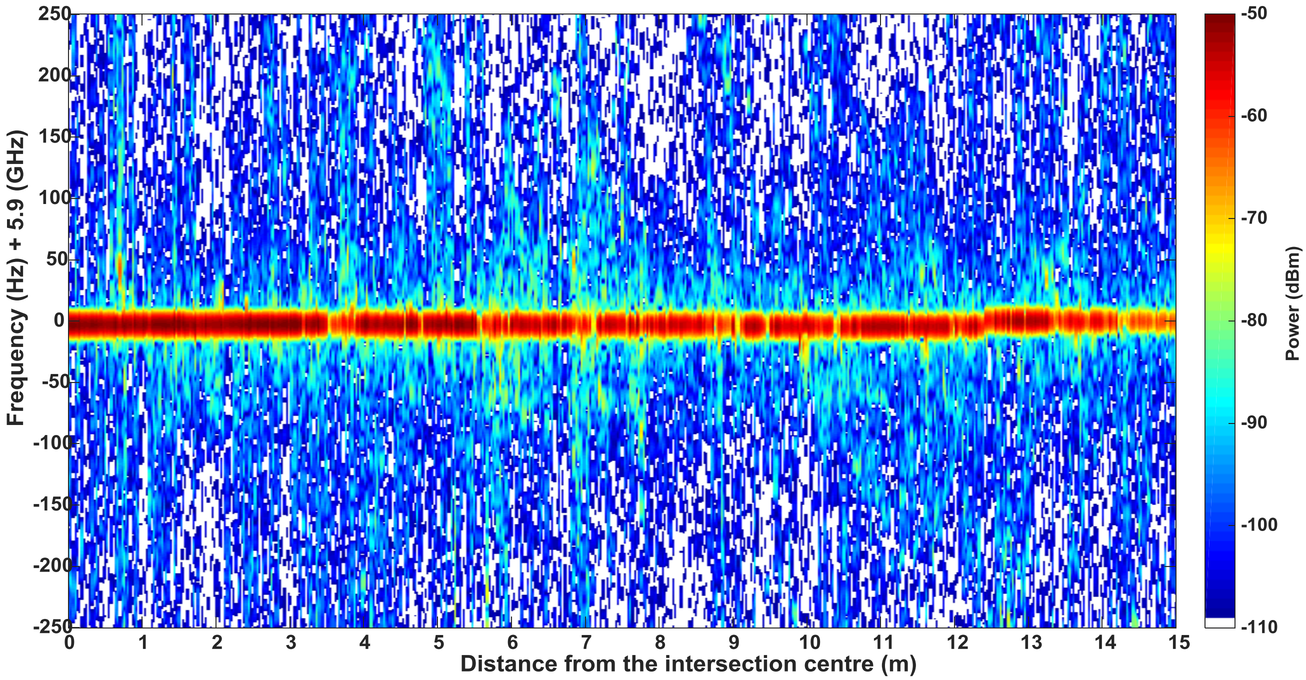

Figure 4.8 All the spectra collected for LOS condition in the north side of the roundabout intersection

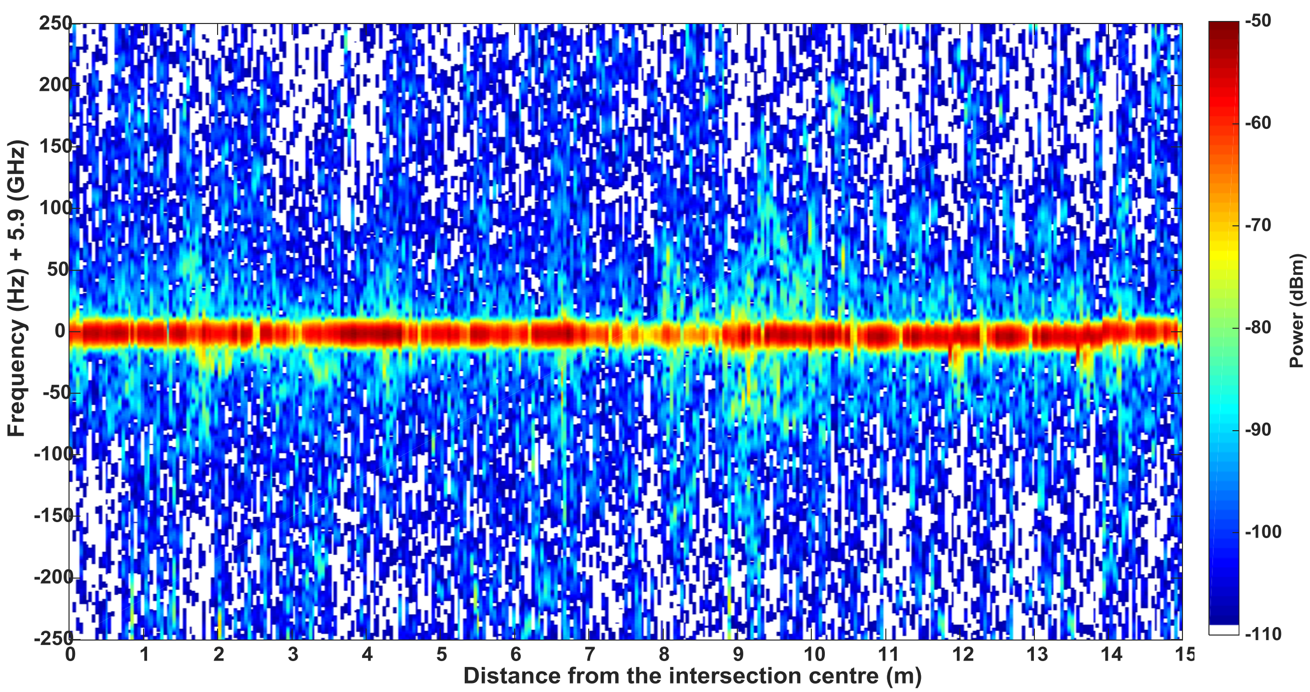

Figure 4.9 All the spectra collected for LOS condition in the south side of the roundabout intersection

The largest Doppler spreads can be found at distances of 3, 7, 10 and 12 m on the north side of the intersection. These Doppler spreads have extended beyond 457 Hz and in the case of data collected at 7 m. Table 4.2 has more significant Doppler spreads have occurred.

Figure 4.10 shows the empirical cumulative distribution functions Doppler spread for data measured in LOS conditions in roundabout scenarios. It shows the values of Doppler spreads that occurs in IVC. Under LOS conditions the Doppler spreads are similar for both the side of this scenario. Despite relatively low speeds in the centre of the intersection, Doppler spreads are still apparent, though 90% are less than 125 Hz and 80% are less than 50 Hz. This may be attributed to the high degree of scattering present in urban environments, leading to multiple angles of arrivals at the receiver.

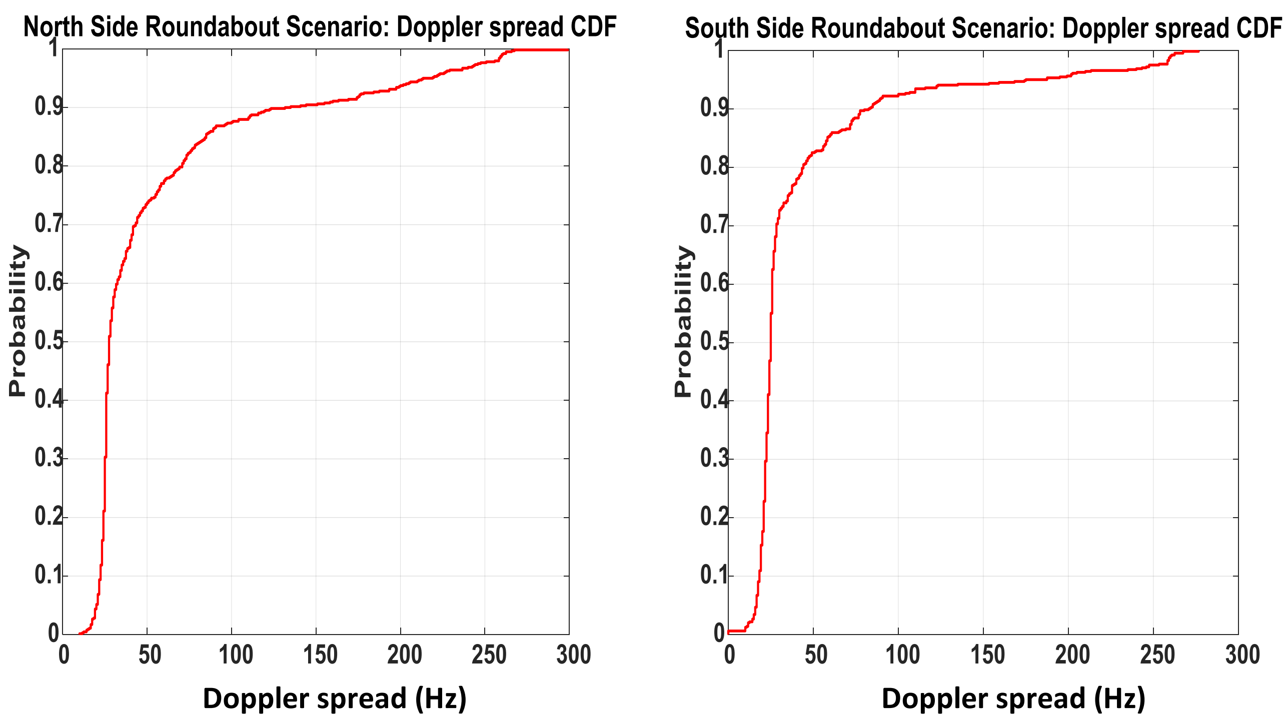

Figure 4.10 Empirical CDF for Doppler spread for the LOS tests of the roundabout intersection

Table 4. 2 Significant Doppler spreads

Scenario Condition	Distance (m)	Doppler spread (Hz)	Observed traffic
LOS (north side of intersection)	1	305	Truck
	3	413	Large van
	4	263	Car
	6	282	Car
	7	457	Traffic burst
	9	266	Truck
	10	450	Large van
	11	372	Sports Utility Vehicle
	12	417	Bus
	13	325	Truck
	14	318	Car
LOS (south side of intersection)	-1	276	Truck
	-3	214	Car
	-6	452	Truck
	-7	301	Large van
	-8	286	Car
	-9	266	Large van
	-10	319	Car
	-12	283	Bus

4.1.3.2. NLOS Test

All spectra collected for NLOS condition in the north and the south sides of the roundabout intersection are shown in Figure 4.11 and Figure 4.12. It is clear in these two Figures that there is less power being received at NLOS condition compared with the LOS that was closer to the centre of the intersection.

Figure 4.11 shows that there are fewer high Doppler spreads than in the LOS area. At 20 m was the largest Doppler spread which was 260 Hz, resulting from a big vehicle passing through the road being used. On the other hand, in the south side of the roundabout intersection (Figure 4.12), many Doppler spreads were observed where the reflected waves reach values close to 300 Hz at different distances away from the centre of the intersection where the CW signal had more power, resulting in the ability to detect larger Doppler spreads. The number of Doppler spreads and their ranges is a direct indication of the increased number of mobile reflectors, in comparison with the data collected on the north side of the intersection. The highest recorded value for Doppler spreads in this side is 24 m away from the intersection centre where it was 380 Hz. Table 4.3 has more significant Doppler spreads in the NLOS scenarios.

Figure 4.13 presents the empirical CDFs of Doppler spread for the data measured in NLOS conditions in the north and south sides of the roundabout intersection. In the figure, 90% of the Doppler spreads are below 19 Hz in the north side of the intersection while 90% of the Doppler spreads are below 20 Hz in the south side of the intersection. This is an expected result, because of open area in the north side and low degrees of mobile reflectivity in the south side were initially anticipated due to the decreasing number of reflectors.

These are a lower value than in the LOS region, and the reason for this is that the received power is lower. The Doppler spreads in the LOS conditions appear to be significant compared with NLOS conditions in the same scenario.

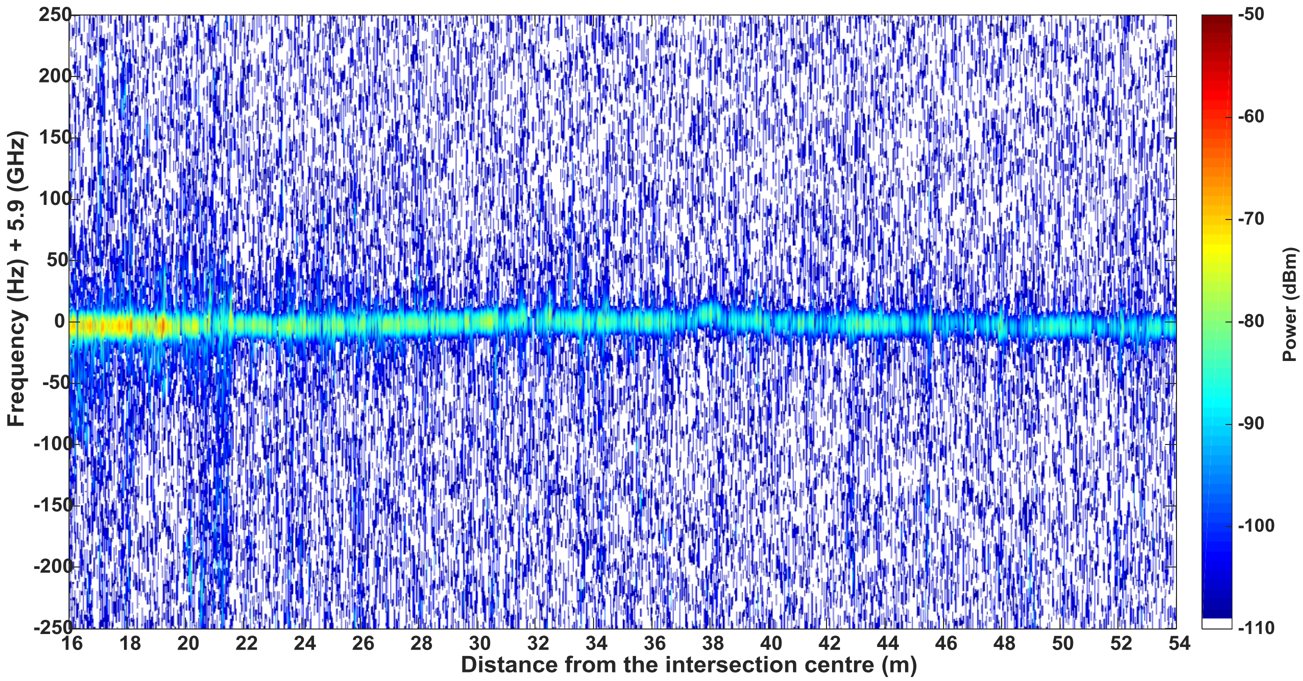

Figure 4.11 All the spectra collected for NLOS condition in the north side of the roundabout intersection

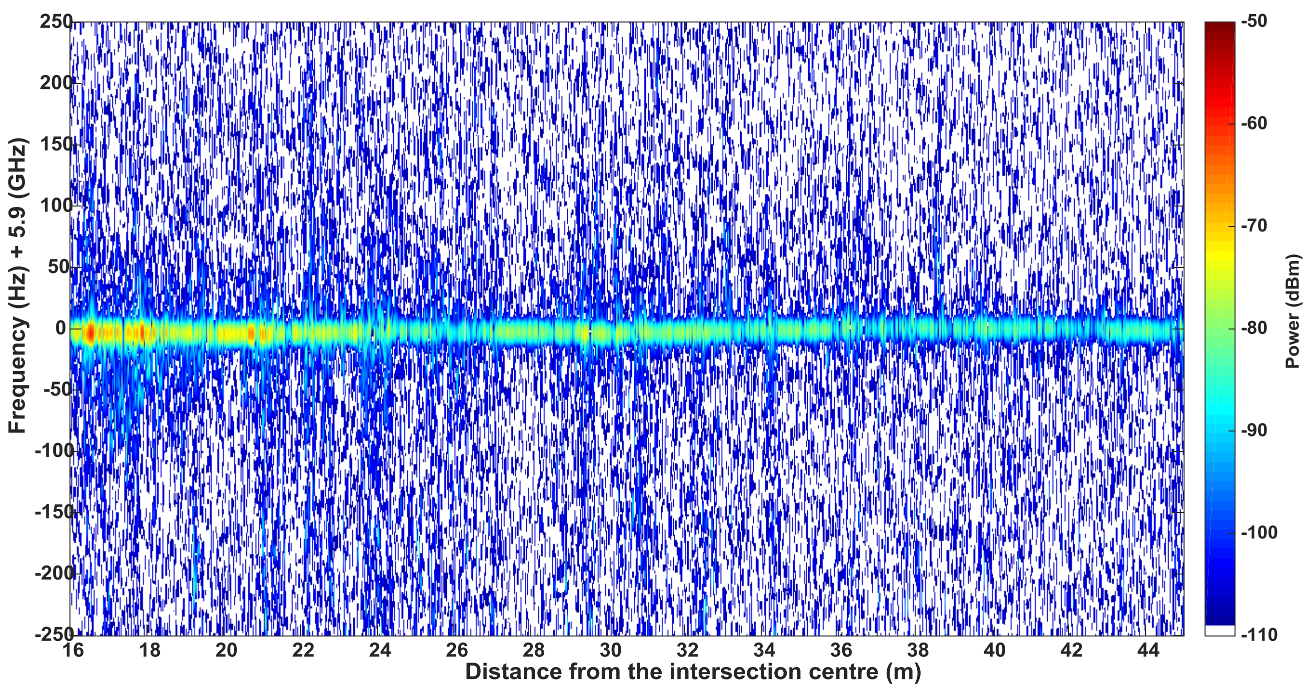

Figure 4.12 All the spectra collected for NLOS condition in the south side of the roundabout intersection

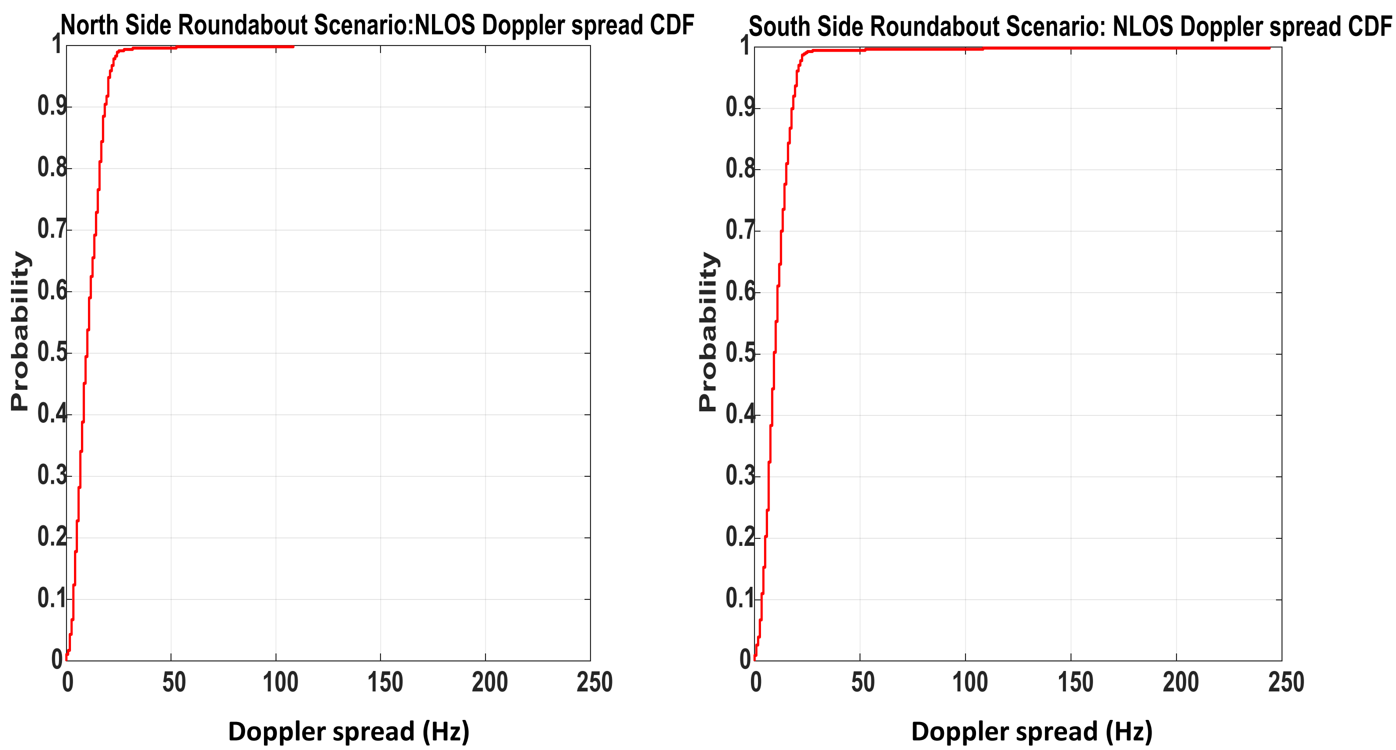

Figure 4.13 Empirical CDF for Doppler spread for the NLOS tests of the roundabout intersection

Table 4.3 Significant Doppler spreads

Scenario Condition	Distance (m)	Frequency (Hz)	Observed traffic
NLOS (North side of intersection)	17	253	Truck
	20	260	Large van
	33	255	van
	42	248	Large van
	47	210	Bus
NLOS (South side of intersection)	-17	222	Sports Utility Vehicle
	-20	251	Large Truck
	-22	255	van
	-23	245	van
	-24	380	Truck
	-31	375	Car
	-34	320	Bus

As previously mentioned, coherence time is used to describe the time-varying nature of the frequency of the channel. In Figure 4.14 the period of time over which the channel is constant and equal to 2 ms in the LOS condition. In the NLOS condition, there is no change in coherence time in the south side of the experimental area until it reaches about 20 m and then a slight change to a distance of 31 m followed by a marked change in time. While it was found that the coherence time in the north side of the experimental area had changed significantly at a distance of 21 m due to the lack of reflections of the signal transmitted compared to the other side.

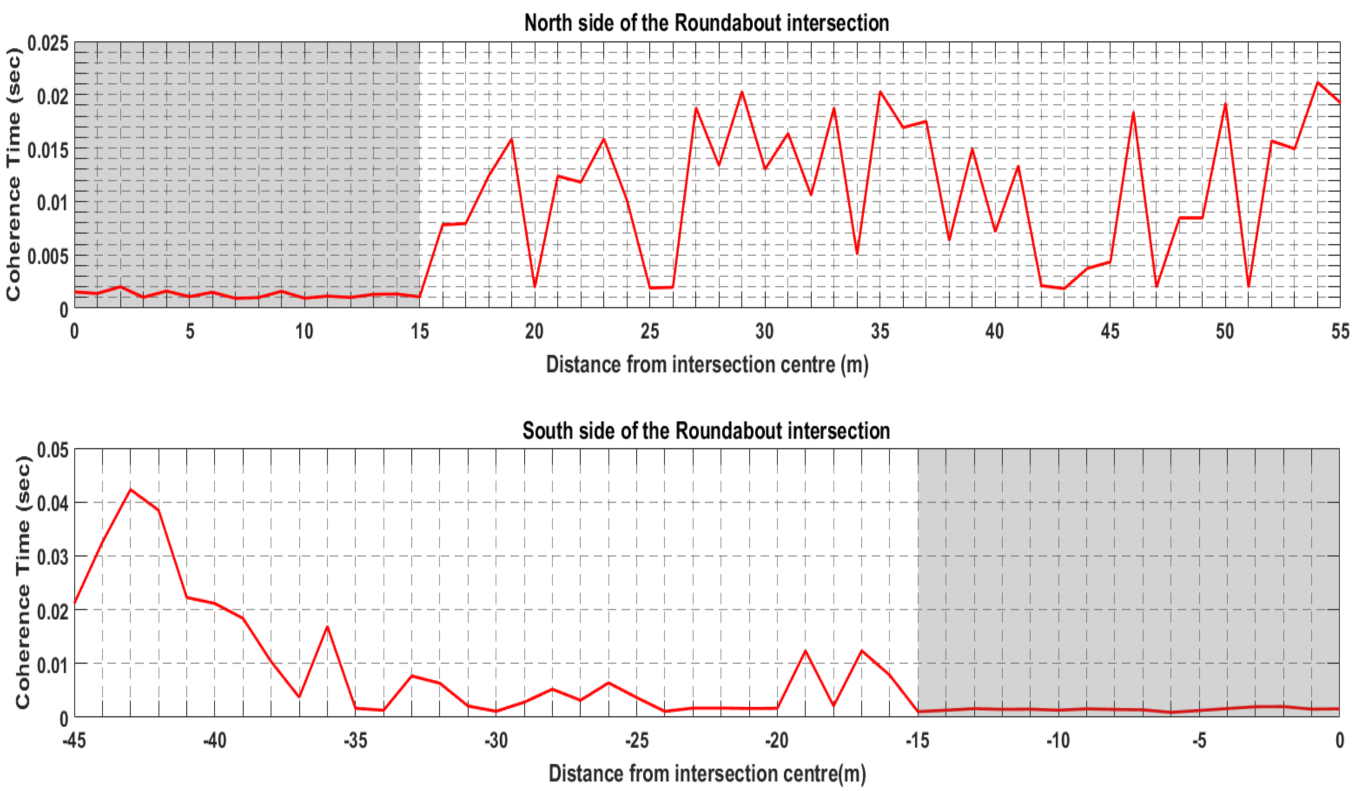

Figure 4.14 Empirical coherence time for the north side and south side of the roundabout intersection

4.2. Scenario Two

Figure 4.15 illustrates the Y-junction scenario which consists of the intersection of Victoria Park Road and Queens Road. An important aspect of this scenario is the possibility of barriers, buildings or trees between intersecting streets. It is a three-way intersection has two lanes in each driving direction. The intersection of Queens Road contains multi-story buildings on both sides, as well as some trees on both sides of the road. The side of Victoria Park Road has multi-story buildings on one side and on the other is a green area surrounded by a fence of trees. The width of the intersection in this scenario is 40 m and the width of the roads was at 20 m at the intersection. Blue circle represent the transmitter location and the yellow circle represent the initial receiver location, respectively. Green-coloured arrows represent the path of the receiver, moving away from the TX. The Y-junction scenario is characterized by the roads that are used to merge two traffic flows into one, e.g., entrance or exit roads. An important part of this scenario is the likelihood of a blocked LOS path because of buildings or trees between the intersecting roads. The size of the buildings between the transmitter and receiver grows as the receiver moves away from the centre of the intersection.

Data were collected at this intersection from 55 positions in three runs; 15 of these positions had line-of-sight (LOS) conditions and 35 had non-line-of-sight (NLOS) conditions. Table 4.4 presented more details about these runs. The transmitter was 30 metres from the intersection centre for all data collected and the receiver was moved along a 55 metres path away from the centre of the intersection. The transmitter and receiver were on the roadside instead of being on the road due to the traffic. Traffic data was recorded by the laptop camera to find out why there was an unexpected difference between the links due to differences in traffic density. In this case, data was collected until the PDR consistently dropped to single digits if not zero.

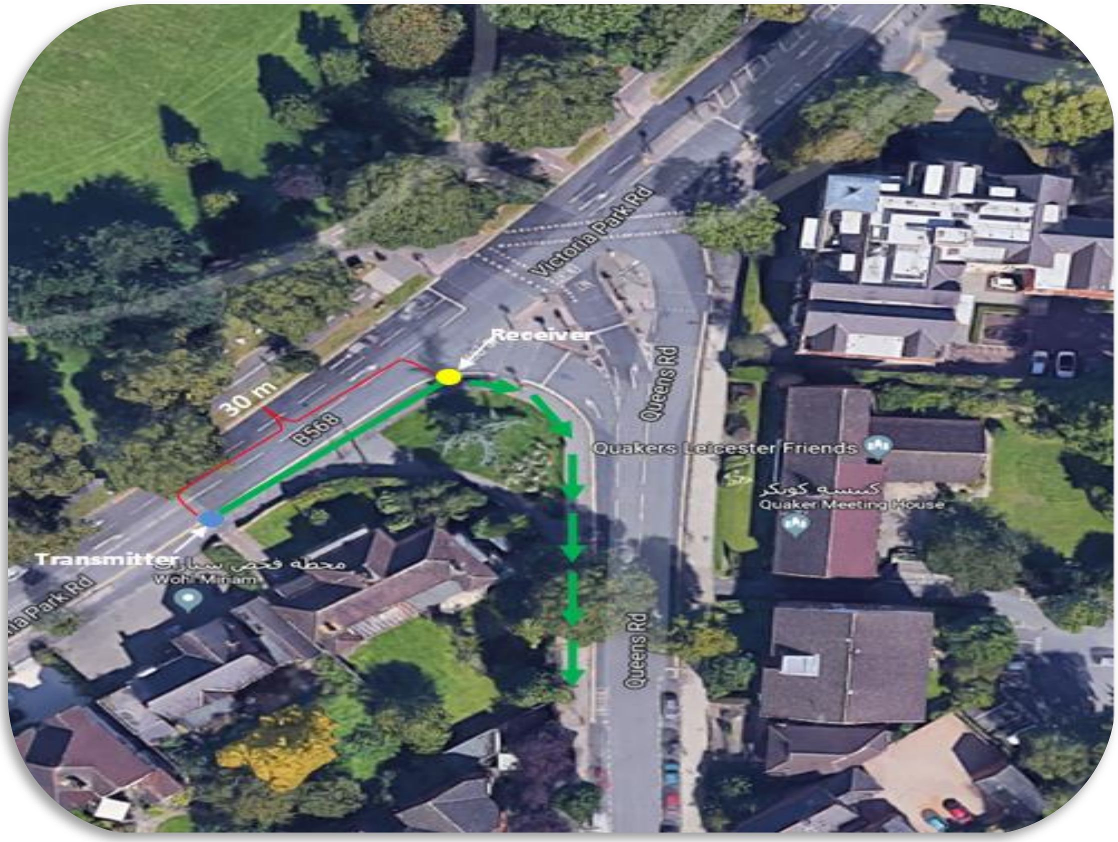

Figure 4.15 Y-junction intersection scenario (second scenario)

Table 4.4 Details of the different measurement runs in the scenario two.

No.	Type of scenario		Distance Range (m)	Distance Resolution (m)	Date	Start time	Vehicles speed (mph)
1	Y-Junction	Run1	0 - 55	1	30-01-2018	10:01	30
		Run2			01-02-2018	13:05	
		Run3			03-02-2018	16:18	

4.2.1. Median Peak Power and Packet Delivery Ratio Analysis

Figure 4.16 shows the PDR and peak power for the data collected in the Y-junction scenario resulting from the data obtained from three data collection attempts which present the general trend for them. Where the shaded part of the graph indicates where LOS communications are located. The first important drop in PDR occurs at a distance of 32 m, where it drops approximately 30%. From the distance of 32 m onwards, there is a great fluctuation in the PDR where it fluctuates between 90% and 50% for most of the rest of the data collected up to 49 metres distance, where it drops to less than 30%. It can be said that up to 49 metres there is an acceptable level of communication although after 41 m it may not be suitable for critical safety operations. The peak power decays slowly and is mixed with fading. There is also a significant difference in the peak power at each point, as described in the error bars. The fluctuation in the LOS region is due to the passage of a number of vehicles of different sizes that acts as reflectors. This significant fluctuation is expected to be noted in that region due to changing environmental conditions (such as reduced vehicular traffic) favourable for communication or improvement due to environmental engineering, causing multipath propagation resulting in increasing the received power.

Figure 4.17 shows all the data collected in the range 0 – 55 m in the Y-junction intersection from the separate runs. The grey shaded area represents the LOS region. The red, black and blue lines are used to represent the data collected in the 1, 2 and 3 runs respectively. An important observation is that the PDR and peak power are very similar to each other closer to the intersection centre. At 24 m the peak power in run 2 is significantly higher and stays higher for most of the distances until 51 m. The PDR is not too different between the three lines. There are a few places where the PDR falls below 90%, but most of the time it ranges between 90% and 98% until 50 m. Beyond 50 m, the PDR fluctuates for most of the positions. It is believed that the propagation conditions were significantly different in the days when these three sets of data were collected, hence the observed differences in both PDR and peak power. The PDR difference at 47 m is about 40%, which is very important and will not be able to support reliable vehicular communications. The peak power seems most closely correlated, with the difference between the runs being less than 10 dB while the PDR seems fairly different, but they rise and fall together most of the time.

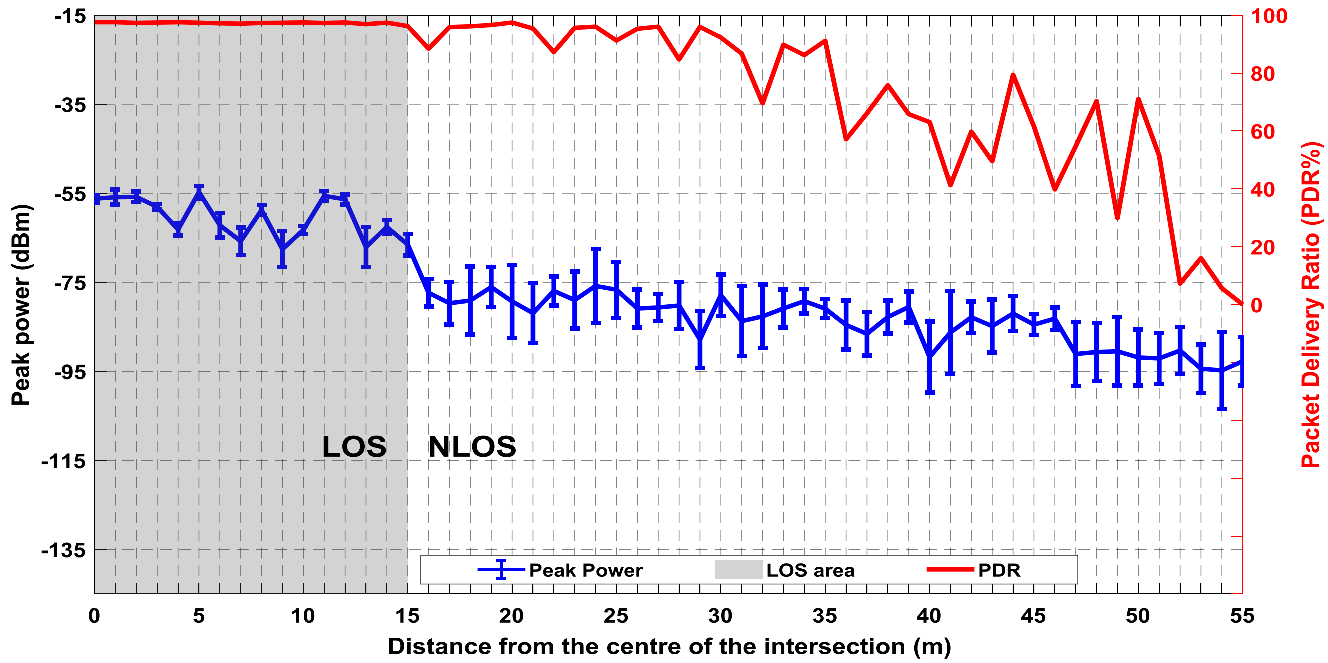

Figure 4.16 Packet delivery ratios and peak power for all the data collected in the Y-junction intersection.

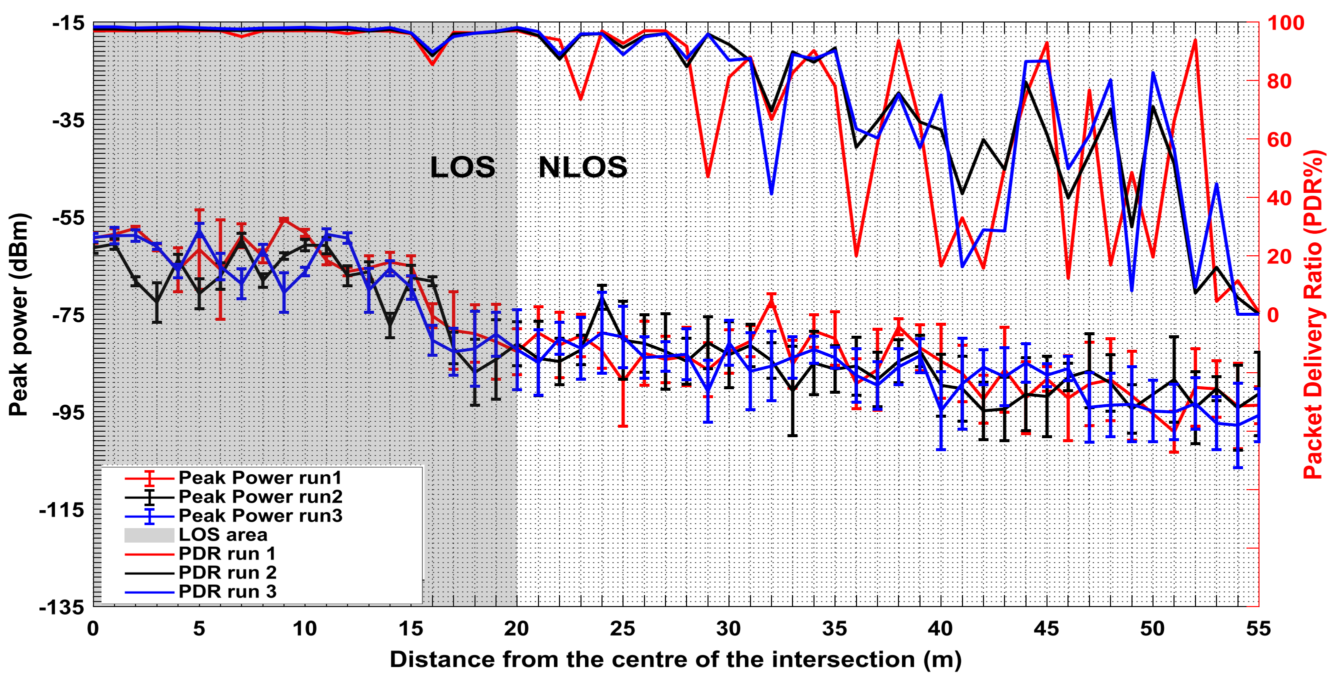

Figure 4.17 Packet delivery ratio and peak power for all the data collected of Y-junction intersection for each run.

4.2.2. Comparison of observations of power with the NLOS model

Figure 4.18 illustrates the NLOS peak power of all data collected from scenario two along with the prediction model provided by virtualsource11p (dashed lines) as a function of distance.

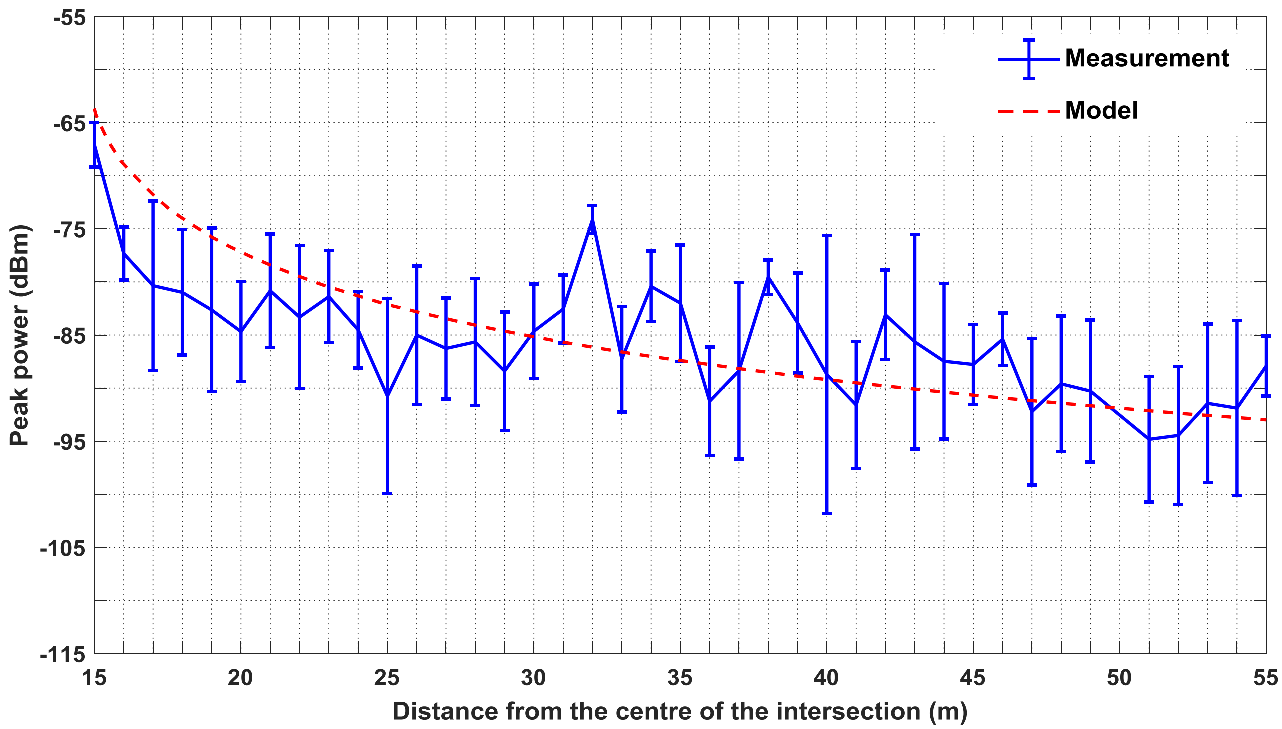

Figure 4.18 Peak power as a function of a distance from the Y-junction intersection: measurement and virtualsource11p model.

it can be observed in this figure that there is a difference in some positions may be due to temporary changes such as the movement of vehicles and the nature of the place, but in general, found that the measurement data on good compatibility with the model.

4.2.3. Doppler Spreads Analysis

4.2.3.1. LOS Test

Figure 4.19 presents all the spectra collected at LOS conditions in the Y-junction intersection. The spectra which were collected at each position are grouped together and the power in the continuous (CW) wave is shown by the horizontal coloured band which goes through the middle of the chart. The centre frequency is located at 5.9 GHz with an observation span of 500 Hz, and the observed noise level has -95 dBm.

In this set, there is a significantly increased occurrence of Doppler spreads, along with larger Doppler spreads, in comparison with the previous intersection. These larger spreads are possibly caused by the presence of vehicles passing near the radio propagation path as well as pedestrians and cyclists. Doppler shifts of reflected waves reach values close to 450 Hz in these measurements, which was data acquired from the LOS area; where the CW signal has more power, resulting in the ability to detect larger Doppler spreads. It is clear from Figure 5.8 that Doppler spreads occurred in most of the positions where data were collected, but the largest value was 14.5 m away from the intersection centre, which was 445 Hz resulting of bus passing during the data collection process. Table 4.5 has more significant Doppler spreads in this scenario.

Figure 4.20 displays the empirical CDFs of Doppler spread for data measured in the LOS condition for Y-junction intersection scenario. For this case, the CDF crosses the 90% threshold at 68 Hz, and the 50% threshold is reached at 28 Hz. The presence of tall buildings as well as trees in the urban environment leads to a high degree of dispersion leading to multiple angles for the future. Again, though the average Doppler spread is only about 2.25% of the 22 Hz subcarrier spacing.

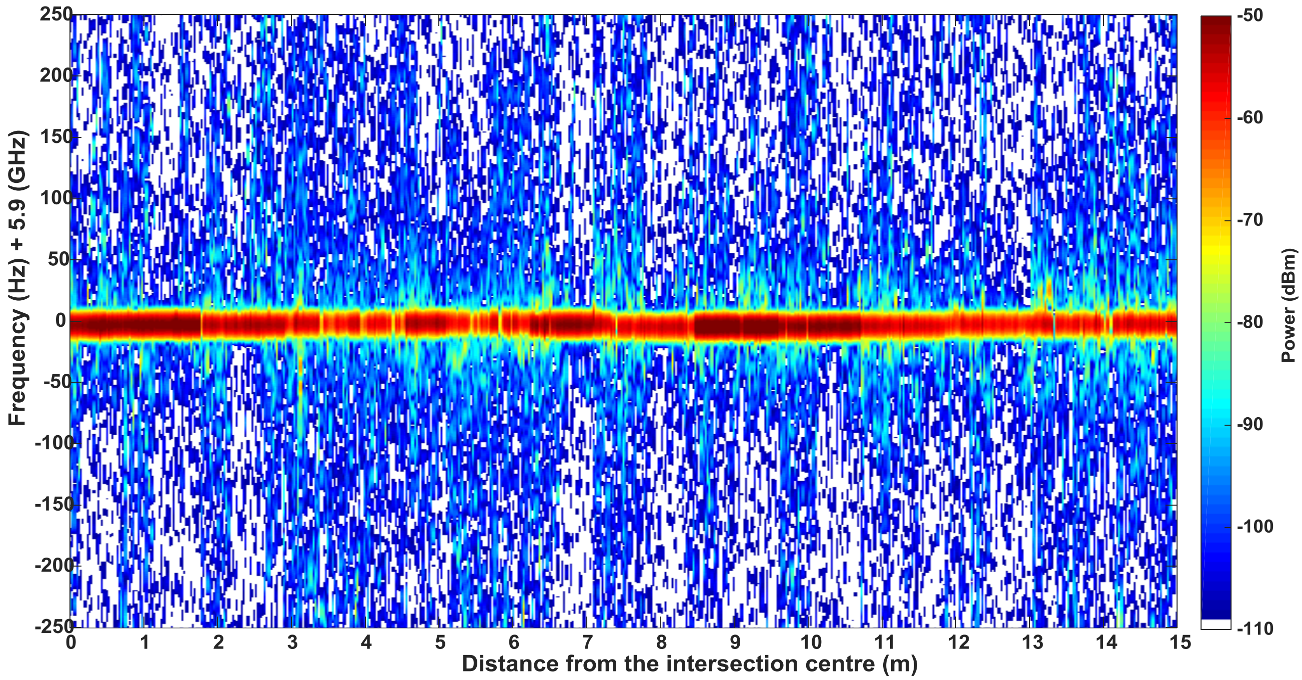

Figure 4.19 All the spectra collected for the LOS condition in the Y-junction intersection

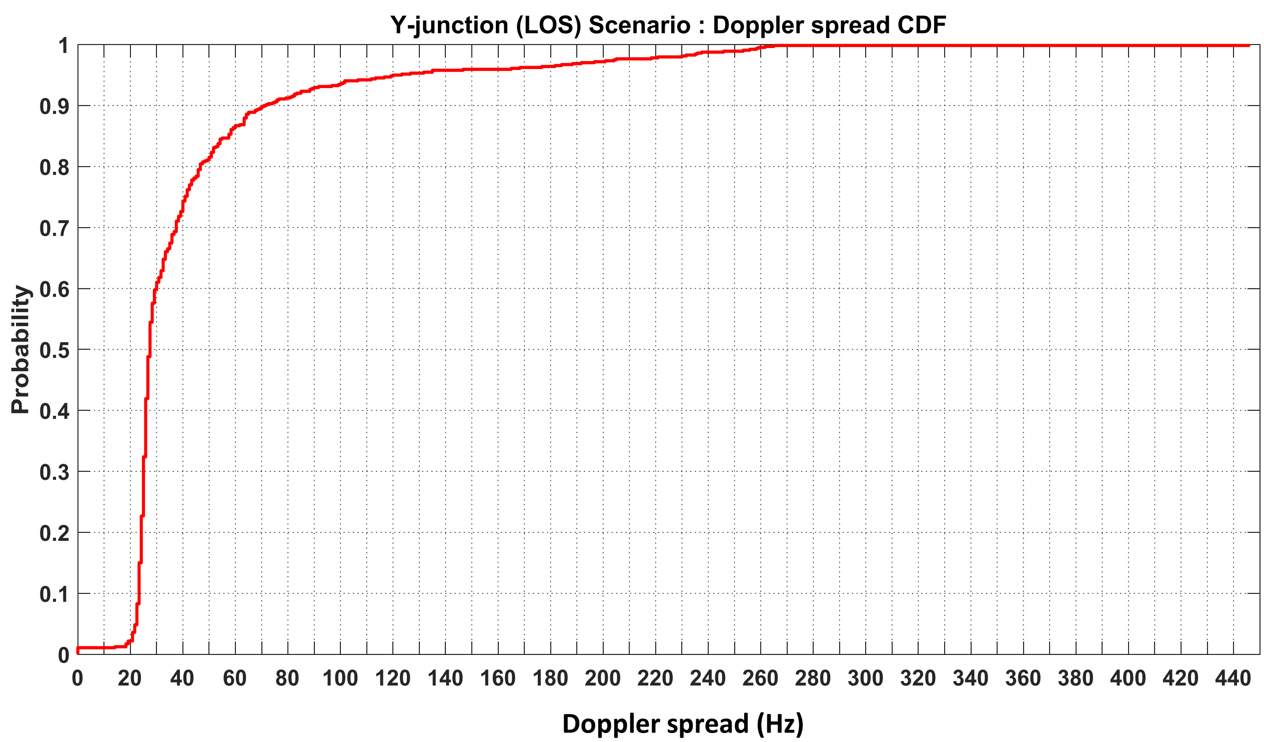

Figure 4.20 Empirical CDF for Doppler spread for the LOS tests of the Y-junction intersection

4.2.3.2. NLOS Test

A spectrum collected at NLOS conditions in the Y-junction intersection is displayed in Figure 4.21. Doppler spreads were much larger and more frequent in this set of data and this is because the received signals at each position have been influenced more by the many moving vehicles of all sizes/shapes and also the pedestrians. The largest Doppler spreads and these can be found at distances of 16, 17, 26and 29 m. These Doppler spreads have extended beyond 250 Hz and in the case of data collected at 26 m, the Doppler spread is greater than 385 Hz. Table 4.5 has more significant Doppler spreads in this scenario.

Figure 4.22 displays the empirical CDF of Doppler spread for the NLOS condition for Y-junction intersection. It can be observed that 90% of Doppler spreads are within 23 Hz which indicates that the reflections from the surroundings are richer than the NLOS area in the previous scenario.

Figure 4.23 shows the coherence time of the Y-junction intersection. The period of time during which the channel is fixed can be assumed to be 1.9ms. There is no change in time in the experimental area until it reaches about 25 m and then a slight change of 34 m followed by a change in time. Increasing in the fixed and mobile scatterers in this intersection leads to increasing of the Doppler spreads and decreasing the coherence time.

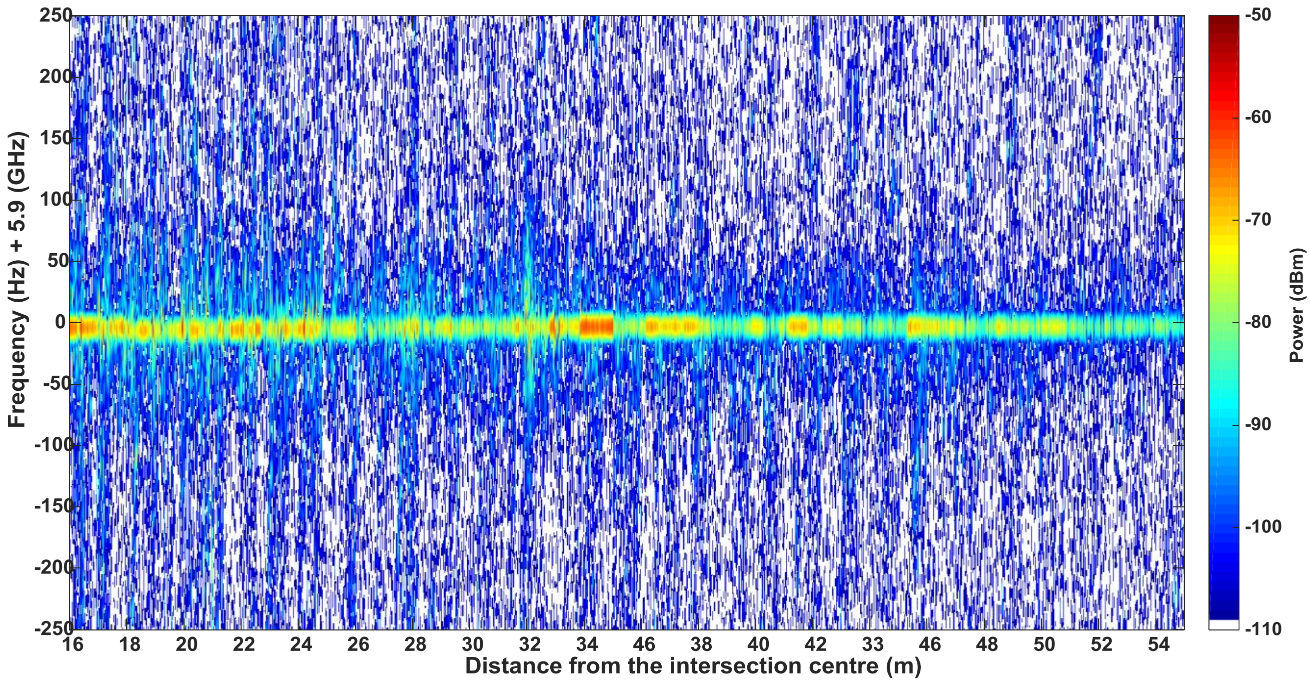

Figure 4.21 All the spectra collected for NLOS condition in the Y-junction intersection

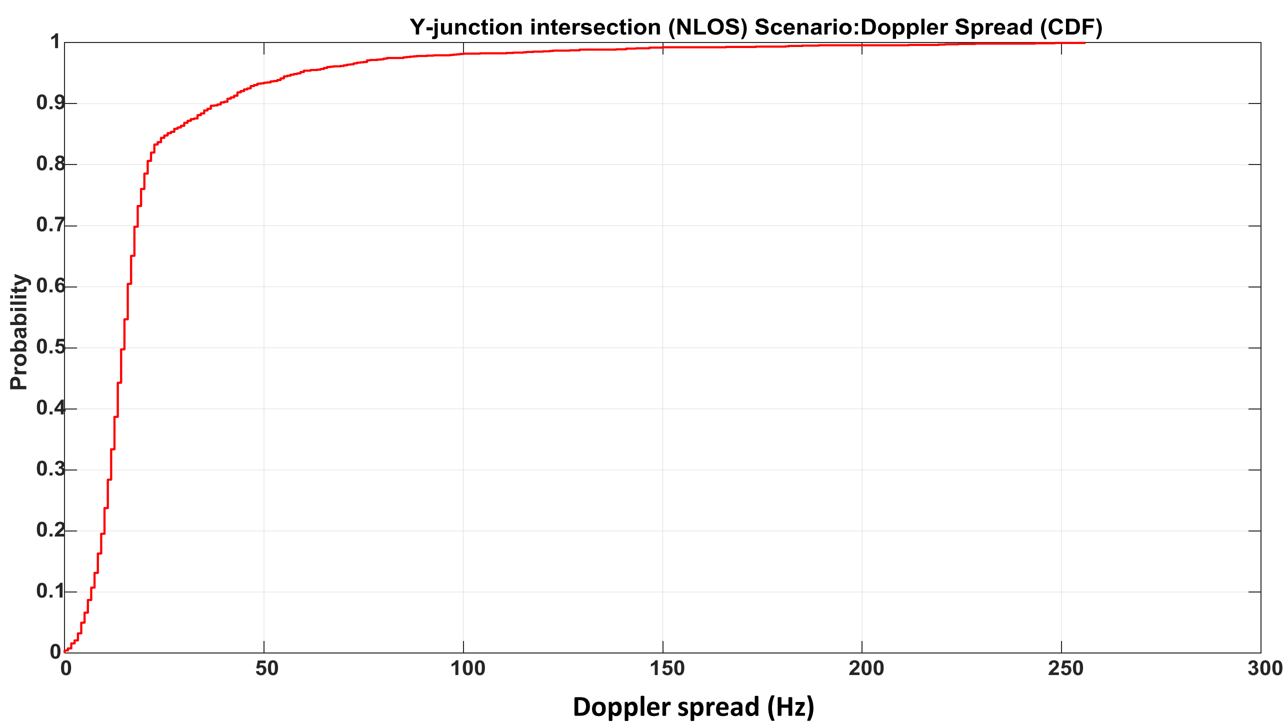

Figure 4.22 Empirical CDF for Doppler spread for the NLOS tests of the Y-junction intersection

Table 4.5 Significant Doppler spreads

Scenario Condition	Distance (m)	Frequency (Hz)	Observed traffic
LOS	3	265	Truck
	9	259.8	Large van
	11	255.8	Large Truck
	13	261.6	VAN
	14.5	445.8	Bus
NLOS	16	265	Sports Utility Vehicle
	17	243	van
	26	385	Large Truck
	29	325	Car

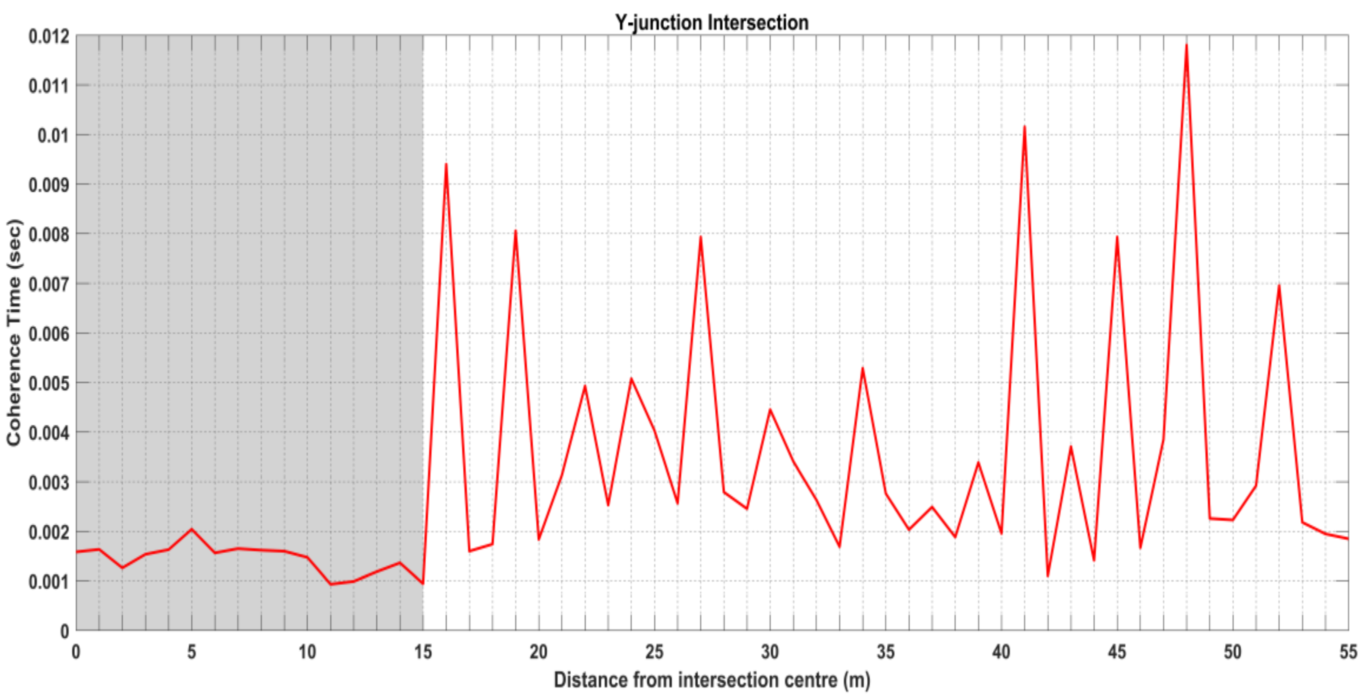

Figure 4.23 Empirical coherence time of the Y-junction intersection

4.3. Scenario Three

This is an irregular three-way intersection resulting from the confluence of University Road with the Welford Road. Figure 4.24 illustrates this intersection. Multi-story buildings border the intersection from Welford Road. The other sides are green spaces containing trees surrounded by a metal fence on the university side and a stone wall from the other side. The width of the intersection in this scenario is 20 m and the width of the roads was at 13 m at the intersection. The blue and yellow circles are the transmitter and receiver respectively. The distance between the transmitter and receiver was 40 m in the initial position, and then the receiver was moved away from this location. Data collected at this intersection from 55 positions in two runs, 20 of these positions line-of-sight (LOS) conditions and 35 were non-line-of-sight (NLOS) conditions. Table 4.6 presented more details about these runs. Green-coloured arrows represent the path of the receiver. This intersection may be similar to a T-junction but at an angle of less than 90^{o}. On the other hand, the path of the receiver trolley has a downward gradient from the intersection centre. There were no street canyons in this propagation environment at all. There was also a wall in front of the receiver path and as the path sloped downwards away from the intersection centre, the height of this wall in relation to the path also rose. Opposite the transmitter, there is a steel fence dividing the pavement from the cemetery next to it and it is believed that this will have influenced the radio propagation. Passage of vehicles at this intersection is not controlled, so the measurements will be affected by the passing of different types of temporary obstacles such as vehicles and pedestrians. However, it was noticed that when a vehicle passed by there was a change in the signal width caused by Doppler spreads, this change depending on the size of the vehicle (more details in Chapter 5).

Table 4.6 Table Details of the different measurement runs in the scenario three.

No.	Type of scenario		Distance Range (m)	Distance Resolution (m)	Date	Start time	Vehicles speed (mph)
1	T-Junction	Run1	0 - 55	1	22-05-2018	10:00	30
		Run2			23-05-2018	12:55	

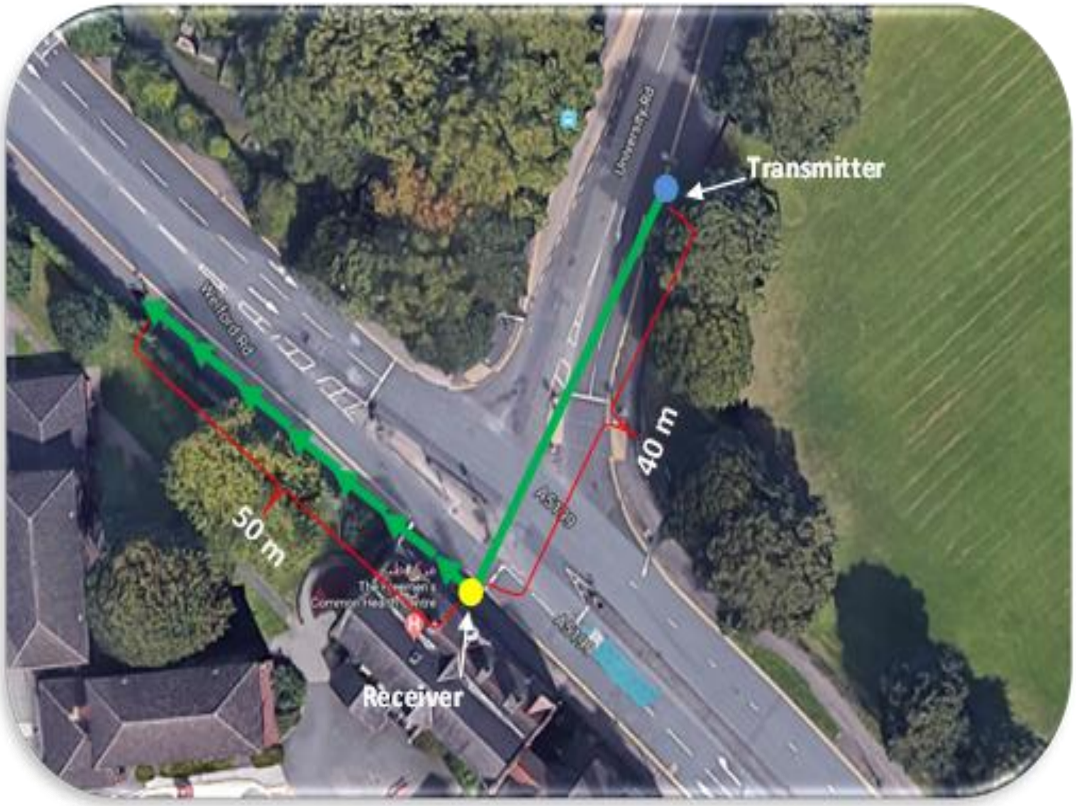

Figure 4.24 Intersection scenario 3

4.3.1. Median Peak Power and Packet Delivery Ratio Analysis

Figure 4.25 displays the PDR and peak power for the data collected in the third intersection with the shaded parts of the graph denoting where LOS communications existed. All the data were collected in two attempts and the receiver was always 5 m away from the centre of the road.

The first significant drop in PDR happens at 38 m where it drops approximately 30%. From 38 m there is considerable fluctuation in the PDR and it swings between 98% and 60% for the majority of the rest of the data collected until the last two points, where it drops to 40%. It can be said that until 55 m there is an acceptable level of communications even though after 38 m it might not be suitable for safety-critical operations. There is also a significant difference in peak power at each point as shown in the long error bars. The LOS region involves some interesting peak power data; the peak power shows to rise (by about 10 dB) compared to the data on NLOS conditions region. These appearances could either be due to the variable conditions in the environment or due to the geometry of the environment causing multipath propagation which has increased the received power.

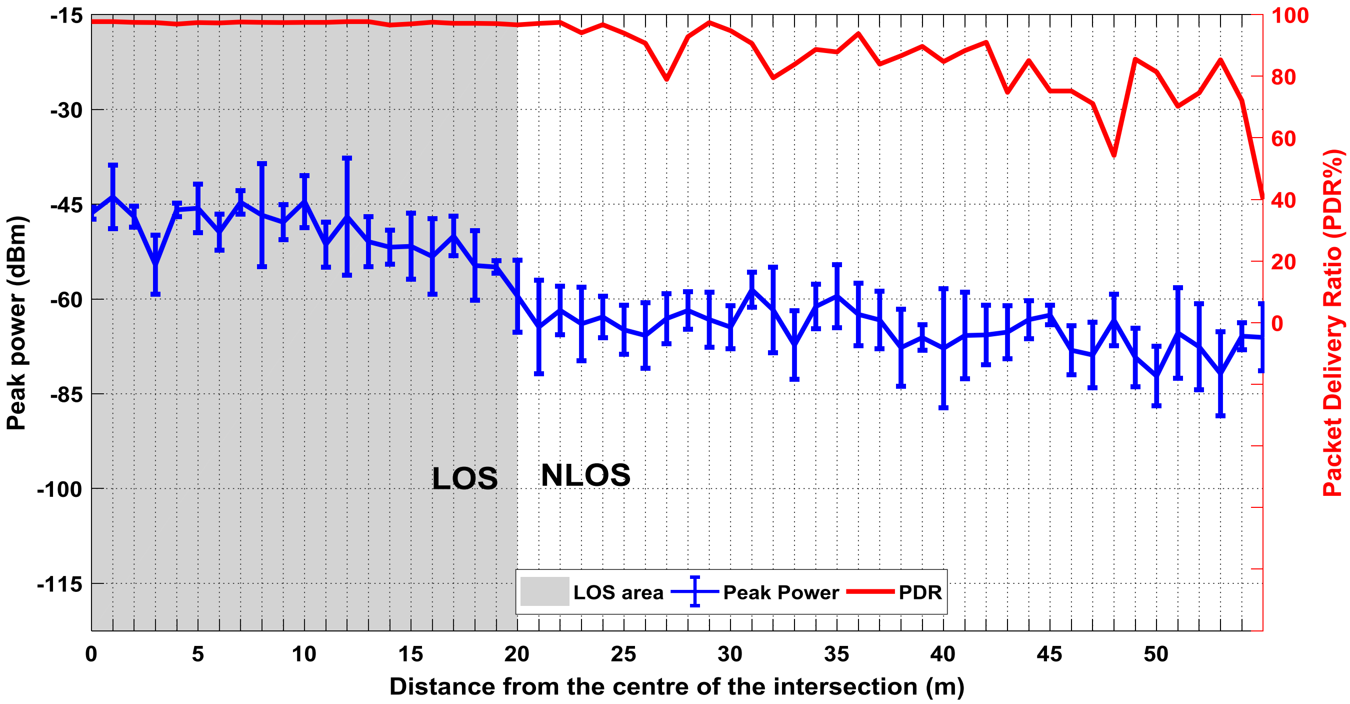

Figure 4.25 Packet delivery ratios and peak power for all the data collected in the third intersection scenario.

The lines on Figure 4.26 are from all the data collected in the range 0 – 55 m in scenario 3. The grey shaded area represents the LOS regions. The red and black lines are used to represent the data collected in the 1 and 2 runs respectively.

The first run was taken in the morning at the rush hour, while the second run was in the afternoon when the traffic was normal.

The PDR appears to be similar in both runs, where it remains about 98% to 30 m and then begins to fluctuate between 98% and 70% to 54 m. It then collapses to 40% at 55 m. The important decline of the PDR in the first run we were at a distance of 27 m about 60%. In the second run, there was a decline in the PDR at a distance of 37 m about 70%. This difference is explained by the temporary reflectors in this first run of the intersection. As well as the pedestrian traffic, because of which some of the radiation pathways that would have been received would be disrupted, will be reflected elsewhere. It can be said that up to 27 m there is an acceptable level of communication although after that may not be suitable for critical safety operations. The fluctuation of peak power in the LOS results from traffic flow. It decreases sharply and not smooth with the entry into the NLOS area but it raises again briefly intersection.

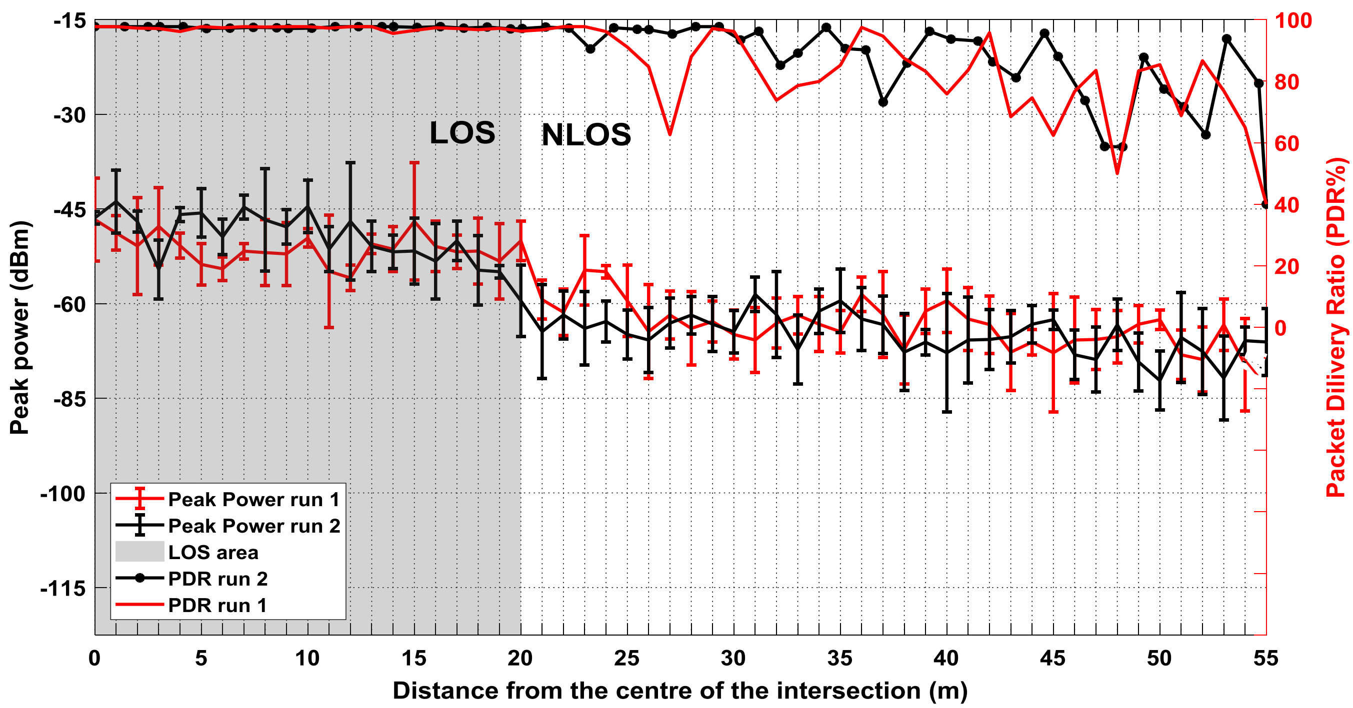

Figure 4.26 Packet delivery ratio and peak power for all the data collected of the third intersection for each run.

4.3.2. Comparison of observations of power with the NLOS model

Figure 4.27 illustrates the NLOS peak power of all data collected from third intersection scenario along with the prediction model provided by virtualsource11p as a function of distance. It can be seen from this Figure the measurement data contain agree well with the NLOS model although the difference in each position and the nature of the signal decay change. The difference in some of these sites may be due to temporary changes such as the passage of vehicles of different sizes or the nature of the place such as in the sloping streets and differences in the forms and sizes of buildings.

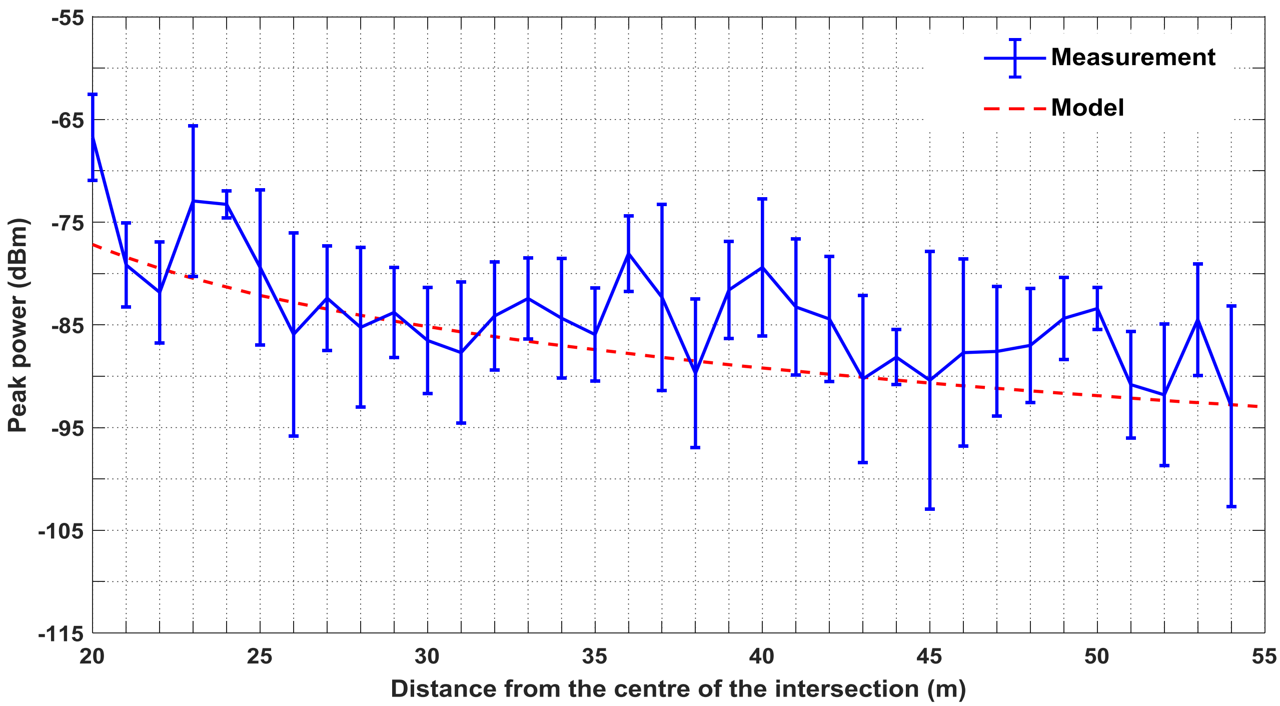

Figure 4.27 Peak power as a function of a distance from the third intersection: measurement and virtualsource11p model.

4.3.3. Doppler Spreads Analysis

4.3.3.1. LOS Test

Figure 4.28 illustrates all the spectra collected at LOS conditions in the T-junction intersection. The spectra which were collected at each position are grouped together and the power in the continuous (CW) wave is shown by the horizontal coloured band which goes through the middle of the chart. The centre frequency is located at 5.9 GHz with an observation span of 500 Hz, and the observed noise level has -95 dBm. Doppler spreads have a large range and are within 270 Hz of where the peak of the CW. It is fluctuated between 150 and 270 Hz. For example, the highest Doppler spread was recorded at a distance of 12 m from the centre of the intersection and was 262.5 Hz due to the passage of a large vehicle near the receiver. All Doppler spreads are recorded high when compared with the previous scenarios, these larger spreads are possibly caused by the presence of vehicles passing near/through the radio propagation path. Table 4.7 shows some of the interesting areas where Doppler spreads have occurred.

Figure 4.29 displays the empirical CDFs of Doppler spread for the LOS condition for the T-junction intersection. For this situation, Doppler spreads are noticeable at an average of 28 Hz while 90% of the Doppler spreads are below 80 Hz.

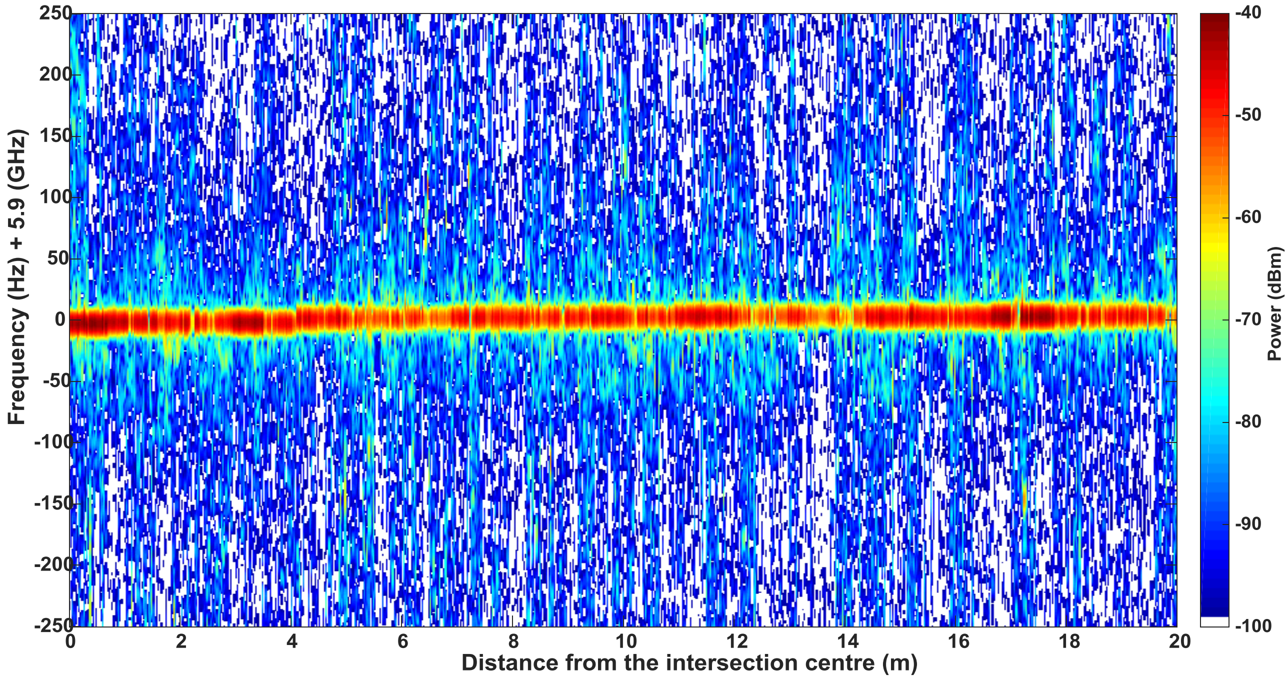

Figure 4.28 All the spectra collected for the LOS condition in the T-junction intersection

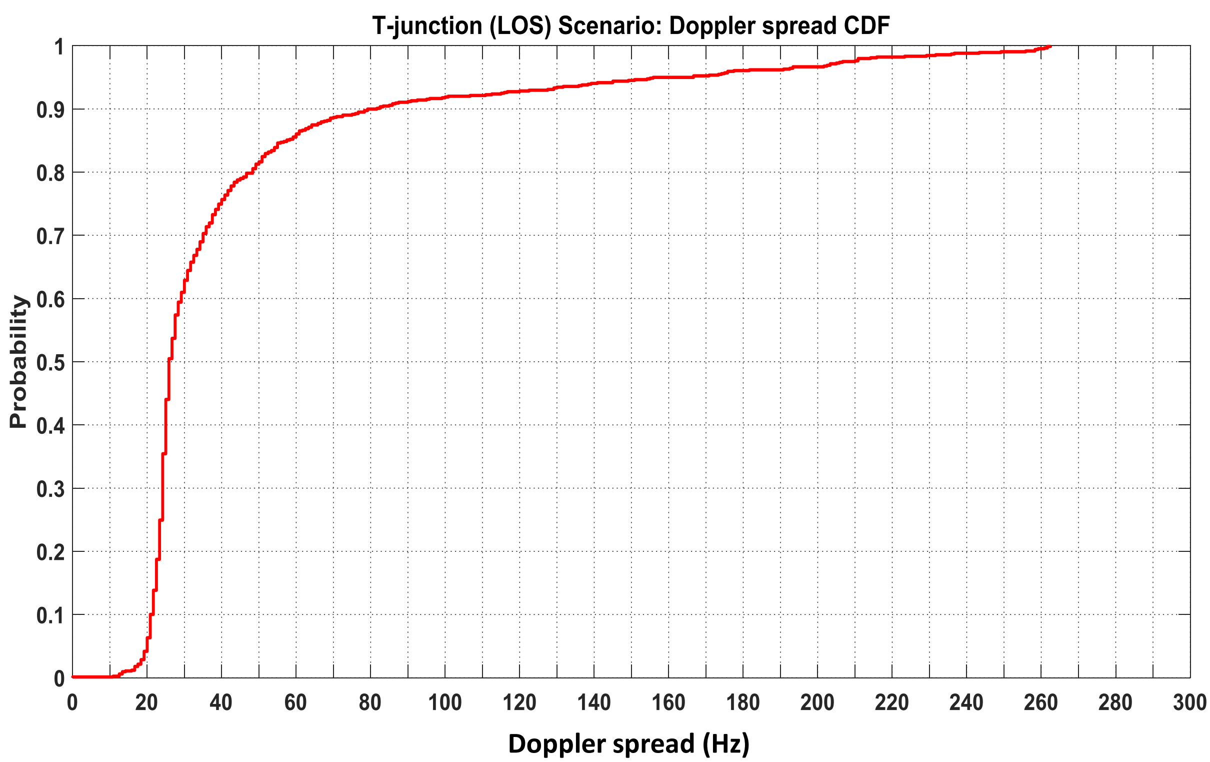

Figure 4.29 Empirical CDF for Doppler spread for the LOS tests of the T-junction intersection

4.3.4. NLOS Test

Figure 4.30 shows all the spectra collected at NLOS conditions in the T-junction intersection. Many Doppler spreads were observed where the reflected waves reach more than 230 Hz at different distances away from the centre of the intersection where the CW signal has more power, resulting in the ability to detect larger Doppler spreads. The highest recorded value for Doppler spreads in this scenario is 32 m away from the intersection centre where you are 238 Hz, which means that the rays that propagate from the transmitter to the receiver at that time were supported by the big waves reflectors. The largest Doppler spreads and these can be found at distances of 21, 24, 32 and 41 m. Table 4.7 shows the value of Doppler spreads at these distances.

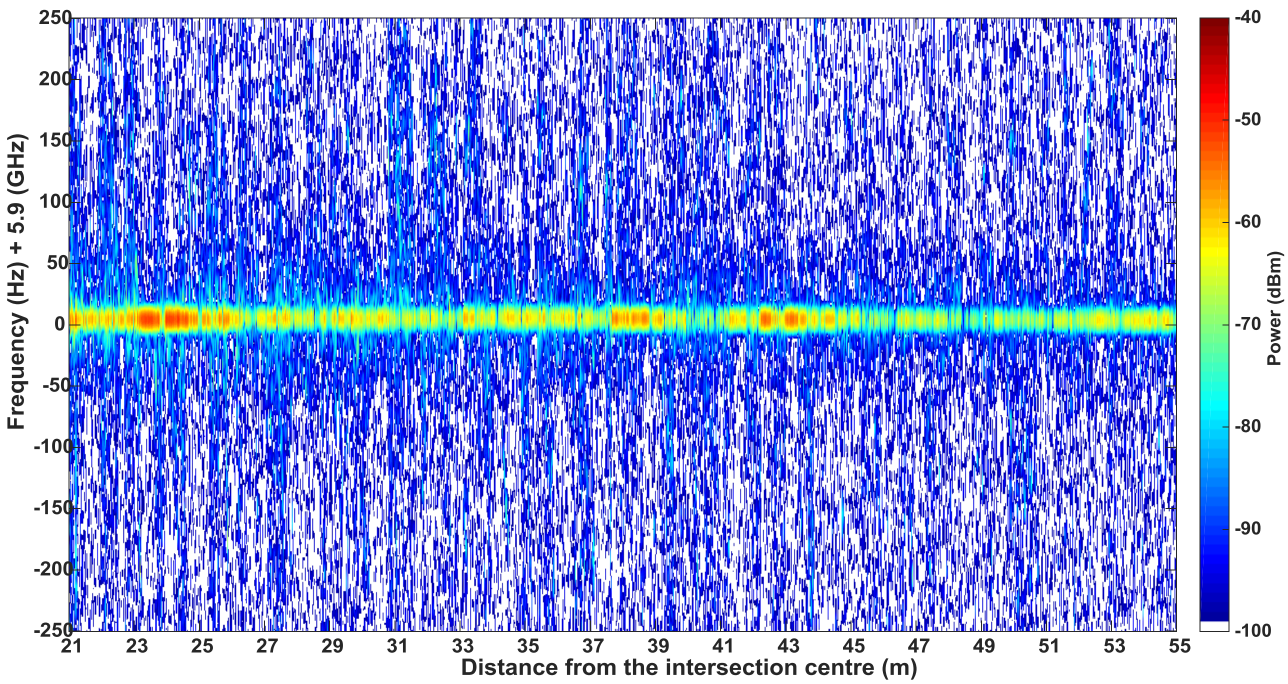

Figure 4.30 All the spectra collected for NLOS condition in the T-junction intersection

Table 4.7 Significant Doppler spreads

Scenario Condition	Distance (m)	Frequency (Hz)	Observed traffic
LOS	1	258.3	Truck
	5	261.6	Large van
	7	260.8	VAN
	12	262.5	Large Truck
	13	261.6	Bus
	16	258.3	Sports Utility Vehicle
NLOS	21	216	Van
	32	238	Truck
	34	226	Car
	41	225	Car

Figure 4.31 presents the empirical CDFs of Doppler spread for the NLOS condition of the T-junction intersection. In the figure, 90% of the Doppler spreads are below 20 Hz. The passage of large vehicles through the wireless transmission path may be the cause of these spreads as well as the slope in the street.

Figure 4.32 shows the coherence time of the T-junction intersection. It should be noted that there is no change in the experimental coherence time in the LOS region where it is approximately 2 ms due to a large number of static and moving waves reflectors. While this time increases when moving away from the centre of the intersection due to the lack of reflectors of the waves, leading to the reduction of the Doppler spreads.

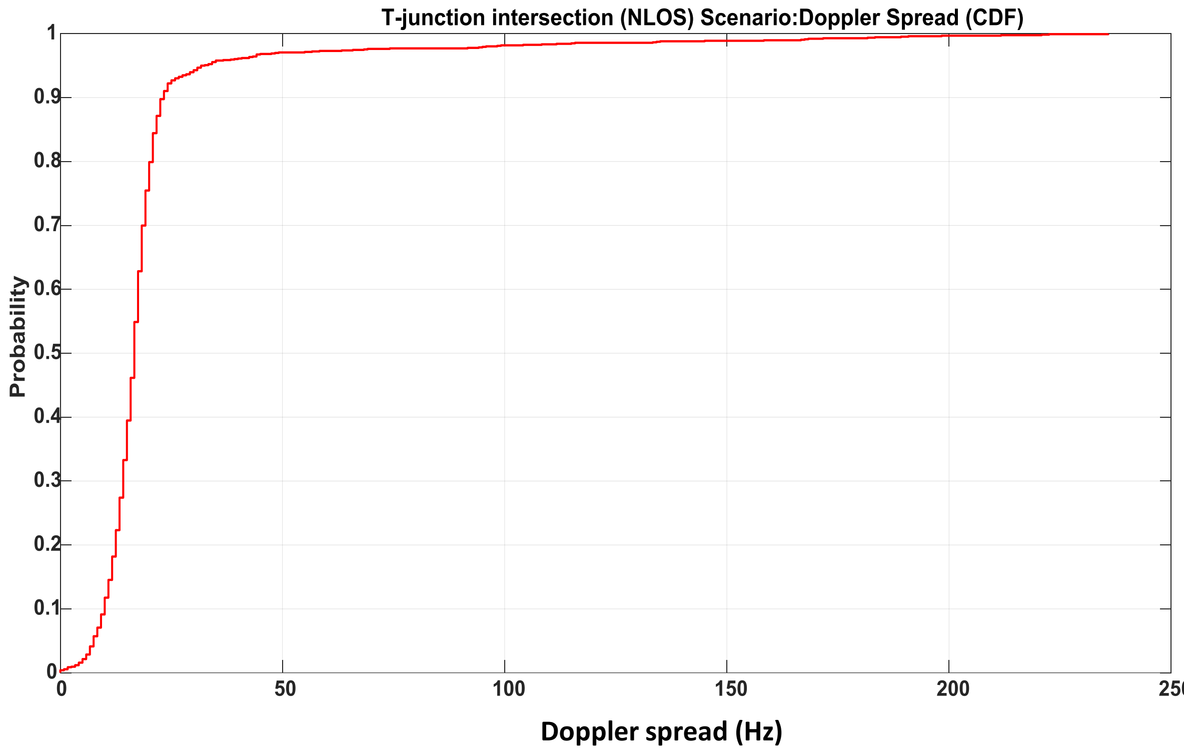

Figure 4.31 Empirical CDF for Doppler spread for the NLOS tests of the T-junction intersection

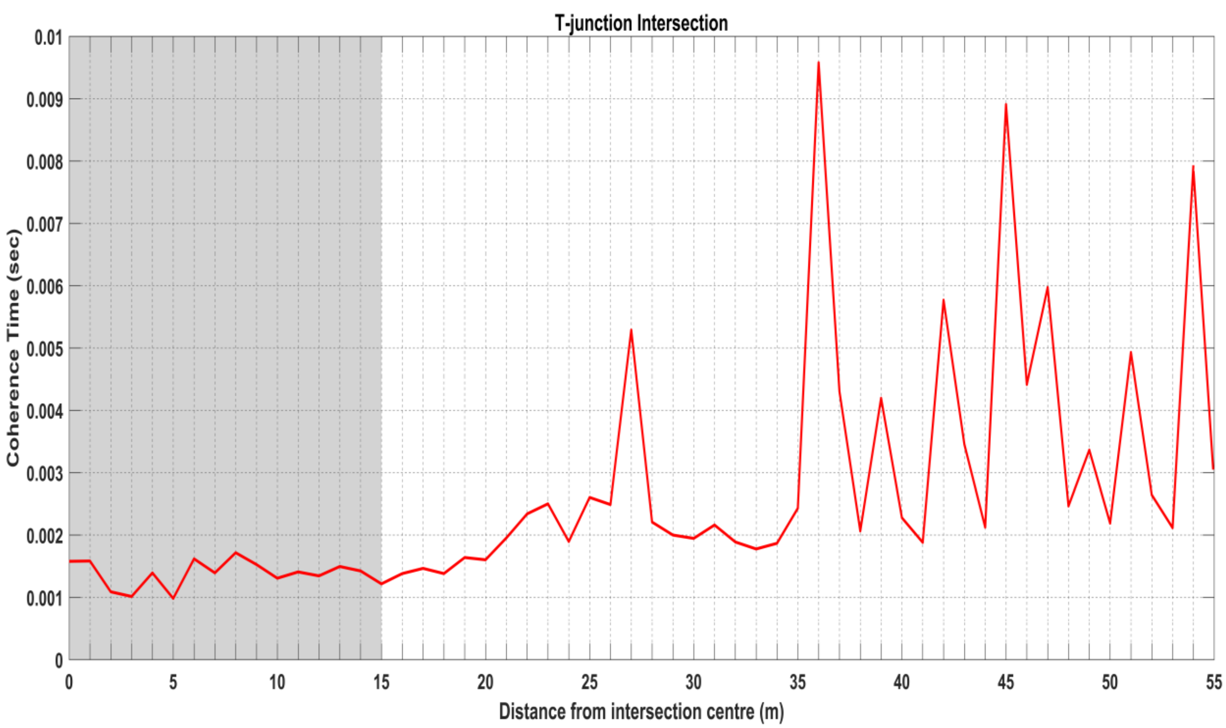

Figure 4.32 Empirical coherence time of the T-junction intersection

4.4. Scenario Four

Figure 4.33 illustrates the fourth scenario that has been deployed in the irregular four-way intersection with wider roads which have two lanes in each driving direction for four-way and width of 20 metres. This intersection is between Welford Road and Victoria Park road. The width of the intersection in this scenario is 30 m and the width of the roads was at 20 m at the intersection. Blue and yellow circles represent the initial Tx and Rx locations, respectively. Green-coloured arrows represent the path of the receiver, moving away from the sender. The distance between the transmitter and receiver was 40 m in the initial position, and then the receiver was moved away from this location. Data collected at this intersection from 55 positions in two runs, 17 of these positions line-of-sight (LOS) conditions and 38 were non-line-of-sight (NLOS) conditions. Table 4.8 presented more details about these runs. The vehicle traffic is not controlled at this intersection. Therefore, the measurements will be affected by passing different types of temporary obstacles such as cars and pedestrians through changes in signal width due to Doppler spreads.

Table 4.8 Details of the different measurement runs in the scenario four.

<table>
<tr><th>No.</th><th colspan="2">Type of scenario</th><th>Distance Range (m)</th><th>Distance Resolution (m)</th><th>Date</th><th>Start time</th><th>Vehicles speed (mph)</th></tr>
<tr><td rowspan="2">1</td><td rowspan="2">Four way intersection</td><td>Run1</td><td rowspan="2">0 - 55</td><td rowspan="2">1</td><td>12-10-2018</td><td>10:30</td><td rowspan="2">30</td></tr>
<tr><td>Run2</td><td>13-10-2018</td><td>14:05</td></tr>
</table>

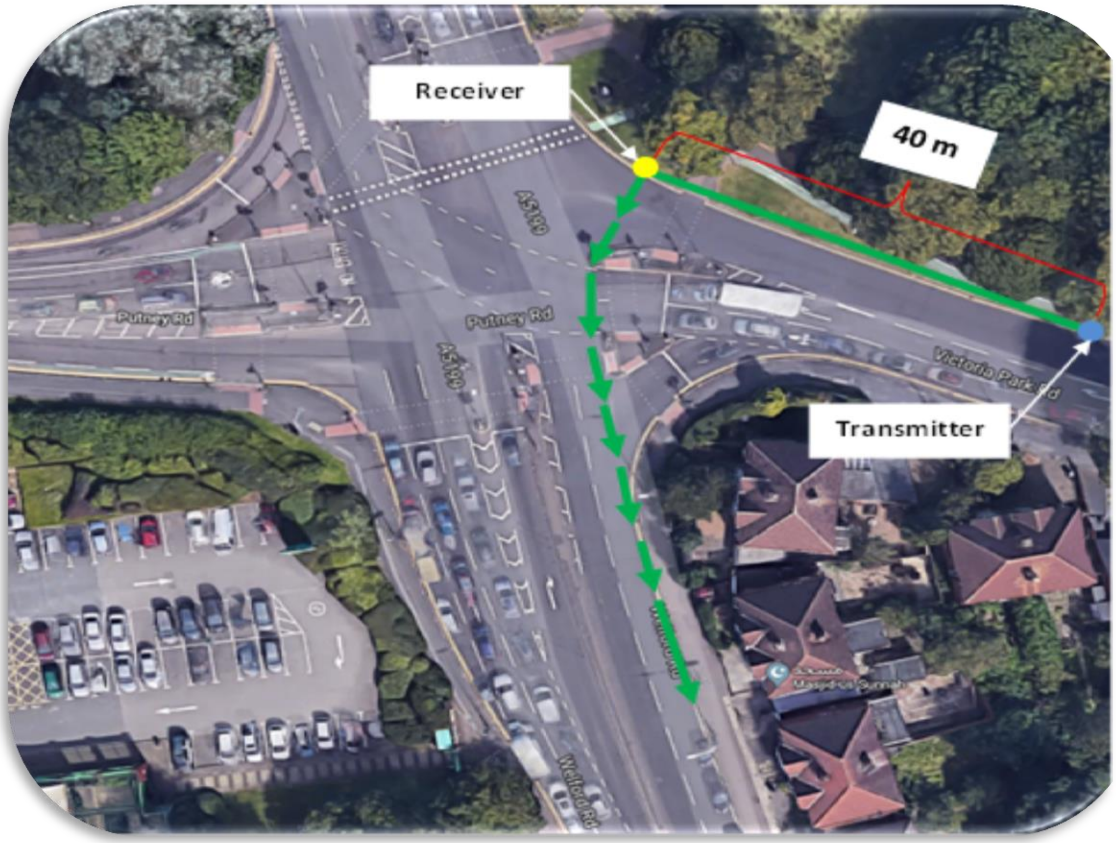

Figure 4.33 Intersection scenario 4

4.4.1. Median Peak Power and Packet Delivery Ratio Analysis

Figure 4.34 shows PDR and peak power resulting from the collection of data obtained from two data collection attempts which present the general trend for them. They varied as the receiver was moved away from the centre of the intersection.

Both the PDR and peak power start high and then decrease as the receiver moves away from the intersection to the NLOS region. The PDR started about 98% to 28m. After this distance starts fluctuation acceptable between 98% and nearly 60% until it reaches about 53 metres after it begins to collapse until it reaches 0%. In this case, it will not be possible to have vehicular safety applications exceeding 53 m.

Depending on the state of traffic, moving objects as obstacles or reflections that cause severe differences in performance.

The peak power in this figure decreases sharply with the entry into the NLOS area but it rises again briefly. The decrease in peak power is not smooth. The fluctuation of peak power in the LOS results from traffic flow obvious.

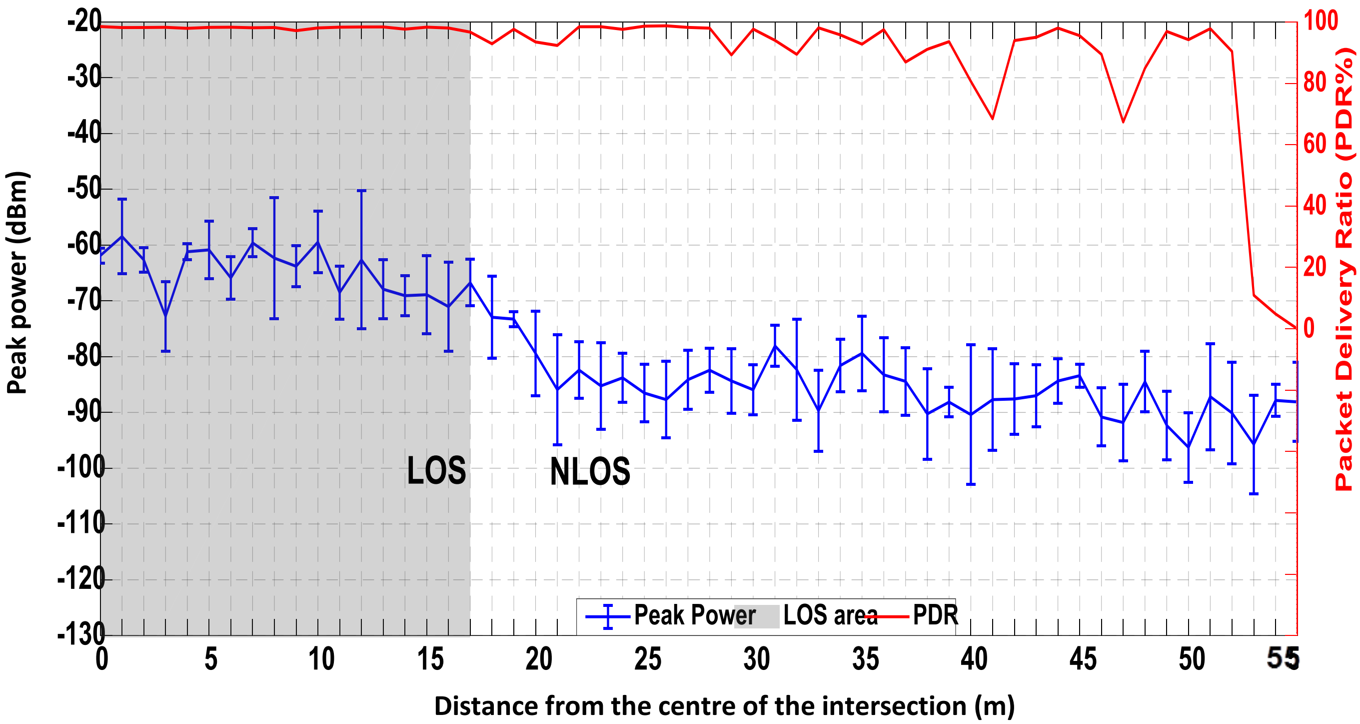

Figure 4.34 Packet delivery ratios and peak power for all the data collected in the fourth intersection scenario.

Figure 4.35 shows all the data collected in the range 0 – 55 m in the fourth scenario of the intersection from the separate runs. The grey shaded area represents the LOS region. The red and black lines are used to represent the data collected in the 1 and 2 runs respectively. A significant observation is that the PDR and peak power are very similar to each other closer to the intersection centre except for some sites that will be explained later.

The PDR is not too different between the two lines. There are a few places where the PDR falls below 85% and 70%, but most of the time it ranges between 90% and 98% until 53 m. Beyond 53 m, the PDR is down to 0%. The fluctuation in the PDR is because the propagation conditions were significantly different in the days when these two sets of data were collected, hence the observed differences in both PDR and peak power. The PDR difference at 10 m is about 70% in the second run. The second significant decline in the PDR at 39 m about 40%. Except for these sites, PDR ratios are acceptable, where it fluctuates between 90% and 98%. The PDR difference at 39 m is about 40%, which is very important and will not be able to support reliable vehicular communications.

The difference in peak strength is less than 10 dBm between two runs while the PDR seems somewhat different.

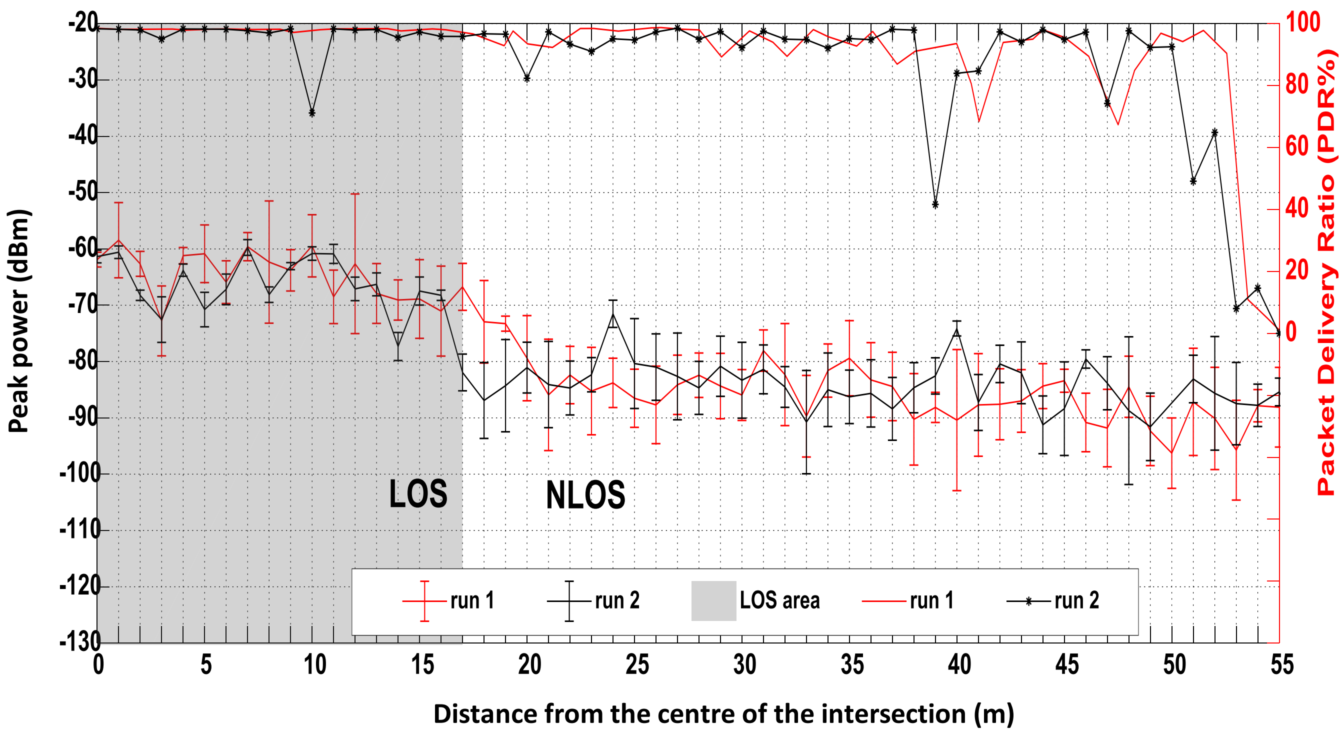

Figure 4.35 Packet delivery ratios and peak power for all the data collected of the fourth intersection for each run.

4.4.2. Comparison of observations of power with the NLOS model

Figure 4.36 illustrates the NLOS peak power of all data collected from forth intersection scenario along with the prediction model provided by virtualsource11p as a function of distance.

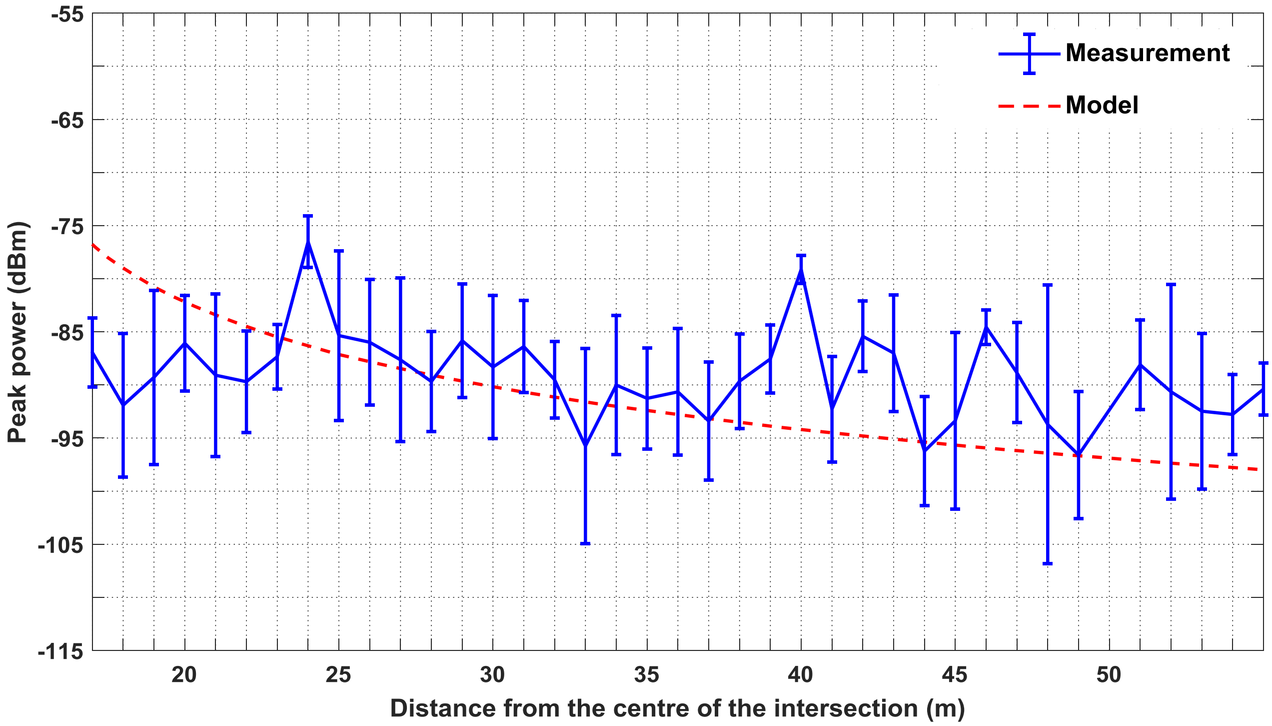

Figure 4.36 Peak power as a function of a distance from the fourth intersections: measurement and virtualsource11p model.

In this intersection, The RX street starts to bend at an approximate distance of 35 m from the intersection centre. Due to that many significant fluctuations in peak power, which are visible at 20 m, and 40 m which start to disappear gradually for distance 45 m, which in turn continuously reduce the total peak power. The reason behind this is the curved RX street.

4.4.3. Doppler Spreads Analysis

4.4.3.1. LOS Test

Figure 4.37 presents all the spectra collected at LOS conditions in the Four-way intersection. The centre frequency is located at 5.9 GHz with an observation span of 500 Hz, and the observed noise level has -95 dBm. The spectra collected at each position are grouped together and the power in the continuous (CW) wave is shown by the horizontal coloured band which goes through the middle of the figure.

In this scenario, the highest values of Doppler spreads were recorded compared to the previous scenarios due to the width of the intersection and a large number of high-speed waves reflectors as well as fixed waves reflectors. Doppler spreads have a large range and are within 488 Hz of where the peak of the CW. Doppler spreads fluctuated between 250 and 488 Hz. For example, the highest Doppler spread was recorded at a distance of 8 m from the centre of the intersection and was 486 Hz due to the passage of a large vehicle near the receiver. Table 4.9 shows some of the interesting areas where Doppler spreads have occurred.

Figure 4.38 displays the empirical CDFs of Doppler spread for the LOS condition for the Four-way intersection. For this case, the CDF crosses the 90% threshold at 230 Hz, and the 50% threshold is reached at 30 Hz. This high range of Doppler spreads is due to the size and the speed of the vehicles that considered as moving waves reflectors.

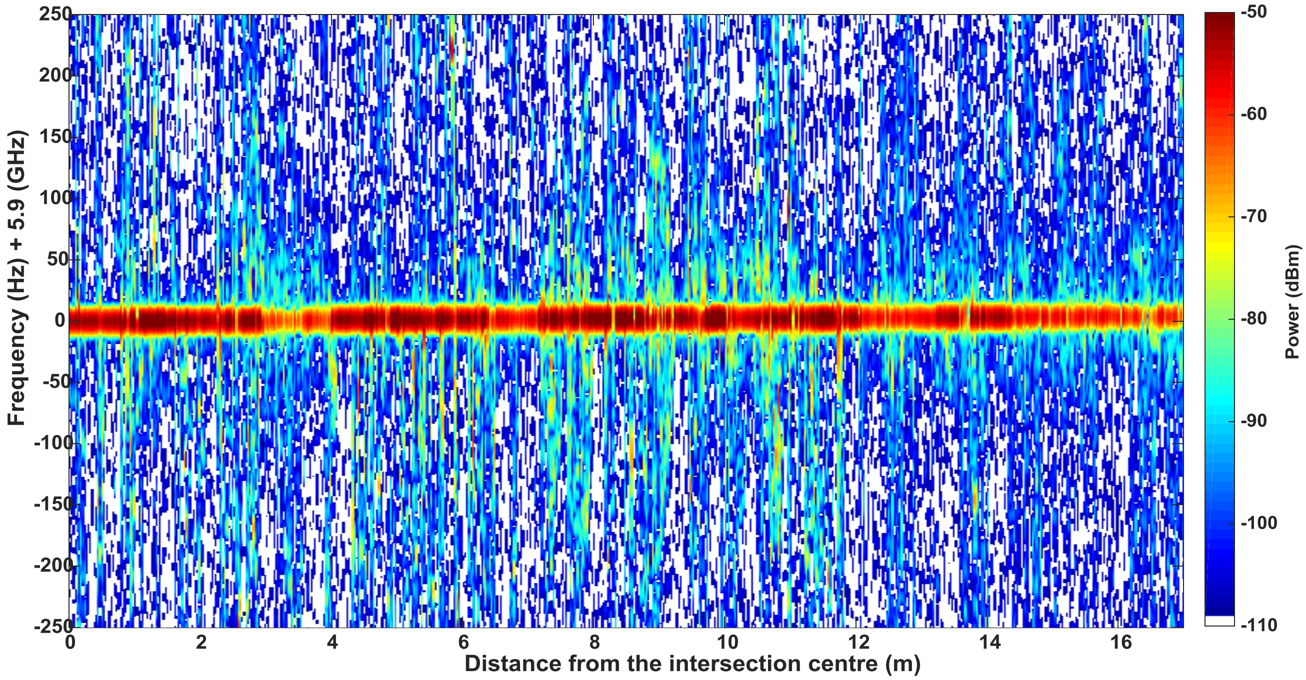

Figure 4.37 All the spectra collected for the LOS condition in the Four-way intersection

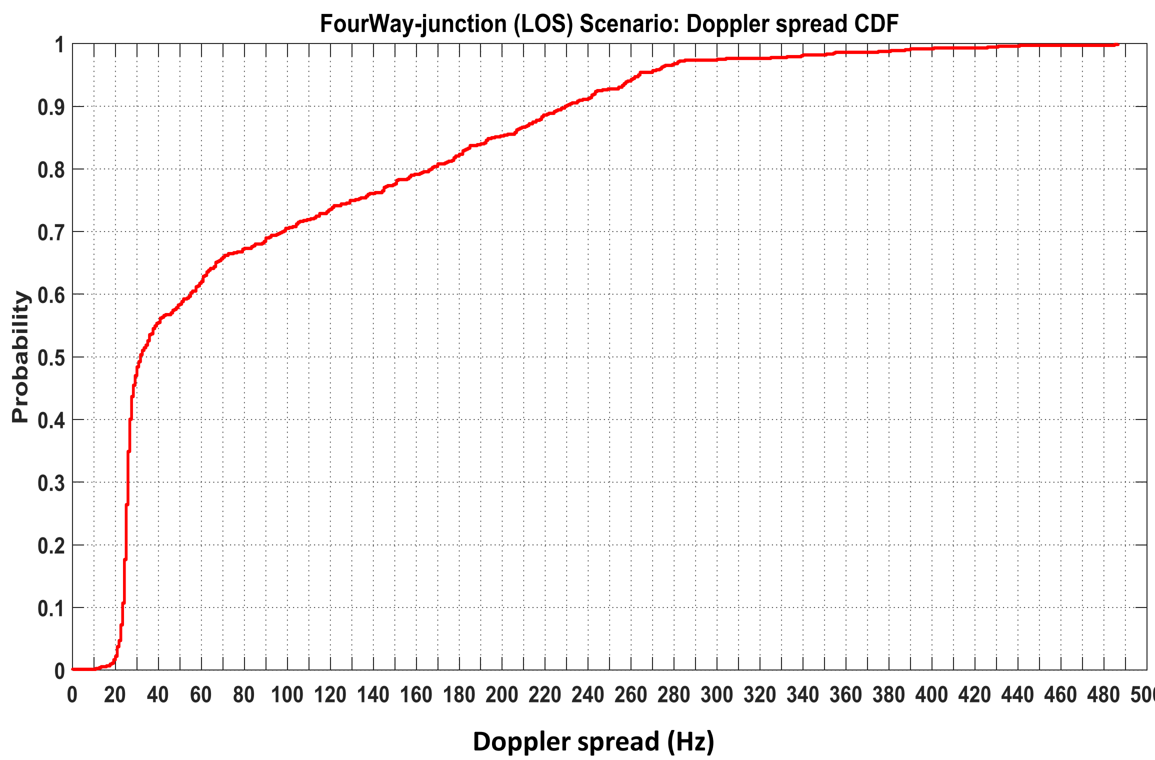

Figure 4.38 Empirical CDF for Doppler spread for the LOS tests of the Four-way intersection

4.4.3.2. NLOS Test

Figure 4.39 shows all the spectra collected at NLOS conditions in the Four-way intersection. There are many Doppler spreads were observed where the reflected waves reach more than 255 Hz at different distances away from the centre of the intersection where the CW signal has more power, resulting in the capability to detect larger Doppler spreads. The highest recorded value for Doppler spreads in this scenario is 22 m away from the intersection centre where you are 260 Hz, which means that the rays that propagate from the transmitter to the receiver at that time were supported by the big waves reflectors. The largest Doppler spreads and these can be found at distances of 18, 21, 22, 51 and 53 m. Table 4.9 illustrates the value of Doppler spreads at these distances.

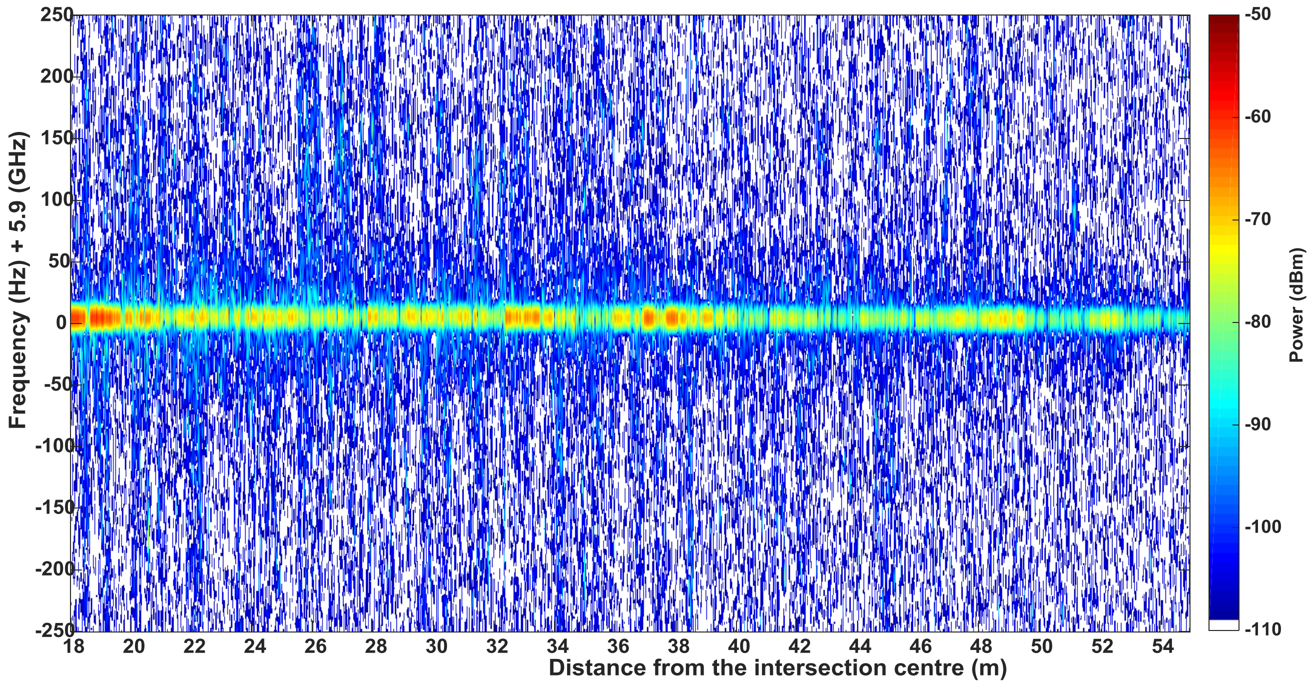

Figure 4.39 All the spectra collected for NLOS condition in the Four-way intersection

Table 4.9 Significant Doppler spreads

Scenario Condition	Distance (m)	Frequency (Hz)	Observed traffic
LOS	3	400.8	Bus
	8	486.6	Large van
	12	485	Large Truck
	14	440	Large Truck
NLOS	18	251	Bus
	21	256	Sports Utility Vehicle
	22	260	Truck
	51	259	Car
	53	250	Van

Figure 4.40 presents the empirical CDFs of Doppler spread for the NLOS condition of the four-way intersection. In the figure, 90% of the Doppler spreads are below 20 Hz. The passage of large vehicles through the wireless transmission path may be the cause of these spreads as well as the slop in the street.

Figure 4.41 shows the coherence time of the Four-way intersection. The period of time during which the channel is fixed can be assumed to be 0.2ms. No change in the time until it reaches about 17 m. increasing in the stationary and mobile scatterers in this intersection lead to increasing of the Doppler spreads and decreasing of the coherence time.

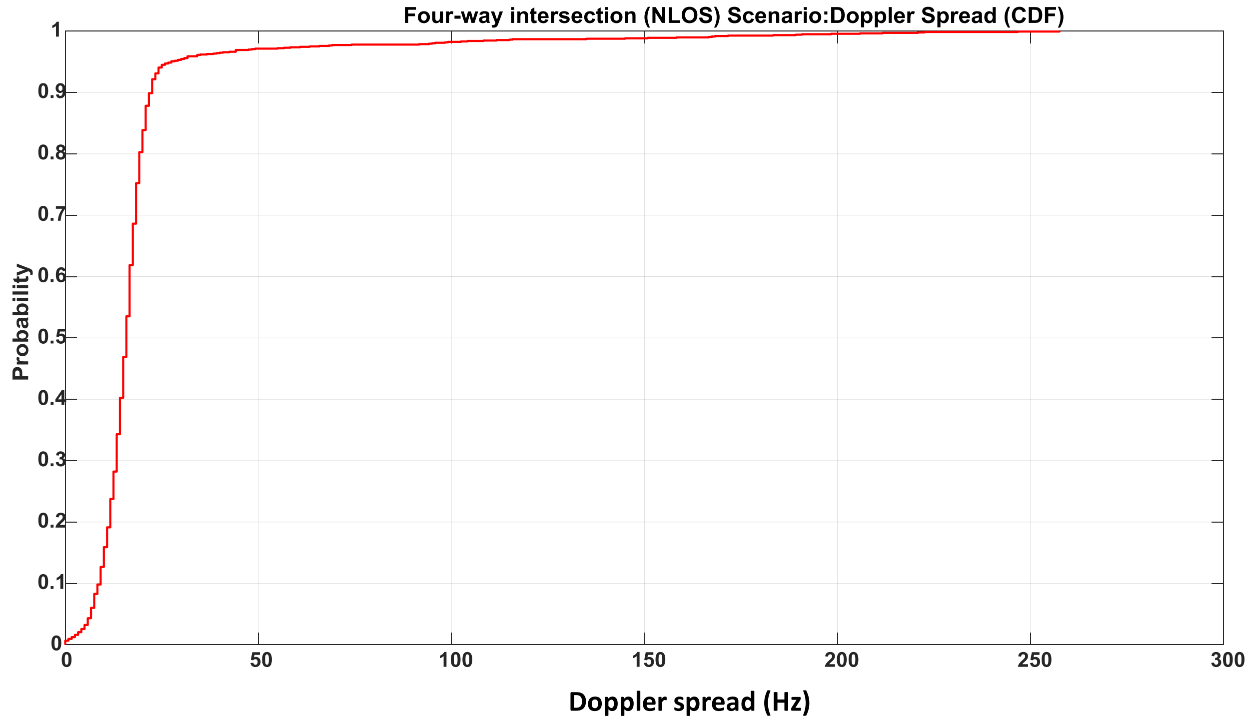

Figure 4.40 Empirical CDF for Doppler spread for the NLOS tests of the Four-way intersection

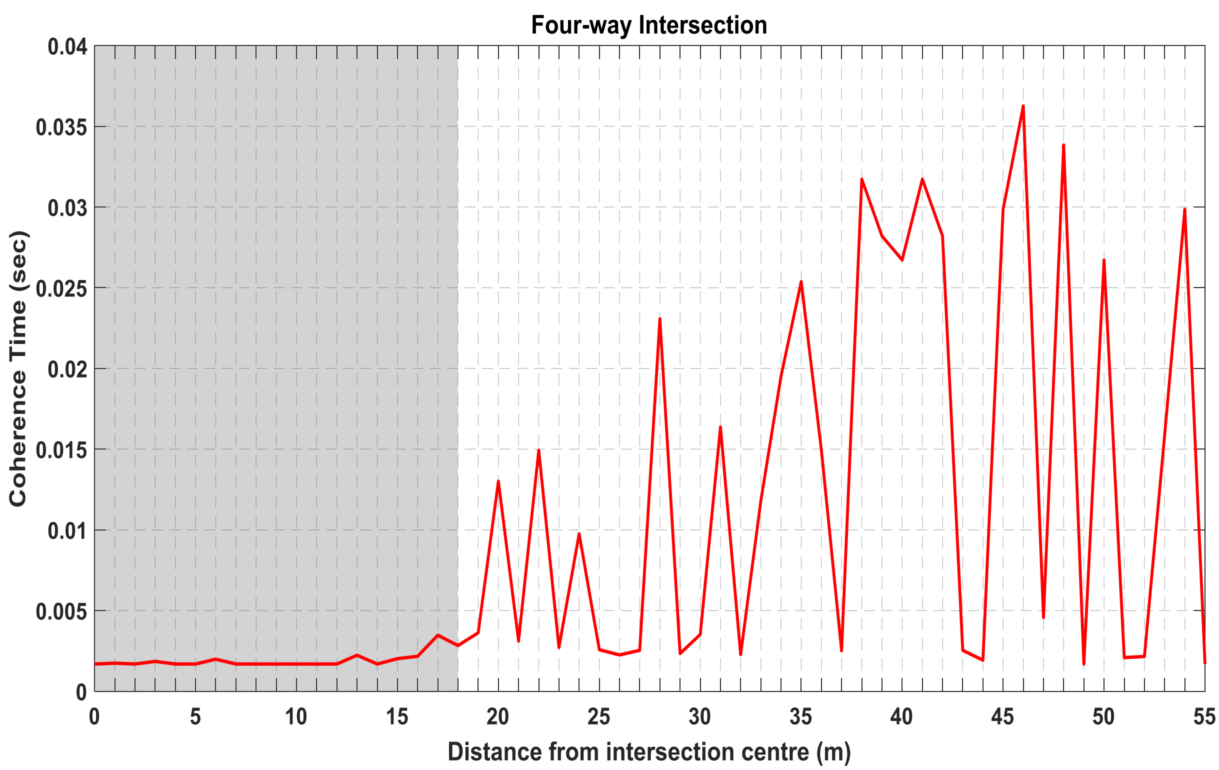

Figure 4.41 Empirical coherence time of the Four-way intersection

4.5. Comparison of the different scenarios

In this section, different scenarios were compared by two parameters. The first one is the median inter-decile range (MIDR), is an indication of the variation in each run. This is the median of the inter-decile ranges of all the positions in a run. The second is the median error (Em = median (MPP – virtualsource11p prediction)) and the distance range for each of the scenarios. Table 4.10 presents details for all the runs in scenarios is indicating the MIDR for all runs in each scenarios as well as Em for each scenarios.

Table 4.10 Details of the different measurement runs in all scenarios

No.	Type of scenario		Distance Range (m)	MIDR (dBm)	Exp. Median (dBm)	Model Median (dBm)	Em (dB)
1	North-side Roundabout intersection	Run1	0 - 55	15.7	-75.04	-76.57	1.5
		Run2		15.8			
		Run3		16			
2	South-side Roundabout intersection	Run1	0 - 45	17.2	-72.93	-74.57	1.6
		Run2		16.9			
		Run3		16.8			
3	Y-Junction	Run1	0 - 55	16.5	-67.56	-69.58	2
		Run2		20.6			
		Run3		19.5			
4	T-Junction	Run1	0 - 55	20.6	-64.39	-67.64	3.25
		Run2		20.2			
5	Four way intersection	Run1	0 - 55	19.3	-66.16	-67.33	1.16
		Run2		18.4			

There is a significant difference between data collected at narrow intersections 3, 4 compared to open intersections 1, 2, 5. For example, Em for the runs in the narrow intersections higher than those in the 5 runs in the most open part, the probable reason for this higher Em on narrow intersections due to increased multipath propagation causing fading of larger magnitude which causes the received power to vary more along the path. The largest error was in T-junction intersection (scenario 3) where was 3.25 dB compared to other scenarios that contain open spaces which were which had fewer buildings.

There is a systematic difference between the collected data and the prediction which contributes towards the relatively large Em value.

The variations observed in narrow intersections 3 and 4 were compared with open intersections 1, 2, and 5, this is due to the density of buildings in narrow intersections that act as signal reflectors

An interesting difference can be found in the shape of the vehicles. The shape of the vehicles in the virtualsource11p module is fixed so we do not see such a fluctuation in the signal of the virtualsource11p model and this is one of the limitations in the model because the cars are not always as one shape. On the other hand, the model assumes that the streets of the intersections are straight and perpendicular to each other, and therefore we do not see the power degradation in the model in the Figures. This is one of the constraints in the model. But in fact the real the streets are not always straight and perpendicular.

After taking a closer look at the intersections and doing some visual inspection with the help of video recordings it is found that there are metallic structures at the corners of the buildings that are situated at the corners of the intersections of the streets north in front of the transmitter and receiver. The strength of the reflected multipath components from these metallic frames is very large, giving an unexpected rise to the received power. In contrast, the model is unable to capture this unusual behaviour in the receiving power due to the properties of the material and placement of scatterers.

Depending on empirical cumulative distribution functions (CDF), It has been observed that Doppler spreads are large in the Los condition, especially in open scenarios such as north-side of the roundabout and the four-way intersection, due to the lack of buildings and a large number of mobile reflectors at high speeds, as in the four-way junction in addition to the high power of the signal.

For example, in Figure 4.38 Doppler spreads are apparent, through 90% are 230 Hz and 80% are 190 Hz. While the narrow area with high buildings density such as Y-junction intersection, the Doppler spreads are 90% less than 90 Hz and 80 % less than 50Hz.

As for the of NLOS conditions, there are no large Doppler spreads except for some places in open areas with mobile reflectors where these reflectors help to reflect the signal to the receiver when they pass near it.

For example, in Figure 4.22, the Doppler spreads were approximately close, for the reasons that were mentioned previously. Table 4.11 Details of the Doppler spread difference in all scenarios.

Table 4.11 Details of the Doppler spread difference in all scenarios.

No.	Type of scenario	Scenario condition	CDF 90%	CDF 80%
1	North-side Roundabout intersection	LOS	150 Hz	70 Hz
		NLOS	30 Hz	25 Hz
2	South-side Roundabout intersection	LOS	100 Hz	40 Hz
		NLOS	25 Hz	20 Hz
3	Y-Junction	LOS	80 Hz	50 Hz
		NLOS	50 Hz	30 Hz
4	T-Junction	LOS	80 Hz	50 Hz
		NLOS	30 Hz	25 Hz
5	Four way intersection	LOS	230 Hz	190 Hz
		NLOS	35 Hz	25 Hz

4.6. Relationship between the PDR and MPP

Figure 4.42 illustrates the relationship between the PDR and the peak power for all the data collected. For all the intersections, when peak power > -90 dBm (green coloured area), the PDR is highly likely to support safety-critical applications. The region between -90 and -120 dBm (yellow coloured area) can be called a transition zone that can be used to transmit data in the network, but important security features will not work efficiently. Finally, in the red coloured area, the peak power < -120 dBm the network cannot be used at all.

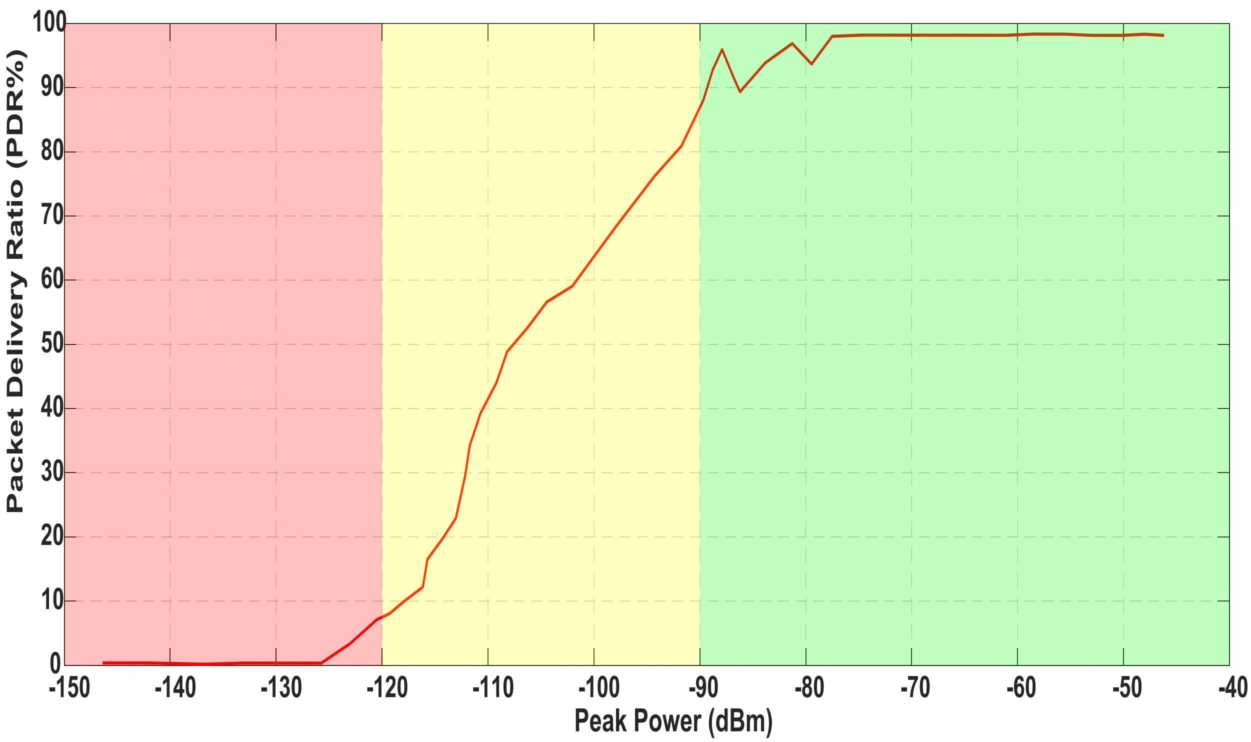

Figure 4.42 The relationship between the average PDR and MPP for all the data collected

4.7. Relationship between the PDR and the Doppler spreads

In Figure 4.3 (which shows the PDR of for the data collected on the south side of the first scenario) it was noticed that there were instances where there were extremely low non-zero PDR values after the receiver was past 37 m from the intersection centre. Compared with Figure 4.9 (which represents Doppler spreads for the south side of the first scenario of the distance between 15 and 55 metres) it was observed that the Doppler diffusion rays had a greater strength again after 37 m.

It has been observed that all scenarios possess values that have a Doppler propagation spectra almost also have a non-zero PDR that are positions where the PDR is greater than zero, though less than 20%. Table 4.12 contains all these non-zero PDR positions.

Table 4.12 The NLOS measurement with a non-zero PDR

Postion	Distance from intersection centre (m)	PDR > 0% (%)
North-side of roundabout intersection	46	19
	47	2
	48	5
	49	10
South-side of roundabout intersection	40	7
	41	5
	43	2
	44	4
Y-junction intersection	53	5
	54	10
	55	2
Four-way intersection	53	10
	54	5

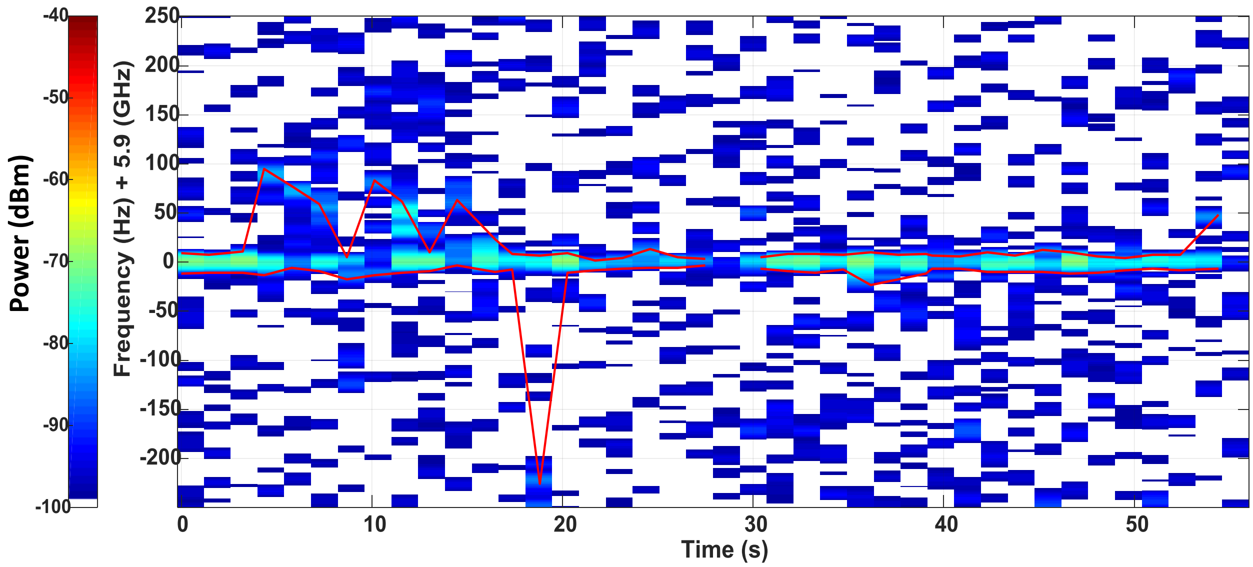

Figure 4.43 The behaviour of frequency at d=38 from the south side of roundabout intersection

Figure 4.43 shows the behaviour of frequency at the distance 38 m from the south side of roundabout intersection when a passing bus near is to the receiver.

Regardless of not seeing (or being able to record) some of the traffic which has improved communications, the Doppler spreads imply that the waves were reflected off moving objects – the vehicular traffic present in the propagation vicinity.

Based on this, 802.11p networks will be deployed in areas with heavy vehicular traffic, which in turn will assist the PDR. However, if each of these vehicles will also contribute to increased network traffic, further study will be needed to determine where the advantages of vehicle traffic are overcome by the disadvantages of increased network traffic.

In addition, almost all of the positions which have Doppler spread spectra also have a non-zero PDR and it can be concluded that the road traffic has directly improved the 802.11p network's performance, albeit for a very short amount of time.

4.8. Conclusion

In conclusion, the dual system described in Chapter 3 was used to collect data at four non-perpendicular intersections in Leicester, UK which provided different propagation environments. A roundabout where NLOS conditions started very close to the centre of the roundabout, Y-junction, non-perpendicular T-junction and a non-perpendicular intersection with a slope in its streets. In all these intersections, traffic was relatively fast during data collection. The collected data displayed how the peak power and PDR deteriorated at each junction as the receiving equipment was moved further away from the centre of the intersection. These data have shown the distances in which vehicle networks will reliably operate critical safety messages in similar environments, which in turn can be useful in network planning. In the north side of the roundabout intersection, it was seen that the traffic increase the variation in the peak power in a path with fewer buildings due to fewer buildings to reflect waves compared to a south side.

In all intersections, it was noticed that the peak power is less when the receiver moves away from the intersection. Scenario three has the best PDR performance furthest from the intersection centre. The roundabout had its PDR drop to zero at least once by 26 m from the centre of the intersection and this the other sides about 35 from the centre of the intersection. In the Y-junction case, the PDR was in single digits long before the receiving equipment was 48 m away from the intersection. The data can also assist in discovering the speed at which a vehicle can travel at and also stop safely if it knows of an approaching vehicle which wants to pass straight through, such as an emergency services vehicle.

The peak power closer to the centre on both sides of the roundabout intersection and was very similar when they were compared with the distance that LOS conditions were lost. On the other hand, away from the intersection centre, the difference in peak power begun to offer as the path with fewer buildings had a lower peak power than the path with buildings on both sides. The PDR did not display similar patterns and started to fall earlier in the path with fewer buildings while it stayed high in the path with more buildings. This reveals importance in building geometry.

The data obtained using the dual-measurement system were compared against an NLOS path-loss model at 5.9GHz frequency. It has been found that the model is flexible and fits well with most of the measurements at different intersections. However, there are some cases where the model does not fit with measurements because of the scattering at some intersections. The model produces results consistent with observations when used in these scenarios and when the receiver is close to the centre of the intersection. The accuracy of predictions for distances far from the intersection is reduced. This difference can be observed by more than -10 dB.

Mangel *et al.* (2011) tried to select the most representative street intersection in Munich but still may not be adequately represented for many other cities. This results in other limitations in the form so that the NLOS model cannot capture unusual behaviours because of in the scattering environment of street intersections.

In this study, the results suggest introducing parameters based on the intersection of the NLOS signal is added dependent on intersection angle and street curvature so that it can overcome the scattering.

The plots in this Chapter provide an overview of all the spectral data collected. These plots are a good index of the size and frequency of Doppler spreads which occurred during the data collection, which is a good indicator of the traffic which was present along with its velocity. In each of the scenarios that were tested, traffic had its individual effect on the data as increasing speeds caused larger Doppler spreads, and when there was more traffic, there were more Doppler spreads. It has been observed that the road with fewer buildings had a greater traffic impact on the data because the proportions of waves being influenced by vehicles were higher.

In addition, another important observation in the data collected was that the size of the Doppler spread seems to be related to the size of the vehicle reflecting the signal. This is because large vehicles have a larger surface to reflect more signals. In this case, the range of Doppler spreads in the signals received increases.

Among the scenarios, the environment with the fewest static scatterers gives the least Doppler spreads. It was observed during data collection near the intersection centre the Doppler spreads caused by traffic have a larger effect.

It can be said that vehicles in the propagation environment can be useful in improving the data network because these vehicles reflect radio waves which in turn operate to extend the coverage of the range allowing reception of packets that would otherwise be lost. It is also clear that the presence of a vehicle, cyclist or pedestrian does not always lead to an increase in PDR and this is because not all visible Doppler spread has an increase in PDR associated with it. Larger vehicles, such as trucks (which have a larger reflector surface), are thought to be better at improving PDR than small cars or sports vehicles.

The amount of traffic affected peak power and PDR in each case and different types of traffic had their individual impact on data; increased speeds caused greater Doppler spreads, and when there was more traffic, more Doppler spreads were observed. Apart from these expected effects, it was observed that on the road with fewer buildings, traffic had a more significant impact on peak power variation because the proportion of waves affected by traffic was higher.

Finally, for close separation values (up to approximately 20 m for all scenarios), 90% of coherence time values are constant but the coherence time becomes more variable with increasing separation between transmitter and receiver for all environments.

Chapter 5: Impact of Environmental Effects on V2V Communication Channel

The two main forms of communication in Vehicular Ad Hoc Networks (VANET): are V2V communication, where vehicles communicate between themselves; and V2I communication, where vehicles communicate with nearby roadside equipment. Because of the comparatively low height of the antennas on the communicating vehicles, it is expected that any change in the environment will affect the signal propagation.

In this Chapter, the focus will be on the impact of temporary changes in the environment such as vehicles that are not connected to the network acting as obstacles to the signal, often affecting propagation even more than static obstacles (e.g. buildings or trees). Also, the antenna height influences the coverage range significantly.

5.1. Effect of traffic on V2V Communication Channel

There is a wide range of empirical studies dealing with the propagation aspects of V2V communication. Many of these studies deal with stationary obstacles, often determined as the key factors that affect signal propagation. However, it is expected that a large part of the V2V communication will be via reflections from the road surface, making the path between two communicating nodes susceptible to interruptions by other vehicles. For example, in urban areas, it is probably other vehicles, especially large transportation and commercial vehicles such as buses and trucks which are considered temporary obstacles, which obstruct the LOS.

However, all modern VANET simulators suppress the impact of vehicles as obstacles to signal propagation, mainly due to the lack of an appropriate methodology capable of effectively integrating vehicle impact. The motivation of this study is to perform measurements to accurately determine the impact of vehicles on the signal power and packet reception rate in different real-world scenarios. Emphasis was placed on measuring the effect of NLOS conditions on the received signal strength and packet delivery ratio. The main goal of this study was to isolate the impact of moving vehicles on the channel quality.

In this Chapter, vehicle traffic and its impact on V2V communication channels were studied in an urban environment at 5.9GHz. In particular, the signal shows variations which depend on the size, speed and location of vehicles relative to the line of sight between the stationary transmitter and receiver. Disturbances in the received signal from different types of vehicles have been studied as they pass through the V2V LOS channel resulting from transmitter and receiver positioning on opposite sides of the road.

5.1.1. Measurement Environment

To facilitate the study of the effect of different vehicles on the V2V channel, the chosen scenario was an intersection between University Road and Welford Road in the centre of Leicester, UK. Figure 5.1 shows the experimental environment. The environment consists of an irregular three-way intersection; one side contains buildings of different sizes. One side of the junction contains two-storey buildings, while on the other two sides large open areas are surrounded by a row of trees. The side-road has a metal fence on the side opposite to where the transmitter is placed. The transmitter and receiver were positioned in LOS contact on either side of the intersection. Three experiments were performed for three different distances between the transmitter and the receiver, which were 20, 40, 60 metres. Measurements of signal strength and Doppler shift were carried out using a CW signal at 5.9 GHz to study of the impact of different size vehicles on the V2V channel. The transmitter and receiver sections were housed in trolleys for easy mobility. The transmitter section consisted of an Anritsu MG3692B signal generator connected via a low-loss coaxial cable to a Hyperlink wireless band 4.9-5.8 GHz 6 dBi omnidirectional antenna (model HVG-4958-06U). The receiver section consisted of an Agilent E4440A the spectrum connected via the same cable to the same antenna (more details in Chapter 3). Table 5.1 presented more details about these measurements. It should be noted that to isolate the impact of traffic, the positions of the two trolleys remained constant throughout each experiment and both were facing each other, allowing the LOS signal path between the trolleys (unless obstructed by traffic) in all measurements. During the measurements, a laptop web camera was used to record all the passing traffic, allowing easy identification of different types of vehicles and permitting their passing to be time synchronized to the measurements. The duration of experiments is about one hour per scenario during the day in order to benefit from the passage of the largest number of cars of different sizes. The flow of traffic was uncontrolled for the duration of the measurements. For each fade, the maximum fade depth (Fmax), duration (T) and Doppler spread (D) were measured. Vehicle speeds varied up to 30mph.

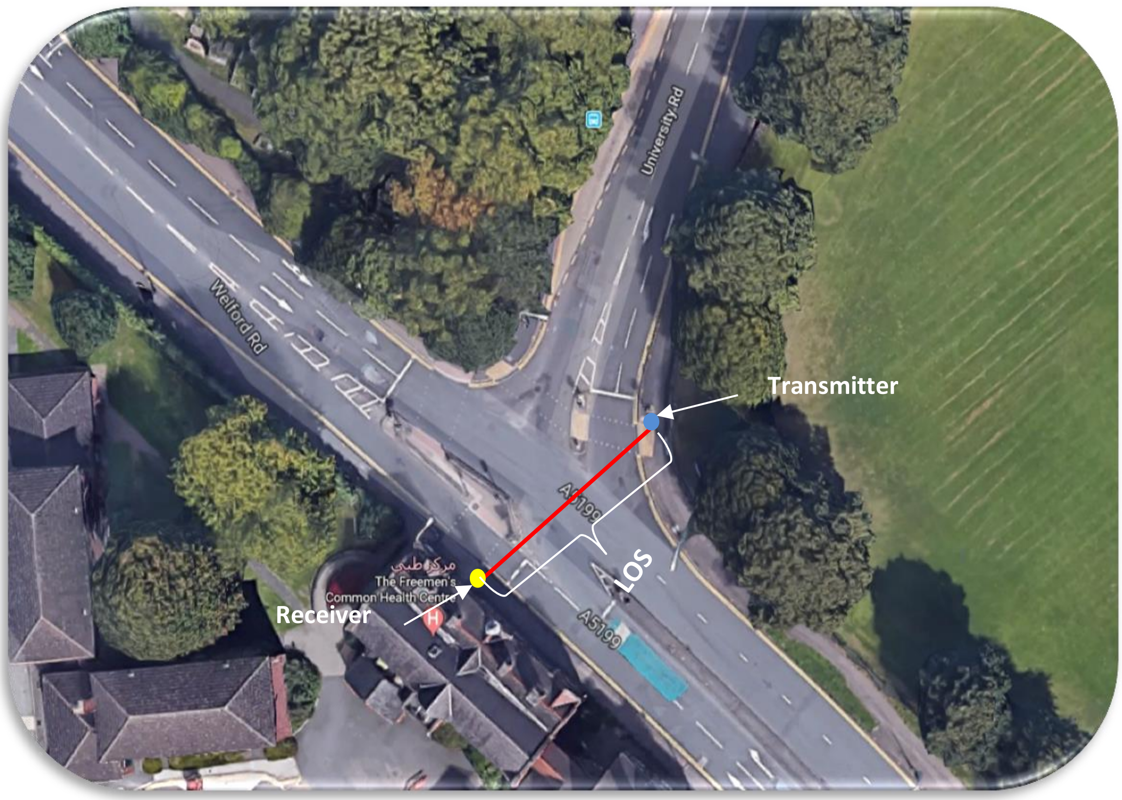

Figure 5.1 The measurements environment.

Table 5.1 Details of the different the three experimants.

No.	Runs	Distance between T_X and R_X (m)	Date	Start time	Vehicles speed (mph)
1	Run1	20	22-10-2018	10:01	30
	Run2	40		12:05	
	Run3	60		16:00	

5.1.2. Vehicle Classification

The internationally recognized vehicle classification system is defined in ISO 3833-1997 (International Organization for Standardisation, 1977). In this system, vehicles are classified according to their structure and design. However, in the United States, another classification system is used by the EPA, this system uses the total internal passenger volume and cargo loads of the vehicle only for assembly performance.

In this study, vehicles that are usually found in urban environments were classified into three groups as follows:

1. Type A includes any small passenger car, multiperson vehicles and small vans such as Mercedes-Benz SLK280, Opel Zafira and Volkswagen Caddy Van and Ford Fiesta.
2. Type B includes light commercial vehicles, such as large vans and large pickup trucks (e.g. Mercedes-Benz Sprinter and Renault Master).
3. Type C includes buses and lorries and any other vehicles that are larger than Type C such as Mercedes-Benz Axor and Iveco Eurocargo.

Figure 5.2 shows examples of each type of vehicle obtained from the video recorded during the measurements.

Figure 5.2 Example snapshots captured from the HD camera showing Type A, Type B, and Type C vehicles.

5.2. The Results

5.2.1. Fading:

To determine and compare the effect of fading and the phenomenon caused by the effect of vehicles on a V2V channel, some measurements were provided those were used to experimentally characterize data. Figure 5.3 illustrates the received signal power that was obtained for a typical vehicle of type A, type B, and type C respectively as they travelled through the LOS between transmitter and receiver at the distance 20 m. The grey area represents the duration of the vehicle's effect on the channel.

As the vehicle approached the LOS, a disturbance in the received signal power of a few seconds was observed. This disturbance resulted from the vehicle blocking the direct signal path between transmitter and receiver. It should be noted that the duration of disturbances in the channel varies depending on the size of the vehicle. To compare the magnitude of fading and the duration of disturbances caused by different types of vehicles, two quantities were determined: the maximum fading depth (Fmax) and duration of disturbance (T). Maximum fading is defined as the maximum decrease in signal power compared to the average signal power in the non-obstructed state, while the duration of the disturbance is defined as the period of time in which the channel is disturbed.

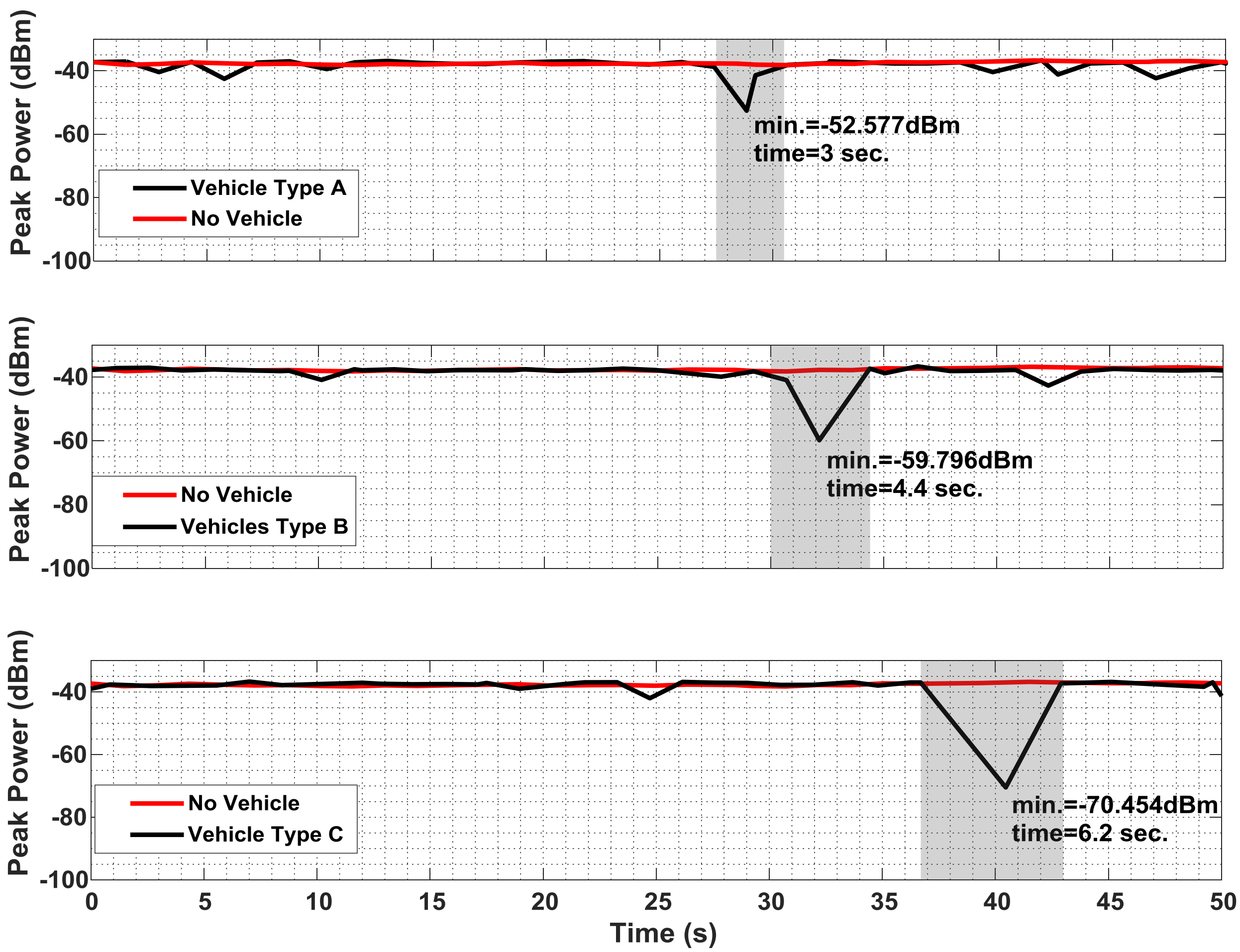

Figure 5.3 Received signal power for types A, B and C vehicles passing through the V2V Channel (20m)

For example, when the vehicle type A approached the channel, disturbances in the received signal power about 3000 ms were observed. These disturbances resulted from the vehicle blocking the direct signal path between transmitter and receiver.

When a vehicle of type B was passing in the link, the receiving signal power started to effect before the vehicle blocked the link. The duration of the disturbance was about 4200 ms. When a vehicle type C blocked the LOS channel, disturbances in the received signal power of about 6200 ms were observed. As seen quite clearly, the channel exhibited different fading behaviour depending on the size of the vehicle relative to the V2V link.

However, the maximum fading showed a significant disparity, with the type A vehicle inducing a much smaller fading when compared with the type C vehicles.

These results indicate that small and medium-sized vehicles can cause the channel's fluctuation to a V2V link from approximately the same distance. However, the size of the disturbance depends on the size of the vehicle. Interestingly, although the type C vehicle type generates a disturbance much longer than the smaller vehicles 6200ms, it is observed that the fading caused by it is bigger to the type A and B where it is by 32 dBm.

Figures 5.4 and 5.5 illustrate the typical received signal power that was obtained for a vehicle of type A, type B, and type C respectively as they travelled through the LOS for distances of 40 m and 60 m respectively. It was observed that increasing the distance between the transmitter and the receiver would cause the Fmax to be significantly reduced because the radio signals attenuate with the increase of the distance.

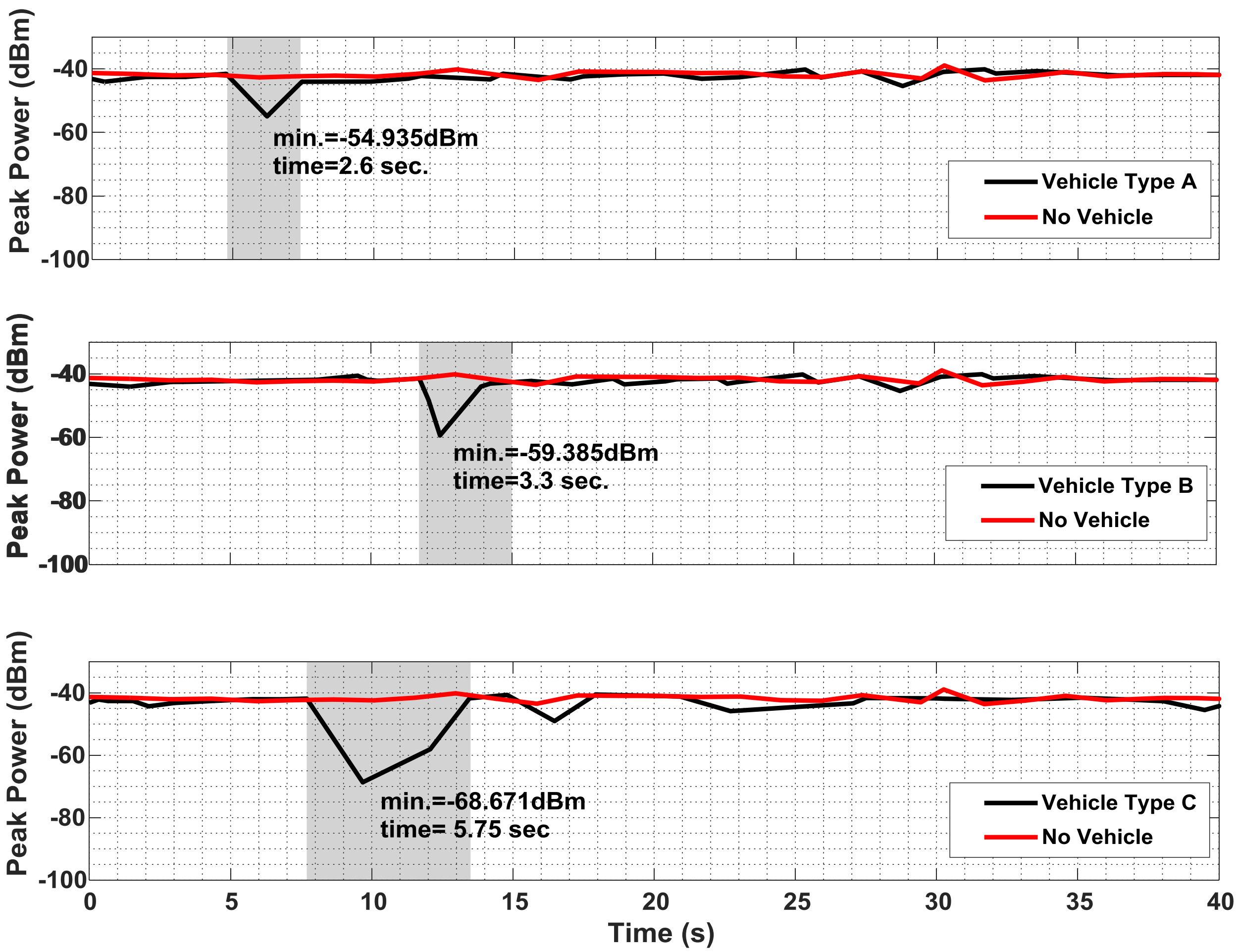

Figure 5.4 Received signal power for types A, B and C vehicles passing through the V2V Channel (40m)

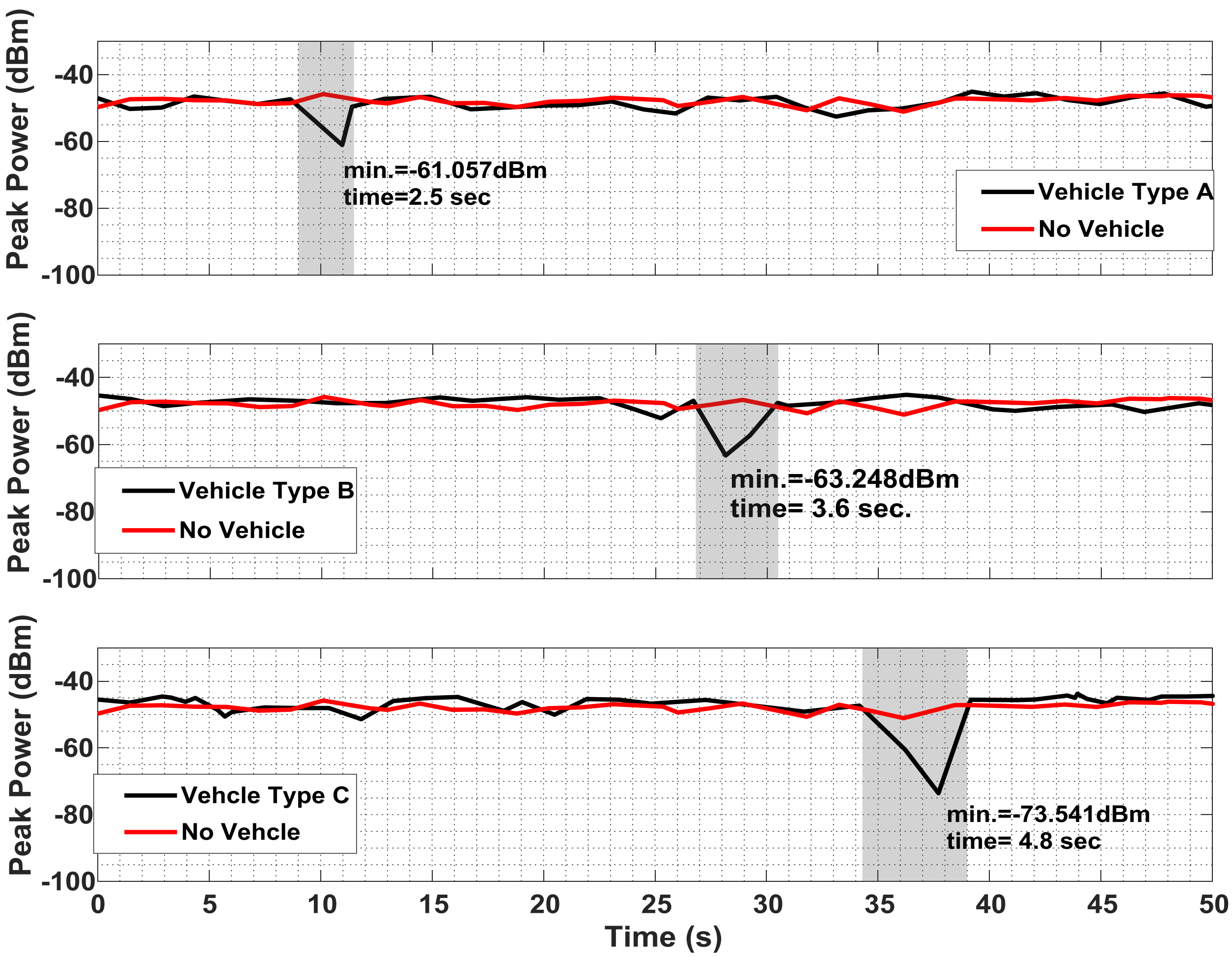

Figure 5.5 Received signal power for types A, B and C vehicles passing through the V2V Channel (60m)

Figure 5.6 shows the cumulative distribution function of the received power. Received power fades when a vehicle pass type A or worse about two-thirds of the time, while those described in the passage of a car of type C occur only 5% of the time.

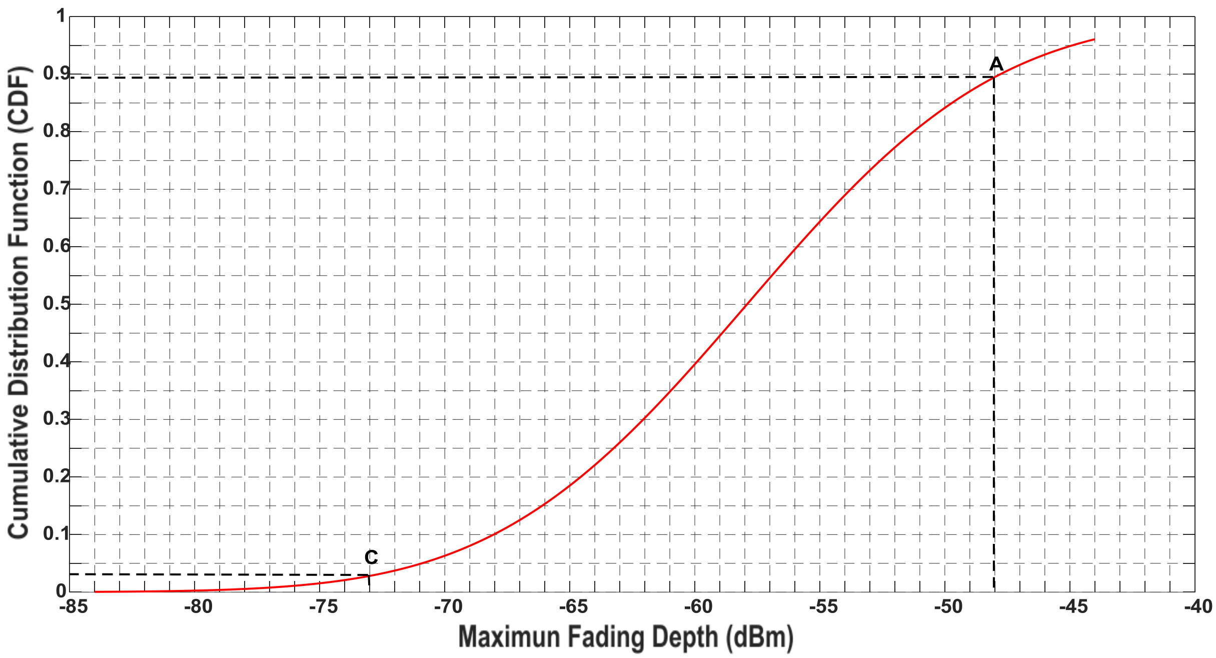

Figure 5.6 Cumulative distribution function of peak power

5.2.2. Doppler behaviour in a LOS condition

In this section, the behaviour of the signal was studied at the maximum fading of each type of vehicle. Figure 5.7, illustrates, the black curves show typical frequency characteristics seen when vehicle of types A, B, and C pass through the LOS link between the transmitter and receiver separated by a distance of 20 m. The red curve represents the signal without an obstacle and the green line represents the noise level. The grey area represents Doppler spread (D) of the vehicle's effect on the channel and is defined by the black and green lines' first intersection away from the peak. The depth of fading, Fmax is seen as the vertical separation between the red and black lines at the peak. This increases as the size of the vehicle increases, from 14.7 dB for type A to 22.0 dB for type B and 32.6 dBm for type C. Furthermore, a clear dependence of Doppler spread on vehicle type is apparent, with D = 185 Hz for type A, 120 Hz for type B and 90 Hz for type C.

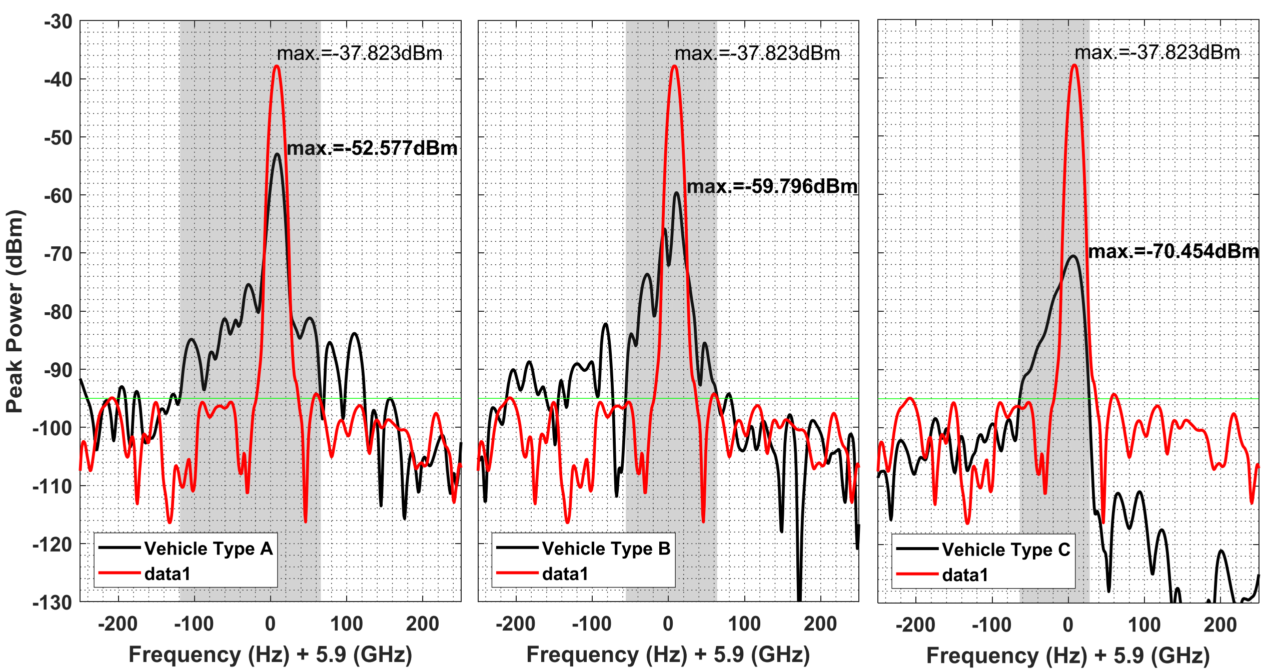

Figure 5.7 Signal behaviour at maximum fading for types a, b and c vehicles passing through the LOS V2V channel (20 m)

The frequency spread is bigger when a vehicle of type A passes through the channel when compared to the frequency spread when a vehicle of type C passes through the channel. The D was 185 Hz when a vehicle of type A was passed, while it was 90 Hz when a vehicle of type C was passed. When a type B vehicle was affecting the channel, the DW was 120 Hz.

Figures 5.8 and 5.9 show the spectra for transmitter - receiver separations of 40 m and 60 m respectively. A similar dependence of Fmax on vehicle type is seen at these separations, but the scale of the difference is diminished, along with the overall signal strength. The pattern of decreasing D with increasing vehicle size is also seen. This pattern seems to be due to the sidebands of the spectrum descending below the noise floor as the fading depth increases. However, comparison with the red curves shows that the sidebands are only significant when the vehicle blocks the LOS path, so the effect of the vehicle is twofold. The larger the vehicle, the more it reduces the overall power reaching the receiver but also, the lower is the main peak above the sidebands, as more is scattered into Doppler shifted reflections. It is difficult to understand exactly how the obstacle can block its own reflections, but maybe this is due to secondary or tertiary reflections. This effect reduces with separation, as the reflections become less significant. It was observed that the Doppler spread was always larger when vehicles of type A was passing through the channel, while it is decreasing when the size of the vehicle increases due to increased temporary shadow time. Interestingly, in Figure 5.9 for vehicle type C, the sidebands reduce even below the sidebands seen in the red curve. This suggests that even when no vehicle is directly in the LOS path, there are reflections from more distant vehicles, and that these, as well as the LOS signal can be blocked by a large vehicle. Figure 5.10 shows the Doppler spectrum bandwidth for each type of vehicles.

Table 5.1 illustrates the duration of disturbance, the maximum fading and the Doppler spectrum bandwidth for each type of vehicle.

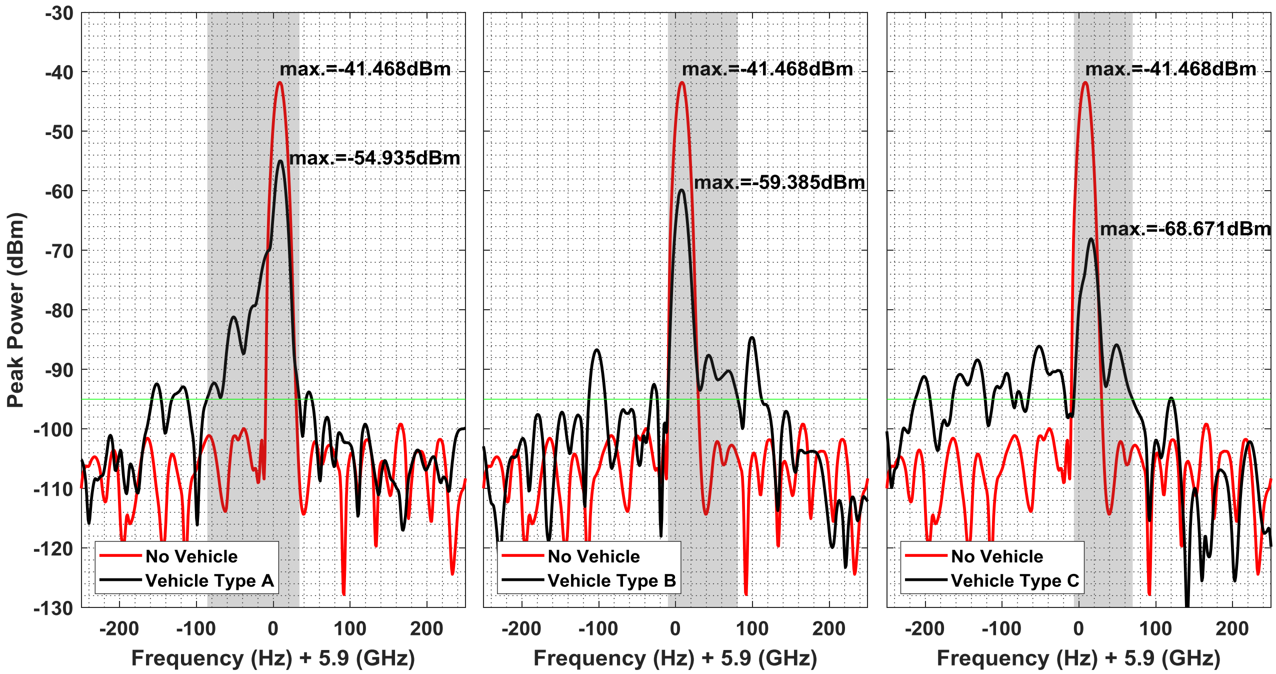

Figure 5.8 Signal behaviour at maximum fading for types a, b and c vehicles passing through the LOS V2V channel (40 m)

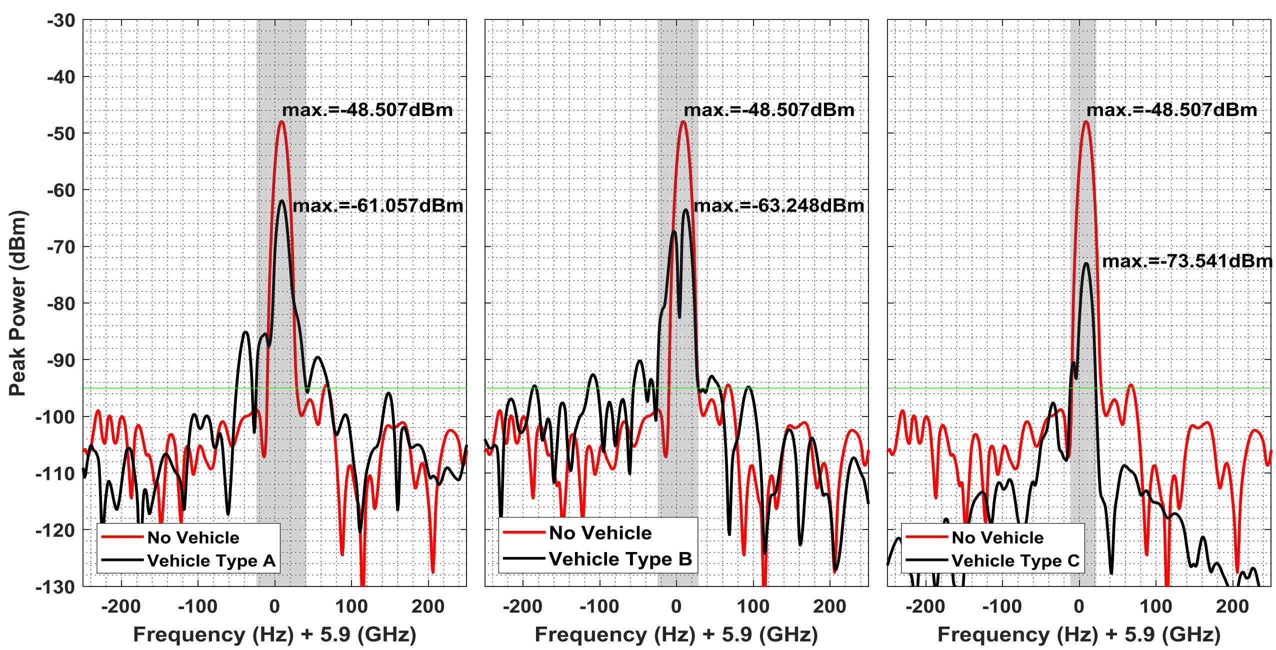

Figure 5.9 Signal behaviour at maximum fading for types a, b and c vehicles passing through the LOS V2V channel (60 m)

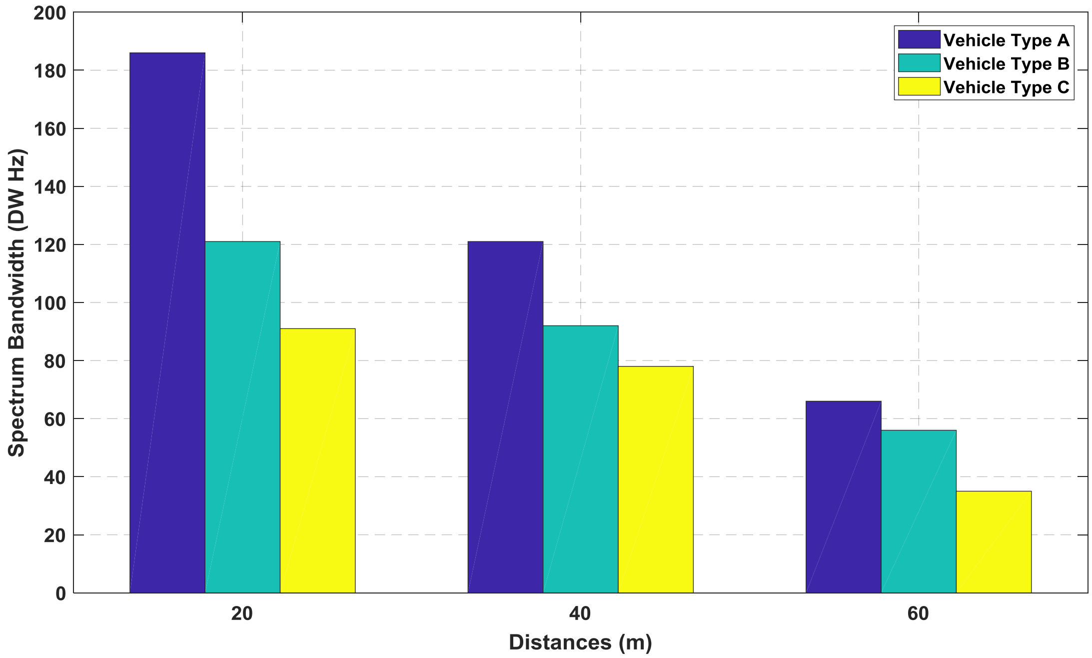

Figure 5.10 Doppler spectrum bandwidth (D) vs. vehicle type and distances

Table 5.2 Duration of disturbance, maximum fading and the Doppler spectrum bandwidth for each type of vehicle

Distance (m)	Vehicle type	Unperturbed Signal Power (dBm)	perturbed Signal Power (dBm)	Fmax (dBm)	T (ms)	D (Hz)
20	**A**	-37.7	-52.5	14.7	3000	185
	B	-37.7	-59.7	22	4200	120
	C	-37.7	-70.4	32.6	6200	90
40	**A**	-41.4	-54.9	13.4	2500	120
	B	-41.4	-59.3	17.9	3300	91
	C	-41.4	-68.6	27.2	6500	77
60	**A**	-48.5	-61	12.5	2500	65
	B	-48.5	-63.2	14.7	3300	55
	C	-48.5	-73.5	25	4800	34

5.3. Effect of Antenna Height on V2V Communication Channel

In general, in wireless communication, the antenna height influences the coverage range and the throughput significantly. In this section, the effect of changing antenna height on the vehicle channel was studied.

5.3.1. Measurement Environment

Figure 5.11 shows the scenario in which measurements were taken was the campus of the University of Leicester. it has narrow roads (single lanes) and many buildings which provide line-of-sight (LOS) and non-line-of-sight (NLOS) propagation conditions at intersections. An intersection is relatively built-up with buildings located along all road. However, the buildings are not uniformly distributed since it is more open from away from the intersection centre (e.g the Library podium is an open space on a raised platform with 1.68 m high walls).

The transmitter and receiver each consisted of Arada LocoMate 2 devices with the Received Signal Strength Indicator being used to measure the signal strength. Secondly, rather than using spot distances, the receiver was moved (at velocities less than 0.5 ms-1) and the median signal levels in 2 m wide bins found (the edges of these bins were positioned using a laser range-finder). The receiver was located within LOS of the transmitter in two positions while the remainders were NLOS. Measurements were taken during a series of five separate runs in different scenarios without control of the pedestrians, cyclists and vehicles. The range of distances (0–18 m) was chosen such that the PDR was close to 100% and hence the median level is a good representation of the actual signal level.

The antenna has an effect on the performance of wireless systems from vehicle to vehicle, such as its altitude, ground plane presence, etc. Measurements were taken for five different configurations of the transmitter antenna, ht=1 m with no ground plane (i.e. on the wooden trolley), ht =1 m with a ground plane (a sheet of aluminum), on the roof of a van with ht=2 m, and for ht =1.5 m and ht =2 m without a ground plane. The transmitter was placed in the centre of a 4.7 m wide street canyon a distance 24 m from a 90^o intersection, while the receiver moved along the middle of the road of intersection from 0 to 18 m

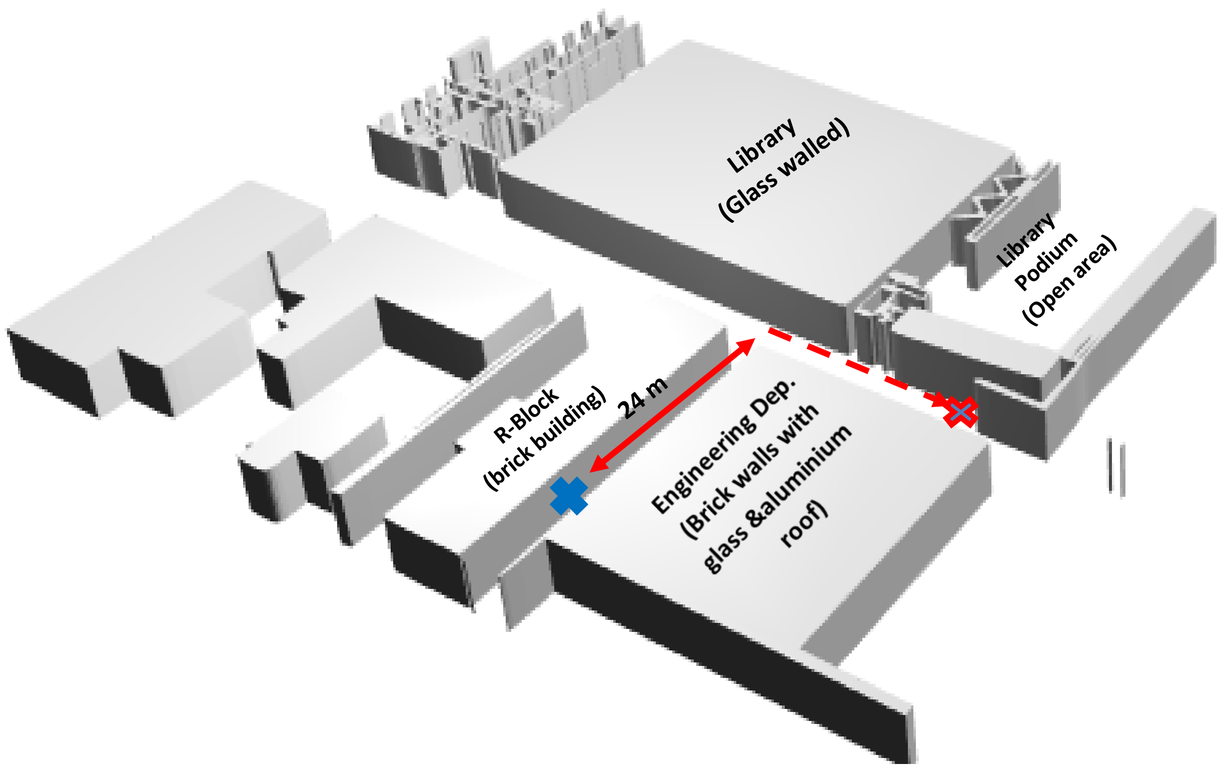

Figure 5. 11 The measurements environment.

5.3.2. Results

Figures 5.12 to 5.16 show the received signal strength (RSS) for the antenna on a trolley, at 1, 1.5 and 2 m height and on the van respectively. The red lines represent the median value of all measurements data respectively.

From these Figures, the height of the antennas (about 1 m from ground level) is lower than that found for a roof-mounted antenna on a typical car (~1.5 m) or small van (~2 m). The changing the height of the transmitter has a strong effect on the received signal at values of the distances within, or a few metres beyond, the LOS region, but the little effect at greater distances.

In addition, placing the antenna on the roof of a van (ht=2 m) has a similar effect to changing the height. Another possible source of divergence of the experiments reported here from vehicle-mounted antennas is that some antennas proposed for use in V2V are omnidirectional antennas on the roof of a vehicle, the geometry of the roof or roof furniture (e.g. roof racks) may result in a non-uniform radiation pattern given the rich multipath environment, and hence the behaviour of the received signal power may be different from that in Figure 5.12.

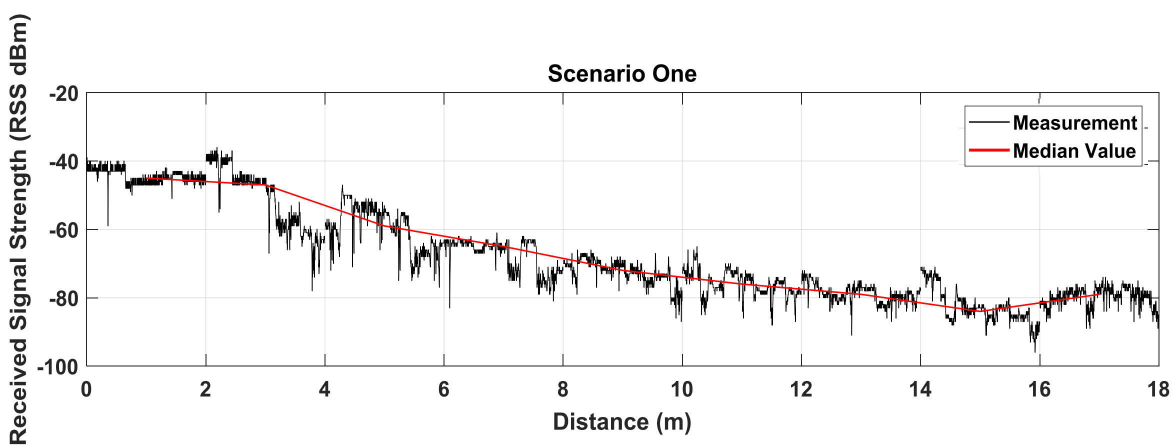

Figure 5.12 RSS measurements for 1 m height on a trolley.

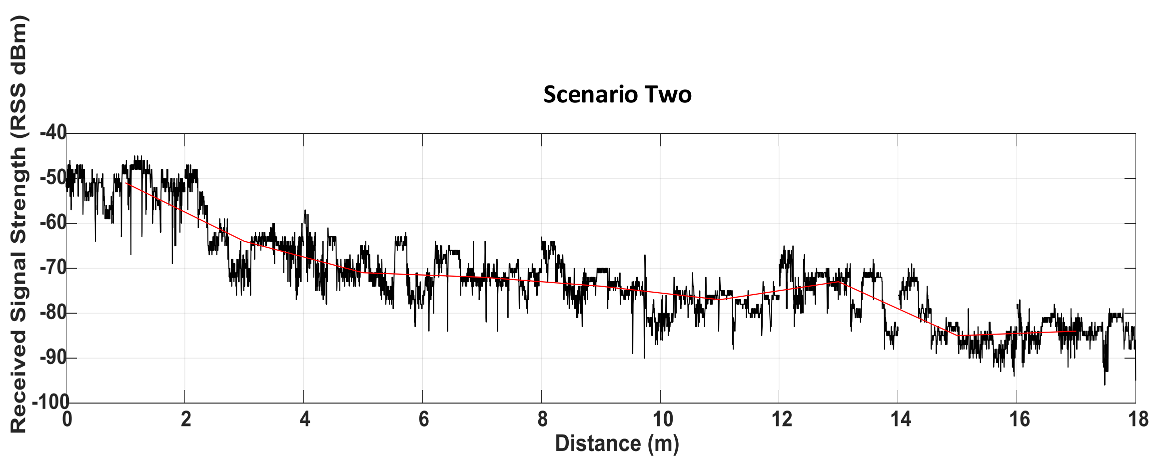

Figure 5.13 RSS measurements for 1 m height with aluminium sheet.

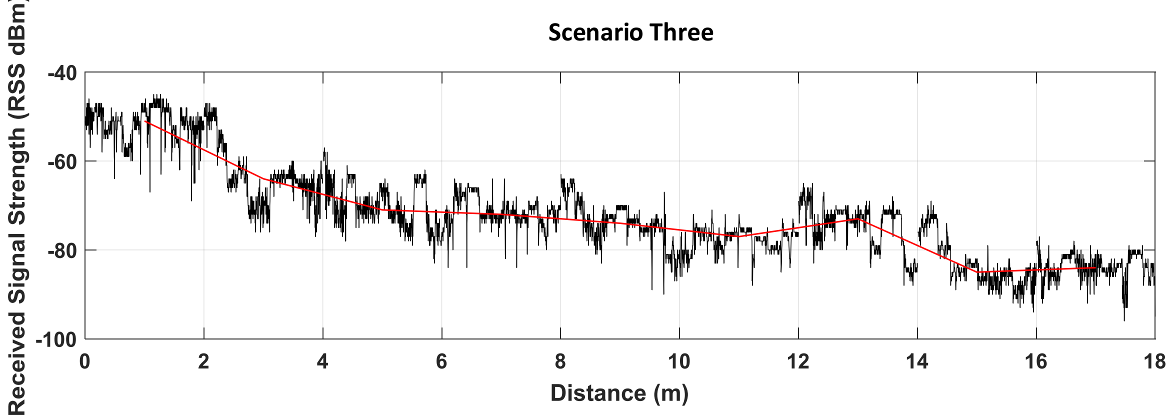

Figure 5.14 RSS measurements for 1.5 m height on a trolley.

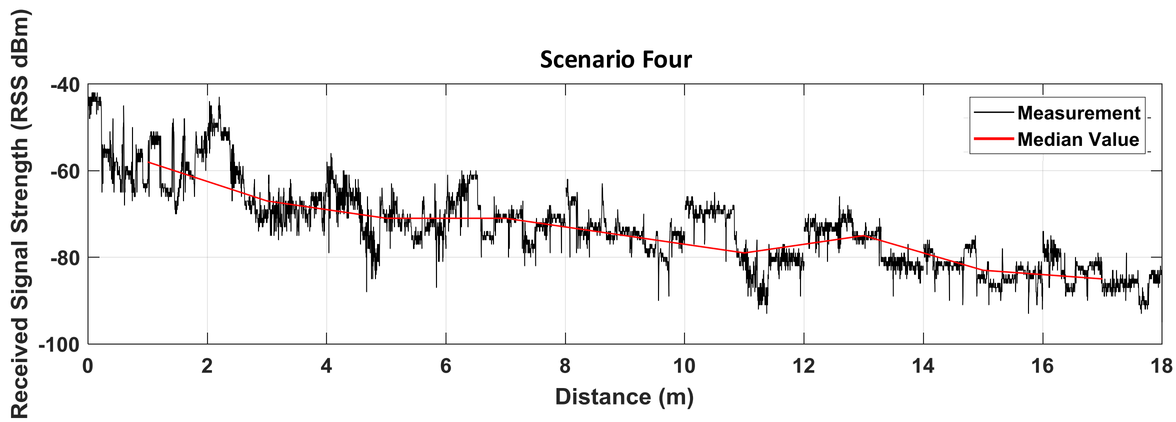

Figure 5.15 RSS measurements for 2 m height on a trolley.

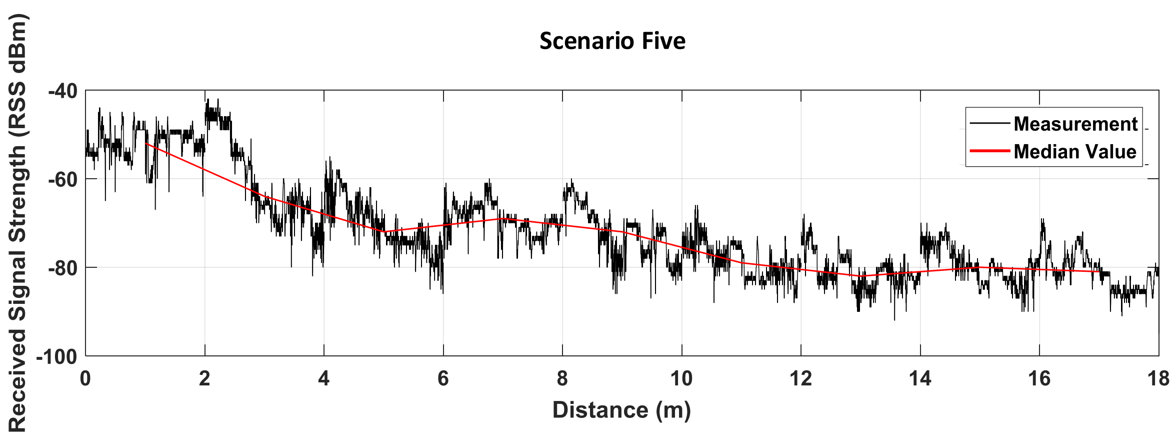

Figure 5.16 RSS measurements for 2 m height on a van.

Figure 5.17 shows the difference between the scenarios shown in Figures 5.13, 5.14, 5.15 and 5.16 with the scenario in figure 5.12.

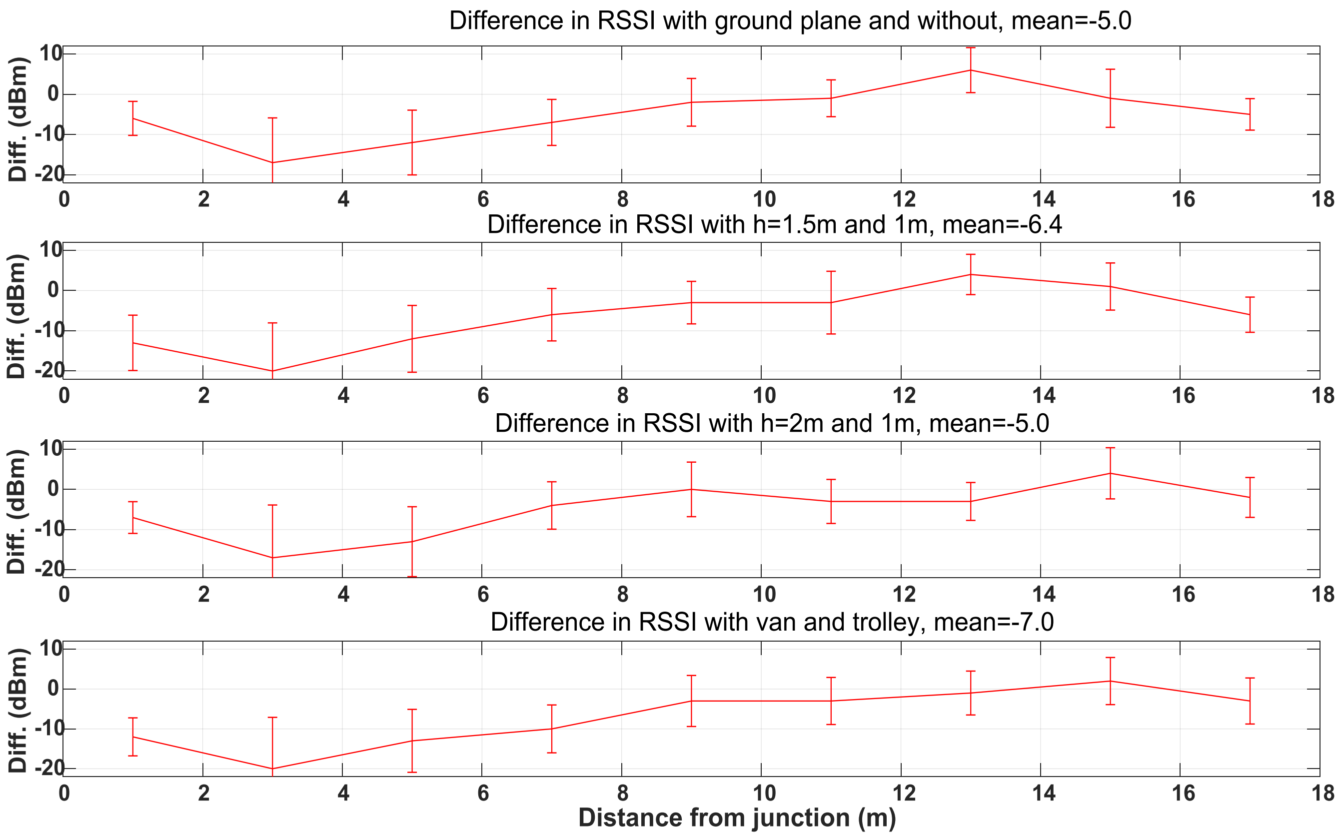

Figure 5.17 The difference in RSSI between the scenarios.

5.4. Conclusions

In this Chapter, the effect of traffic on a V2V channel was studied at 5.9 GHz in an urban environment. The impact of the size of three different types of vehicles has been studied when they block a V2V LOS link. In particular, the statistical characteristics of the fading in the signal observed in a V2V link formed by two trolleys, one being the transmitter and the other being the receiver

The effect of blocking by the vehicle is to reduce the average signal power significantly when compared to the LOS case and to decrease the Doppler spread depending on the size of vehicles. It has been observed that the obstructing vehicles significantly decrease the received signal power compared to when the LOS path is clear. This decrease is directly correlated to vehicle size. The reduced power and spreading in frequency both have a detrimental effect on the quality of V2V communication.

The duration of disturbance of the channel depends on the size of the vehicle passing through the V2V link, which obscures the LOS. It is worth noting that the characteristics of a V2V signal are expected to vary in traffic in different environments (e.g. city centre, urban and rural areas) depending on the traffic density and the speed of vehicles that have a clear impact on the characteristics of the link. This duration of fading is strongly correlated to vehicle size.

To conclude that, in order to design a V2V connection model correctly, the impact of vehicles as obstacles cannot be neglected

The changing the height of the transmitter has a strong effect on the received signal at values of distance within, or a few metres beyond, the LOS region, but the little effect at greater distances. In addition, the antenna ground has a similar effect in changing the height as in placing the antenna on the surface of the truck (ht = 2 m).

Chapter 6: Simulations and Performance Evaluation of V2V Communication Perspective

Vehicle channel modelling plays an important role in assessing the performance of communication systems for V2V (Filali, 2017). Future developments of such models depend on a good performance in different environments such as highways, urban, rural and suburban areas. The main challenge in this area is to develop a precise and efficient vehicle channel model that can take into account the random and variable characteristics over time of different environments. An accurate radio channel model provides a better understanding and thus a better design for vehicular communication systems (Al-Bado *et al.* 2012).

Geometry-based channel models are able to represent the propagation environment more accurately (Cheng *et al*. 2013). These modelling techniques rely on a variety of information about what surrounds the vehicles, which include building engineering data obtained from available sources (Boban *et al.* 2014). For example, using satellite images to model a V2V environment for channel characterization on a city-scale.

Simulating a practical vehicle environment requires an assortment of information from numerous sources. Moreover, because of the complication included in implementing vehicle channel models to simulate a large-scale network, one simulator cannot assess the performance of an entire system (Filali *et al.* 2017).

6.1. Simulation Framework for V2V Ad Hoc Network

A new three-phase simulation framework was proposed that combines multiple layers of simulations in three distinct phases. The first stage of a realistic environment configuration is characterized by the passage of cars using OpenStreetMap as well as Simulation of Urban Mobility (SUMO). The second stage created LOS and NLOS links GEMV2 in a realistic communication environment for V2V. Finally, the last stage involves producing two sets of files that help to analyse the results. The first group of files is the Keyhole Markup Language (KML) format to visualize the result by using Google Earth. The second group is comma-separated values (.csv files) suitable for analysing the results. Figure 6.1 illustrates the framework of the simulation.

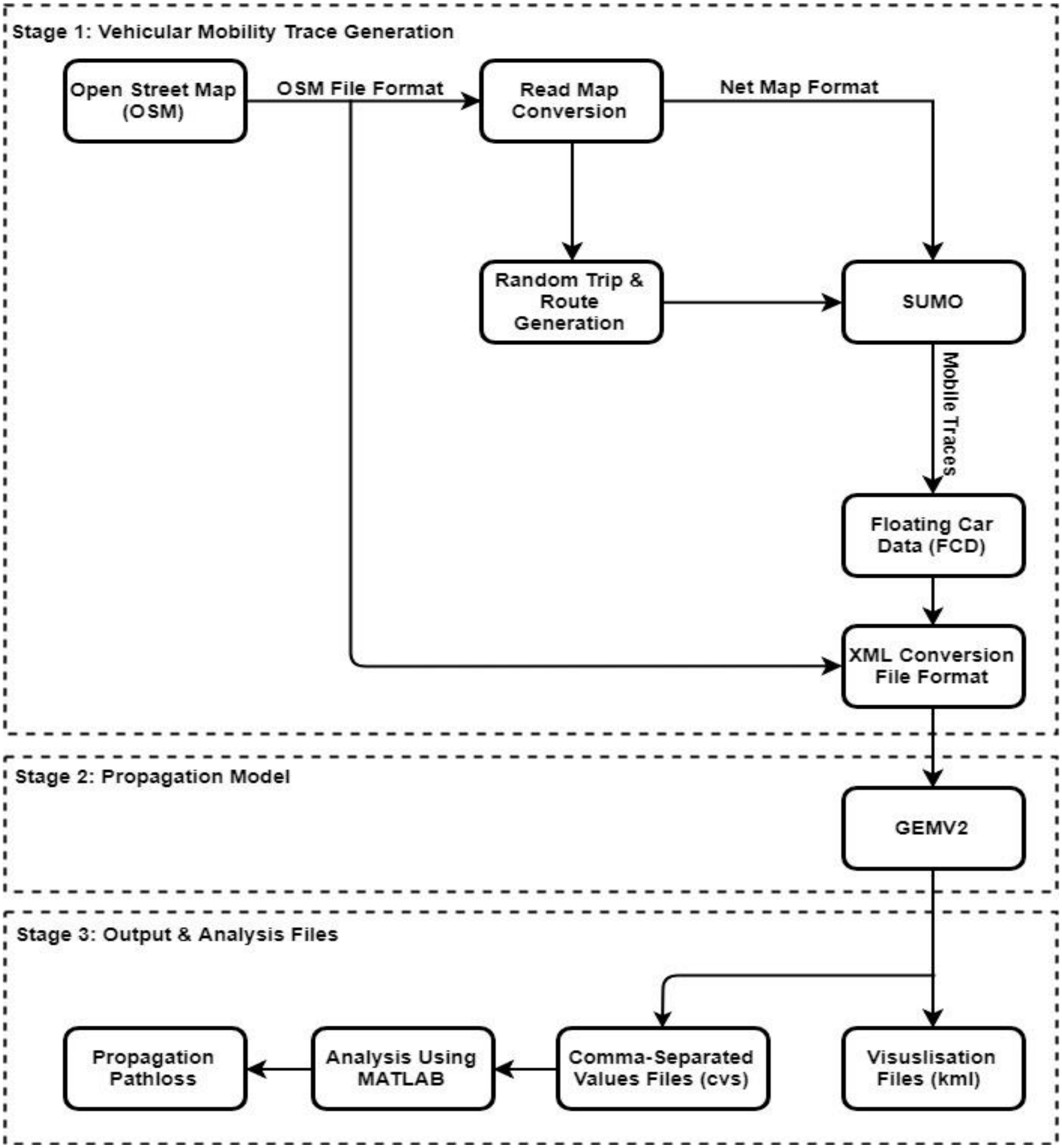

Figure 6.1 Framework of Simulation of V2V Propagation Model

6.1.1. Vehicular Mobility Trace Generation

To generate the impact of city-wide transport on the map of real road infrastructure Simulation of Urban Mobility (SUMO) has been used (SUMO, 2018). The road network layout is extracted for the selected area such as Leicester from OpenStreetMap (OSM) which provides global maps through an extensive network of shareholders and a large user base (Haklay, *et al.* 2008). For this purpose, the OSM has to pass through several necessary conversion processes before it is integrated with the randomly generated trips and route information. The Net-Map file format which has the road network and the route information produces vehicular mobility patterns in Floating Car Data (FCD) format. Figure 6.2 shows the extracted road topology from OSM and the mobility scenario in SUMO-GUI.

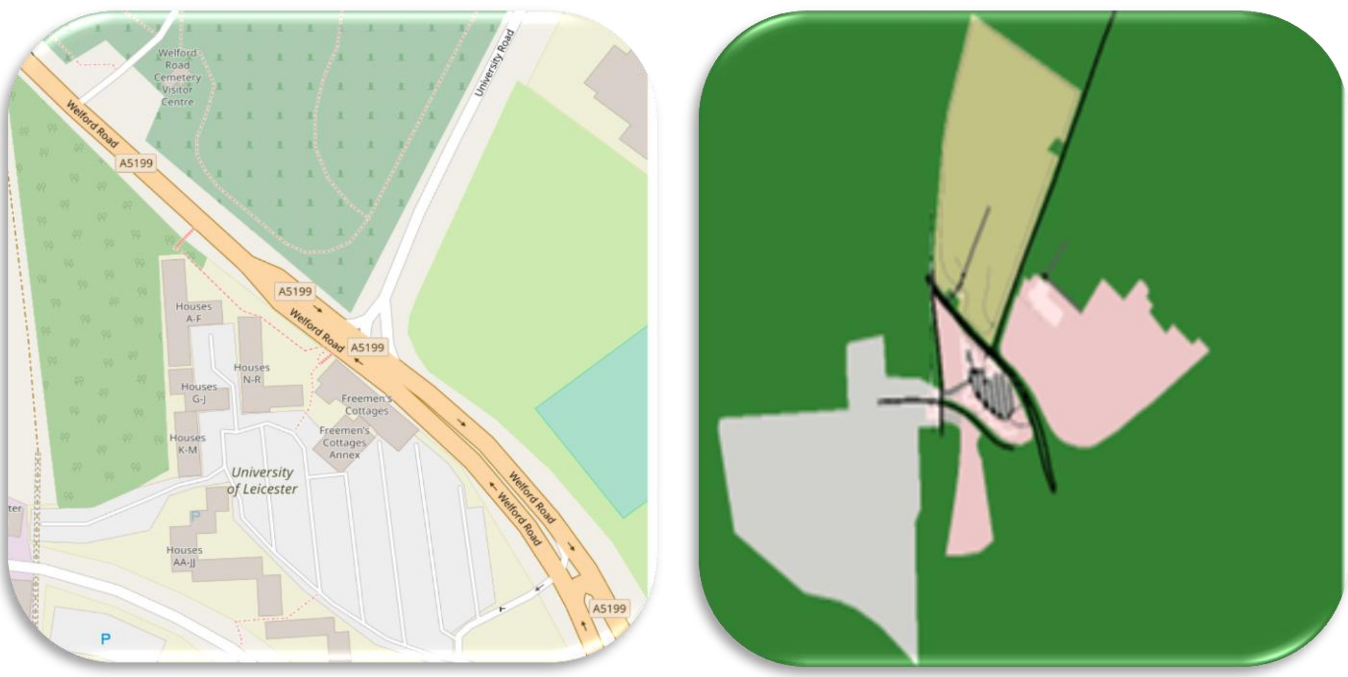

a **b**

Figure 6.2 Road Infrastructure Map obtained from OSM and displayed in SUMO-GUI respectively

6.1.2. GEMV2 Propagation Model

Before it is discussed the structure of GEMV2, it is introduced the spatial tree structure which used for efficient VANET object manipulation. As previously mentioned buildings and foliage outlines are provided through free geographic databases such as OpenStreetMap. SUMO has also been used to provide outlines and vehicle locations. The dimensions of the vehicles can be measured from statistical distributions.

To model large networks with hundreds (or thousands) of vehicles, R-trees was used (Luo, *et al.* 2012). It is a tree data structure in which objects in the field are bound by rectangles and hierarchically structured based on their location in space. Because of the inherent geometrical structure, VANET data lend themselves to an efficient R-tree representation. The outlines of the vehicles are stored in an R-tree separate from the outlines of buildings and foliage is that, unlike vehicles, buildings and foliage do not move; therefore, their R-tree needs to be computed only once. On the other hand, the vehicle R-tree changes at each simulation time step. The algorithm starts with all objects (i.e., vehicles, buildings, or foliage) and splits them into two child nodes (i.e., we use a binary R-tree). To keep the tree balanced, the objects at each node were sorted splitting based on the currently longer axis so that each created child node contains about half of the objects.

The Geometry-based efficient propagation Model (GEMV2) was used, which provides a geometry-based propagation model for V2V communication. It is a MATLAB implementation which is free and openly distributed. This model is a hybrid of the deterministic and stochastic channel modelling techniques, where it can distinguish and measure the characteristics of the channels for three different types of links (LOS, NLOSv and NLOSb) by considering the geometrical information such as height, width, etc.

GEMV2 uses outlines of vehicles, buildings, and foliage to calculate large-scale signal variations (path-loss and shadowing). It calculates the small-scale signal variations using the number and size of objects around the communicating vehicles. To simulate the V2V communication channel by using GEMV2, it is necessary to import both vehicular mobility file from SUMO and outlines of buildings and foliage from OpenStreetMap.

As mentioned in Chapter 2, GEMV2 classifies V2V communication links into three groups: the first one is LOS-links that have an unobstructed optical path between the transmitting and receiving antennas. The second one is NLOSv–links whose LOS is obstructed by other vehicles. Finally, NLOSb–links whose LOS is obstructed by buildings or foliage.

For these three groups, GEMV2 calculates large scale signal variations for effects roughly pertaining to path loss and large-scale fading deterministically. Whereas it calculates small scale signal variations stochastically and models the effect by combining multipath due to diffractions, reflections, and scattering, and Doppler spread. The other objects such as traffic signs and traffic lights are considered because of neither readily available geographic databases nor computationally feasible to model.

In order to calculate large and small-signal differences, GEMV2 implements different propagation models for each type of link. For LOS links, the two-ray ground reflection model is used, while for NLOSv links, it uses an experimental model (Boban *et al.*, 2011) which includes diffraction off the sides and the roofs of vehicles. For NLOSb links, GEMV2 calculates reflection and diffraction and long-distance path loss model.

After large and small scale signal variations are calculated, the two-ray ground reflection model is used to obtain the total loss of the path as in Equation 6.1.

$$|E_{TOT}| = \frac{E_o d_o}{d_{LOS}}\, cos\left(w_c\left(t - \frac{d_{LOS}}{c}\right)\right) + R_{ground}\frac{E_o d_o}{d_{ground}}\, cos\left(w_c\left(t - \frac{d_{ground}}{c}\right)\right) \ldots\ldots\ldots\ldots\ 6.1$$

Where the total received E-field, E_{TOT}, is then a result of the direct line-of-sight component E_{LOS}, and the ground reflected component. E_o is the free space E-field, d_o is a reference distance, d_{LOS} is distance the that direct wave travels, d_{ground} is distance that the reflected wave travels, w_c is angular frequency, and c is the speed of light. Unlike other simulators, GEMV2 takes into its calculation the antenna height due to the importance it obtained from the measurement results while calculating the reflection coefficient R_{ground} and distance d_{ground}.

The received power was found by long-distance path loss model PL for distance d is given by (Srinivasa *et al.*, 2009).

$$PL(d) = PL(d_o) + 10_{\gamma} \log\left(\frac{d}{d_0}\right) \dots \dots \dots \dots 6.2$$

Where path loss exponent γ = 2.9, which extracted from (Fernando, 2011). $PL(d_o)$ is reference path loss at a reference distance d_o.

6.1.3. Output Flies

After the simulation is finished, two types of files are obtained:

- The first type is Keyhole Markup Language (KML) to visualize the results. Google Earth or any program that provides support KML format is used.
- The second type of these files is comma-separated values (CSV) with each variable saved in a different file which suitable for analyzing the results in/outside MATLAB.

6.2. Performance Evaluation

6.2.1. Simulation Environment

V2V channel parameters change as vehicles move across different environments with different traffic conditions. The aim of this study is to display how path loss changes according to various traffic scenarios.

For performance evaluation, the scenarios described in Chapter 3 were simulated which were characterized by the heterogeneous heights of the buildings. The simulation was performed twice per scenario in a different number of vehicles to study the effect of vehicles density on the parameters of a V2V communication channel. These vehicles were moving between a randomly selected origin and destination. Table 6.1 illustrates the simulation parameters and their corresponding values. The values of the communication range in the table were taken from the results of previous studies (Boban *et al.*, 2011).

Table 6.1 Description of simulation parameters

Parameter	Values
Number of Vehicles	10, 100
Data Rate	6 Mbps
Minimum Receiver Sensitivity	-95 dBm
Transmission Power	18 dBm
Frequency	5.89 GHz
Antenna Height	0.2 m
Vehicle Speed	20 mph to 60 mph
Simulation Duration	100 s
Path Loss Exponent	2.9
Max. Range (NLOSb link)	300 m

6.2.2. Simulation Study

Figures 6.3 to 6.6 show the Google Earth visualization in term of received power calculated by the model for all scenarios in Chapter 3. The coloured lines representing received signal strength in dBm between the transmitter and the receiver.

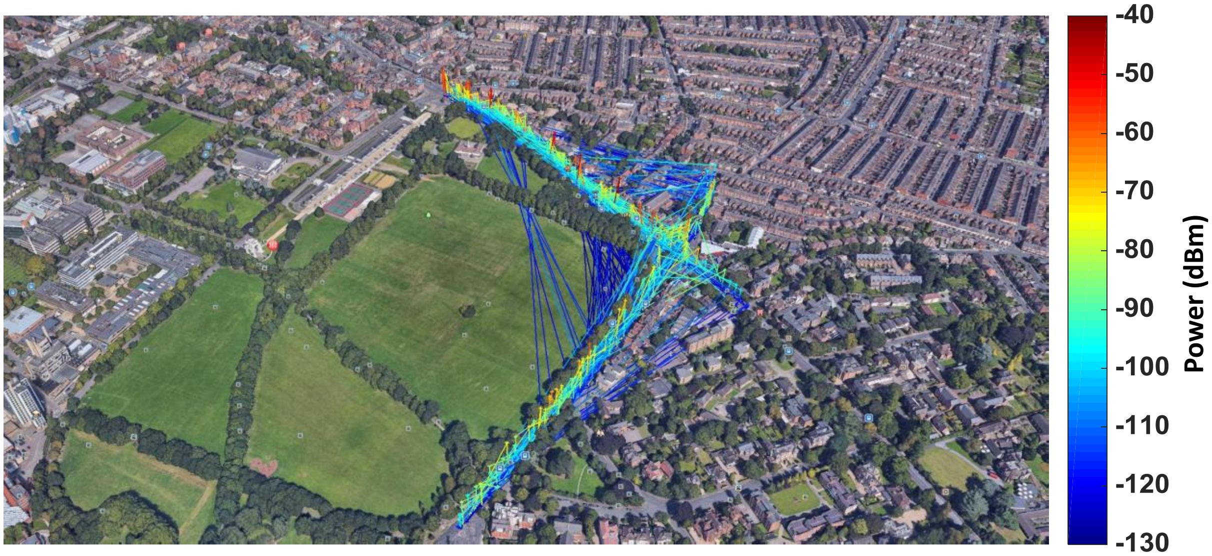

Figure 6.3 The google earth visualization for the first scenario

Figure 6.4 The google earth visualization for the second scenario

Figure 6.5 The google earth visualization for the third scenario

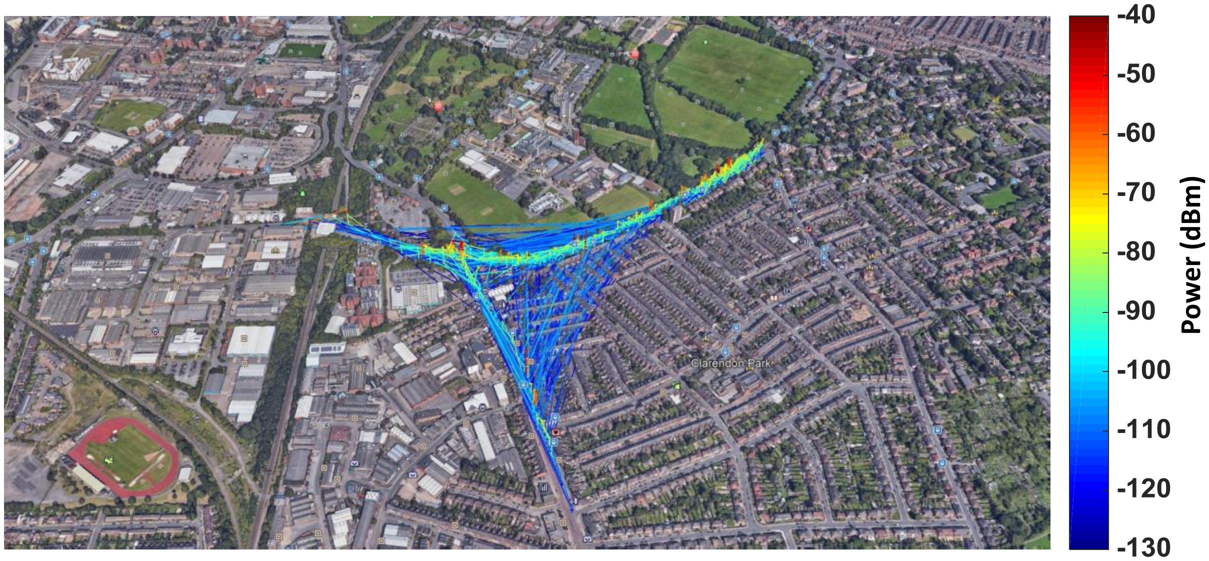

Figure 6.6 The google earth visualization for the fourth scenario

Figures 6.7 to 6.10 show the difference in the received power for all scenarios in Chapter 3 by using 10 and 100 vehicles. In all graphics, the x-axis shows the distance in metres between communication pairs while the y-axis shows the received power value in dBm. Additionally, the standard deviation (σ) and the mean (μ) values are given below the related graphics.

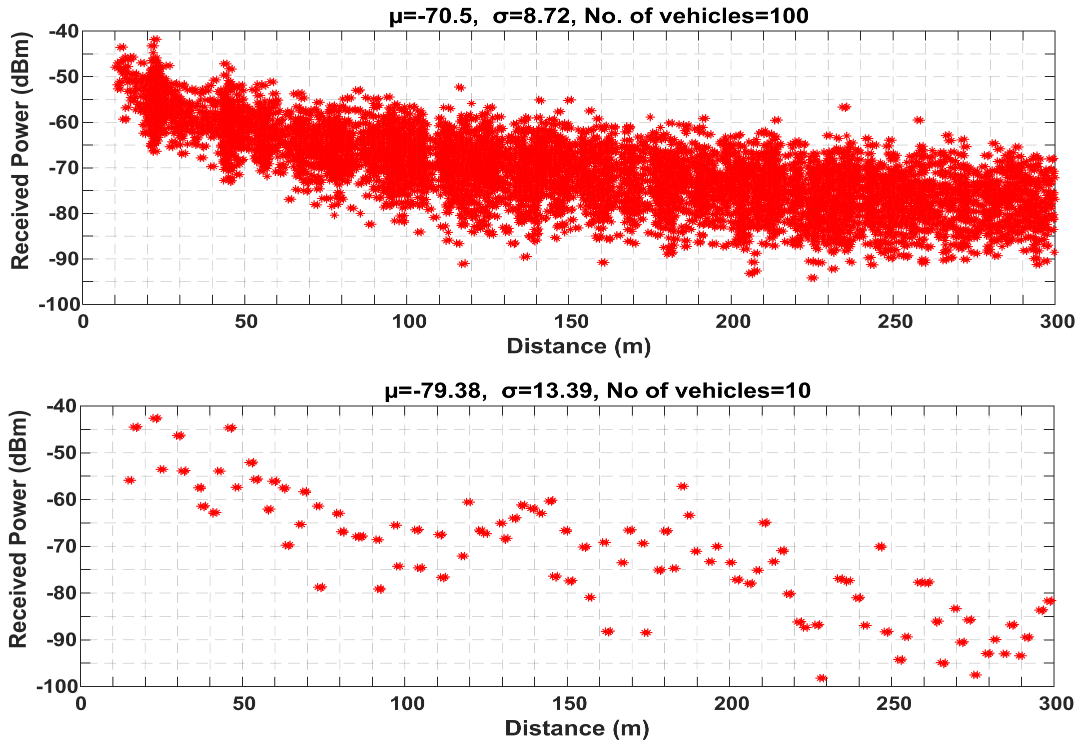

Figure 6.7 Comparison of received power (dBm) for the roundabout intersection on GEMV2 V2V communication simulations

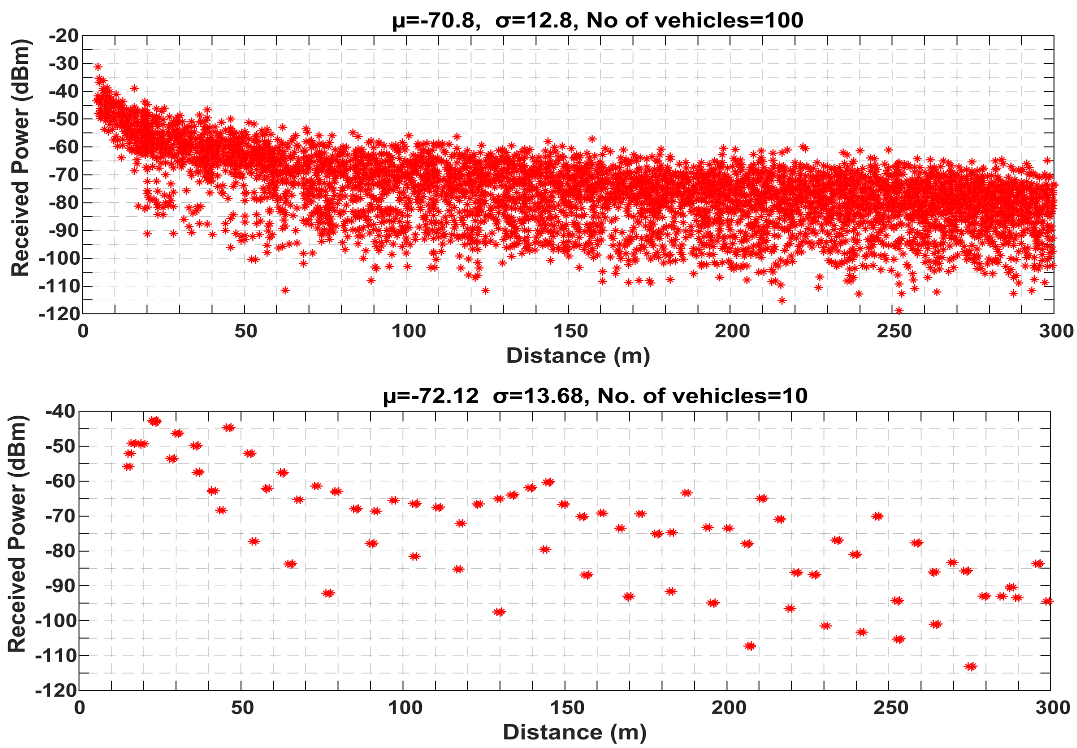

Figure 6.8 Comparison of received power (dBm) for the Y-junction intersection on GEMV2 V2V communication simulations

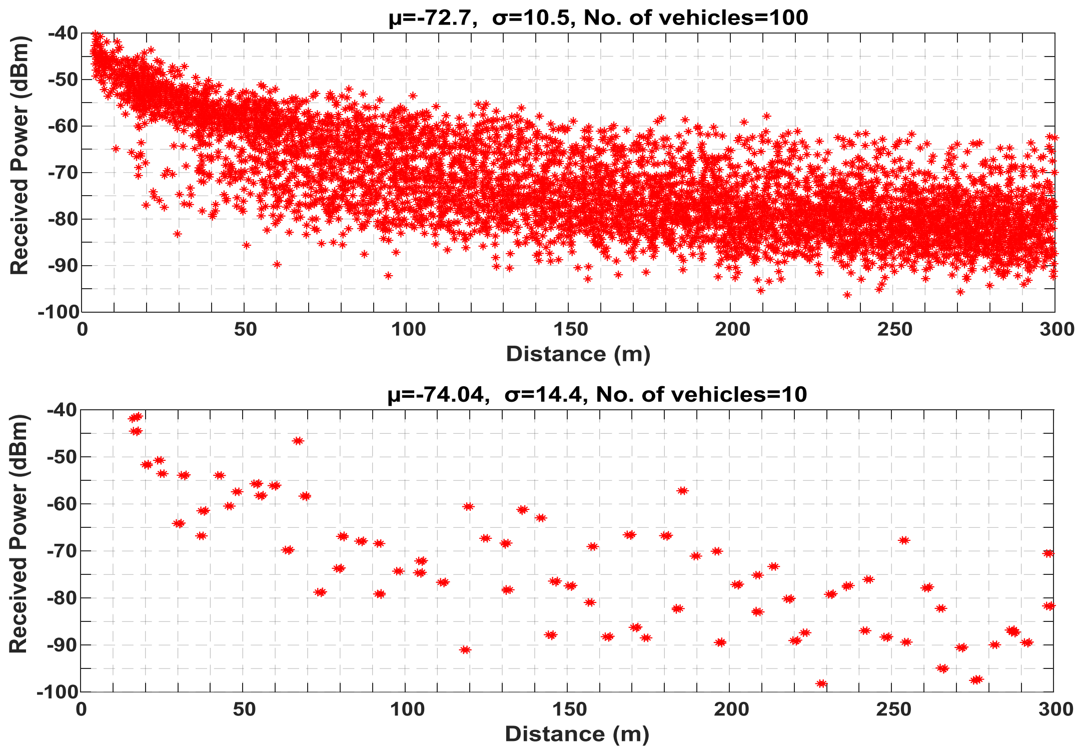

Figure 6.9 Comparison of received power (dBm) for the T-Junction intersection on GEMV2 V2V communication simulations

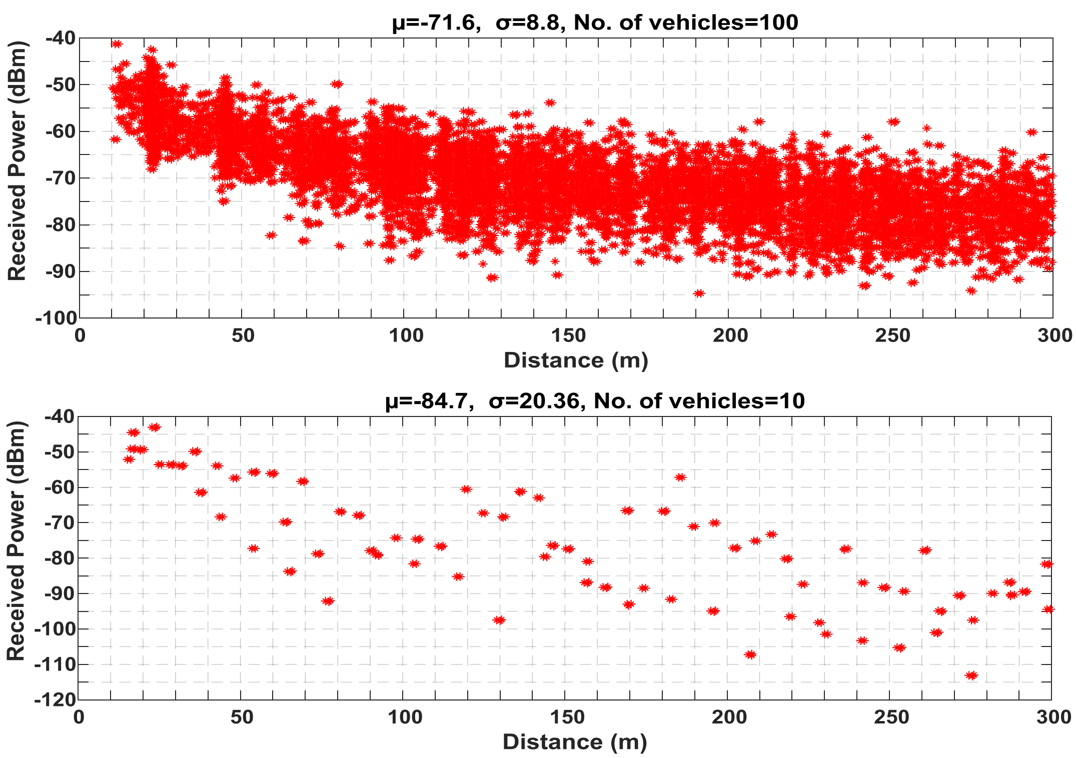

Figure 6.10 Comparison of received power (dBm) for the four-way intersection on GEMV2 V2V communication simulations

The receiver power differentials in the previous scenario indicate the fact that blocking cars and buildings causes a significant reduction in the received signal strength.

It is noticeable that the received power decreases significantly in the case of decreasing the number of cars in the open intersections that contain a few of the number of buildings as in the forms 6.7 and 6.10 where the standard deviation that is indicative of how to spread out data are 13.39 dB and 20.36 dB, respectively. In the narrow intersections, the decrease in the number of cars does not affect much because of the density of the buildings as in Figures 6.8 and 6.9.

As a result, it can be said that the buildings have more effect than the number of vehicles between communication pairs on the received power degradation.

6.3. Conclusion

The aim of this study is to investigate the effect of the buildings and the number of vehicles on the V2V communication channel. For this purpose, OpenStreetMap, SUMO and GEMV2 simulation tools were used to generate simulation framework which implements the typical simulation for V2V communication channel with different scenarios was mentioned detailed in Chapter 3. The effect of the buildings and the number of vehicles on the received power level were compared in different intersections which have different geometry information.

It is concluded that increasing the number of vehicles causes more attenuation than the surrounding buildings on an open intersection. On the other hand, in the narrow intersections, the buildings between communication pairs have a more decreasing effect on the received power than the number of vehicles on the V2V communication channel.

This study shows the effects of the buildings and the number of vehicles on the V2V communication channel. Preliminary results obtained from this work can be a good motivation for this research area. However, it still needs both much more theoretical and experimental studies to support the simulation results.

Chapter 7: Conclusions

Wireless communication systems are likely to be used to exchange information between vehicles as part of driving towards independent autonomous systems. The accepted standard of communication for this is presently the IEEE 802.11p which runs at 5.9 GHz. However, the number of study on radio wave propagation at 5.9 GHz with a focus on vehicular communication is not too big. This raises many questions about this type of communication. Various physical environments (such as urban, suburban, highways and rural intersections) provide difficult channel characteristics (such as Doppler increase, delay differentials due to multipath propagation. The study in this thesis has focused on propagation at non-perpendicular intersections such as the roundabout and Y-junction.

This thesis includes seven Chapters as follows.

- Chapter 1 outlined the research area that interests this research (channel characterization in the Vehicular environment). As well as indented VANET applications and their related requirements.
- The literature on Vehicular Ad-hoc Networks (VANETs) has presented in chapter 2. It is providing a compendium of the states of the art proceeded to evaluate V2V channel characterization and modelling by including analytical as well as measurement-based research on V2V channels. Different propagation environments and their impact on propagation are discussed.
- Chapter 3 is the methodology. The dual measurement system is similar to that used by C.J. Clayton. (2016) was used but the network system is developed by using a MIMO system. The Signal strength, Doppler spreads and network performances have been measured simultaneously using the equipment configuration described in this Chapter. The 802.11p network system (NS) has been measured network performance and a continuous wave system (CWS) has been measured channel parameters. Two unique aspects were used in this system. The first one was used the MIMO in the network system (NS) that it can give the best throughput and efficiency of signals transmissions by using multiple antennas both at transmitting & receiving end. Another feature is the type of locations used for data collection which are

represented by non-perpendicular intersections with the transmitter placed on the branched road hence causing NLOS conditions. Whilst studies have been performed to model propagation at intersections this is the first that entirely focusses on radio propagation at 5.9 GHz at non-perpendicular intersections.

- Chapter 4 includes measurements of signal strength and packet delivery ratio which showed that the performance of the network suffered a huge loss in NLOS conditions at non-perpendicular intersections. When the transmitter was 30 m away from the intersection centre in a single lane roundabout intersection and transmitting a CW 18 dBm, 90% PDR (which would be marginal in supporting safety critical communications) was consistently observed only for 20 m north side and 35 m south side which was under NLOS conditions. The part with the larger coverage was south-side (which acts as a waveguide) whereas the other part had an open space which led to less power being received in that part of the intersection. These ranges are short compared to the coverage of 100s of metres on highways or open areas.

  The network performance was worse on the north-side of the roundabout intersection which had fewer buildings to reflect signals. A consistent PDR greater than 90% was not observed at all with the transmitter 30 m away from the intersection centre and the receiver collecting data from 20 m away from the intersection centre. The PDR was consistently less than 10% once the receiver was beyond 25 m from the intersection centre.

  The PDR was consistently greater than 90% for just over 47 m in the Y-junction because of the density of buildings in this intersection. The PDR was also consistently greater than 60% up to a distance of 55 m away from the intersection centre.

  To support safety-critical systems designers may have using a communications repeater at the centre of the intersections with buildings at the edges assuming that the increased latency and network congestion does not adversely affect the system more.

  The path loss predictions from a recent model, VirtualSource11p were compared against the signal strength measurements for the four intersections. The virtualsource11p model is a site generic model which does not consider the layout of buildings surrounding a junction. It was found that the median error was within 4 dB for measurement runs up to 55 m away from the intersection centre. It has been found that the model is flexible and well with most of the measurements at different intersections. However, there are some cases where the model does not fit with measurements because of the scattering at some intersections. Users of this model should, therefore, realize that the model works best in environments with many surfaces to reflect waves.

In this Chapter, Doppler spreads were found to be high in LOS regions, compared with NLOS, taking into account traffic density as well as buildings. It was also found that the larger vehicles resulted in a larger Doppler spread with stronger amplitudes, which in turn would assist in the PDR process. However, if each of these vehicles will also contribute to increased network traffic, further study will be needed to determine where the advantages of vehicular traffic are overcome by the disadvantages of increased network traffic. It can be concluded that road traffic has directly improved the 802.11p network performance, albeit for a very short period of time.

- Chapter 5 shows another contribution of this study – the effect of the environment on the communication channel. An experimental evaluation of the impact of obstructing vehicles on V2V communications. A series of experiments on 802.11p devices were carried out in three different distance scenarios between transmitter and receiver: 20 m, 40 m and 60 m. The results indicate that vehicles that block the line of sight greatly reduce signal when compared to line-of-sight conditions in all scenarios. Also, the effect seems to be clearer the closer the obstacle of the transmitter with the attenuation varies depending on the vehicle type.

  The effect of vehicle volume on frequency behaviour was also investigated in this Chapter. As the size of the vehicle affects frequency disturbances, so that the larger the size of the vehicle the less Doppler spreads due to the increased duration of obstruction between the transmitter and the receiver. The effect of antenna height was also investigated in this Chapter. The changing the height of the transmitter has a strong effect on the received signal at values of the distances within, or a few metres beyond, the LOS region, but the little effect at greater distances. In addition, the antenna ground plane has a similar effect in changing the height as in placing the antenna on the surface of the truck (ht = 2 m).

- Chapter 6: The effect of the buildings and the number of vehicles on the V2V communication channel was studied in this Chapter. The OpenStreetMap, SUMO, and GEMV2 simulation tools were used to create a simulation framework that performs typical simulation of a V2V connection channel with different scenarios.
  It has been found that the increase in the number of vehicles will lead to more attenuation of the signal received compared to the surrounding buildings at the open intersections, while the impact of buildings between communication pairs in narrow intersections is greater.

7.1. Contributions

- A dual measurement system using 802.11p MIMO transceiver (LocoMate mini 2) radio propagation and network performance data at non-perpendicular intersections in five different intersections located in the centre of Leicester to determine the channel characteristics such as PDR and peak power.
- The data obtained in real-time measurements were compared against path loss modelling under NLOS conditions which are called virtualsource11p. This model is flexible with the urban environment and it is not fit with suburban or rural environments because of a few buildings
- Physical traffic was analyzed to assist communications by measuring Doppler changes and the time of coherence of the channel.
- The effect of the LOS-obstructing vehicles on inter-vehicle communication was described in terms of received power and the behaviour of frequency by considering the size of the vehicle and the distances between transmitter and receiver. It was found that larger vehicles led to larger Doppler spreads with stronger amplitudes.

- The difference in antenna height on the communication channel as well as the antenna base was studied. It influences the coverage range significantly.
- A framework was introduced to study the effect of the density of vehicles and structures on the V2V communication channel depends on The OpenStreetMap, SUMO, and GEMV2 simulation tools. It shows the effects of the number of vehicles on the V2V communication channel.

7.2. Future Work

The following are possible directions in which the work is done in this thesis could be extended.

- A more comprehensive measurement campaign and develop a channel model for V2V and V2I that takes into account the contributions of terrain, morphology, topography and path loss for each type of terrain.
- Develop methods of recording traffic density during measurements would be beneficial. These methods can be used to create relationships between physical traffic and the network performance, signal strength and the Doppler spread.
- Extend this research to include channel characterization, parameterization and modelling for time-bound communication and high-speed communications networks. Furthermore, the MIMO channel characterization is also explored for high-speed wireless systems.
- Develop a simulation framework of several stages combining several layers of simulation tools. These stages are the integration of actual traffic and then used to analyze the impact of physical traffic on the signal strength and Doppler spreads. For example, use the engineering-based propagation model (GEMV2) to characterize the received signal strength between transmitter and receiver pairs. As well as the use of building engineering data at the regional level and the effects of vehicular mobility to represent the environment in the real world. After that, the output is collected and fed as inputs to simulate the network. The difference between the proposed

framework and the standard propagation models applied in network simulations and their impact on network performance measures such as packet loss and latency.

References

Abbas, T., Karedal, J., Tufvesson, F., Paier, A., Bernad, L., and Molisch, A. (2011), 'Directional analysis of vehicle-to-vehicle propagation channels', IEEE Vehicular Technology Conference, (May). doi: 10.1109/VETECS.2011.5956706.

Abbas, T., Bernado, L., Thiel, A., Mecklenbrauker, C., and Tufvesson, F. (2013), 'Measurements based channel characterization for vehicle-to-vehicle communications at merging lanes on highway', 2013 IEEE 5th International Symposium on Wireless Vehicular Communications, WiVeC 2013 - Proceedings. doi: 10.1109/wivec.2013.6698241.

Abbas, T., Thiel, A., Zemen , T., Mecklenbrauker, C., and Tufvesson, F. (2013), 'Validation of a non-line-of-sight path-loss model for V2V communications at street intersections', 2013 13th International Conference on ITS Telecommunications, ITST 2013, pp. 198–203. doi: 10.1109/ITST.2013.6685545.

Abbas, T. (2014), 'Measurement based channel characterization and modeling for vehicle-to-vehicle communications', PhD thesis, Lund University, Sweden.

Abbas, T., Sjöberg, K., Karedal, J., and Tufvesson, F. (2015), 'A measurement based shadow fading model for vehicle-to-vehicle network simulations', International Journal of Antennas and Propagation, 2015. doi: 10.1155/2015/190607.

Abbas, T., Nuckelt, J., and K¨urner, T. (2015), 'Simulation and measurement-based vehicle-to-vehicle channel characterization : accuracy and constraint analysis', IEEE Transactions on Antennas and Propagation, October 2015.

Abbas, T., Karedal, J. and Tufvesson, F. (2013), 'Measurement-based analysis: the effect of complementary antennas and diversity on vehicle-to-vehicle communication', IEEE Antennas and Wireless Propagation Letters, 12, pp. 309–312. doi: 10.1109/LAWP.2013.2250243.

Acosta, G. and Ingram, M. A. (2007), 'Six time- and frequency- selective empirical channel models for vehicular wireless LANs', IEEE Vehicular Technology Magazine, 2(4), pp. 4–11. doi: 10.1109/MVT.2008.917435.

Acosta, G. and Ingram, M. A. (2006), 'Model development for the wideband expressway vehicle-to-vehicle 2.4 ghz channel', IEEE Wireless Communications and Networking Conference, 2006. WCNC 2006., 3(c), pp. 1283–1288. doi: 10.1109/WCNC.2006.1696471.

Agilent (2012), PSA series spectrum analyzers getting started guide (E4448A)', TestWorld, Inc. Unitrd States.

Al-Bado, M., Sengul, C. and Ruben Merz (2012), ‘What details are needed for wireless simulations? - a study of a site-specific indoor wireless model’, pp. 1–12. doi: 10.1109/INFCOM.2012.6195724.

Alexander, P., Haley, D., and Grant, A. (2011), ‘Cooperative intelligent transport systems: 5.9-GHz field trials’ IEEE Vehicular Technology Conference, July 2011.

Almers, P., Bonek, E., Burr, A., Czink, N., Debbah, M., Degli-Esposti, V., Hofstetter, H., and Kyosti, P. (2007), ‘Survey of channel and radio propagation models for wireless MIMO systems’, Eurasip Journal on Wireless Communications and Networking, 2007(Section 3). doi: 10.1155/2007/19070.

Alsuhli, G.H., Khattab, A.K., & Fahmy, Y.A. (2019), 'Double-head clustering for resilient VANETs' *Wireless Communications and Mobile Computing, 2019*, 2917238:1-2917238:17.

Amadeo, M., Campolo, C. and Molinaro, A. (2012), ‘Content-centric networking’, Proceedings of the ninth ACM international workshop on Vehicular inter-networking, systems, and applications - VANET ’12, (Cid), p. 99. doi: 10.1145/2307888.2307906.

Anritsu Company (2009), ‘Synthesized signal generators operation manual’, (June).

Arada Systems (no date), ‘LocoMate mini 2 TM | DSRC with external GPS and DSRC Antenna’, pp. 2–4.

Avazov, N., Islam, S.M., Park, D., & Kwak, K.S. (2017), 'Statistical characterization of a 3-d propagation model for v2v channels in rectangular tunnels' *IEEE Antennas and Wireless Propagation Letters, 16*, 2392-2395.

Aygün, B., Boban, M., Vilela, J.P., & Wyglinski, A.M. (2016), 'Geometry-based propagation modeling and simulation of vehicle-to-infrastructure links' *IEEE 83rd Vehicular Technology Conference (VTC Spring)*, 1-5.

Azimi, S. (Reza), Bhatia, G., and Rajkumar, R. (2013), ‘Reliable intersection protocols using vehicularnetworks’, Proceedings of theACM/IEEE 4th International Conference on Cyber-Physical Systems, pp. 1–10. doi: 10.1145/2502524.2502526.

Bai, F., Stancil, D. D. and Krishnan, H. (2010), ‘Toward understanding characteristics of dedicated short range communications (DSRC) from a perspective of vehicular network engineers’, Proceedings of the sixteenth annual international conference on Mobile computing and networking - MobiCom ’10, (May 2014), p. 329. doi: 10.1145/1859995.1860033.

Bernad, L. (2012), 'Non-stationarity in vehicular wireless channels', PhD thesis. University of Technology, Wien.

Bernadó, L., Zemen, T., Tufvesson, F., Molisch, A., and Mecklenbrauker, C. (2013), 'Delay and doppler spreads of non-stationary vehicular channels for safety relevant scenarios', *IEEE Transactions on Vehicular Technology*, vol. 63, no. 1, pp. 82-93,

Boban, M., Vinhoza, T., Ferreira, M., Barros, J., and Tonguz, O. K. (2011), 'Impact of vehicles as obstacles in vehicular ad hoc networks', IEEE Journal on Selected Areas in Communications, 29(1), pp. 15–28. doi: 10.1109/JSAC.2011.110103.

Boban, M., Meireles, R., Barros, J., Steenkiste, P., and Tonguz, O. K. (2014), 'TVR - Tall vehicle relaying in vehicular networks', IEEE Transactions on Mobile Computing, 13(5), pp. 1118–1131. doi: 10.1109/TMC.2013.70.

Boban, M., Barros, J. and Tonguz, O. K. (2014), 'Geometry-based vehicle-to-vehicle channel modeling for large-scale simulation', IEEE Transactions on Vehicular Technology, 63(9), pp. 4146–4164. doi: 10.1109/TVT.2014.2317803.

Boban, M., Dupleich, D.A., Iqbal, N., Luo, J., Schneider, C.M., Müller, R., Yu, Z., Steer, D., Jämsä, T., Li, J., and Thomä, R.S. (2019), 'Multi-band vehicle-to-vehicle channel characterization in the presence of vehicle blockage' *IEEE Access, 7*, 9724-9735.

Boban, M., Gong, X., & Xu, W. (2017), 'Modeling the evolution of line-of-sight blockage for v2v channels' *IEEE 84th Vehicular Technology Conference (VTC-Fall)*, 1-7.

Borhani, A. and Patzold, M. (2013), 'Modelling of non-stationary mobile radio channels using two-dimensional brownian motion processes', International Conference on Advanced Technologies for Communications, pp. 241–246. doi: 10.1109/ATC.2013.6698114.

Bosch, GLM 80 Professional Laser Measure Laser measures | Bosch Professional.Available at: http://www.bosch-professional.com/gb/en/glm-80-26171-ocs-p/ [Accessed October 2, 2018]

Cai, X., Peng, B., Yin, X., & Yuste, A.P. (2018), 'Hough-transform-based cluster identification and modeling for v2v channels based on measurements' *IEEE Transactions on Vehicular Technology, 67*, 3838-3852.

Campuzano, A. J., Fernández, H., Balaguer, D., Vila, A., Reig, J., and Rubio, L. (2012), 'vehicular-to-vehicular channel characterization and measurement results', Waves, no. 4, pp. 15–24.

Cheng, L., Henty, B., Bai, F., Mudalige, P. (2007), 'A fully mobile, GPS enabled, vehicle-to-vehicle measurement platform for characterization of the 5.9 GHz DSRC channel', IEEE Antennas and Propagation Society, AP-S International Symposium (Digest), pp. 2005–2008. doi: 10.1109/APS.2007.4395917.

Cheng, L., Henty, B. E., Bai, F., Mudalige, P. (2007), ‘Mobile vehicle-to-vehicle narrow-band channel measurement and characterization of the 5.9 GHz Dedicated Short Range Communication (DSRC) frequency band’, IEEE Journal on Selected Areas in Communications, 25(8), pp. 1501–1516. doi: 10.1109/JSAC.2007.071002.

Cheng, L., Stancil, D. D. and Bai, F. (2013), ‘A roadside scattering model for the Vehicle-To-Vehicle communication channel’, IEEE Journal on Selected Areas in Communications, 31(9), pp. 449–459. doi: 10.1109/JSAC.2013.SUP.0513040.

Chisb, R. and Shukla, C. (2014), ' Performance evaluation of 4g-lte-scfdma scheme under sui and itu channel models', International Journal of Engineering and Technology, 14(01), pp 58-69.

Chouhan, P., Kaushal, G. and Prajapat, U. (2016), ‘Comparative study MANET and VANET’, International Journal of Engineering and Computer Science, 05(16079), pp. 16079–16083. doi: 10.18535/ijecs/v5i4.04.

Clayton C. J. (2016), 'Effect of physical traffic & t-junction layout on radio signal characteristics & network performance at 5 . 9 GHz.', PhD thesis, University of Leicester, Leicester .

Convoys, P. (2016), ‘Vehicle-to-Vehicle communications in mixed passenger-freight convoys’, final report, University of Southern California Los Angeles, (September).

Cozzetti, H., Campolo, C., Scopigno, R., Molinaro, A. (2012), ‘Urban VANETs and hidden terminals: Evaluation through a realistic urban grid propagation model’, 2012 IEEE International Conference on Vehicular Electronics and Safety, ICVES 2012, pp. 93–98. doi: 10.1109/ICVES.2012.6294332.

Davis, J. and Linnartz, J. (1994), ‘Vehicle to vehicle RF propagation measurements’, Signals, Systems and Computers, 1, pp. 470–474. doi: 10.1109/ACSSC.1994.471498.

Dudley, D. G., Lienarc, M., . Mahmouc, S., and Degauque, P. (2007), ‘Wireless propagation in tunnels’, IEEE Antennas and Propagation Magazine, 49(2), pp. 11–26. doi: 10.1109/MAP.2007.376637.

Eggers, P. C. F., Brown, T., Olesen, K., and Pedersen, G. (2007), ‘Assessment of capacity support and scattering in experimental high speed vehicle to vehicle MIMO links’, IEEE Vehicular Technology Conference, pp. 466–470. doi: 10.1109/VETECS.2007.107.

El-Sallabi, H. M. (2000), ‘Fast path loss prediction by using virtual source technique for urban microcells’, IEEE 51st Vehicular Technology Conference Proceedings - VTC 2000-Spring, 3, pp. 2183–2187. doi: 10.1109/VETECS.2000.851659.

ETSI TS 102 (2010), ‘Intelligent transport systems (ITS) vehicular communications ; basic set of applications’, Intelligent Transport Systems, 1, pp. 1–60.

Eurecom (2014), VanetMobiSim-Newcom. Available at: http://vanet.eurecom.fr/.

Fernandez, H., Rubio, L., and Reig, J. (2014), ‘Path loss characterization for vehicular communications at 700 MHz and 5.9 GHz under LOS and NLOS conditions’, IEEE Antennas and Wireless Propagation Letters, 13, pp. 931–934. doi: 10.1109/LAWP.2014.2322261.

Fernández, H., Rubio, L., and Reig, J. (2013), ‘Path loss modeling for vehicular system performance and communication protocols evaluation’, Mobile Networks and Applications, 18(6), pp. 755–764. doi: 10.1007/s11036-013-0463-x.

Fernandez, J. A., Pittsburgh, PA, U. and Bai, ; Kevin Borries ; Lin Cheng ; B. V. K. Vijaya Kumar ; Daniel D. Stancil ; Fan (2012), ‘Performance of the 802.11p Physical Layer in Vehicle-to-Vehicle Environments’, Department of Electrical and Computer Engineering, Carnegie Mellon University, (Jan). Available at: http://citeseerx.ist.psu.edu/viewdoc/download?doi=10.1.1.307.7302&rep=rep1&type=pdf.

Fernando Jose Casadevall Palacio, Ramon Agustí, Jordi Pérez-Romero, M. L.-B. (2011), ‘Radio environmental maps: information models and reference model’, Faramir, (April), pp. 1–95.

Filali, Z., and Hameed M. (2017), ‘LTE and IEEE 802.11p for vehicular networking: a performance evaluation’, EURASIP Journal on Wireless Communications,1, pp. 1–15.

Giordano, E., Frank, R., Pau, G. and Gerla, M. (2010), ‘CORNER : a realistic urban propagation model for VANET’, pp. 57–60.

Gozalvez, J., Sepulcre, M. and Bauza, R. (2012), ‘Impact of the radio channel modelling on the performance of VANET communication protocols’, Telecommunication Systems, 50(3), pp. 149–167. doi: 10.1007/s11235-010-9396-x.

Granda, F., Azpilicueta, L., Rosales, C.V., Celaya-Echarri, M., López-Iturri, P., Aguirre, E., Astrain, J.J., Medrano, P., Villadangos, J.E., & Falcone, F. (2018), 'Deterministic propagation modeling for intelligent vehicle communication in smart cities' *Sensors*.

Granda, F., Azpilicueta, L., Vargas-Rosales, C., López-Iturri, P., Aguirre, E., Astrain, J.J., Villandangos, J., and Falcone, F. (2016), 'Characterization of radio propagation channel in urban vehicle to infrastructure environments to support WSNs'.

Hafner, M. R., Cunningham, D., Caminiti, L., Vecchio, D. (2011), ‘Automated vehicle-to-vehicle collision avoidance at intersections’, Proceedings of the 18th ITS World Congress, IS05(1314), pp. 1–11.

Haklay, M. and Weber, P. (2008), “OpenStreetMap: User-generated street maps,” *IEEE Pervasive Comput.*, vol. 7, no. 4, pp. 12–18, Oct.–Dec.

Hameed Mir, Z. and Filali, F. (2017), ‘Large-scale simulations and performance evaluation of connected cars - A V2V communication perspective’, Simulation Modelling Practice and Theory. Elsevier B.V., 72, pp. 88–103. doi: 10.1016/j.simpat.2017.01.004.

Hartenstein, H. and Laberteaux, K. P. (2010), VANET: vehicular applications and inter networking technologies, Karlsruhe Institute ofTechnology (KIT), Germany.

Hofer, M., Xu, Z., Vlastaras, D., Schrenk, B., Löschenbrand, D., Tufvesson, F., and Zemen, T. (2019), 'Real-time geometry-based wireless channel emulation' *IEEE Transactions on Vehicular Technology, 68*, 1631-1645.

IEEE Std. 802.11p-2010, P. 11 (2010), 'Wireless lan medium access control (mac) and physical layer (phy) specifications, wireless access in vehicular environment', IEEE Std., July 2010. doi: 10.1002/9780470978238.

Islam, T., Hu, Y., Onur, E., Boltjes, B., and Jongh, J. (2013), ‘Realistic simulation of IEEE 802.11p channel in mobile vehicle to vehicle communication’, Proceedings of 13th Conference on Microwave Techniques, COMITE 2013 - MAREW 2013: Microwave and Radio Electronics Week 2013, pp. 156–161. doi: 10.1109/COMITE.2013.6545061.

Jain, A. and Bharti, R. (2014), ‘Simulation and performance analysis of throughput and delay on varying time and number of nodes in MANET’, VII(2), pp. 113–117.

Jiang, D., Chen, Q. and Delgrossi, L. (2008), ‘Optimal data rate selection for vehicle safety communications’, Proceedings of the fifth ACM international workshop on VehiculAr Inter-NETworking - VANET ’08, p. 30. doi: 10.1145/1410043.1410050.

Karedal, J., Tufvesson, F., Czink, N., and Zemen, T. (2009), ‘A geometry-based stochastic MIMO model for vehicle-to-vehicle communications’, IEEE Transactions on Wireless Communications, 8(7), pp. 3646–3657. doi: 10.1109/TWC.2009.080753.

Karedal, J., Tufvesson, F., Abbas, T., Klemp, O., and Paier, A. (2010), ‘Radio channel measurements at street intersections for vehicle-to-vehicle safety applications’, IEEE Vehicular Technology Conference. doi: 10.1109/VETECS.2010.5493955.

Karedal, J., Czink, N., Paier, A., Tufvesson, F., and Molisch, a. (2011), ‘Path loss modeling for vehicle-to-vehicle communications’, IEEE Transactions on Vehicular Technology, 60(1), pp. 323–328. doi: 10.1109/TVT.2010.2094632.

Karnadi, F. K., Mo, Z. H. and Lan, K. C. (2007), ‘Rapid generation of realistic mobility models for VANET’, IEEE Wireless Communications and Networking Conference, WCNC, pp. 2508–2513. doi: 10.1109/WCNC.2007.467.

Kaul, S., Ramachandran, K., Shankart, P., Gruteser, M., Seskar, I., and Nadeem, T. (2007), 'Effect of antenna placement and diversity on vehicular network communications', 2007 4th Annual IEEE Communications Society Conference on Sensor, Mesh and Ad Hoc Communications and Networks, SECON, pp. 112–121. doi: 10.1109/SAHCN.2007.4292823.

Kenney, J. B. (2011), 'Dedicated short-range communications (DSRC) standards in the United States', Proceedings of the IEEE, 99(7), pp. 1162–1182. doi: 10.1109/JPROC.2011.2132790.

Kunisch, J. and Pamp, J. (2008), 'Wideband car-to-car radio channel measurements and model at 5.9 GHz', IEEE Vehicular Technology Conference, pp. 1–5. doi: 10.1109/VETECF.2008.64.

Liu, P., Ai, B., Matolak, D., Sun, R.,and Li, y. (2016), '5-GHz vehicle-to-vehicle channel characterization for example overpass channels', IEEE Transactions on Vehicular Technology, 65(8), pp. 5862–5873. doi: 10.1109/TVT.2015.2476382.

Longair, M. (2015), '"...a paper ...I hold to be great guns": a commentary on Maxwell (1865) "A dynamical theory of the electromagnetic field"', Philosophical Transactions of the Royal Society A: Mathematical, Physical and Engineering Sciences, 373(2039), pp. 20140473–20140473. doi: 10.1098/rsta.2014.0473.

Luan, T. H., Shen, X. and Bai, F. (2013), 'Integrity-oriented content transmission in highway vehicular ad hoc networks', Proceedings - IEEE INFOCOM, pp. 2562–2570. doi: 10.1109/INFCOM.2013.6567063.

Luo, L., Wong, M. and Leong, L. (2012), "Parallel implementation of R-trees on the GPU," in *Proc. 17th ASP-DAC*, 2012, pp. 353–358.

Maier, G., Paier, A. and Mecklenbrauker, C. F. (2012), 'Performance evaluation of IEEE 802.11p infrastructure-to-vehicle real-world measurements with receive diversity', IWCMC 2012 - 8th International Wireless Communications and Mobile Computing Conference, pp. 1113–1118. doi: 10.1109/IWCMC.2012.6314362.

Mangel, T. Michl, M., Klemp, O., and Hartenstein, H. (2011), 'Real-world measurements of non-line-of-sight reception quality for 5.9 GHz IEEE 802.11 p at intersections', … Technologies for Vehicles, pp. 189–202. doi: 10.1007/978-3-642-19786-4_17.

Mangel, T. and Hartenstein, H. (2011), '5.9GHz IEEE 802.11p inter-vehicle communication: non-line-of-sight reception under competition', 2011 IEEE Vehicular Networking Conference (VNC), 2, pp. 155–162.

Mangel, T., Klemp, O. and Hartenstein, H. (2011a), '5.9 GHz inter-vehicle communication at intersections: a validated non-line-of-sight path-loss and fading model', EURASIP Journal on Wireless Communications and Networking, 2011(1), p. 182. doi: 10.1186/1687-1499-2011-182.

Mangel, T., Klemp, O. and Hartenstein, H. (2011b), ‘A validated 5.9 GHz non-line-of-sight path-loss and fading model for inter-vehicle communication’, 2011 11th International Conference on ITS Telecommunications, ITST 2011, pp. 75–80. doi: 10.1109/ITST.2011.6060156.

Mao, C., Gao, S., & Wang, Y. (2018), 'Dual-band full-duplex Tx/Rx antennas for vehicular communications' *IEEE Transactions on Vehicular Technology, 67*, 4059-4070.

Matolak, D., Sen, I. and Xiong, W. (2005), ‘5 GHz wireless channel characterization for vehicle to vehicle communications’, Military Communications, pp. 5–11. Available at: http://ieeexplore.ieee.org/xpls/abs_all.jsp?arnumber=1606122.

Maurer, J., Fugen, T. and Wiesbeck, W. (2002), ‘Narrow-band measurement and analysis of the inter-vehicle transmission channel at 5.2 GHz’, Vehicular Technology Conference. IEEE 55th Vehicular Technology Conference. VTC Spring 2002 (Cat. No.02CH37367), 3, pp. 1274–1278. doi: 10.1109/VTC.2002.1002820.

Mecklenbraüker, C. F., Molisch, A., Karedal, J., Tufvesson, F., and Klemp, O. (2011), ‘Vehicular channel characterization and its implications for wireless system design and performance’, Proceedings of the IEEE, 99(7), pp. 1189–1212. doi: 10.1109/JPROC.2010.2101990.

Meireles, R., Boban, M., Steenkiste, P., Tonguz, O., and Barros, J. (2010), ‘Experimental study on the impact of vehicular obstructions in VANETs’, 2010 IEEE Vehicular Networking Conference, VNC 2010, pp. 338–345. doi: 10.1109/VNC.2010.5698233.

Molisch. F. (2005), 'Wireless communications' second edition, University of Southern California, USA .

Molisch, A. F., Tufvesson, F., Karedal, J., and Mecklenbräuker, C. (2009), ‘A survey on vehicle-to-vehicle propagation channels’, IEEE Wireless Communications, 16(6), pp. 12–22. doi: 10.1109/MWC.2009.5361174.

Nilsson, M.G., Gustafson, C., Abbas, T., & Tufvesson, F. (2018), ' A Path Loss and Shadowing Model for Multilink Vehicle-to-Vehicle Channels in Urban Intersections' *Sensors*.

Nilsson, M. G. Hallbjörner, P., Arabäck, N., Bergqvist, B., Abbas, T., and Tufvesson, F. (2015), ‘Measurement uncertainty, channel simulation, and disturbance characterization of an over-the-air multiprobe setup for cars at 5.9 GHz’, IEEE Transactions on Industrial Electronics, 62(12), pp. 7859–7869. doi: 10.1109/TIE.2015.2475423.

Nimay Ch. Giri1, Anwesha Sahoo2, J. R. Swain3, P. Kumar4, A. Nayak5, P. D. (2014), ‘Capacity and performance comparison of SISO and MIMO system for next generation network (NGN)’, 3(9), pp. 3031–3035.

Office, U. S. G. A. (2013), ‘intelligent transportation systems: vehicle-to-vehicle technologies expected to offer safety benefits, but a variety of deployment challenges exist’, GAO Reports, (November), pp. 1–53. Available at: http://search.ebscohost.com/login.aspx?direct=true&db=bth&AN=91862107&site=ehostlive.

Olariu, S. (2009), 'Vehicular networks from theory to practice, Ad Hoc Networks', Old dominion University Norfolk,Virginia, U.S.A. . doi: 10.1016/j.adhoc.2010.01.001.

Onubogu, O. J. (2016), 'Simulation and measurement based MIMO and vehicular channel characterization at 920 MHz and 5.8 GHz', PhD thesis, Queensland University of Technology, Australia .

Otto, J. S., Bustamante, F. E. and Berry, R. A. (2009), ‘Down the block and around the corner: The impact of radio propagation on inter-vehicle wireless communication’, Proceedings - International Conference on Distributed Computing Systems, pp. 605–614. doi: 10.1109/ICDCS.2009.60.

Paier, A., Karedal, J., Czink, N., Dumard, C., Zemen, T., Tufvesson, F., Molisch, A., and Mecklenbräuker, C. (2009), ‘Characterization of vehicle-to-vehicle radio channels from measurements at 5.2 GHz’, Wireless Personal Communications, 50(1), pp. 19–32. doi: 10.1007/s11277-008-9546-6.

Paier, A., Bernad, L., Karedal, J., Klemp, O., and Kwoczek, A. (2010), ‘Overview of vehicle-to-vehicle radio channel measurements for collision avoidance applications’, IEEE Vehicular Technology Conference, pp. 4–8. doi: 10.1109/VETECS.2010.5493975.

Paier, A. (2010), ‘The Vehicular Radio Channel in the 5 GHz Band’, PhD thesis. University of Technology, Wien .

Park, J.J., Lee, J., Kim, K., Kim, M.D., and Lee, K. (2018), '28 GHz doppler measurements in high-speed expressway environments' *IEEE 29th Annual International Symposium on Personal, Indoor and Mobile Radio Communications (PIMRC)*, 1132-1133.

Park, J., Lee, J., Kim, K., Lee, K., and Kim, M. (2018), 'Vehicle antenna position dependent path loss for -wave V2V communication' *11th Global Symposium on Millimeter Waves (GSMM)*, 1-3.

Paschalidis, P., Wisotzki, M., Kortke, A., Keusgen, W., and Peter, M. (2008), ‘A wideband channel sounder for car-to-car radio channel measurements at 5.7 GHz and results for an urban scenario’, IEEE Vehicular Technology Conference, pp. 1–5. doi: 10.1109/VETECF.2008.62.

Paschalidis, P., Mahler, K., Kortke, A., Peter, M., and Keusgen, W. (2011a), ‘Pathloss and multipath power decay of the wideband car-to-car channel at 5.7 GHz’, IEEE Vehicular Technology Conference, (May). doi: 10.1109/VETECS.2011.5956721.

Paschalidis, P., Mahler, K., Kortke, A., Peter, M., and Keusgen, W. (2011b), ‘Pathloss and multipath power decay of the wideband car-to-car channel at 5.7 GHz’, IEEE Vehicular Technology Conference. doi: 10.1109/VETECS.2011.5956721.

Pätzold, M., Hogstad, B. O. and Youssef, N. (2008), ‘Modeling, analysis, and simulation of MIMO mobile-to-mobile fading channels’, IEEE Transactions on Wireless Communications, 7(2), pp. 510–520. doi: 10.1109/TWC.2008.05913.

Puñal, O., Aguiar, A. and Gross, J. (2012), ‘In VANETs we trust ? characterizing rf jamming in vehicular networks’, Proceedings of the ninth ACM international workshop on Vehicular inter-networking, systems, and applications,VANET’12, pp. 83–92. doi: 10.1145/2307888.2307903.

Rashdan, I., Müller, F.D., Jost, T., and Sand, S. (2019), 'Measurement-based geometrical characterization of the vehicle-to-pedestrian channel' *13th European Conference on Antennas and Propagation (EuCAP)*, 1-5.

Rashdan, I., Müller, F.D., Wang, W., Schmidhammer, M., & Sand, S. (2018), 'Vehicle-to-pedestrian channel characterization: wideband measurement campaign and first results'.

Rappaport, T. (2002), Wireless communication principles and practice, second edition, University of Texas, Austin .

Renaudin, O., Kolmonen, V., Vainikainen, P., and Oestges, C. (2008), ‘Wideband MIMO car-to-car radio channel measurements at 5.3 GHz’, IEEE Vehicular Technology Conference, pp. 1–5. doi: 10.1109/VETECF.2008.65.

Renaudin, O., Kolmonen, V., Vainikainen, P., and Oestges, C. (2009), ‘Car-to-car channel models based on wideband {MIMO} measurements at 5.3 {GHz}’, 3rd European Conference on Antennas and Propagation (EuCAP). IEEE, pp. 635–639.

Rodriguez, I., Almeida, E.P., Lauridsen, M., Assefa, D., Gimenez, L.C., Nguyen, H.C., Sørensen, T.B., and Mogensen, P. (2016), 'Measurement-based evaluation of the impact of large vehicle shadowing on v2x communications'.

Rubio, L., Reig, J. and Fernandez, H. (2012), ‘Propagation aspects in vehicular networks’, Vehicular Technologies: Increasing Connectivity, (April 2011). doi: 10.5772/15650.

Schneider, J. (2017), 'Understanding the finite-difference time-domain method', Artech House antennas and propagation library.

Schumacher, H., Tchouankem, H., Nuckelt, J., Kürner, T., Zinchenko, T., Leschke, A., and Wolf, L. (2012), ‘Vehicle-to-Vehicle IEEE 802.11p performance measurements at urban intersections’, IEEE International Conference on Communications, (February 2015), pp. 7131–7135. doi: 10.1109/ICC.2012.6364714.

Schwartz, R. S., Das, K., Scholten, H., and Havinga, P. (2012), 'Exploiting beacons for scalable broadcast data dissemination in VANETs', Proceedings of the ninth ACM international workshop on Vehicular inter-networking, systems, and applications - VANET '12, p. 53. doi: 10.1145/2307888.2307899.

Segata, M., Bloessl, B., Joerer, S., Sommer, C., Cigno, R. and Dressler, F. (2013), 'Short paper: vehicle shadowing distribution depends on vehicle type: results of an experimental study', IEEE Vehicular Networking Conference, VNC, pp. 242–245. doi: 10.1109/VNC.2013.6737623.

Sen, I. and Matolak, D. W. (2008), 'Vehicle-vehicle channel models for the 5-GHz band', IEEE Transactions on Intelligent Transportation Systems, 9(2), pp. 235–245. doi: 10.1109/TITS.2008.922881.

Sengar, K., Rani, N., Singhal, A., Sharma, D., Verma, S., and Singh, T. (2014), 'Study and capacity evaluation of SISO, MISO and MIMO RF wireless communication systems', International Journal of Engineering Trends and Technology, 9(9), pp. 436–440. doi: 10.14445/22315381/IJETT-V9P283.

Sepulcre, M. and Gozalvez, J. (2014), 'Experimental evaluation of cooperative active safety applications based on V2V communications', Proceedings of the ninth ACM international workshop on Vehicular inter-networking, systems, and applications - VANET '12, (April 2014), p. 13. doi: 10.1145/2307888.2307893.

Shah, C. R. (2017), 'Performance and comparative analysis of SISO ,SIMO,MISO, MIMO', International Journal of Wireless Communication and Simulation, 9(1), pp. 1–14.

Sharafkandi, S., Bansal, G., Kenney, J. B., and Du, D. H. C. (2012) 'A novel use of EDCA to improve vehicle safety communication', Proceedings of the ninth ACM international workshop on Vehicular inter-networking, systems, and applications - VANET '12, p. 115. doi: 10.1145/2307888.2307910.

Shivaldova, V., Paier, A., Smely, D., and Mecklenbrauker, C. (2012), 'On roadside unit antenna measurements for vehicle-to-infrastructure communications', IEEE International Symposium on Personal, Indoor and Mobile Radio Communications, PIMRC, pp. 1295–1299. doi: 10.1109/PIMRC.2012.6362546.

Simons, R. W. (1996), 'Guglielmo Marconi and early systems of wireless communication', Communication, 11(1), pp. 37–55.

Sommer, C., Eckhoff, D., German, R., and Dressler, F. (2011), 'A computationally inexpensive empirical model of IEEE 802.11p radio shadowing in urban environments', 2011 8th International Conference on Wireless On-Demand Network Systems and Services, WONS 2011, pp. 84–90. doi: 10.1109/WONS.2011.5720204.

Srinivasa, S. and Haenggi, M. (2009), ‘Path loss exponent estimation in large wireless networks’, Information Theory and Applications Workshop, ITA 2009, (March 2009), pp. 124–129. doi: 10.1109/ITA.2009.5044933.

Subramanian, S., Werner, M., Liu, S., Jose, J., Lupoaie, R., and Wu, X. (2012), ‘Congestion control for vehicular safety: synchronous and asynchronous mac algorithms’, Proceedings of the ninth ACM international workshop on Vehicular inter-networking, systems, and applications - VANET ’12, p. 63. doi: 10.1145/2307888.2307900.

SUMO (2018). Available at: http://sumo.dlr.de/wiki/Main.

Sukuvaara, T., Ylitalo, R., Katz, M., (2013), ‘IEEE 802.11p based vehicular networking operational pilot field measurement’.

Takahashi, S., Kato, A., Sato, K., and Fujise, M. (2004), ‘Distance dependence of path loss for millimeter wave inter-vehicle communications’, Radioengineering, 13(4), pp. 8–13. doi: 10.1109/VETECF.2003.1284971.

Tan, I., Tang, W., Laberteaux, K., and Bahai, A. (2008), ‘Measurement and analysis of wireless channel impairments in DSRC vehicular communications’, IEEE International Conference on Communications, pp. 4882–4888. doi: 10.1109/ICC.2008.915.

Tatham, S. (2017), ‘PuTTY 0.70 is released’. Available at: https://lists.tartarus.org/pipermail/putty-announce/2017/000026.html.

Torres, R.P., Pérez, J.M., Basterrechea, J., Valle, L., Domingo, M., Fernández, H., Rubio, L., Rodrigo-Peñarrocha, V.M., & Reig, J. (2017), 'On the applicability of ray-tracing propagation models to V2V-intersection environments' *IEEE International Symposium on Antennas and Propagation & USNC/URSI National Radio Science Meeting*, 615-616

Turkka, J. and Renfors, M. (2008), ‘Path loss measurements for a non-line-of-sight mobile-to-mobile environment’, Proceedings - 2008 8th International Conference on Intelligent Transport System Telecommunications, ITST 2008, pp. 274–278. doi: 10.1109/ITST.2008.4740270.

Uzcategui, R. and Acosta-Marum, G. (2009), Wave: A tutorial, Communications Magazine, IEEE. doi: 10.1109/MPC.1994.298461.

Vega, C.A., Gutierrez, C.A., Rodríguez, J.J., Castillo, J.V., Delgado, D.U., Rivera, J.L., & Ibarra, M. (2019), ‘Doppler spectrum measurements of vehicular radio channels using a narrowband sounder’.

Vinel, A. (2012), ‘3GPP LTE versus IEEE 802.11p/WAVE: Which technology is able to support cooperative vehicular safety applications?’, IEEE Wireless Communications Letters, 1(2), pp. 125–128. doi: 10.1109/WCL.2012.022012.120073.

Vlastaras, D., Abbas, T., Nilsson, M., Whiton, R., Olback, M., and Tufvesson, F. (2014), 'Impact of a truck as an obstacle on vehicle-to-vehicle communications in rural and highway scenarios', 2014 IEEE 6th International Symposium on Wireless Vehicular Communications, WiVeC 2014 - Proceedings. doi: 10.1109/WIVEC.2014.6953226.

VMEbus Extensions for Instrumentation (2010), 'TCP/IP instrument protocol specification VXI-11'.

Wiesbeck, W. and Knorzer, S. (2007), 'Characteristics of the mobile channel for high velocities', *International Conference on Electromagnetics in Advanced Applications*, Torino, 2007, pp. 116-120.

Wang, S., Guan, K., He, D., Li, G., Lin, X., Ai, B., and Zhong, Z. (2018), 'Doppler Shift and coherence time of 5g vehicular channels at 3.5 GHz' *IEEE International Symposium on Antennas and Propagation & USNC/URSI National Radio Science Meeting*, 2005-2006.

Wang, S., Huang, A. and Zhang, T. (2013), 'Performance evaluation of IEEE 802.15.4 for V2V communication in VANET', Proceedings - 2013 International Conference on Computational and Information Sciences, ICCIS 2013, pp. 1603–1606. doi: 10.1109/ICCIS.2013.420.

Wang, X. Anderson, E., Steenkiste, P., and Bai, F. (2012), 'Improving the accuracy of environment-specific vehicular channel modeling', 7th ACM International Workshop on Wireless Network Testbeds, Experimental Evaluation and Characterization, WiNTECH 2012, pp. 43–50. doi: 10.1145/2348688.2348699.

World Health Organization (2015), 'Global status report on road safety', Injury prevention, p. 318. doi: http://www.who.int/violence_injury_prevention/road_safety_status/2015/en/.

Yang, M., Ai, B., He, R., Chen, L., Li, X., Li, J., Zhang, B., Huang, C., and Zhong, Z. (2019), 'A cluster-based three-dimensional channel model for vehicle-to-vehicle communications' *IEEE Transactions on Vehicular Technology, 68*, 5208-5220.

Yang, M., Ai, B., He, R., Chen, L., Li, X., Huang, Z., Li, J., and Huang, C. (2018), 'Path Loss analysis and modeling for vehicle-to-vehicle communications with vehicle obstructions' *10th International Conference on Wireless Communications and Signal Processing (WCSP)*, 1-6.

Yi, G., Shengchu, W., Yupeng, Z., Feng, L., & Lin, Z. (2018), 'Exploring LTE-V link level performance by geometry enhanced winner ii channel model' *International Conference on Information Networking (ICOIN)*, 346-351.

Yusuf, M.S., Tanghe, E., Martens, L., Laly, P., Gaillot, D.P., Liénard, M., Degauque, P., & Joseph, W. (2019), 'Experimental investigation of v2i radio channel in an arched tunnel' *13th European Conference on Antennas and Propagation (EuCAP)*, 1-5.

Zaji, A. G., and Stüber, G. L. (2008), 'Space-time correlated mobile-to-mobile channels : modelling and simulation', in *IEEE Transactions on Vehicular Technology*, vol. 57, no. 2, pp. 715-726, March 2008.